Physical models for Gravitational Wave experiments on Ground and in Space

Jean-Yves VINET
ARTEMIS
Observatoire de la Côte d'Azur
06304 NICE (France)

September 26, 2006

Contents

Foreword

Since about fourty years, a new field of theoretical and experimental research field has emerged: Gravitational Wave Astronomy. At the beginning, in the sixties, the scientific status of this research was so fuzzy and the profile of the pioneers so variable that it took some years to the science community to acknowledge the legitimacy of that new branch despite of its originality. The mixing of several specialities such as electronics, vacuum, cryogenics, laser optics, signal processing and General Relativity, all pushed at the limit by the extreme weakness of the effects to record, made this field overlapping a number of classical academic departments and did not facilitate its integration as a specific activity.

This has changed since the realization of large instruments around the world like LIGO (U.S.), Virgo (France+Italy), GEO600 (Germany+GB), TAMA (Japan) and progresses of the ESA/NASA space mission called LISA. These projects and their foreseable future improvements need trained young searchers.

The aim of the present course is to present the theoretical bases of the above mentionned projects, and to introduce some special fields on which the R&D is now focusing, so that the major part of the present document addresses physical issues not directly related to General Relativity. But most people of the Fundamental Physics community have already understood that General Relativistic effects will be revealed by a metrology of the extreme, which means an extreme metrology.

The course consists of 6 chapters.

Chapter 1

Theory of GW Interferometers

1.1 Shot noise limited interferometry

1.1.1 Spectral density of power equivalent to SN

Shot noise is produced by photodetectors currently used in all domains of photonics. Even with very stable lasers and cooled detectors, the photocurrent appears, at the microscopic level as a random stationnary process having a mean in agreement with a classical theory, but a variance that can be understood only by reference to quantum theory. In fact the light is produced and received as a flux of photons, and it is shown, for instance, that during a time interval Δt, the number photons that a photodiode can detect is a random variable N whose probability law is Poissonnian (a general law for all processes consisting in random arrivals). This means that the probability of detecting exactly n photons is:

$$p_n \;=\; \mathrm{e}^{-m}\,\frac{m^n}{n!}$$

where m is the only parameter of the Poisson probability distribution, and in concrete terms, represents the mean photon flux. In fact, if the mean number of photons is larger than about 50, the Poisson law is identical to a gaussian law having the same moments. It is classically shown that the expectation value of a random variable N obeying a Poisson law of parameter m is $E[N] = m$, and it variance is $V[N] = m$. On the other hand, during the time interval Δt, the energy deposited on the diode is

$$\Delta e \;=\; \eta P \Delta t \;=\; N h_P \nu$$

where P is the power of the light beam, and ν its frequency (h_P is the Planck constant). η is the *quantum efficiency* of the detector, a quantity very close to 1 in present infra-red detectors, so that we shall ignore η in all the sequel. In other words, consider P as the power actually detected. Now, it is clear that there is an equivalence between saying that N is a random variable, and saying that P is a random variable. Calling P_0 the averaged value of P, we see that

$$E[N] = \frac{P_0 \Delta t}{h_P \nu}$$

and consequently (Poisson) :

$$V[N] = \frac{P_0 \Delta t}{h_P \nu}$$

It is now possible to consider the variance of P :

$$V[P] = V[N] \frac{h_P^2 \nu^2}{\Delta t^2}$$

$$= \frac{P_0 h_P \nu}{\Delta t}$$

The quantity $1/\Delta t$ may be regarded as the ideal bandwidth of the detector, then the quantity $P_0 h\nu$ appears as a white spectral density. We shall consider in the sequel that given an incoming power P_0, the two-sided spectral density of power equivalent to shot noise is

$$S'_P(f) = P_0 h_P \nu \tag{1.1}$$

The fact that the preceding formula gives actually the two-sided SD can be shown as follows. On successive time slices of duration Δt, the detected energy (and consequently the averaged power) is a random variable of mean P_0, so that, calling x the statistical variable $P - P_0$, $x(t)$ defines a stationary centered stochastic process. We can write the function $x(t)$ as :

$$x(t) = x_k \quad \text{for} \quad k\Delta t < t < (k+1)\Delta t$$

The spectral density of any stationary centered process has the general definition :

$$S_x(\Omega) = \lim_{T \to \infty} \frac{1}{T} E \left[\left| \int_0^T \mathrm{e}^{-i\Omega t} x(t)\, dt \right|^2 \right]$$

If we choose T an integer multiple of Δt, we get easily :

$$\int_0^T \mathrm{e}^{-i\Omega t} x(t)\, dt \;=\; \sum_{k=0}^{n-1} x_k\, \mathrm{e}^{-i(k+\frac{1}{2})\Omega\Delta t}\, \Delta t\, \mathrm{sinc}(\Omega\Delta t/2)$$

so that

$$\left| \int_0^T \mathrm{e}^{-i\Omega t} x(t)\, dt \right|^2 = \sum_{k,m} x_k x_m\, \mathrm{e}^{-i(k-m)\Omega\Delta t}\, \Delta t^2\, \mathrm{sinc}(\Omega\Delta t/2)^2$$

The variables x_k are uncorrelated, so that

$$E[x_k x_m] \;=\; V[P]\, \delta_{km}$$

and

$$E\left[\left| \int_0^T \mathrm{e}^{-i\Omega t} x(t)\, dt \right|^2 \right] \;=\; \sum_k V[P] \Delta t^2\, \mathrm{sinc}(\Omega\Delta t/2)^2$$

$$=\; n\Delta t V[P] \Delta t \mathrm{sinc}(\Omega\Delta t/2)^2$$

(with the definition: $\mathrm{sinc}(x) \equiv \sin(x)/x$), and with $T = n\Delta t$, this is finally

$$S'_P(\Omega) \;=\; P_0\; h_P\nu\; \mathrm{sinc}(\Omega\Delta t/2)^2$$

One easily sees that the total variance is recovered by integrating over negative and positive frequencies (and remembering that $\int_{-\infty}^{\infty} \mathrm{sinc}(x)^2\, dx = \pi$) The single-sided spectral density is thus :

$$S_P(\Omega) \;=\; 2P_0\; h_P\nu\; \mathrm{sinc}(\Omega\Delta t/2)^2$$

The integration time Δt can be chosen very short, so that the preceding function is almost flat in the audio region, and the one sided spectral density to be used in practical problems is simply :

$$S_P(\Omega) \;=\; 2P_0\; h_P\nu$$

as for a white noise.

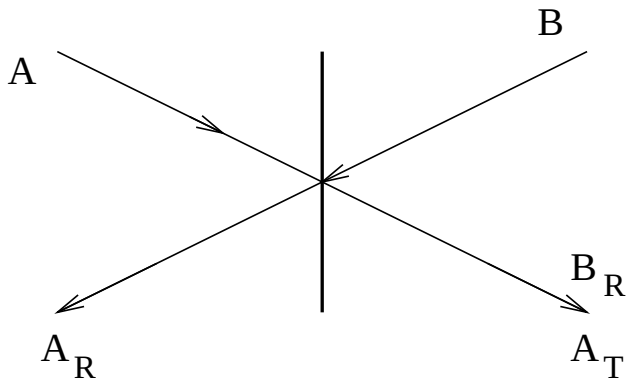

Figure 1.1: Partially reflecting mirror

1.1.2 Partially reflecting mirrors

In interferometry, a light source provides a beam that is often split into two or more waves propagating along different paths. It is mandatory to take into account the phase jumps caused by reflection or transmission at a mirror surface. We consider a mirror as a plane surface of vanishing thickness. There are two complex numbers z_R and z_T expressing respectively the relative reflected and transmitted waves. Namely, when a wave of complex amplitude A reaches the mirror's surface, we have (see Fig.1.1 for notation):

$$A_R \;=\; z_R A \;\;,\;\; A_T \;=\; z_T A$$

Conservation of the total power requires that

$$|z_R|^2 + |z_T|^2 \;=\; 1 - p$$

where p expresses possible absorption (dissipation) in the mirror. For our present purposes, it is mandatory to have a very small p (usually a few ppm, i.e. a few 10^{-6}). Requirements on the arguments of z_R and z_T come from the mirror viewed as a 4 ports element. If a second wave of amplitude B reaches the mirror coming from the opposite direction, the source of A being switched off, it undergoes exactly the same processes with the same coefficients. If now the two amplitudes are present simultaneously, we have thus:

$$A_R = z_R A + z_T B$$

$$B_R = z_T A + z_R B$$

Remark that we call A_R the sum of all waves going to the left, and B_R the sum of all waves going to the right; we could as well call B_T and A_T the same waves. If we consider the power balance, we must have

$$|A_R|^2 + |B_R|^2 = (1-p)\left(|A|^2 + |B|^2\right)$$

on the other hand, using the preceding equations, we get

$$|A_R|^2 + |B_R|^2 = \left(|z_R|^2 + |z_T|^2\right)\left(|A|^2 + |B|^2\right) + (z_R\overline{z_T} + \overline{z_R}z_T)\left(\overline{A}B + A\overline{B}\right)$$

we therefore must have for any couple (A, B) of complex numbers

$$(z_R\overline{z_T} + \overline{z_R}z_T)\left(\overline{A}B + A\overline{B}\right) \;=\; 0$$

which clearly requires

$$z_R\overline{z_T} + \overline{z_R}z_T \;=\; 0$$

or, in terms of arguments:

$$Arg(z_R) - Arg(z_T) \;=\; (2n+1)\frac{\pi}{2} \quad (n \in \mathbf{N})$$

In order to preserve the power balance at each interference occuring at the surface of a mirror, we must, in the calculation, take into account this phase jump of $\pi/2$ between the reflected and the transmitted wave. One possible choice, that will be kept throughout this document, is

$$z_R = i\,r \;,\quad z_T \;=\; t$$

where (r, t) are real numbers verifying

$$r^2 + t^2 = 1 - p$$

1.1.3 Elementary Michelson

A simple interferometer design is shown on Fig.1.2. The light coming from a laser is split into two distinct paths ended by mirrors, then reflected and recombined on the splitter where the interference occurs. We call r_s and t_s the reflection and transmission coefficients of the splitter, and k the wave number ($k \equiv 2\pi/\lambda$, λ being the wavelength. The amplitude of the laser wave is A and the outgoing is B. One has

$$B \;=\; r_s t_s\left(r_1 \mathrm{e}^{2ika} + r_2 \mathrm{e}^{2ikb}\right)$$

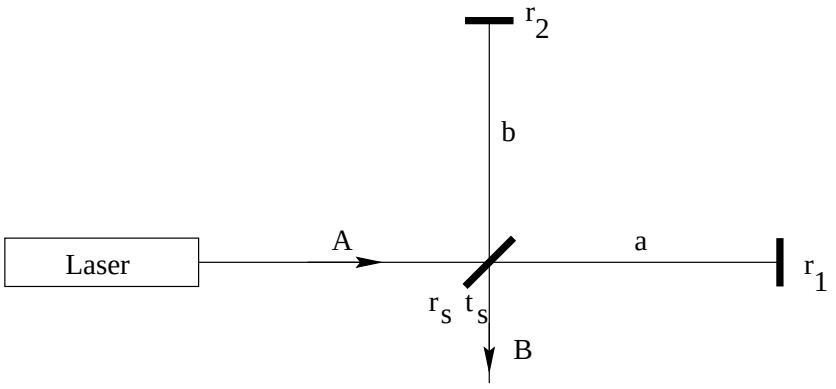

Figure 1.2: A simple Michelson experiment

so that

$$B\overline{B} \;=\; r_s^2 t_s^2 A\overline{A}\,\left(r_1^2 + r_2^2 + 2r_1 r_2\cos[2k(a-b)]\right)$$

Suppose now that the device aims to measure a very small variation of the length of one arm. For instance, the length of arm 1 is $a = a_0 + x(t)$, where $|x(t)| \ll \lambda$. We can consider for brevity that the splitter is well balanced and $r_s^2 = t_s^2 = 1/2$. The outgoing power is :

$$P(t) \;=\; P_{DC} + \Delta P(t)$$

with

$$P_{DC} \;=\; \frac{1}{4}P_0\,\left(r_1^2 + r_2^2 + 2r_1 r_2\cos\alpha\right)$$

where $\alpha = 2k(a_0 - b)$ is the static tuning of the interferometer. if $x(t) = 0$, we see that the outgoing power can be controlled by α. If $\alpha = 2n\pi$,

$$P_{DC,b} \;=\; \frac{(r_1 + r_2)^2}{4}\,P_0$$

which is almost 1 if both r_1, r_2 are reasonably near unity, we say that the interferometer is tuned at a *bright fringe*, if now $\alpha = (2n+1)\pi$,

$$P_{DC,d} \;=\; \frac{(r_1 - r_2)^2}{4}\,P_0$$

which can be made as small as wanted by equalizing r_1 and r_2. We say that the interferometer is tuned at a *dark fringe*. In practice, it is not so easy to

make $r_1 = r_2$, and this determines the *contrast* of the inteferometer. If x is not zero, there is a time varying component

$$\Delta P(t) \;=\; r_1 r_2 P_0 k x(t) \sin\alpha$$

The question is now : What is the minimum variation x that we could detect, knowing that there is a fluctuation of the power, even in the absence of signal, due to shot noise. The answer is given by computing the signal to noise ratio ρ :

$$\rho(f) \;=\; \frac{S_{\Delta P(f)}}{S_P(f)}$$

The spectral density S_P of power equivalent to shot noise is :

$$S_P(f) \;=\; \frac{1}{2} P_0 h_P \nu \left(r_1^2 + r_2^2 + 2 r_1 r_2 \cos\alpha\right)$$

The spectral density of signal is :

$$S_{\Delta P}(f) \;=\; r_1^2 r_2^2 P_0^2 \sin^2\alpha\, k^2 S_x(f)$$

where $S_x(f)$ is the SD of x viewed as a stationnary process. We have thus

$$\rho(f) \;=\; 2 r_1^2 r_2^2 \frac{P_0}{h_P \nu} f(\alpha)\, k^2 S_x(f)$$

where

$$f(\alpha) \;=\; \frac{\sin^2\alpha}{r_1^2 + r_2^2 + 2 r_1 r_2 \cos\alpha}$$

(see Fig.1.3). It is easily seen that the optimal value α_0 is such that

$$\cos\alpha_0 = -\,\frac{r_<}{r_>}$$

where $r_<$ is the smallest of r_1, r_2 ,and $r_>$ the largest. One already sees that if the two coefficients are close to 1 , the tuning of the interfometer is near a dark fringe. When optimally tuned, we have

$$f(\alpha_0) \;=\; \frac{1}{r_>^2}$$

so that the optimal SNR is

$$\rho(f) \;=\; 2 r_<^2 \frac{P_0}{h\nu}\, k^2\, S_x(f)$$

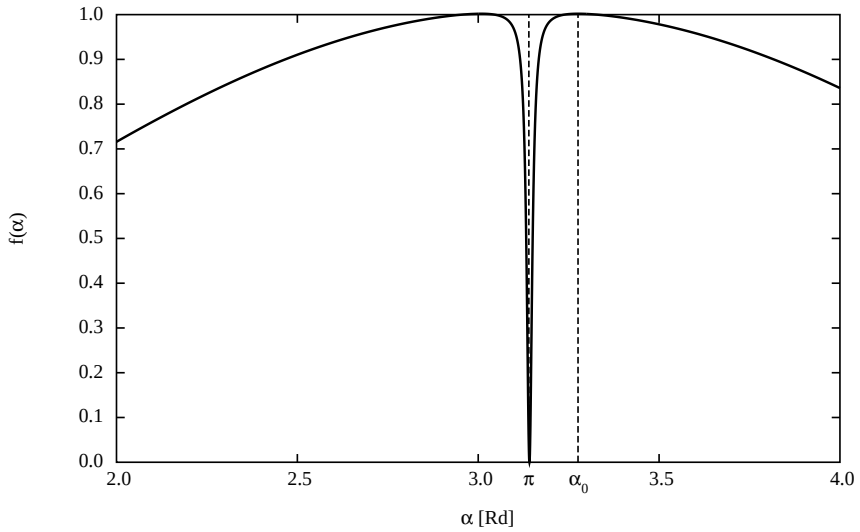

Figure 1.3: Optimization of the SNR

The minimum detectable x can be evaluated by taking $\rho = 1$, and this gives

$$S_x(f)_{\min} \;=\; \frac{1}{2r_<^2}\frac{h_P\nu}{k^2 P_0}$$

It is more physical to consider the root spectral density :

$$S_x^{1/2}(f) \;=\; \frac{\lambda}{4\pi}\sqrt{\frac{2h_P\nu}{P_0}}$$

where we have set $r_< \sim 1$. If further we assume that the small displacement $x(t)$ is caused by a gravitational wave $h(t)$, we have

$$x(t) = L\,h(t)$$

where L is the roughly equal arm lengths of the arms, and we have replaced the motion of both mirrors of $hL/2$ by a unique motion of mirror 1 by hL. The root spectral density of h equivalent to shot noise is finally:

$$S_h^{1/2}(f) \;=\; \frac{\lambda}{4\pi L}\sqrt{\frac{2h_P\nu}{P_0}}$$

With the Virgo laser ($P_0 \sim 20$ W) and the wavelength $\lambda \sim 1.064\,\mu$m of the Nd:YAG amplifier, we get

$$S_x^{1/2}(f) \;\sim\; 1.2 \times 10^{-17}\,\mathrm{m\,Hz^{-1/2}}$$

With a 3 km arm length, this gives

$$S_h^{1/2}(f) \;\sim\; 3.8 \times 10^{-21}\,\mathrm{Hz^{-1/2}}$$

In fact, according to the theoretical litterature, this means that two orders of magnitude are missing for having some hope to detect gravitational waves. We shall see that these two orders can be gained by

- enhancing the laser power, not by upsizing the laser itself, but by creating a resonance surtension on the Michelson
- increase the arm length, not by adding kilometers of tunnels, but by creating a resonance in the 3 km arms

Creation and characterics of resonances are thus a very important item we are going to analyze and discuss in details.

1.1.4 Frequency stability requirements

The shot noise is not the only limitation to laser metrology. The laser source is not in practice a purely monochromatic source. The laser frequency is determined by the optical length of the laser cavity, which means the distance between mirrors, but also the index in the amplifier medium, and the index of the medium in between mirrors and amplifier medium. All these parameters are in general coupled to external sources of mechanical or thermal noise, so that the instantaneous frequency of the laser may be viewed as a random process. We shall represent the laser optical amplitude as:

$$A_{\mathrm{laser}} = A_0\ \mathrm{e}^{-i\omega_0 t}\,\mathrm{e}^{i\Psi(t)}$$

where $\omega_0/2\pi$ is the nominal frequency of the laser, and $\Psi(t)$ a random centered process. The power reaching the photodetector is:

$$P(t) \;=\; \frac{1}{4}\left[r_1^2 + r_2^2 + 2r_1 r_2 \cos[2k(b-a) + \Psi(t-2a/c) - \Psi(t-2b/c)]\right]$$

We have thus a spurious phase:

$$\phi(t) \;=\; \frac{1}{2}\left[\Psi(t-2a/c)-\Psi(t-2b/c)\right] \;=$$

$$\frac{1}{2}\left[\Psi(t-(a+b)/c+(b-a)/c)-\Psi(t-(a+b)/c-(b-a)/c)\right]$$

$$\simeq\; \frac{b-a}{c}\frac{\partial\Psi}{\partial t}(t-(a+b)/c)$$

assuming the difference $d \equiv b-a$ small compared to the coherence length of the laser. We have thus

$$\phi(t) \;=\; \frac{d}{c}\times 2\pi\nu(t)$$

where $\nu(t)$ is the instantaneous frequency. This implies that if we want to reduce the corresponding phase noise to a level comparable to the shot noise, which is:

$$\phi_{\mathrm{sn}} \;=\; \sqrt{\frac{2h_P\nu}{P}}$$

we must obtain a spectral density of frequency noise:

$$\delta\nu(f) < \frac{c}{2\pi d}\sqrt{\frac{2h_P\nu}{P}}$$

we see the importance of having a good symmetry (a small d) between the two arms. If we take the parameters already used above, the shot noise induced phase was about $10^{-10}\mathrm{Rd/Hz^{1/2}}$, if we admit a 1% relative asymmetry, this results in a requirement of

$$\delta\nu(f) < 2.10^{-4}\mathrm{Hz/Hz^{1/2}}$$

The realistic situation is even more demanding, because firstly we want a safety margin of at least 1 order of magnitude with respect to the shot noise, secondly the shot noise will be reduced by 1 order of magnitude by recycling, and finally, the arm lengths will be seen to result from resonance effects, less easy to symmetrize than actual geometrical lengths, so that the requirement is rather in the range of $10^{-6}\mathrm{Hz/Hz^{1/2}}$.

1.2 The Fabry-Perot resonant cavity

Installing resonant cavities on the arms of an interferometer has been proposed by R. Drever [1] in order to increase the effective length of the arms. Let us discuss this idea.

1.2.1 Conventions used throughout this section

We assume a monochromatic light source, and we describe in the present section the (ideal) light beam circulating inside the interferometer as a plane wave, and moreover, we consider a given component of the electric field, so that the optical field at any place x of an optical system is of the scalar form

$$A(t,x) \;=\; A(x)\; \mathrm{e}^{-i\omega t}$$

A simple propagation step along a path of length L in a vacuum is therefore represented by a phase factor, and the relation between amplitudes will be

$$A(x+L) \;=\; \mathrm{e}^{ikL}\; A(x)$$

with $k \;=\; \omega/c \;=\; 2\pi/\lambda$, c being the velocity of light. As seen above, when a light ray encounters a mirror, it is partially reflected, transmitted and absorbed. We keep the convention explicited above: A_{in} being the incoming amplitude, A_{ref} the reflected, A_{trans} the transmitted, we have :

$$A_{ref} \;=\; ir\; A_{in} \quad , \quad A_{trans} \;=\; t\; A_{in}$$

r, t being respectively the reflection and transmission coefficients of the mirror (real numbers).. We have the power balance :

$$r^2 + t^2 \;=\; 1 - p$$

where p is the loss coefficient, accounting for absorption in the coating or scattering into a different mode due to mirror geometrical imperfections (p can be as low as a few ppm (10^{-6}) for supermirrors as Virgo's).

A Fabry-Perot cavity is made of two parallel mirrors. When light enters the cavity through mirror 1, it is partially reflected and partially transmitted. The transmitted wave is reflected by mirror 2, then returns to mirror 1 where it is recombined with the incoming wave and partially transmitted to the exterior. On Fig.1.4, we have spatially separated the left and right

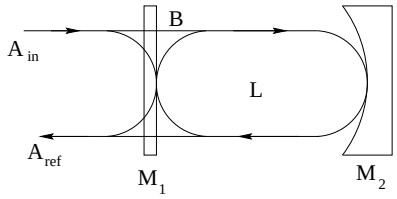

Figure 1.4: Fabry-Perot cavity

propagating waves for the sake of clarity. If the phase after a round trip in the cavity allows it, the interference of the incoming wave and the returning wave is constructive and a strong intracavity wave builds up. light can be stored. We call $r_i,\ t_i\ , p_i\ \ (i = 1, 2)$, the parameters of the mirrors, and $A_{\rm in}$ the incoming wave. The length of the cavity is L. We can write the interference at M_1 for the intracavity wave as :

$$B \ = \ t_1\, A_{\rm in} \ - \ r_1 r_2\, {\rm e}^{2ikL} B$$

so that

$$B \ = \ \frac{t_1}{1 + r_1 r_2 {\rm e}^{2ikL}}\, A_{\rm in}$$

Clearly a resonance occurs when ${\rm e}^{2ikL} \ = \ -1$. We first discuss the case when the length of the cavity is fixed, and the frequency of light variable. The inverse case will be presented later. For a given L, we have a series of resonant frequencies

$$\nu_n \ = \ \left(n + \frac{1}{2}\right)\, \frac{c}{2L}$$

The spacing between two successive resonances is called *Free spectral Range* (FSR), and noted $\Delta\nu_{FSR}$.

$$\Delta\nu_{FSR} \ = \ \frac{c}{2L}$$

For a 3 kilometers cavity (as in VIRGO), the FSR is close to 50 kHz, whereas the optical frequency (at $\lambda \ = \ 1.06\,\mu$m) is about 3×10^{14} Hz, so that the integer n is close to 6×10^9. The ratio $S \ = \ B/A_{\rm in}$ is called *surtension factor* . Its maximum value is

$$S_{\rm max} \ = \ \frac{t_1}{1 - r_1 r_2}$$

Remark that if r_2 is fixed, for instance because the end mirror is assumed "Rmax", the maximum surtension is a function of r_1, which can take any

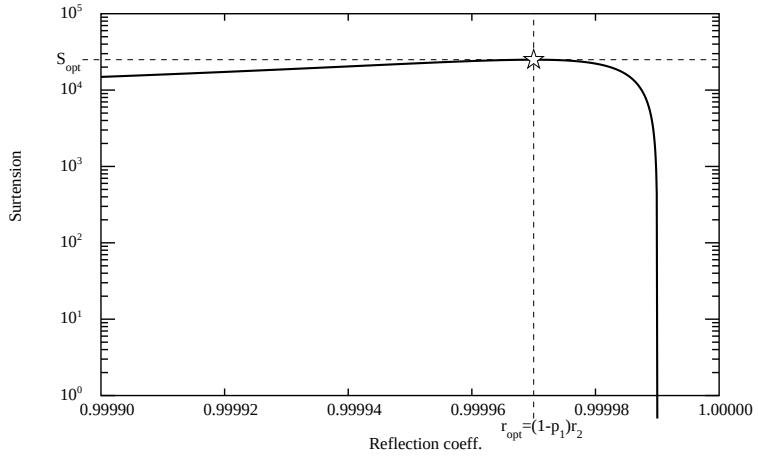

Figure 1.5: Surtension vs reflectivity of M1, assuming 20 ppm losses on each mirror, and no transmission for M2

value between 0 and $\sqrt{1-p1}$. It is easily seen that the value of r_1 for which $S_{\mathbf{max}}$ is a maximum is:

$$r_{\mathrm{opt}} \;=\; (1-p_1)\, r_2$$

and the corresponding value of $S_{\mathbf{max}}$ is

$$S_{\mathrm{opt}} \;=\; \frac{1-p_1}{1-(1-p1)(1-p2)} \;\sim\; \frac{1}{p_1+p_2}$$

(see Fig.1.5).

The width of the resonance line may be evaluated as follows. We assume that the frequency is close a resonance, so that

$$\nu \;=\; \nu_n \;+\; \delta\nu$$

with $\delta\nu \ll \Delta\nu_{FSR}$. We have

$$2kL \;=\; (2n+1)\pi \;+\; 2\pi\,\frac{\delta\nu}{\Delta\nu_{FSR}}$$

The surtension coefficient takes on the form

$$S \;=\; \frac{t_1}{1 \;-\; r_1 r_2\, \exp\left(2i\pi\frac{\delta\nu}{\Delta\nu_{FSR}}\right)}$$

Its square modulus gives the ratio between the intensities :

$$|S|^2 \;=\; \frac{t_1^2}{(1-r_1r_2)^2 \;+\; 4r_1r_2\,\sin\left(\pi\,\frac{\delta\nu}{\Delta\nu_{FSR}}\right)}$$

This is

$$|S|^2 \;=\; S^2_{\max} \;\times\; \frac{1}{1+\left[\frac{2\sqrt{r_1r_2}}{1-r_1r_2}\,\sin\left(\pi\,\frac{\delta\nu}{\Delta\nu_{FSR}}\right)\right]^2}$$

Proximity of the resonance allows to replace the sine by its argument, so that

$$|S|^2 \;=\; S^2_{\max} \;\times\; \frac{1}{1+\left[2\mathcal{F}\frac{\delta\nu}{\Delta\nu_{FSR}}\right]^2}$$

with the following definition

$$\mathcal{F} \;=\; \frac{\pi\sqrt{r_1r_2}}{1-r_1r_2} \tag{1.2}$$

for the *finesse* of the cavity. The values of $\delta\nu$ such that the surtension is half its maximum are :

$$\delta\nu \;=\; \pm\,\frac{\Delta\nu_{FSR}}{2\mathcal{F}}$$

and the *Full Width at Half Maximum* (FWHM) of the resonance is finally :

$$\delta\nu_{FWHM} \;=\; \frac{\Delta\nu_{FSR}}{\mathcal{F}}$$

One can note that we have described the cavity by an extra set of parameters $\mathcal{F}$ and $\Delta\nu_{FSR}$ equivalent to r_1r_2 and L. $\mathcal{F}$ contains only a photometric information about mirrors, whereas $\Delta\nu_{FSR}$ contains a geometrical information about the cavity. The exact expression for the resonance can be written under the form

$$|S|^2/S^2_{\max} \;=\; \frac{1}{1+\left[\frac{2\mathcal{F}}{\pi}\,\sin\left(\pi\,\frac{\delta\nu}{\Delta\nu_{FSR}}\right)\right]^2}$$

see Fig.1.6. The wave reflected off the cavity can be computed by

$$A_{\text{ref}} \;=\; ir_1A_{\text{in}} \;+\; ir_2t_1\mathrm{e}^{2ikL}B$$

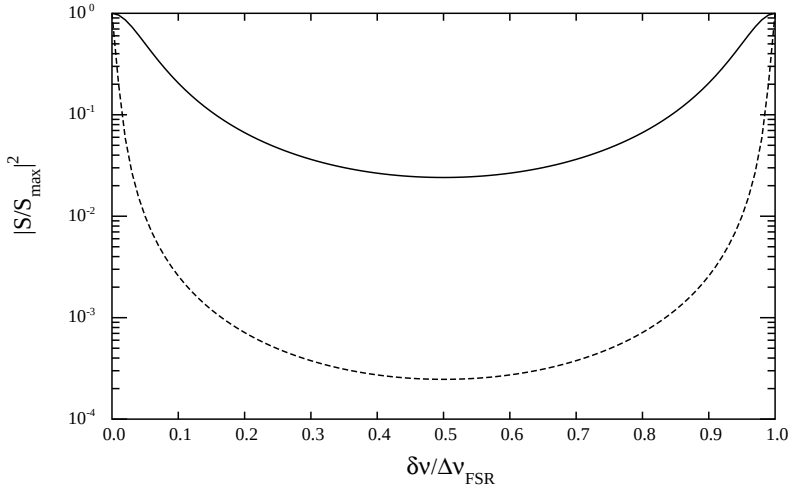

Figure 1.6: Resonance line shape for a finesse of $\mathcal{F} = 10$ (solid line), and $\mathcal{F} = 100$ (dotted line). Frequency unit is $\Delta\nu_{FSR}$

by substituting the value of B, we get

$$A_{\text{ref}} \;=\; i\,\mathcal{R}\,A_{\text{in}}$$

Where $\mathcal{R}$ is the reflectance of the cavity, defined as

$$\mathcal{R} \;=\; \frac{r_1 \;+\; (1-p_1)r_2\,\mathrm{e}^{2ikL}}{1 \;+\; r_1 r_2\,\mathrm{e}^{2ikL}} \tag{1.3}$$

For a cavity operated in the reflection mode, having a finite reflectivity of the input mirror (M_1), a high reflectivity end mirror (M_2) and reasonable losses (p_1, p_2), it can be seen that the global reflectance is about unity, with a small peak of absorption at resonance. The phase of the reflected wave undergoes a rapid transition of 2π when crossing the resonance (see Fig.1.7 and Fig.1.8). This is classical in all oscillators, and can be better understood in a simplified model. Note that $\delta\nu = \pm\,0.5 \times \delta\nu_{FWHM}$ correspond to half the maximum absorption and to a dephasing of $\pm\pi/2$ with respect to resonance. If now, the frequency of the light source is fixed and the length of the cavity variable, which is ideally the case in a GW interferometer, instead of resonant frequencies, we have resonant lengths given by

$$L_n \;=\; \left(n + \frac{1}{2}\right)\,\frac{\lambda}{2}$$

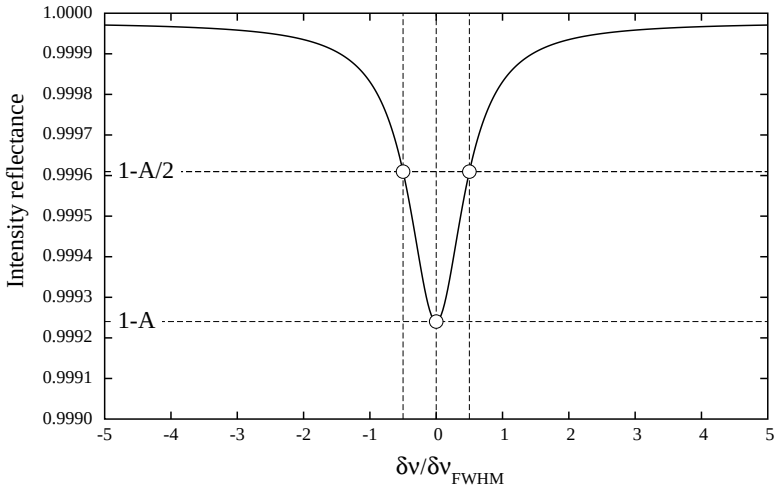

Figure 1.7: Absorption line of a cavity for r_1=0.85 and r_2=0.99998.(Finesse $\mathcal{F} \simeq 19.3$). A is the maximum of absorption.

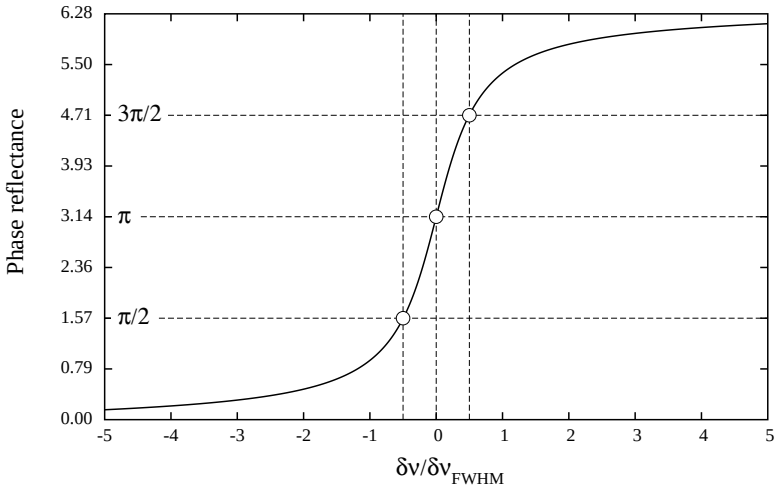

Figure 1.8: Phase reflectance of a cavity for r_1=0.85 and r_2=0.99998

showing that the displacement separating two successive resonances is :

$$\Delta L_{FSR} \;=\; \frac{\lambda}{2}$$

It is easy to show that the width of the resonance, in terms of displacement, is

$$\delta L_{FWHM} \;=\; \frac{\lambda}{2\mathcal{F}}$$

We develop now an approximate model of a cavity relying on the fact that the finesse is large compared to unity. It will prove useful for our further discussions of more complex systems involving cavities. A key parameter is indeed the finesse, defined by eq.(1.2) and depending only on the parameter $r_1 r_2$. Conversely, it is possible to compute $r_1 r_2$ from $\mathcal{F}$:

$$r_1 r_2 \;=\; 1 - \frac{\pi}{\mathcal{F}}\sqrt{1+\frac{\pi^2}{4\mathcal{F}^2}} - \frac{\pi^2}{2\mathcal{F}^2}$$

If $\mathcal{F}$ is much larger than 1, we can limit the expression at the first order in $1/\mathcal{F}$, and take

$$r_1 r_2 \;=\; 1 - \frac{\pi}{\mathcal{F}}$$

Consider now the reflectance of the cavity Eq.(1.3), and the phase factor $2kL$. We assume a frequency ν that is slightly detuned with respect ot resonance by an amount $\delta\nu$ so that :

$$2kL \;=\; 2k_0 L + 2\pi\frac{\delta\nu}{\Delta\nu_{FSR}} \;=\; \pi + \;2\pi\,\frac{1}{\mathcal{F}}\,f$$

where the *reduced frequency* f is the ratio of the offset to linewidth :

$$f \equiv \frac{\delta\nu}{\delta\nu_{FWHM}}$$

with $2k_0 L \equiv \pi \bmod[2\pi]$, we have :

$$r_2\mathcal{R} = \frac{r_1 r_2 - (1-p_1) r_2^2\, \mathrm{e}^{2i\pi f/\mathcal{F}}}{1 - r_1 r_2\, \mathrm{e}^{2i\pi f/\mathcal{F}}} \tag{1.4}$$

We set $(1-p_1)r_2^2 = (1-p)$, where p accounts for all losses in the cavity. By expanding $r_2\mathcal{R}$ at first order in $1/\mathcal{F}$ we get :

$$r_2\mathcal{R} \;=\; -\;\frac{1 - p\mathcal{F}/\pi + 2if}{1-2if}$$

The quantity $\sigma = p\mathcal{F}/\pi$ is called *coupling rate* and it is easily seen that $0 < \sigma < 2$. We have indeed obviously

$$0 < r_1^2 < 1 - p_1$$

$$\rightarrow 0 < r_1^2 r_2^2 < (1 - p_1) r_2^2 = 1 - p$$

then, assuming p very small,

$$\rightarrow 0 < r_1 r_2 < \sqrt{1 - p} = 1 - p/2$$

whence

$$0 < 1 - \frac{\pi}{\mathcal{F}} < 1 - p/2$$

$$\rightarrow 0 < \frac{p\mathcal{F}}{\pi} < 2$$

Most of the properties of the FP cavity can be known by only knowing its coupling rate. The reflectance of the cavity can thus be written (by putting $r_2 \simeq 1$ at this point) :

$$\mathcal{R} \;=\; -\frac{1 - \sigma + 2if}{1 - 2if}$$

We see that the reflectance at resonance is

$$\mathcal{R}(0) \;=\; -(1 - \sigma)$$

so that $\sigma = 1$ corresponds to total absorption of light, or *optimal coupling.* For σ running from 0 to 1 the cavity is overcoupled, this means that, at resonance, the incoming field is increasingly absorbed by the cavity until total absorption. then past 1, the field is decreasingly absorbed until total reflection. The intensity reflection coefficient is :

$$|\mathcal{R}|^2 \;=\; 1 - \frac{\sigma(2 - \sigma)}{1 + 4f^2}$$

The reflected phase is :

$$\mathrm{Arg}\,[\mathcal{R}] = \pi + \tan^{-1}\left(\frac{2f}{1 - \sigma}\right) + \tan^{-1}(2f) \tag{1.5}$$

Increasing values of σ progressively decouples the cavity from the incoming field, the reflectivity becomes near unity (because the input mirror becomes

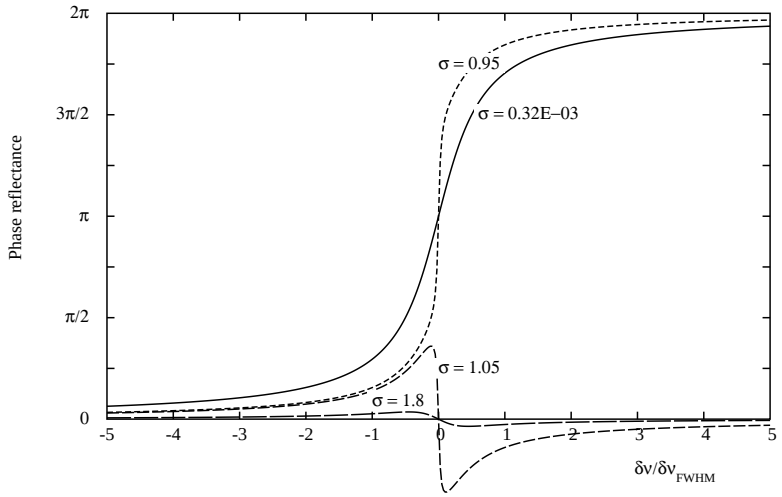

Figure 1.9: Transition from over to undercoupling. (NB : For σ=1, there is no reflected wave)

the only part of the FP visible from the exterior) , and the reflected phase becomes more and more unsensitive to frequency detuning (see Fig.1.9). Note that the coupling is strong when the coupling constant is weak, and vice-versa. We should better therefore, call σ the *undercoupling constant*, but we keep the present definition for the sake of brevity. The surtension coefficient is defined by

$$\mathcal{S} \;=\; \frac{t_1^2}{|1 + r_1 r_2 \mathrm{e}^{2ikL}|^2}$$

In the coupling rate notations, it becomes

$$\mathcal{S} \;=\; \frac{\sigma(2-\sigma)}{p(1+4f^2)}$$

showing that the maximum of intracavity power is reached at optimal coupling ($\sigma = 1$). In general, at resonance we have therefore

$$\mathcal{S}_0 \;=\; \frac{2\mathcal{F}}{\pi}\left(1 - \frac{\sigma}{2}\right)$$

and simply

$$\mathcal{S}_0 \;=\; \frac{2\mathcal{F}}{\pi}$$

in the strong overcoupling regime ($\sigma \ll 1$). The phase reflectance (see eq.1.5) is

$$\Phi(f) \;=\; \pi + \tan^{-1}\left(\frac{2f}{1-\sigma}\right) + \tan^{-1}(2f)$$

For f very small, this is at first order :

$$\Phi(f) \;=\; \frac{2(2-\sigma)}{1-\sigma}\, f \;=\; \frac{2(2-\sigma)}{1-\sigma}\, \mathcal{F}\, \frac{\delta\nu}{\Delta\nu_{FSR}}$$

In terms of the coupling rate, and absolute frequency detuning, the slope of $\Phi(\delta\nu)$ is

$$\frac{d\Phi}{d\delta\nu} \;=\; \frac{2\sigma(2-\sigma)}{1-\sigma}\, \frac{\pi}{p\,\Delta\nu_{FSR}}$$

In terms of the coupling rate and absolute displacement of the mirrors, we have the slope

$$\frac{d\Phi}{d\delta L} \;=\; \frac{2\sigma(2-\sigma)}{1-\sigma}\, \frac{2\pi}{p\,\lambda}$$

It could seem that the optimum detectivity is near the optimal coupling, where the slope is a maximum. The infinite slope at optimal coupling is very appealing, but unfortunately corresponds to total absorption, so that there is no reflected wave... This will be discussed later, in the Michelson interferometer section, when we shall study the conversion of a phase change into an amplitude change, detectable by a diode. If the coupling rate is small (i.e. the losses small and the finesse moderate), which is the current case in GW interferometers, the slope is simply :

$$\frac{d\Phi}{d\delta L} \;=\; \frac{8\mathcal{F}}{\lambda}$$

This allows to find a relation with an equivalent number n of non interfering round trips in a multipass cell of same length : in such a situation, the slope would be:

$$\frac{d\Phi}{d\delta L} \;=\; \frac{4\pi n}{\lambda}$$

so that

$$n \;\sim\; 2\mathcal{F}/\pi$$

note that this is exactly the surtension at resonance :

$$n \;=\; \mathcal{S}_0$$

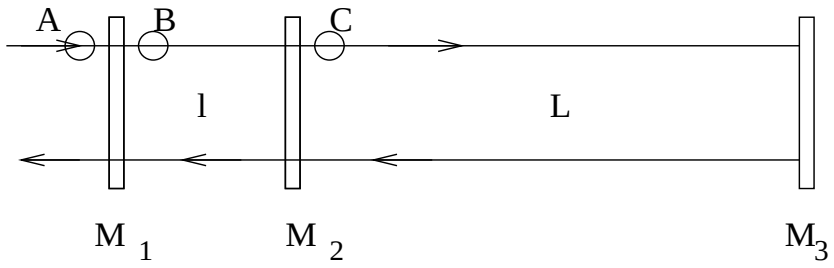

Figure 1.10: Double Fabry-Perot

In the undercoupling regime ($1 < \sigma < 2$), the phase reflectance has two extrema, for

$$f \;=\; \pm\frac{1}{2}\sqrt{\sigma - 1}$$

these two extrema being

$$\Phi \;=\; \pm\,\tan^{-1}\left(\frac{2-\sigma}{\sigma\sqrt{\sigma-1}}\right)$$

showing that the phase reflectance becomes flat as $\sigma \to 2$.

1.2.2 The double Fabry-Perot cavity

It is interesting to investigate what happens when we install a Fabry-Perot cavity inside a Fabry-Perot cavity, because it is the basis of the so-called "power recycling" setup, used in GW interferometers for enhancing the laser power, that we shall discuss in details in a foregoing section. The system we are considering is described on Fig.1.10: it consists of three mirrors, M_1, M_2, M_3, spaced by distances l and L. We assume $L \gg l$. This offers us the opportunity to calculate the transmittance of a Fabry-Perot cavity having mirrors M_1, M_2. Call $r_1,\ r_2,\ t_1,\ t_2$ the corresponding parameters, and for the sake of simplicity, let us neglect the losses, and in the same spirit, take $r_3 = 1$. We can write the stored amplitude when M_3 is removed:

$$B \;=\; A\,\frac{t_1}{1 + r_1 r_2\,\mathrm{e}^{2ikl}}$$

as already seen. Now the amplitude tranmitted through mirror M_2 in absence of mirror M_3 defines the transmittance:

$$\mathcal{T} = \frac{t_1 t_2 \mathrm{e}^{ikl}}{1 + r_1 r_2 \mathrm{e}^{2ikl}}$$

whereas the reflectance for a wave coming from the right is, according to a preceding study:

$$\mathcal{R} = \frac{r_2 + r_1 \mathrm{e}^{2ikl}}{1 + r_1 r_2 \mathrm{e}^{2ikl}}$$

For the compound cavity, we can evaluate the amplitude C just as we would do for a cavity having a virtual mirror of parameters $\mathcal{R}$, $\mathcal{T}$, and an end mirror M_3:

$$C = \frac{\mathcal{T}}{1 + \mathcal{R}\,\mathrm{e}^{2ikL}} A$$

Now the question is: How to choose the phases $2kl$ and $2kL$ in order to maximize the intracavity power $|C|^2$? It is worth to compute explicitly the result:

$$C = \frac{t_1 t_2 \,\mathrm{e}^{ikl}}{1 + r_1 r_2 \,\mathrm{e}^{2ikl} + \mathrm{e}^{2ikL}\,(r_2 + r_1 \,\mathrm{e}^{2ikl})} A$$

we see that for $2kl \equiv 0 \ [\mathrm{mod}\ 2\pi]$, and $2kL \equiv \pi \ [\mathrm{mod}\ 2\pi]$, we get

$$|C|^2 = \frac{t_1^2 t_2^2}{(1 - r_1)^2 (1 - r_2)^2} |A|^2$$

which is clearly the maximum value. It means that the short cavity must be *antiresonant*, and the long one resonant. We can write the result as a global surtension:

$$S_0 = \left[\frac{|C|^2}{|A|^2}\right]_{\mathrm{reso}} = \frac{(1 + r_1)(1 + r_2)}{(1 - r_1)(1 - r_2)}$$

We know that a cavity at antiresonance is far more reflective than any of its two simple mirrors: if we assume $r_1 = 1 - \varepsilon_1$ and $r_2 = 1 - \varepsilon_2$, with $\varepsilon_1, \varepsilon_2 \ll 1$, we have

$$\mathcal{R}_{\mathrm{antireso}} = \mathcal{R}_0 = \frac{r_1 + r_2}{1 + r_1 r_2} \sim 1 - \frac{\varepsilon_1 \varepsilon_2}{2}$$

which shows that the global transmittance is second order with respect to the individual transmittances. Moreover, we know that both the transmittance and the reflectance of an antiresonant cavity are almost independent on the

frequency over a large interval in between two successive resonances. If we assume $L \gg l$, the free spectral range Δ_L of the long cavity is much shorter than that Δ_l of the short cavity. If we therefore take a frequency excursion $\delta\nu$ small compared to Δ_L, it will be a fortiori small compared to Δ_L, and owing to the preceding remark, we can consider $\mathcal{T}$ and $\mathcal{R}$ as constants. Its is easy to check that the phase of $\mathcal{R}$ changes by a negligible amount. We have:

$$2kl \;=\; 2\pi\frac{\delta\nu}{\Delta_l}$$

so that

$$\begin{aligned}\mathcal{R} \;&=\; \frac{r_2 + r_1 + 2i\pi r_1\delta\nu/\Delta_l}{1 + r_1r_2 + 2i\pi r_1r_2\delta\nu/\Delta_l}\\ &=\; \mathcal{R}_0\;\frac{1 + 2i\pi\frac{r_1}{r1+r_2}\frac{\delta\nu}{\Delta_l}}{1 + 2i\pi\frac{r_1r_2}{1+r_1r_2}\frac{\delta\nu}{\Delta_l}}\\ =\; \mathcal{R}_0\;&\left\{1 + 2i\pi\frac{\delta\nu}{\Delta_l}\left[\frac{r_1(1-r_2^2)}{(r_1+r_2)(1+r_1r_2)}\right]\right\}\end{aligned}$$

thus, not only $\delta\nu/\Delta_l$ is much smaller than $\delta\nu/\Delta_L$, but it is multiplied by $(1-r_2)$. We can consequently definitely neglect the phase change in $\mathcal{R}$. We have

$$2kL \;\equiv\; \pi + 2\pi\frac{\delta\nu}{\Delta_L}$$

and the surtension is

$$S \;=\; \frac{|C|^2}{|A|^2} \;=\frac{|\mathcal{T}|^2}{\left|1 - \mathcal{R}\mathrm{e}^{2i\pi\delta\nu/\Delta_L}\right|^2}$$

where $\mathcal{R}$, $\mathcal{T}$ have their antiresonant values. This is:

$$\begin{aligned}S \;&=\; \frac{\mathcal{T}^2}{1 + \mathcal{R}^2 - 2\mathcal{R}\cos\left(2\pi\frac{\delta\nu}{\Delta_L}\right)}\\ &=\; S_0\;\frac{1}{1 + \frac{4\mathcal{R}\sin^2(\pi\delta\nu/\Delta_L)}{(1-\mathcal{R})^2}}\end{aligned}$$

If we replace the sine by its argument, this gives:

$$S \;=\; S_0\;\frac{1}{1 + \left(2\mathcal{F}_{\mathrm{super}}\frac{\delta\nu}{\Delta_L}\right)^2}$$

where $\mathcal{F}_{\rm super}$ is the *superfinesse*, defined by

$$\mathcal{F}_{\rm super} \equiv \frac{\pi\sqrt{\mathcal{R}}}{1-\mathcal{R}}$$

The linewidth is accordingly:

$$\delta_L = \frac{\Delta_L}{\mathcal{F}_{\rm super}}$$

For instance, assume the length of the long cavity to be $L = 3$ km. The free spectral range is thus $\Delta_L \sim 50$ kHz. If we put a simple input mirror with reflectivity $r_2^2 = 0.882$, the finesse is near 50, so that the linewidth of the cavity is near 1 kHz. Now if we add a second mirror, of same reflectivity $r_1^2 = 0.882$ and if we tune the short cavity at antiresonance, we get a reflectance of 0.998 for the short cavity, giving a superfinesse of 1595, and a linewidth of ~ 31 Hz.

1.3 Optics in a wavy spacetime

The most promising ground based GW detectors are interferometric optical systems. GW are detectable through their geometrical signature: they modulate the light distances between a pair of freely falling test masses. GW passing through our small region in the Galaxy are extremely weak, so that in a coordinate system $(t, \mathbf{x})$ linked to two freely falling masses initially at rest in this system, the metric tensor $g_{\mu\nu}$ may have the form:

$$g_{\mu\nu}(t,\mathbf{x}) = \eta_{\mu\nu} + h_{\mu\nu}(t,\mathbf{x}) \tag{1.6}$$

where $\eta_{\mu\nu} \equiv \mathrm{diag}(1,-1,-1,-1)$ is the Minkowski tensor of the locally flat background spacetime (freely falling frame), and $h_{\mu\nu}$ a very small dimensionless tensor field representing the GW amplitude. A photon travelling in a vacuum is expected to follow a null geodesic of the spacetime, which means that the invariant spacetime element is zero along its trajectory:

$$ds^2 \equiv g_{\mu\nu}dx^\mu dx^\nu = 0 \tag{1.7}$$

It is allowed to make a choice of gauge such that the tensor field $h_{\mu\nu}$ is traceless and transverse. It is also allowed to rotate the frame in such a

way that the z axis coincides with the direction of the GW source and the (x, y) axes with its polarization principal directions. Then $h_{\mu\nu}$ has only two independent components called $h'_+(t, \mathbf{x})$ and $h'_\times(t, \mathbf{x})$, so that

$$h_{\mu\nu}(t, \mathbf{x}) = \begin{pmatrix} 0 & 0 & 0 & 0 \\ 0 & h'_+(t-z) & h'_\times(t-z) & 0 \\ 0 & h'_\times(t-z) & -h_+(t-z)' & 0 \\ 0 & 0 & 0 & 0 \end{pmatrix} \tag{1.8}$$

(we use units such that the speed of light is $c = 1$). More generally, if the GW vector $\mathbf{w}$ has the angular coordinates (θ, ϕ), we may define the following unit vectors (forming a direct orthonormal frame):

$$\mathbf{w} = \begin{bmatrix} \sin\theta\cos\phi \\ \sin\theta\sin\phi \\ \cos\theta \end{bmatrix} \tag{1.9}$$

$$\vartheta = \frac{\partial \mathbf{w}}{\partial \theta}, \quad \varphi = \frac{1}{\sin\theta}\frac{\partial \mathbf{w}}{\partial \phi} \tag{1.10}$$

In the cartesian frame having $(\mathbf{w}, \vartheta, \varphi)$ as unit vectors, the unit polarization vectors $(\mathbf{a}, \mathbf{b})$ of the source are in the (ϑ, φ) plane, making with those an angle ψ (polarization angle):

$$\begin{cases} \mathbf{a} = \cos\psi\,\vartheta - \sin\psi\,\varphi \\ \mathbf{b} = \sin\psi\,\vartheta + \cos\psi\,\varphi \end{cases} \tag{1.11}$$

In the same frame, the tensor field h has the following components (latin indices take values 1,2,3):

$$h_{0i} = 0, \quad h_{ij}(t, \mathbf{x}) = h_+(t - \mathbf{w}.\mathbf{x}).(\vartheta_i\vartheta_j - \varphi_i\varphi_j) + h_\times(t - \mathbf{w}.\mathbf{x}).(\vartheta_i\varphi_j + \vartheta_j\varphi_i)$$

The new polarization components $h_+, h_\times$ are deduced from the initial ones $h'_+, h'_\times$ by the rotation:

$$\begin{cases} h_+ = \cos 2\psi\ h'_+ + \sin 2\psi\ h'_\times \\ h_\times = -\sin 2\psi\ h'_+ + \cos 2\psi\ h'_\times \end{cases} \tag{1.12}$$

showing the spin 2 geometrical status of the GW amplitude.

In our new frame fully determined by the source direction, the null spacetime element (1.7) is now:

$$ds^2 = 0 = dt^2 - dx^2 - dy^2 - dz^2 + h_{ij}dx^i dx^j \tag{1.13}$$

Assume our photon is emitted at point A of coordinates $\mathbf{x}_A$ and detected at B of coordinates $\mathbf{x}_B$. Let L be the ordinary spatial distance between A and B, and $\mathbf{n}$ the unit vector $(\mathbf{x}_B - \mathbf{x}_A)/L$. If the trip from A to B is parametrized by the scalar parameter u, we can write along the optical path:

$$\mathbf{x} \;=\; \mathbf{x}_A + u\mathbf{n} \quad (u \in [0, L])$$

(1.13) becomes:

$$0 \;=\; dt^2 - du^2 + h_{ij}n^i n^j du^2 \tag{1.14}$$

At first order in h this gives:

$$du \;=\; dt\left[1 + \frac{1}{2}H(t - \mathbf{w}.\mathbf{x})\right] \tag{1.15}$$

where

$$H \;=\; h_{ij}n^i n^j \;=\; h_+\xi_+ + h_\times\xi_\times$$

with the following definitions of the directional functions $\xi_{+,\times}$:

$$\xi_+ \;=\; (\vartheta.\mathbf{n})^2 - (\varphi.\mathbf{n})^2, \quad \xi_\times \;=\; 2\,(\vartheta.\mathbf{n})(\varphi.\mathbf{n}) \tag{1.16}$$

If we call t_r the date of emission of the photon (retarded time) and t the current date, the $\mathbf{x}$ that appears in the argument of H has its zeroth order expression:

$$\mathbf{x} \;=\; \mathbf{x}_A + (t - t_r).\mathbf{n}$$

so that by integrating (6.47) we find

$$L \;=\; t - t_r + \frac{1}{2}\int_{t_r}^{t} H(t' - \mathbf{w}.(\mathbf{x}_A + (t' - t_r)\,\mathbf{n})\,dt'$$

or as well

$$t_r \;=\; t - L + \frac{1}{2}\int_{t-L}^{t} H((1 - \mathbf{w}.\mathbf{n})t' - \mathbf{w}.\mathbf{x}_A + \mathbf{w}.\mathbf{n}\,t_r)\,dt' \tag{1.17}$$

1.3.1 Ground based antennas

For ground antennas, the upper bound of the sensitivity frequency band is about a few kHz, giving a GW wavelength larger than 50 km and about 3,000 km at the maximum of sensitivity. The physical size of these antennas is at most 4 km (LIGO). The variation of the integrand is thus small within the

integration range, and for the retarded time corresponding to a round trip along a straight path of length L, we have simply

$$t_r \;=\; t - 2L \;+ L\,H(t) \tag{1.18}$$

If the photons are emitted by a laser of wavelength λ, the result after a simple propagation is a phase modulation:

$$\Phi(t) \;=\; \frac{2\pi L}{\lambda}\,H(t) \tag{1.19}$$

If we assume the interferometer arms respectively along the x (north) and y (west) axes, we have explicitly

$$\Phi_{\rm north}(t) \;=\; \frac{2\pi L}{\lambda}\,\Big[h_+(t)(\cos^2\theta\cos^2\phi - \sin^2\phi) - h_\times(t)\cos\theta\sin 2\phi\Big] \tag{1.20}$$

$$\Phi_{\rm west}(t) \;=\; \frac{2\pi L}{\lambda}\,\Big[h_+(t)(\cos^2\theta\sin^2\phi - \cos^2\phi) + h_\times(t)\cos\theta\sin 2\phi\Big] \tag{1.21}$$

1.3.2 LISA

For the space antenna LISA, the sensitivity band has a minimum at about 10 mHz, corresponding to a wavelength of 30 Mkm. On the other hand, the interspacecraft distance is 5 Mkm, so that in a large domain of frequencies, the ratio is not negligible. We can resume integration of (6.49) as follows. Assume $H(t)$ admits a Fourier transform $\tilde H(\Omega)$. we obtain from (6.49):

$$t_r \;=\; t - L \;+$$

$$+\,\frac{1}{2}\int_{\mathbf{R}} d\Omega\,\tilde H(\Omega)\;\int_{t-L}^{t}\exp\left[-i\Omega(1-\mathbf{w}.\mathbf{n})t' + i\Omega\mathbf{w}.\mathbf{x}_A - i\Omega\mathbf{w}.\mathbf{n}\,(t-L)\right]$$

giving

$$t_r \;=\; t - L + \frac{1}{2}\int_{\mathbf{R}} d\Omega\,\tilde H(\Omega)\,{\rm e}^{-i\Omega t}\;\frac{{\rm e}^{i\Omega\mathbf{w}.\mathbf{x}_B} \;-\; {\rm e}^{i\Omega(\mathbf{w}.\mathbf{x}_A+L)}}{-i\Omega(1-\mathbf{w}.\mathbf{n})} \tag{1.22}$$

The modulated phase detected at B is $\Phi(t) = 2\pi\nu t_r$ where ν is the laser frequency. This induces a frequency modulation which is the main observable of LISA:

$$\delta\nu(t) \;=\; \frac{1}{2\pi}\,\frac{d\Phi(t)}{dt} \;=\; \frac{\nu}{2(1-\mathbf{w}.\mathbf{n})}\int_{\mathbf{R}} d\Omega\,\tilde H(\Omega)\,{\rm e}^{-i\Omega t}\;\Big[{\rm e}^{i\Omega\mathbf{w}.\mathbf{x}_B} \;-\; {\rm e}^{i\Omega(\mathbf{w}.\mathbf{x}_A+L)}\Big]$$

this is finally equivalent to a modulated Doppler shift:

$$\left[\frac{\delta\nu(t)}{\nu}\right]_{A\to B} = \frac{H(t-\mathbf{w}.\mathbf{x}_B) - H(t-\mathbf{w}.\mathbf{x}_A - L)}{2(1-\mathbf{w}.\mathbf{n})} \tag{1.23}$$

This expression is often called 2-pulses response, because a short GW pulse is thus seen twice in the phasemeter output. Remark that the time delay between the two pulses is:

$$\Delta t_{AB} = L - \mathbf{w}.[\mathbf{x}_B - \mathbf{x}_A] = L(1-\mathbf{w}.\mathbf{n})$$

Note that if the GW and the light travel in the same direction, $\mathbf{w}.\mathbf{n} = 1$ (with the same velocity), the delay is zero: the first pulse produced at A reaches B at the time at which the second pulse in B is produced. The observable (1.23) is nevertheless zero because in this case the $\xi_{+,\times}$ are zero.

In the case of purely h_+ sources (binaries in a plane perpendicular to the line of sight), we have the following pattern (see fig.1.11).

1.3.3 The Sideband Algebra

Let us now turn to wave optics. Our light ray is in fact a monochromatic plane wave of frequency $\nu = \omega/2\pi$. Call $B(t)$ the (complex) amplitude at the end of the round trip, and $A(t)$ its value at the beginning. We have

$$B(t) = A(t_r)$$

If we note

$$A(t) = A\mathrm{e}^{-i\omega t}$$

we get

$$B(t) = A\mathrm{e}^{-i\omega t_r} = A\mathrm{e}^{-i\omega(t-2L/c)} \exp\left[ih\frac{\omega L}{c}\mathrm{sinc}(\Omega L/c)\cos\left(\Omega(t-L/c)\right)\right]$$

Since we are always at first order in h, we write

$$\begin{aligned} B(t) &= A\mathrm{e}^{-i\omega t}\mathrm{e}^{2i\omega L/c} + \\ &\tfrac{i}{2}hA\ \tfrac{\omega L}{c}\mathrm{sinc}(\Omega L/c)\ \mathrm{e}^{2i\omega L/c}\mathrm{e}^{i\Omega L/c}\mathrm{e}^{-i(\omega+\Omega)t} + \\ &\tfrac{i}{2}hA\ \tfrac{\omega L}{c}\mathrm{sinc}(\Omega L/c)\ \mathrm{e}^{2i\omega L/c}\mathrm{e}^{-i\Omega L/c}\mathrm{e}^{-i(\omega-\Omega)t} \end{aligned}$$

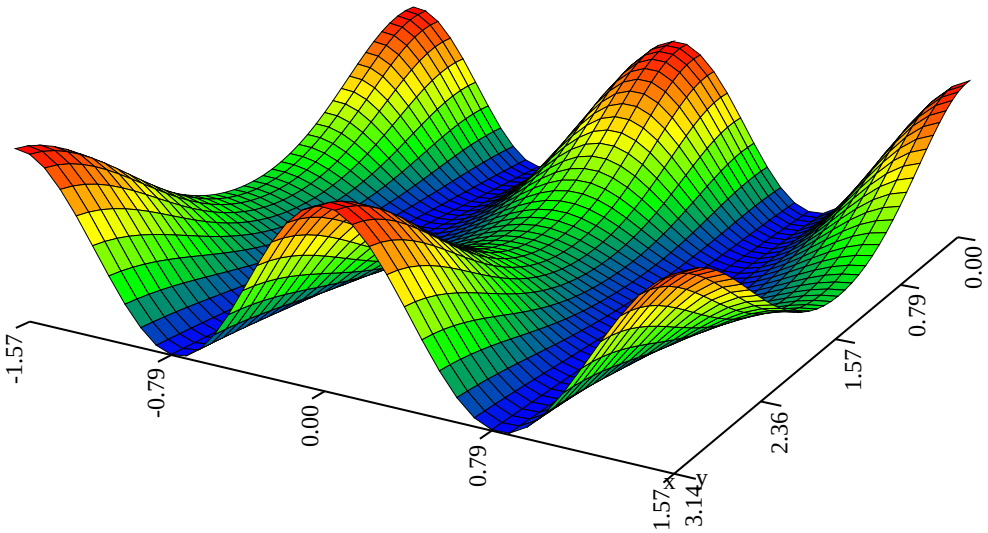

Figure 1.11: Directivity pattern for h_+ sources. Angle θ runs from 0 to π, angle ϕ from $-\pi/2$ to $\pi/2$.

It clearly appears that the action of the GW was to create two sidebands of very low amplitude, of frequencies $\nu \pm \nu_g$ from one single frequency ν. Now let us see what happens if the incoming optical wave is already modulated and exhibits two sidebands. This is necessary because in interferometers, light undergoes several times the action of the GW in order to enhance the signal production. Let the incoming amplitude be of the form

$$A(t) \;=\; \left(A_0 \;+\; \frac{1}{2}\,h\,A_1 \mathrm{e}^{-i\Omega t} \;+\; \frac{1}{2}\,h\,A_2 \mathrm{e}^{i\Omega t}\right) \mathrm{e}^{-i\omega t}$$

The scaling factor is h because we assume the GW to be the only cause of generation of sidebands in the whole (arbitrary) optical system. We have then

$$B(t) \;=\; A(t_r) \;= \left[A_0 + \frac{1}{2}hA_1\mathrm{e}^{-i\Omega t}\mathrm{e}^{2i\eta} + \frac{1}{2}hA_2\mathrm{e}^{i\Omega t}\mathrm{e}^{-2i\eta}\right] \;\times$$

$$\times\; \mathrm{e}^{-i\omega t}\mathrm{e}^{2i\xi}\mathrm{e}^{-i\epsilon h\xi \mathrm{sinc}(\eta)\cos(\Omega t - \eta)}$$

For shortening the formula, we have used the abbreviations: $\xi \equiv \omega L/c$ and $\eta \equiv \Omega L/c$. After a 1st order expansion of the exponential, we get

$$B(t) \;=\; \left(B_0 \;+\; \frac{1}{2}\,h\,B_1 \mathrm{e}^{-i\Omega t} \;+\; \frac{1}{2}\,h\,B_2 \mathrm{e}^{i\Omega t}\right) \mathrm{e}^{-i\omega t}$$

with the following notation :

$$B_0 \;=\; \mathrm{e}^{2i\xi} A_0$$

$$B_1 \;=\; \mathrm{e}^{2i(\xi+\eta)} A_1 - i\epsilon\xi \mathrm{sinc}(\eta)\mathrm{e}^{i(2\xi+\eta)} A_0$$

$$B_2 \;=\; \mathrm{e}^{2i(\xi-\eta)} A_2 - i\epsilon\xi \mathrm{sinc}(\eta)\mathrm{e}^{i(2\xi-\eta)} A_0$$

We see that if we define "generalized amplitudes" as rank 3 vectors having the carrier amplitude, the upper sideband and the lower sideband respectively as coordinates, by setting

$$\mathcal{A} \;=\; (A_0,\; A_1,\; A_2)$$

and

$$\mathcal{B} \;=\; (B_0,\; B_1,\; B_2)$$

the amplitude after a round trip that we have precedently computed may be written in the form :

$$\mathcal{B} \;=\; \mathbf{X}\mathcal{A}$$

where $\mathbf{X}$ is the linear round trip operator defined as

$$\mathbf{X} = \begin{pmatrix} e^{2i\xi} & 0 & 0 \\ -i\epsilon\xi \mathrm{sinc}(\eta) e^{i(2\xi+\eta)} & e^{2i(\xi+\eta)} & 0 \\ -i\epsilon\xi \mathrm{sinc}(\eta) e^{i(2\xi-\eta)} & 0 & e^{2i(\xi-\eta)} \end{pmatrix} \tag{1.24}$$

It is easy to check that the set of all operators having the form

$$\mathbf{O} = \begin{pmatrix} O_{00} & 0 & 0 \\ O_{10} & O_{11} & 0 \\ O_{20} & 0 & O_{22} \end{pmatrix}$$

is stable for any algebraic operation, and even may be given the structure of a non commutative field which means that it can be viewed as a set of ordinary numbers, except that the product is not commutative in general. We call it $\mathcal{S}$ for brevity. The basic algebraic operations are defined by ($a, b = 0, 1, 2, i, j = 1, 2$):

- The sum :
$$(\mathbf{A} + \mathbf{B})_{ab} = \mathbf{A}_{ab} + \mathbf{B}_{ab}$$
- The product by a complex number:
$$(z.\mathbf{A})_{ab} = z\,(\mathbf{A})_{ab}$$
- The product :
$$(\mathbf{A}\ \mathbf{B})_{ii} = A_{ii}B_{ii}$$
$$(\mathbf{A}\ \mathbf{B})_{i0} = A_{i0}B_{00} + A_{ii}B_{i0}$$
- The inverse :
$$(\mathbf{A}^{-1})_{ii} = \frac{1}{A_{ii}}$$
$$(\mathbf{A}^{-1})_{i0} = -\frac{A_{i0}}{A_{00}\ A_{ii}}$$

An $\mathcal{S}$ operator may be associated to any optical element of a complex optical system. The diagonal elements $\mathbf{O}_{ii}$ represent action of that element on the carrier and the sidebands. Often (mirrors, lenses) there is no frequency dependence because the gravitational perturbation causes a negligible frequency shift, well inside the tolerances of the mirror coatings, and in this case, the

corresponding operator is simply scalar. In fact the only non-diagonal operators are those corresponding to propagation of light in a vacuum over long distances. The result is that, after some $\mathcal{S}$ algebra, the whole optical system has an associated $\mathcal{S}$ operator describing its behaviour. This approachhas been proposed fistly by [2].

1.4 Signal to Noise Ratio

We can start with a pure monochromatic wave

$$\mathcal{A}_{\text{in}} \;=\; (A,\ 0\ ,0)$$

S being the system's $\mathcal{S}$ operator, we know that the output wave is given by :

$$\mathbf{A}_{\text{out}} \;=\; A\left[S_{00} + \frac{h}{2}S_{10}\,\mathrm{e}^{-i\Omega t} + \frac{h}{2}S_{20}\,\mathrm{e}^{i\Omega t}\right]\mathrm{e}^{-i\omega t}$$

The corresponding detectable power is, up to a normalization factor, and calling P_{in} the incoming power :

$$P(t) \;=\; \mathbf{A}_{\text{out}}\,\overline{\mathbf{A}_{\text{out}}} \;=$$

$$=\; P_{\text{in}}\left[|S_{00}|^2 + \frac{h}{2}\left(S_{10}\overline{S_{00}} + \overline{S_{20}}S_{00}\right)\mathrm{e}^{-i\Omega t} + \frac{h}{2}\left(S_{20}\overline{S_{00}} + \overline{S_{10}}S_{00}\right)\mathrm{e}^{i\Omega t}\right]$$

The signal amplitude at frequency ν_g is thus

$$S(\nu_g) \;=\; |S_{10}\overline{S_{00}} + \overline{S_{20}}S_{00}|$$

The DC component of the output is proportional to $|S_{00}|^2$, so that our main concern, the SNR is proportional to :

$$\mathrm{SNR}(\nu_g) \;\propto\; |S_{10}\,\mathrm{e}^{-i\varphi_{00}} + \overline{S_{20}}\,\mathrm{e}^{i\varphi_{00}}|$$

where φ_{ij} is the argument of S_{ij}. We have as well, with the correct normalisation :

$$\mathrm{SNR}(\nu_g) \;=\; \sqrt{\frac{P_{\text{in}}}{2h_P\nu}}\,\left||S_{10}| + |\overline{S_{20}}|\,\mathrm{e}^{i(\varphi_{10}+\varphi_{20}-2\varphi_{00})}\right|\,h(\nu_g) \qquad (1.25)$$

Inversely, the spectral density $h_{\rm SN}(\nu_g)$ equivalent to the quantum noise is obtained by taking a unitary SNR :

$$h_{\rm SN}(\nu_g) \;=\; \sqrt{\frac{2h_P\nu}{P_{\rm in}}}\,\frac{|S_{00}|}{|S_{10}\overline{S_{00}}+\overline{S_{20}}S_{00}|}$$

We see that evaluation of the SNR of any optical GW detector eventually reduces to calculation of the S_{i0} of the whole system.

1.5 Resonant cavities in a GW

The first element we need, before addressing more complex structures, is the $\mathcal{S}$ operator associated to a Fabry-Perot cavity. We take the same notations as in Fig.1.6. The intracavity (vector) amplitude $\mathcal{B}$ obeys:

$$\mathcal{B} \;=\; t_1\mathcal{A}_{\rm in} - r_1r_2\mathbf{X}\,\mathcal{B}$$

where $\mathbf{X}$ is the round trip operator just defined above (Eq.1.24). We have thus

$$\mathcal{B} \;=\; [1+r_1r_2\mathbf{X}]^{-1}\;t_1\,\mathcal{A}_{\rm in}$$

The reflected amplitude is :

$$\mathcal{A}_{\rm ref} \;=\; i\,r_1\,\mathcal{A}_{\rm in} + i\,t_1r_2\,\mathbf{X}\,\mathcal{B}$$

$$=\; i\;[r_1+(1-p_1)r_2\,\mathbf{X}]\;[1+r_1r_2\mathbf{X}]^{-1}\;\mathcal{A}_{\rm in}$$

so that the reflectance of the cavity is the operator

$$\mathbf{F} \;=\; [r_1+(1-p_1)r_2\,\mathbf{X}]\;[1+r_1r_2\mathbf{X}]^{-1} \qquad (1.26)$$

It is possible to compute the components of $\mathbf{F}$:

$$\mathbf{F} \;=\; \begin{pmatrix} F & 0 & 0 \\ G_+ & F_+ & 0 \\ G_- & 0 & F_- \end{pmatrix}$$

F is the ordinary reflectance of the FP for the carrier, $F_\pm$ the ordinary reflectance of the FP for the upper and lower sidebands respectively. For the sake of simplicity, we use again the notation :

$$\begin{aligned} \xi \;&=\; kL \\ \eta \;&=\; \Omega L/c \end{aligned}$$

(recall that $\Omega/2\pi$ is the GW frequency). We have then, after direct evaluation of $\mathbf{F}$ according to Eq.1.26 :

$$F = \frac{r_1 + (1-p_1)r_2 e^{2i\xi}}{1 + r_1 r_2 e^{2i\xi}}$$

$$F_\pm = \frac{r_1 + (1-p_1)r_2 e^{2i(\xi\pm\eta)}}{1 + r_1 r_2 e^{2i(\xi\pm\eta)}} \tag{1.27}$$

$$G_\pm = -i\epsilon \frac{t_1^2 r_2 \xi \mathrm{sinc}(\eta) e^{i(2\xi\pm\eta)}}{(1 + r_1 r_2 e^{2i\xi})(1 + r_1 r_2 e^{2i(\xi\pm\eta)})} \tag{1.28}$$

In the coupling rate (σ) formalism, this can be approximated by

$$F = -\frac{1 - \sigma + 2i\Delta f}{1 - 2i\Delta f} \tag{1.29}$$

$$F_\pm = -\frac{1 - \sigma + 2i(\Delta f \pm f_g)}{1 - 2i(\Delta f \pm f_g)} \tag{1.30}$$

$$G_\pm = i\epsilon \frac{2\mathcal{F}L}{\lambda} \frac{2 - \sigma}{(1 - 2i\Delta f)[1 - 2i(\Delta f \pm f_g)]} \tag{1.31}$$

where $\Delta f = \delta\nu/\delta\nu_{\mathrm{FWHM}}$ is the reduced detuning of the light source from resonance, and $f_g = \nu_g/\delta\nu_{\mathrm{FWHM}}$ the reduced gravitational frequency. When we vary the detuning, we see that the modulus of G_+ has a resonance for $\Delta f = 0$ (resonance of the carrier) and a second resonance when $\Delta f = -f_g$, the upper sideband becoming resonant. The modulus of G_- has also a resonance for $\Delta f = 0$ and for $\Delta f = f_g$, the lower sideband becoming resonant (see Fig.1.12). A symmetrical figure can be obtained with $|G_+|$.

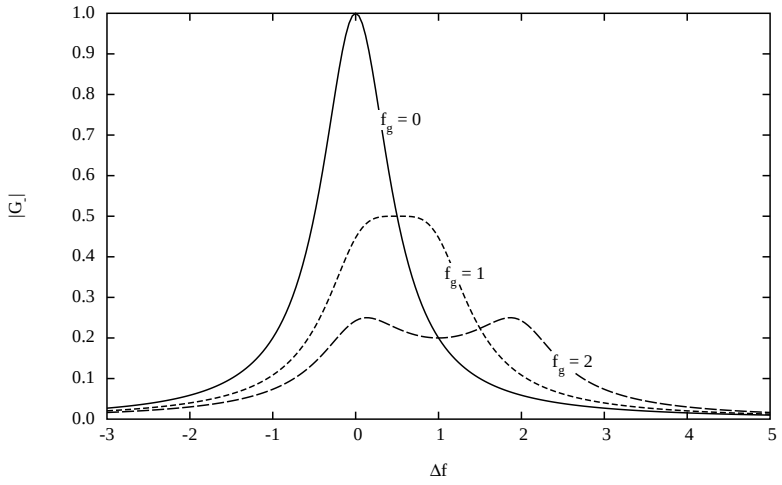

Figure 1.12: Efficiency of lower sideband generation vs detuning of the source for three reduced GW frequencies. Solid line :$f_g = 0$, short dashed line : $f_g = 1$, long dashed line : $f_g = 2$

1.6 Michelson Interferometer involving FP cavities

We take the classical Michelson geometry, but replace the end mirrors by two identical Fabry-Perot cavities, F_1 and F_2. Note that even when optically identical, the effect of a GW on them will be different, and consequently we must denote the corresponding operators by different notations (see Fig.1.13). We neglect in this first aapproach, small phases of order $2\pi\nu_g a/c$. The transmitted amplitude is

$$\mathcal{A}_{\rm trans} \;=\; -r_s t_s \left(\mathrm{e}^{2ika}\mathbf{F}_1 + \mathrm{e}^{2ikb}\mathbf{F}_2\right)\; \mathcal{A}_{\rm in}$$

whereas the reflected amplitude is

$$\mathcal{A}_{\rm ref} \;=\; i\left(t_s^2\mathrm{e}^{2ika}\mathbf{F}_1 - r_s^2\mathrm{e}^{2ikb}\mathbf{F}_2\right)\; \mathcal{A}_{\rm in}$$

Note that we neglect phases of the order of $2\pi\nu_g a/c$. The expressions of $\mathbf{F_1}$ and $\mathbf{F_2}$ for perfectly identical but orthogonal cavities lying respectively along

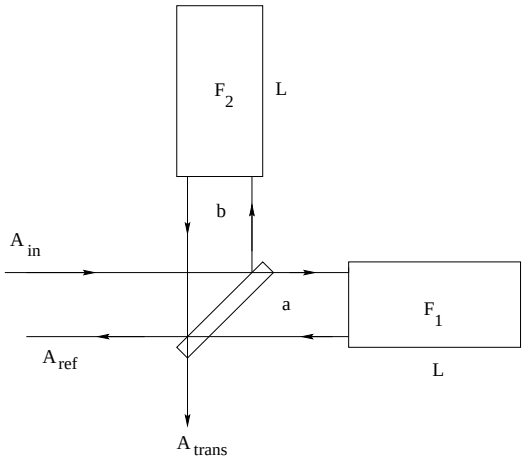

Figure 1.13: Geometry of a Michelson with FP cavities

the x and y directions, are :

$$\mathbf{F}_1 = \begin{pmatrix} F & 0 & 0 \\ G_+ & F_+ & 0 \\ G_- & 0 & F_- \end{pmatrix} \quad , \quad \mathbf{F}_2 = \begin{pmatrix} F & 0 & 0 \\ -G_+ & F_+ & 0 \\ -G_- & 0 & F_- \end{pmatrix}$$

The opposite signs of the off-diagonal elements reflect the signature of a + polarized gravitational wave having the x, y axes as polarization directions. We can define a transmittance and a reflectance $\mathcal{S}$ operator an obvious way, by

$$\begin{aligned} \mathcal{A}_{\text{trans}} &= \mathbf{T}_{\text{Mic}}\, \mathcal{A}_{\text{in}} \\ \mathcal{A}_{\text{ref}} &= i\, \mathbf{R}_{\text{Mic}}\, \mathcal{A}_{\text{in}} \end{aligned}$$

The elements of these operators are as follows, assuming a perfectly symmetrical splitter ($r_s = t_s = \sqrt{1-p_s}/2$), for the transmittance:

$$\begin{aligned} T_{\text{Mic},00} &= -(1-p_s)\mathrm{e}^{ik(a+b)} \cos[k(a-b)]\, F \\ T_{\text{Mic},11} &= -(1-p_s)\mathrm{e}^{ik(a+b)} \cos[k(a-b)]\, F_+ \\ T_{\text{Mic},22} &= -(1-p_s)\mathrm{e}^{ik(a+b)} \cos[k(a-b)]\, F_- \\ T_{\text{Mic10}} &= -i(1-p_s)\mathrm{e}^{ik(a+b)} \sin[k(a-b)]\, G_+ \\ T_{\text{Mic20}} &= -i(1-p_s)\mathrm{e}^{ik(a+b)} \sin[k(a-b)]\, G_- \end{aligned}$$

and for the reflectance :

$$\begin{aligned}
R_{\mathrm{Mic},00} &= i(1-p_s)\mathrm{e}^{ik(a+b)}\sin[k(a-b)]\,F \\
R_{\mathrm{Mic},11} &= i(1-p_s)\mathrm{e}^{ik(a+b)}\sin[k(a-b)]\,F_+ \\
R_{\mathrm{Mic},22} &= i(1-p_s)\mathrm{e}^{ik(a+b)}\sin[k(a-b)]\,F_- \\
R_{\mathrm{Mic},10} &= (1-p_s)\mathrm{e}^{ik(a+b)}\cos[k(a-b)]\,G_+ \\
R_{\mathrm{Mic},20} &= (1-p_s)\mathrm{e}^{ik(a+b)}\cos[k(a-b)]\,G_-
\end{aligned}$$

It is evident that when the interferometer is tuned at a dark fringe for the carrier, the sidebands are transmitted, and conversely. The SNR takes the form :

$$\mathrm{SNR}(\nu_g) \;\propto\; (1-p_s)\sin[k(a-b)]\left|G_+\frac{\overline{F}}{|F|}-\overline{G_-}\frac{F}{|F|}\right| \tag{1.32}$$

If we assume the carrier at a dark fringe, we get

$$\mathbf{T}_{\mathrm{Mic}} = (1-p_s)\mathrm{e}^{ik(a+b)}\begin{pmatrix} 0 & 0 & 0 \\ -iG_+ & 0 & 0 \\ -iG_- & 0 & 0 \end{pmatrix} \;,\; \mathbf{R}_{\mathrm{Mic}} = (1-p_s)\mathrm{e}^{ik(a+b)}\begin{pmatrix} iF & 0 & 0 \\ 0 & iF_+ & 0 \\ 0 & 0 & iF_- \end{pmatrix}$$

This allows to study the SNR of a simple Michelson having FP cavities as arms. We have in the coupling rate formalism, neglecting p_s at this level :

$$\mathrm{SNR}(f_g) \;\propto\; \frac{4\mathcal{F}L}{\lambda}\frac{2-\sigma}{\sqrt{1+4\Delta f^2}}\frac{1}{2}\left|\frac{\mathrm{e}^{i\Psi_+}}{\sqrt{1+4(\Delta f+f_g)^2}}+\frac{\mathrm{e}^{-i\Psi_-}}{\sqrt{1+4(\Delta f-f_g)^2}}\right|$$

where

$$\begin{aligned}
\Psi_+ &= \tan^{-1}\left(2(\Delta f+f_g)\right)-\tan^{-1}\left(\frac{2\Delta f}{1-\sigma}\right) \\
\Psi_- &= \tan^{-1}\left(2(\Delta f-f_g)\right)-\tan^{-1}\left(\frac{2\Delta f}{1-\sigma}\right)
\end{aligned}$$

After some algebra, we find the following result :

$$\mathrm{SNR}(f_g) \;\propto\; \frac{8(1-\sigma/2)\mathcal{F}L}{\lambda}\times$$

$$\left[\frac{(1-\sigma+4\Delta f)^2+4(1-\sigma)^2f_g^2}{(1+4\Delta f)^2\left((1-\sigma)^2+4\Delta f)^2\right)\left(1+8(\Delta f^2+f_g^2)+16(\Delta f^2-f_g^2)^2\right)}\right]^{1/2} \tag{1.33}$$

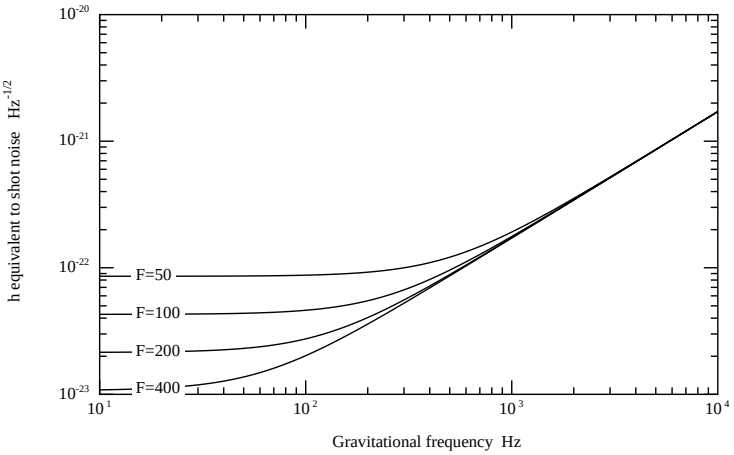

Figure 1.14: Simple Michelson with FP cavities : Spectral density of h equivalent to shot noise

if the cavities are at resonance ($\Delta f = 0$), we have simply

$$\mathrm{SNR}(f_g) \;=\; \frac{8\mathcal{F}L}{\lambda}\,\frac{1-\sigma/2}{\sqrt{1+4f_g^2}}\,\sqrt{\frac{P_L}{2h_P\nu}}\,h(f_g)$$

q we plot hereafter the spectral density of equivalent h for various values of $\mathcal{F}$ for a 20W light source at $\lambda = 1.064\,\mu$m. (see Fig.1.14). The sensitivity at low frequency is a function of $\mathcal{F}$. The optimum value of $\mathcal{F}$ occurs theoretically for $\sigma = 1$, i.e. for the optimal coupling of the cavities. This corresponds to $\mathcal{F} = \pi/p$. For $p = 3\,10^{-5}$, this corresponds to a finesse of 10^5. On the other hand, when $\sigma = 1$, the surtension coefficient is $\mathcal{S} = 1/p$, and this means here a surtension of $\simeq 3\,10^4$. For a 10 W laser source, this is is 0.3 MW stored light power. Let us keep however in mind that the improvement due to increasing the finesse occurs only at low frequency. But at low frequency, the limitation of the sensitivity is due to thermal noise, and it is worthless to try higher finesses as long as a means of reducing thermal noise has'nt been found . Better idea is to increase the laser power, because the whole curve is then globally lowered. But 20W (as assumed in Fig.1.14) is the maximum presently reasonable for a CW monomode, stabilized laser. For

gaining 1 order of magnitude, we would have to lock in phase an array of 3 such lasers. This is quite feasible, but the result can be achieved with a much more elegant and convenient solution, as explained hereafter. Let us remark that for given ν_g, the SNR is of the form

$$SNR \;=\; \frac{8\pi L}{\lambda}\,\frac{1}{p}\,\frac{\sigma(1-\sigma/2)}{\sqrt{1+q^2\sigma^2}}\,\sqrt{\frac{P_L}{2h_P\nu}}\,h(\nu_g)$$

with $q \equiv 2\pi\nu_g/p\Delta\nu_{\rm FSR}$ and consequently is a maximum for a finite value of σ. The parameter q is very high even for $\nu_g = 10\,$Hz, and a good approximation of the optimal coupling rate is :

$$\sigma_{opt} \;=\; \left(\frac{2}{q^2}\right)^{1/3} \;=\; \left(\frac{p\Delta\nu_{\rm FSR}}{\sqrt{2}\,\pi\,\nu_g}\right)^{2/3}$$

The optimal finesse is therefore :

$$\mathcal{F}_{opt}(\nu_g) \;=\; \left(\frac{\pi}{p}\right)^{1/3}\left(\frac{\Delta\nu_{\rm FSR}}{\nu_g}\right)^{2/3}$$

For instance, with $p = 3\,10^{-5}$, $\Delta\nu_{\rm FSR} = 50\,$kHz, this gives

$$\mathcal{F}_{opt}(\nu_g) \;=\; 13782 \times \left(\frac{10{\rm Hz}}{\nu_g}\right)^{2/3}$$

But the maximum is very flat, and it is not necessary to require the true optimum. A value of σ such that $q\sigma = 2$ is quite sufficient, the SNR differing from its true optimum by only 10%. this corresponds to

$$\mathcal{F}_{opt}(\nu_g) \;=\; \frac{\Delta\nu_{\rm FSR}}{\nu_g}$$

The pseudo-optimal finesse for $\nu_g = 1$ kHz is for instance $\mathcal{F} = 50$. The pseudo-optimal finesse depends of a reference frequency $\nu_g^{(0)}$ which is an equivalent parameter, the length of the cavities being fixed. In terms of this reference frequency, we have :

$$\mathrm{SNR}(\nu_g) \;=\; \frac{4\,\frac{\nu_{\rm opt}}{\nu_g^{(0)}}}{\sqrt{1+\left(2\,\frac{\nu_g}{\nu_g^{(0)}}\right)^2}}\sqrt{\frac{P_L}{2h_P\nu}}h(\nu_g)$$

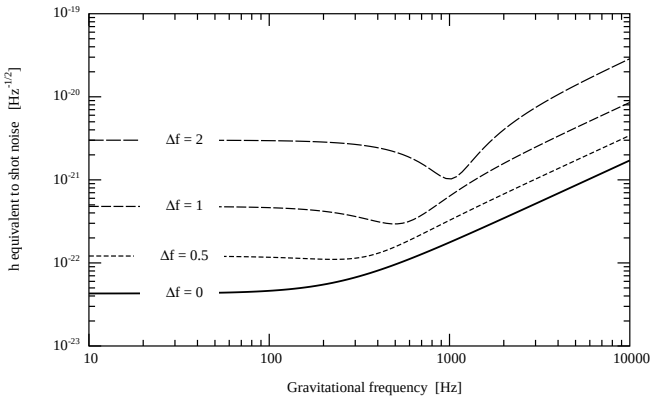

Figure 1.15: Michelson with detuned cavities (F=100)

where $\nu_{\rm opt}$ is the optical frequency. This formula is valid except for too small values of $\nu_g^{(0)}$. For the interval [10 Hz, 10kHz], it is valid. We see the huge scale factor provided by the cavities. When the two cavities have a common detuning, the SNR is reduced, as can be red directy on Eq.(1.33). But a resonance occurs when the upper sideband created by the GW becomes resonant (for $f_g = \Delta f$). At this frequency, the loss due to the frequency offset of the carrier is somewhat compensated by the resonance (see Fig1.6) One important point is that, working out of resonance, the reflectances of the cavities are much higher than in the tuned case. This regime of operation, of no benefit in the simple Michelson configuration, becomes interesting when recycling is applied, as will be shown later.

1.7 Recycling

1.7.1 standard power recycling

It is clear from conservation laws in general, and namely from the previous section that when tuned at a dark fringe, the transmittance of the Michelson being a minimum, its reflectance is a maximum. It has been proposed a long time ago by R. Drever to build a cavity with one extra mirror (the recycling mirror) and the Michelson as a second mirror (see Fig.1.16 for notation). By

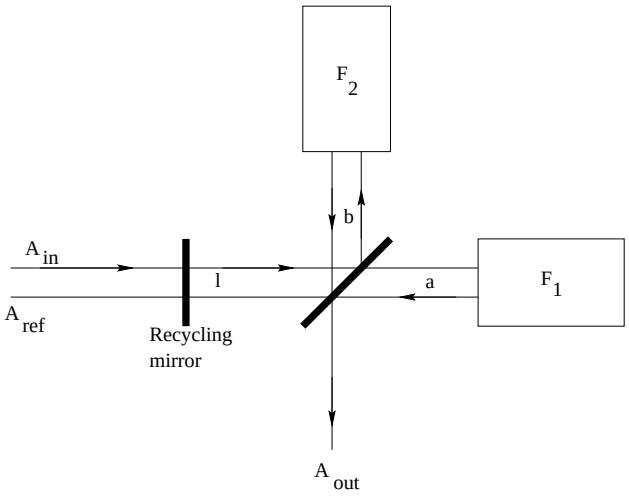

Figure 1.16: Recycled Michelson with FP cavities

controlling the resonance of this *recycling cavity* , the surtension coefficient enhances the power reaching the splitter, and the SNR is increased. The $\mathcal{S}$ operator corresponding to this configuration is easily obtained by copying the simple Fabry-Perot operators. The Michelson operators for reflection and transmission being respectively $\mathbf{R}_{\rm Mic}$ and $\mathbf{T}_{\rm Mic}$, and l the length of the recycling cavity, we have for the reflectance and transmittance of the complete interferometer :

$$\mathbf{R}_{\rm Itf} \;=\; \left[r_r + (1-p_r)\mathrm{e}^{2ikl}\mathbf{R}_{\rm Mic}\right]\,\left[1+\mathrm{e}^{2ikl}r_r\mathbf{R}_{\rm Mic}\right]^{-1} \tag{1.34}$$

$$\mathbf{T}_{\rm Itf} \;=\; \mathrm{e}^{ikl}t_r\mathbf{T}_{\rm Mic}\left[1+\mathrm{e}^{2ikl}r_r\mathbf{R}_{\rm Mic}\right]^{-1} \tag{1.35}$$

We are especially interested in the $T_{\rm Itf\ 10,20}$ components, giving the SNR. Using the preceding results about the Michelson operators, after some algebra, we obtain ($\delta \equiv k(a-b)$) :

$$T_{\rm Itf\ 10,20} \;=\; -i\,\frac{t_r(1-p_s)\mathrm{e}^{ik(l+a+b)}\,G_\pm\left[\sin\delta + i\,r_r(1-p_s)\mathrm{e}^{ik(2l+a+b)}\,F_\pm\right]}{D\,D_\pm}$$

$$T_{\rm Itf\ 00} \;=\; -\,\frac{t_r(1-p_s)\mathrm{e}^{ik(l+a+b)}\,\cos\delta\,F}{D}$$

with the following definition ($a = -1, 0, 1$) :

$$D_a \;=\; 1 + i\, r_r(1-p_s)\mathrm{e}^{ik(2l+a+b)} \sin\delta\, F_a$$

It is always possible to tune the path difference between the two arms at a dark fringe ($\delta \equiv \pi/2[\mathrm{mod}2\pi]$), and the length l of the recycling cavity in order to obtain resonance, i.e. :

$$D \;=\; 1 - r_r(1-p_s)\,|F|$$

where F refers to the (assumed common) reflectance of the cavities. At this point, the SNR is simply the SNR of a Michelson, multiplied by the surtension factor :

$$\mathrm{SNR}(f_g) \;=\; \mathrm{SNR}_{\mathrm{Mic}}(f_g) \times \frac{t_r}{1 - r_r(1-p_s)\,|F|} \tag{1.36}$$

In the so called *standard recycling* sheme, we assume the FP cavities at resonance ($\Delta f = 0$). The SNR takes on the simple form

$$\mathrm{SNR} \;=\; \frac{4\frac{\mathcal{F}L}{\lambda}(2-\sigma)}{\sqrt{1+4f_g^2}}\; \frac{t_r(1-p_s)}{1 - r_r(1-p_s)|1-\sigma|}\; \sqrt{\frac{P_L}{2h_P\nu}}\; h(\nu_g)$$

Where we see directly how increasing the coupling factor increases the Michelson SNR, but decreases the recycling factor. Anyway, we are free to choose the best recycling reflectance r_r, i.e. that maximizing the recycling surtension factor. This happens when

$$r_{r\ opt} \;=\; (1-p_r)(1-p_s)|1-\sigma|$$

giving

$$S_{r\ opt} \;=\; (1-p_s)\sqrt{\frac{1-p_r}{1-(1-p_r)(1-p_s)^2(1-\sigma)^2}}\; \frac{4\frac{\mathcal{F}L}{\lambda}(2-\sigma)}{\sqrt{1+4f_g^2}}\; \sqrt{\frac{P_L}{2h_P\nu}}\; h(\nu_g)$$

The mirror losses will be taken very small (of the order of 10 ppm), and we have seen that the coupling rate in a simple Michelson must be relatively small. It will be even smaller here, because the recycling factor would be

destroyed by a large cavity absorption. It is therefore not unrealistic to consider that the total losses are dominated by the cavity resonant absorption, and however, small ($p_r + 2p_s \ll 2\sigma \ll 1$). The optimal SNR is then

$$\mathrm{SNR}(\nu_g) \;=\; \frac{4\pi L}{\sqrt{2}\lambda}\,\frac{1}{p}\;\frac{\sigma^{1/2}(2-\sigma)}{\sqrt{1+\left(2\pi\frac{\nu_g}{p\,\Delta\nu_{\mathrm{FSR}}}\,\sigma\right)^2}}\,\sqrt{\frac{P_L}{2h_P\nu}}\,h(\nu_g)$$

When searching for the optimal value of σ, we get the following equation, with $q = 2\pi\nu_g/p\Delta\nu_{\mathrm{FSR}}$:

$$\frac{1}{2}q^2\sigma^3 + q^2\sigma^2 + \frac{3}{2}\sigma^2 - 1 \;=\; 0$$

for avoiding an exact but useless and cumbersome resolution of this equation, we rather solve it in q:

$$q^2 \;=\; \frac{1-3\sigma^2/2}{\sigma^2(1+\sigma/2)}$$

Now we remark that, even for low GW frequencies (10 Hz), q^2 is very large: Consequently, σ must be very small, and we can take the approximation

$$\sigma_{opt} \;=\; \frac{1}{q}$$

or, in terms of finesse,

$$\mathcal{F}_{opt} \;=\; \frac{\Delta\nu_{\mathrm{FSR}}}{2\nu_g^{(0)}}$$

Where $\nu_g^{(0)}$ is the GW frequency for which the SNR is optimized. But here, the maximum is sharp (see Fig.1.17). Remark that this value is half the pseudo-optimum for the simple Michelson. This sharp maximum makes the SNR very sensitive to the GW frequency at which the SNR is optimized. With physically significant parameters (frequencies in the detection range [10 Hz,10 kHz], and small losses), the SNR can be approximated by a simple formula. Call p_{ITF} the losses encountered in the recycling mirror and the splitter, i.e. the losses external to FP's : we have

$$1 - p_{\mathrm{ITF}} \;=\; (1-p_r)(1-p_s)^2 \;\Rightarrow p_{\mathrm{ITF}} \;\simeq\; p_r + 2p_s$$

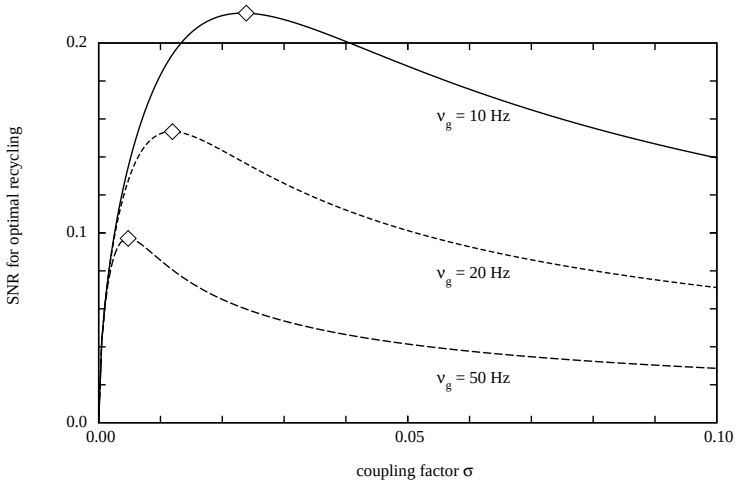

Figure 1.17: SNR vs σ for three GW frequencies. The small diamonds show the approximate optima theoretically derived

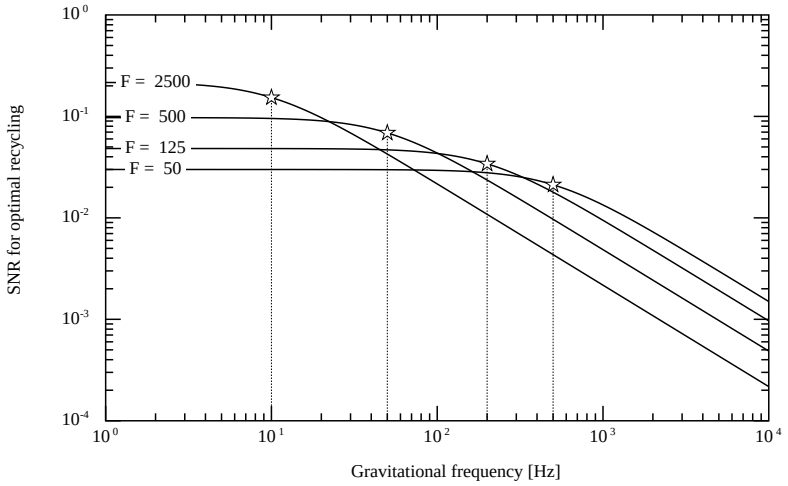

Figure 1.18: SNR vs frequency for four finesses. The small stars point the GW frequency at which the SNR was optimized.

The losses internal to FP's are still $p = 1-(1-p_1)r_2^2$. Neglecting non essential small terms leads to :

$$\mathrm{SNR}(\nu_g) \;=\; \frac{1}{\sqrt{p_{\mathrm{ITF}} + \frac{p\Delta\nu_{\mathrm{FSR}}}{\pi\nu_g^{(0)}}}} \frac{2\frac{\nu_{\mathrm{opt}}}{\nu_g^{(0)}}}{\sqrt{1+\left(\frac{\nu_g}{\nu_g^{(0)}}\right)^2}} \sqrt{\frac{P_L}{2h_P\nu}}\, h(\nu_g) \qquad (1.37)$$

the parameter $p\Delta\nu_{\mathrm{FSR}}/2\pi$ has the dimension of a frequency, and is of order 1 Hz. The first term represents the gain due to optimal recycling, the second is the SNR of a simple Michelson. We can conclude that a power recycled Michelson, having an optimal recycling rate, and an optimal finesse for a given GW frequency is not significantly better that a simple Michelson when that frequency is very low. In this subsection and in the next one, we see how the reflectivity of the Fabry-Perot cavities play a central role. The efficiency of recycling crucially depends on the quality of the reflectivity. This is the reason why at low frequency, a high finesse being needed, the coupling rate increases, the reflectivity decreases, and the effect of recycling becomes negligible. This strong requirement of very reflecting cavities was the cause of a number of numerical optics studies that in turn, motivated section 3.

The amplitude in the recycling cavity has a peak at the recycling resonance. It is interesting to evaluate the width of the resonance line when the frequency of the source varies. The surtension factor reads :

$$S_r \;=\; \left|\frac{t_r}{1+ir_r(1-p_s)\,\mathrm{e}^{ik(2l+a+b)}\sin\delta F}\right|^2$$

in this expression, the dominating phase is obviously given by the reflectance F. Since the phase reflected by cavities has already a sharp slope, we can expect this slope to be reinforced by the recycling finesse. We can take for the modulus of the reflectance its value $|F| = 1-\sigma$ at resonance, assume $\delta = \pi/2$ and $\pi/2 + k(2l+a+b) \equiv \pi$. The only frequency dependent quantity (in this approximation) is the phase Φ of the reflectance, given by

$$\Phi \;\sim\; 2\tan^{-1}(2\Delta f)$$

where we have assumed a small σ. If the frequency excursion is small compared to the cavity linewidth, then Δf is small, so that we can write :

$$S_r \;=\; S_r^{(0)} \left|\frac{1}{1+(4\mathcal{F}_R\Delta f/\pi)^2}\right|^2$$

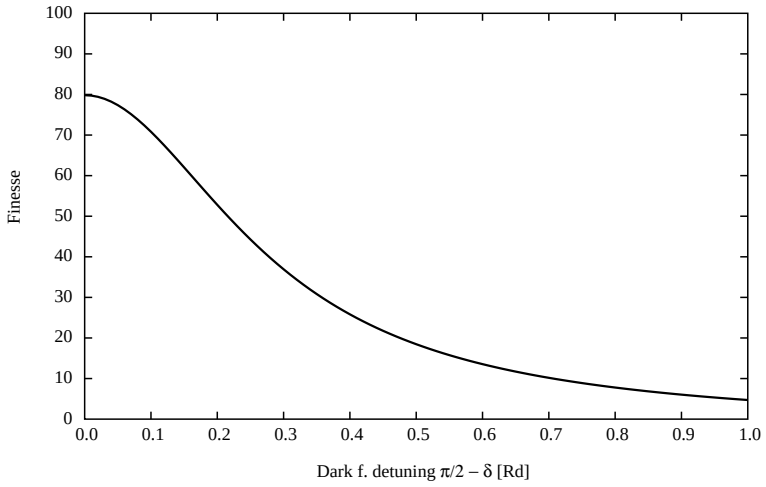

Figure 1.19: Variable finesse by detuning the dark fringe

where $S_r^{(0)}$ is the peak height for a given detuning of the dark fringe δ, Δf the reduced frequency excursion, and

$$\mathcal{F}_R \;=\; \frac{\pi\sqrt{r_r(1-p_s)(1-\sigma)\sin\delta}}{1-r_r(1-p_s)(1-\sigma)\sin\delta}$$

the recycling finesse. This finesse depends obviously of the tuning of the Michelson. Detuning reduces the reflectance of the Michelson, as can be seen on Fig.1.19.

The full width at half maximum of the surtension peak can be therefore estimated by

$$\delta\nu_{\rm rec} \;=\; \frac{\pi}{2\mathcal{F}_R}\,\delta\nu_{\rm FWHM}$$

(recall that $\delta\nu_{\rm FWHM}$ i the linewidth of the cavity). For standard values, say $p_s = 2\ 10^{-5}$, $S_r^{(0)} = 50$, (hence $r_r = 0.962$, $\sigma = 6.366\ 10^{-4}$, (corresponding to a cavity finesse of 50), we find $\mathcal{F}_R \sim 78$. For a 3 km long, 50 finesse cavity, the linewidth is 1 kHz, so that

$$\delta\nu_{\rm rec} \;\sim\; 20{\rm Hz}$$

very near the exact value, numerically obtained, of 19.64 Hz (on Fig. 1.20, we show the exact line shape for such parameters). It is also clear that

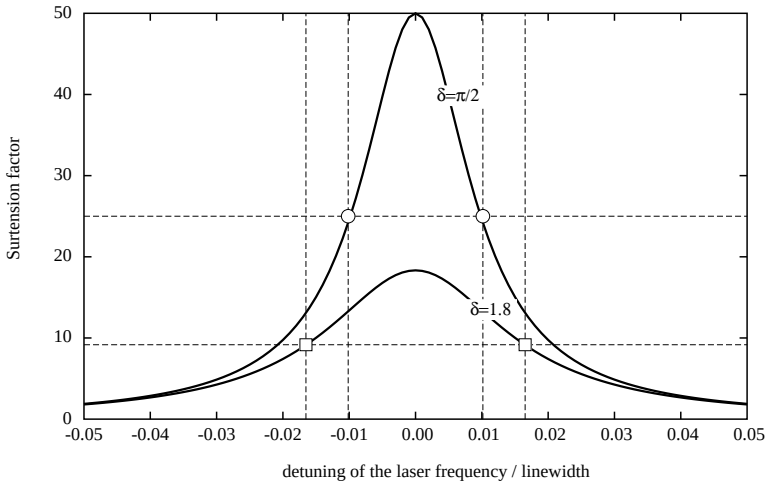

Figure 1.20: Linewidth of the recycling cavity / linewidth of the long cavities. A detuning wrt darkfringe increases the recycling width

a detuning with respect to the dark fringe ($\delta \neq \pi/2$) not only decreases the maximum recycling gain, but also increases the recycling linewidth. On Fig.1.21 the full width at half maximum of the recycling width is plotted. This helps tuning the interferometer.

1.7.2 detuned power recycling

We consider the case of a power recycled Michelson with detuned cavities. The basic idea is to exploit at the same time the resonance (frequency ν_0) of a cavity for one sideband (such that $\nu_L \pm \nu_g = \nu_0$) and the fact that the carrier being out of resonance, the reflectivity of the cavities is enhanced, and consequently the recycling efficiency also. We restrict our attention to two special cases giving the same result for the SNR : The *symmetrical* detuning, in which the two cavities have the same detuning Δf, and the *antisymmetrical* detuning, in which one cavity is detuned by Δf, and the other one by $-\Delta f$. In the first case, the upper sideband is resonant in the two arms, and never the lower sideband, in the second case, the upper sideband is resonant in the first arm, and the lower sideband in the second arm, so that finally, the effect is identical. We develop the symmetrical case. Owing

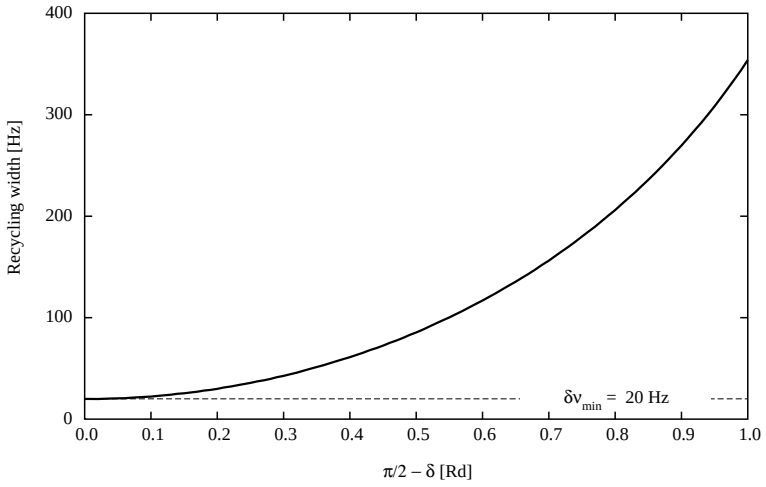

Figure 1.21: Linewidth of the recycling cavity vs dark fringe detuning $\delta \equiv 2\pi(a-b)/\lambda$

to the general Eq.1.33, the SNR for a detuned, power recycled Michelson is :

$$\mathrm{SNR}(f_g) \;=\; \frac{8\mathcal{F}L(1-\sigma/2)}{\lambda}\,\frac{t_r}{1-r_r(1-p_s)\rho}\,\sqrt{S}\,\sqrt{\frac{P_L}{2h_P\nu}}\,h(\nu_g)$$

where $\rho(\Delta f)$ is the FP's modulus reflectance, and

$$S \;=\; \frac{(1-\sigma+4\Delta f^2)^2+4(1-\sigma)^2 f_g^2}{(1+4\Delta f^2)((1-\sigma)^2+4\Delta f^2)(1+8(\Delta f^2+f_g^2)+16(\Delta f^2+f_g^2)^2)}$$

recall that

$$\rho(\Delta f) \;=\; \sqrt{1-\frac{\sigma(2-\sigma)}{1+4\Delta f^2}}$$

The optimal recycling is obtained when

$$r_r \;=\; (1-p_r)(1-p_s)^2\rho^2$$

The efficiency of recycling essentially depends on the reflectivity of the cavities. When the detuning is not zero, it simultaneously happens, for $f_g = \Delta f$ that one of the sidebands is resonant, and the reflectivity of the cavities,

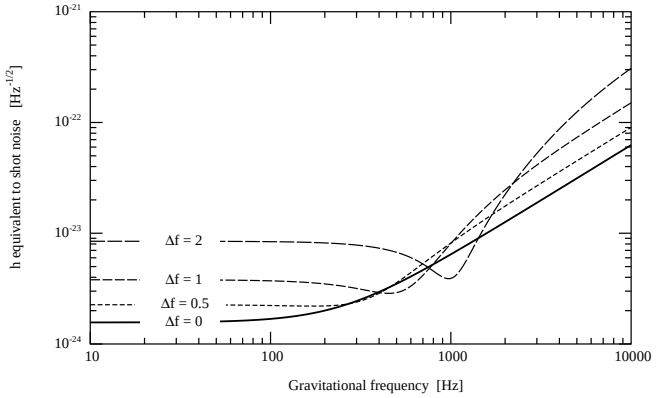

Figure 1.22: Detuned recycled Michelson (F=100)

higher than when the carrier is resonant. This is the reason why it is possible to have a better SNR for f_g in the neighborhood of Δf. (see Fig.1.22).

The maximum SNR is

$$\mathrm{SNR_{max}} = \frac{8\mathcal{F}L(1-\sigma/2)}{\lambda}\frac{1}{\sqrt{1-(1-p_r)(1-p_s)\rho^2}}\times$$

$$\times\sqrt{\frac{(1-\sigma)^2+4(1-\sigma)(3-\sigma)\Delta f^2+16\Delta f^4}{(1+4\Delta f^2)((1-\sigma)^2+4\Delta f^2)(1+16\Delta f^2)}}\sqrt{\frac{P_L}{2h_P\nu}}\,h(\nu_g)$$

1.7.3 Synchronous Recycling

The title of the present section could have been "how to make a narrow band optical detector by 6 orders of magnitude better than bar detectors". The basic idea of synchronous recycling is to have two identical cavities, and a coupling. In such a system a system of *supermodes* exists, corresponding to combinations of the individual eigenmodes of one cavity. For instance, to a given $\mathrm{TEM_{00}}$ mode of frequency ν_0, corresponds two supermodes, a symmetrical (S) and an antisymmetrical (A). The eigenfrequencies ν_S, ν_A differ from ν_0 by an amount depending of the coupling. When the coupling tends to zero, the frequencies ν_S, ν_A tend to the same limit ν_0, and to degeneracy. If the coupling is very weak, the difference $\nu_S - \nu_A$ may fall in

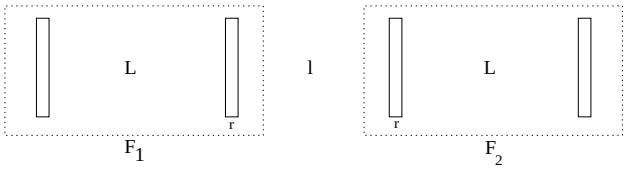

Figure 1.23: System of coupled cavities

the audio range, and a gravitational perturbation is able to pump energy from one mode in the other. The principle of operation is thus to tune the coupling at a minimum, the light source on the A mode, and waiting the signal on the S frequency (or vice-versa). Another way of understanding what happens in coupled cavities is to consider the beat note between these A and S modes. The result is that the stored energy is periodically exchanged between the two cavities, at a frequency which is the gap $\nu_S - \nu_A$ (Think to coupled pendulums). We feel that if the GW frequency is exactly this beat note, the light will accumulate positive phase shifts during the first half GW period, then will be transferred to the second cavity at the moment when the phase becomes negative in the first, and positive in the second, so that, roughly speaking, it sees always a long arm, (or a short one) and we can expect the phase modulation to increase indefinitely. It has been first proposed by Ph. Bernard and E. Picasso [4] to use this effect in high Q superconducting microwave cavities.

It is worth studying the effect on a simplified model involving only two coupled optical cavities (see Fig.1.23). The two cavities (of length L) are facing each other. The light can be transmitted through the central region of length l. In fact, this region is itself a cavity and we call it the central cavity. Without changing the two FP's, it is possible to tune the central cavity by changing the distance l. When the central cavity is at resonance, its tranmittance is a maximum, and the coupling is strong. When the central cavity is at antiresonance, its transmittance is a minimum, and the coupling is weak. We assume in the following simple model no losses, a reflectivity of 1 for the two end mirrors, and of r for the two inner mirrors. Let us consider the resonance condition for a wave to remain stored in the system. If we call F the reflectances of the (identical) cavities, we have for a round trip in the central cavity :

$$(iF\,\mathrm{e}^{ikl})^2 = 1$$

Two series of solutions can be obtained by taking

$$iF\,\mathrm{e}^{ikl} = 1 \quad \text{symmetrical mode}$$

$$iF\,\mathrm{e}^{ikl} = -1 \quad \text{antisymmetrical mode}$$

in case of zero losses, the reflectance of one cavity is of modulus 1 :

$$F \;=\; \frac{r + \mathrm{e}^{2ikL}}{1 + r\,\mathrm{e}^{2ikL}} \;=\; \mathrm{e}^{2ikL}\,\frac{1 + r\,\mathrm{e}^{-2ikL}}{1 + r\,\mathrm{e}^{2ikL}}$$

If we take the resonance as a reference frequency, we can write

$$2kL \;=\; \frac{4\pi\nu_0 L}{c} + \frac{4\pi L\delta\nu}{c}$$

where ν_0 is the resonance frequency of the (isolated) cavity, and $\delta\nu$ the unknown detuning giving a resonance in the coupled system. We have thus $4\pi\nu_0/\lambda \equiv \pi\,[\mathrm{mod}2\pi]$, and we can work with the reduced detuning already used above, $\Delta f = \delta\nu/\delta\nu_{\mathrm{FWHM}}$ which is simply the ratio of the detuning to the linewidth of the cavity. The round trip phase becomes simply

$$2kL = \pi + \frac{2\pi}{\mathcal{F}}\,\Delta f$$

so that the reflectance reduces to the pure phase factor

$$\mathrm{Arg}(F) = \pi + \frac{2\pi}{\mathcal{F}}\,\Delta f + 2\,\tan^{-1}\left[\frac{r\,\cos(2\pi\Delta f/\mathcal{F})}{1 - r\,\sin(2\pi\Delta f/\mathcal{F})}\right]$$

For the phase factor corresponding to the central cavity, we have

$$kl = \frac{2\pi\nu_0 l}{c} + \frac{\pi l}{\mathcal{F}\,L}\,\Delta f$$

The constant phase $\varphi = 2\pi\nu_0 l/c$ can be considered as the tuning of the central cavity. The resonance conditions become

$$2\,\tan^{-1}\left[\frac{r\,\cos(2\pi\Delta f/\mathcal{F})}{1 - r\,\sin(2\pi\Delta f/\mathcal{F})}\right] \;=\; (2n+1)\pi - \frac{\pi}{2} - \varphi - \frac{2\pi}{\mathcal{F}}\Delta f - \frac{\pi l}{\mathcal{F}\,L}\,\Delta f$$

leading to the S-modes equation :

$$\frac{r\,\cos(2\pi\Delta f/\mathcal{F})}{1 - r\,\sin(2\pi\Delta f/\mathcal{F})} \;=\; \tan\left[\frac{\varphi}{2} + \frac{\pi}{4} + \left(1 + \frac{l}{2L}\right)\Delta f\right]^{-1} \qquad (1.38)$$

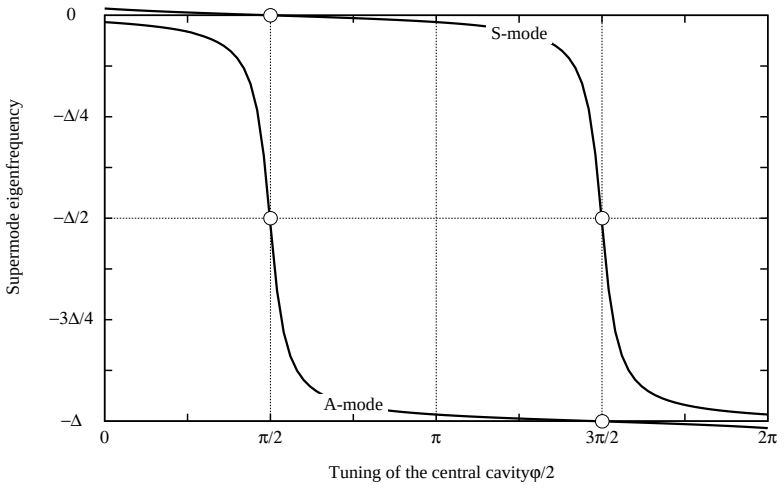

Figure 1.24: Relative detuning of the A and S supermodes vs tuning of the central cavity

The A-modes equation can be obtained a similar way :

$$\frac{r\,\cos(2\pi\Delta f/\mathcal{F})}{1-r\,\sin(2\pi\Delta f/\mathcal{F})} \;=\; -\tan\left[\frac{\varphi}{2}+\frac{\pi}{4}+\left(1+\frac{l}{2L}\right)\Delta f\right] \qquad (1.39)$$

These are implicit equations in the unknown detuning Δf. The numerical solutions are plotted on Fig.1.24. The round trip phase in the central cavity is equal to 2φ. The value $\varphi = 0$ corresponds thus to *antiresonance*, then to a minimum of coupling, and a weak splitting of the resonance lines. The tuning has period π, so that we retrieve a similar situation at $\varphi = \pi$ where the S-frequency is near the preceding A-frequency. The value $\varphi = \pi/2$ corresponds to *resonance* of the central cavity, thus to a maximum of coupling, and a maximum of line splitting This maximum is half the FSR (the interval between the two white spots on the figure). In order to study the minimum of coupling, and the frequency gap between the A and S modes at this tuning, we turn to our simplified model, which will be of some use anyway in the sequel. For zero losses, the parameter σ is zero, and we have for the phases :

$$\frac{\pi}{2}+2\,\tan^{-1}(2\Delta f)+\frac{2\pi l}{c}\,(\nu_0+\delta\nu) \;\equiv\; 0 \quad (\mathrm{S}-\mathrm{modes})$$

$$\frac{\pi}{2} + 2\,\tan^{-1}(2\Delta f) + \frac{2\pi l}{c}\,(\nu_0 + \delta\nu) \;\equiv\; \pi \quad (\mathrm{A-modes})$$

We can write as well

$$\Delta f_S \;=\; \frac{1}{2}\tan\left[\frac{\varphi}{2} + \frac{\pi}{4} + \frac{\pi l}{2\mathcal{F}L}\Delta f_S\right]^{-1}$$

The term $\pi l/2\mathcal{F}L$ is very small for kilometric cavities of finesse $\simeq 100$ and a metric central cavity. If we neglect it, we have the very simple results :

$$\Delta f_S \;=\; \frac{1}{2}\tan\left[\frac{\varphi}{2} + \frac{\pi}{4}\right]^{-1}$$

$$\Delta f_A \;=\; -\frac{1}{2}\tan\left[\frac{\varphi}{2} + \frac{\pi}{4}\right]$$

The following plot (Fig.1.25) is to be compared with the preceding. The approximation used is valid only for detunings much smaller than the FSR. For $\varphi = \pi/2$, we have seen that the detuning of the A-mode is half the FSR, the model consequently fails, this is the reason of the divergence of the A-mode at this point. The same reason causes the divergence of the S-mode at $-\pi/2$. If we restrict our attention to the neighbourhood of $\varphi = 0$, i.e. the validity range of the present model, we can see a good agreement with the exact calculation. It is in particular easy to compute the minimum line splitting :

$$[\Delta f_S - \Delta f_A]_{\min} \;=\; \frac{1}{2}\left[\frac{1}{\tan(\pi/4)} + \tan(\pi/4)\right] \;=\; 1$$

corresponding, in terms of frequency, to

$$[\delta\nu_S - \delta\nu_A]_{\min} \;=\; \delta\nu_{\mathrm{FWHM}} \;=\; \frac{c}{2\mathcal{F}L}$$

In other words, the minimum splitting is nothing but the linewidth of the cavity. If we intend to use this device to detect GW by coupling the A and S modes with the gravitational perturbation, we see that we have to use high finesse and long cavities. For the current situation (L=3 km and $\mathcal{F}$=100), the frequency gap is ν_g=500 Hz. Higher values can be obtained by a different tuning of the central cavity : The general result is

$$\nu_g \;=\; \delta\nu_S - \delta\nu_A \;=\; \frac{1}{\cos\varphi}\,\frac{c}{2\mathcal{F}L}$$

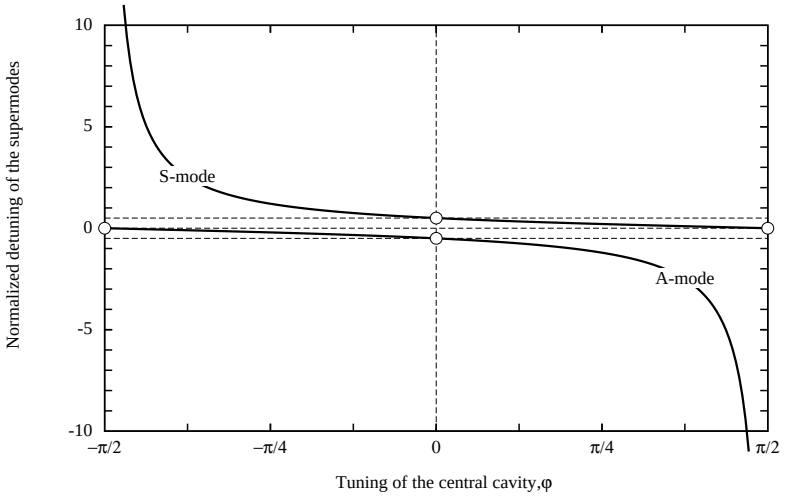

Figure 1.25: Approximate model of degeneracy removing by coupling

We have now to study the response of a real system involving a light source and a detector. The scheme of Fig.1.26 was suggested years ago by R. Drever [1] after a very different approach than Ph. Bernard & E. Picasso. The coupled cavities are in what we call *ring cavity* on the figure. The optical path has been split for clarity, and it could seem strange to separate between the incident and the reflected wave off a cavity. It is however possible by using polarization rotators and polarization sensitive reflectors, so that the situation is almost that of the figure. If (as likely) these switching elements induce losses, these losses can be localized in the mirror r_t. The splitter and the square path allow to launch two rotating waves in the ring cavity, one clockwise and one counterclockwise, these waves are recombined on the splitter. We first consider the counterclockwise wave (see Fig.1.27) and evaluate the $\mathcal{S}$ reflection operator. We have firstly for the intracavity wave :

$$B \;=\; t_r A_{in} + r_r r_t \mathrm{e}^{2ikl} \mathbf{F_2 F_1}\, B$$

or :

$$B \;=\; t_r \left[1 - r_r r_t \mathrm{e}^{2ikl} \mathbf{F_2 F_1}\right]^{-1}$$

then

$$A_{out} = i\, r_r\, A_{in} - i\, t_r r_t \mathrm{e}^{2ikl} \mathbf{F_2 F_1}\, B$$

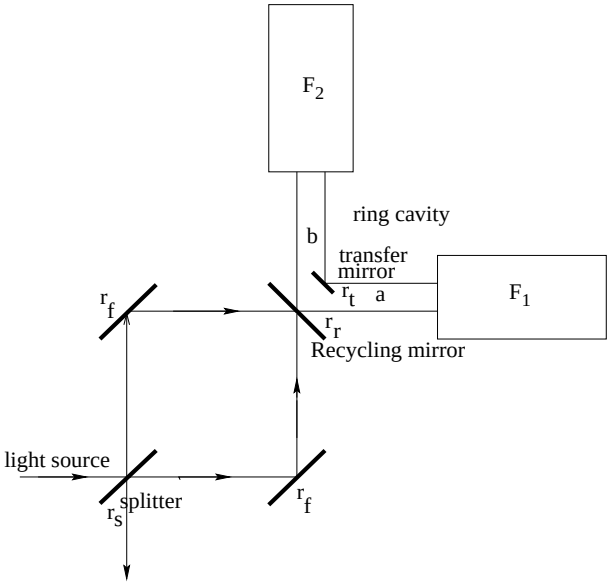

Figure 1.26: Sketch of the synchronous recycling configuration

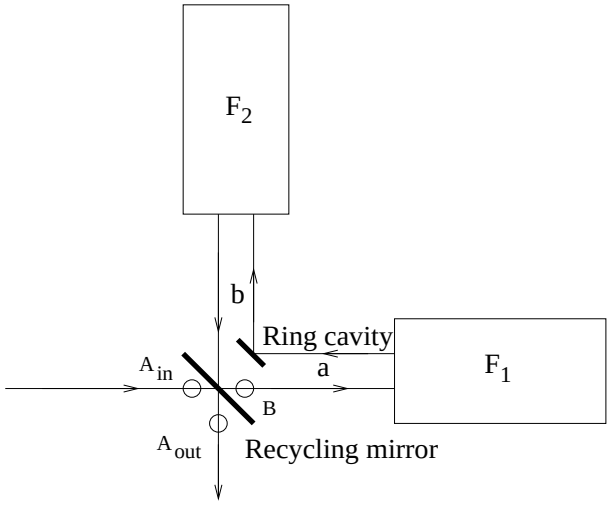

Figure 1.27: Ring cavity and counterclockwise optical path

so that the reflectance is :

$$\begin{aligned}\mathbf{R_+} &= r_r - t_r^2 r_t \mathrm{e}^{2ikl}\mathbf{F_2F_1}\left[1 - r_r r_t \mathrm{e}^{2ikl}\mathbf{F_2F_1}\right]^{-1} \\ &= \left[r_r - (1-p_r) r_t \mathrm{e}^{2ikl}\mathbf{F_2F_1}\right]\left[1 - r_r r_t \mathrm{e}^{2ikl}\mathbf{F_2F_1}\right]^{-1}\end{aligned}$$

Obviously, for the clockwise optical path, we have the reflectance :

$$\mathbf{R_-} = \left[r_r - (1-p_r) r_t \mathrm{e}^{2ikl}\mathbf{F_1F_2}\right]\left[1 - r_r r_t \mathrm{e}^{2ikl}\mathbf{F_1F_2}\right]^{-1}$$

Now, if we return to the splitter, we can compute the transmittance of the whole system :

$$\mathbf{T} = -i\, t_s^2 r_f^2\, \mathrm{e}^{i\phi}\mathbf{R_-} + i r_s^2 r_f^2\, \mathrm{e}^{i\phi}\mathbf{R_+}$$

Where the two transfer mirrors of the square cavity have been assumed identical. ϕ is the optical path inside the square cavity. If further we assume a perfectly symmetrical splitter, we can write

$$\mathbf{T} = -i\,\frac{1}{2}(1-p_s) r_f^2 \mathrm{e}^{i\phi}\,(\mathbf{R_-} - \mathbf{R_+})$$

A direct calculation gives

$$[R_- - R_+]_{10} = -t_r^2 r_t\, \mathrm{e}^{2ikl}\,\frac{2G_+(F_-F_+)}{DD_+}$$

Where the definitions of $G_\pm$, $F_\pm$ are the same as in section 7 , and

$$D_a = 1 - r_r r_t\, \mathrm{e}^{2ikl} F_a^2 \quad (a = -1, 0, 1)$$

The [10] component of $\mathbf{T}$ is thus :

$$T_{10} = \frac{\mathcal{F}L}{\lambda}\,\frac{4i(2-\sigma)^2(1-p_s) r_f^2 r_t \mathrm{e}^{i\phi} t_r^2 f_g}{(1-2i\Delta f)^2[1-2i(\Delta f + f_g)]^2\,[1 - r_r r_t \mathrm{e}^{2ikl}F^2]\,[1 - r_r r_t \mathrm{e}^{2ikl}F_+^2]}$$

One would obtain a similar expression for T_{20} by changing the sign of f_g. The preceding expression exhibits a sharp resonance peak when the resonance condition

$$2kl + 2\mathrm{Arg}(F) \equiv 0 \quad [\mathrm{mod} 2\pi]$$

is met. The difference of π with respect to the preceding subsection (two isolated cavities) is due to the fact that we have now two extra mirrors, for

recycling (M_r) and transfer (M_t) each adding a phase of $\pi/2$. This should be kept in mind in any comparison. In particular, the resonance condition for the central cavity is now $2kl \equiv 0$, and the antiresonance is $2kl \equiv \pi$. We assume the laser frequency given, so that kl is a constant, representing the tuning of the central cavity. The long cavities are detuned by a microscopic change in length making their new resonance shifted by an amount Δf. For Δf corresponding to a resonance of the ring cavity, we have thus to solve

$$\tan^{-1}\left(\frac{2\Delta f}{1-\sigma}\right) + \tan^{-1}(2\Delta f) \;=\; -kl$$

or,

$$\frac{2(2-\sigma)\Delta f}{1-\sigma-4\Delta f^2} = -\tan(kl)$$

this gives two solutions :

$$\Delta f_S \;=\; \frac{1}{2}\left[\frac{1-\sigma/2}{\tan(kl)} + \sqrt{\left(\frac{1-\sigma/2}{\tan(kl)}\right)^2 + 1 - \sigma}\right]$$

and

$$\Delta f_A \;=\; \frac{1}{2}\left[\frac{1-\sigma/2}{\tan(kl)} - \sqrt{\left(\frac{1-\sigma/2}{\tan(kl)}\right)^2 + 1 - \sigma}\right]$$

Note that

$$\Delta f_A \times \Delta f_S \;=\; -\frac{1-\sigma}{4} \tag{1.40}$$

and

$$\Delta f_S - \Delta f_A \;=\; \sqrt{\left(\frac{1-\sigma/2}{\tan(kl)}\right)^2 + 1 - \sigma} \tag{1.41}$$

We remark that the minimum frequency gap, is

$$[\Delta f_S - \Delta f_A]_{\min} = \sqrt{1-\sigma}$$

For having a large SNR at the normalized GW frequency $f_g^{(0)} \;>\; \sqrt{1-\sigma}$, we follow the following scheme :

- Tune the central cavity in such a way that $\Delta f_S - \Delta f_A = f_g^{(0)}$, which happens for

$$kl = \tan^{-1}\left[\frac{1-\sigma/2}{\sqrt{f_g^{(0)2} - (1-\sigma)}}\right]$$

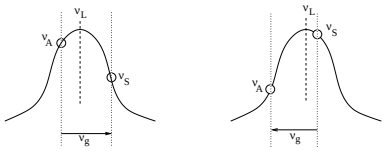

Figure 1.28: Gravito-optical pumping

- Δf_A and Δf_S are now determined. Tune the cavities in such a way that $\Delta f = \Delta f_A$.

Obviously, a similar process can be carried out starting from the upper frequency Δf_S and going to the lower level Δf_A : this is described by the T_{20} component of the $\mathcal{S}$ transmittance (see Fig.1.28). Unfortunately, only one of the two components T_{10} and T_{20} can be made resonant. If we work on T_{10}, we can therefore neglect T_{20}, and vice-versa. At the end of this process, we see that the resonance condition is met simultaneously, for

$$1 - r_r r_t \mathrm{e}^{2ikl} F^2 = 1 - r_r r_t \rho_A^2$$

because the tuning satisfies the modes A equation, and for

$$1 - r_r r_t \mathrm{e}^{2ikl} F_+^2 = 1 - r_r r_t \rho_S^2$$

because the tuning satisfies the modes S equation when $f_g = f_g^{(0)}$. ρ_A and ρ_S are the modulus reflectances :

$$\rho_{A,S}^2 \;=\; 1 - \frac{\sigma(2-\sigma)}{1 + 4\Delta f_{A,S}^2}$$

We have then, at resonance, when $f_g = f_g^{(0)}$,

$$|T_{10}| \;=\; \frac{\mathcal{F}L}{\lambda} \frac{16(1-\sigma/2)^2 t_r^2 f_g^{(0)}}{(1+4\Delta f_A^2)(1+4\Delta f_S^2)(1 - r_r r_t \rho_A^2)(1 - r_r r_t \rho_S^2)}$$

We can still fix the recycling rate by opimizing T_{10} with respect to r_r. In the general case, when the gravitational frequency is larger than the minimum gap, it is cumbersome to derive the optimal r_r. We have :

$$[r_r]_{\mathrm{opt}} = \frac{1 + (1-p_r) r_t^2 \rho_A^2 \rho_S^2}{r_t(\rho_A^2 + \rho_S^2)} - \sqrt{\left(\frac{1 + (1-p_r) r_t^2 \rho_A^2 \rho_S^2}{r_t(\rho_A^2 + \rho_S^2)} \right)^2 - (1-p_r)}$$

If we use the definitions of ρ_A and ρ_S, it is possible to show that

$$\rho_A \times \rho_S = 1 - \sigma$$

which is particularly remarkable, being independent on the tuning of the cental cavity. After that, the sum $\rho_A^2 + \rho_S^2$ will obviously depend on the tuning :

$$\rho_A^2 + \rho_S^2 = 1 + (1-\sigma)^2 - \frac{\sigma^2(2-\sigma)^2}{\sigma^2 + 4f_g^{(0)2}}$$

It is however reasonable to optimize the SNR for the lowest possible GW frequency, i.e when $f_g^{(0)} = f_m = \sqrt{1-\sigma}$, situation in which we have $\rho_A = \rho_S = \sqrt{1-\sigma}$. The optimum value of the recycling mirror reflection coefficient is simply

$$[r_r]_{\text{opt}} = (1-p_r) r_t (1-\sigma)$$

And the optimal peak value of $|T_{10}|$ is

$$|T_{10}|_{\text{peak}} = \frac{2\pi L}{\lambda p} K(\sigma)$$

with the form factor

$$K(\sigma) = \frac{2\sigma\sqrt{1-\sigma}}{1-(1-p_{RC})(1-\sigma)^2}$$

and $1 - p_{RC} = (1-p_r) r_t^2$. The form factor K has the maximum value 1, obtained for the approximate value $\sigma = (2p_{RC})^{1/3}$. But the shape of the curve is so flat, that this value is misleading, a value of K very close to 1 is obtained already for the pseudo- optinum $\sigma \simeq 20 p_{sr}$ (see fig.1.29). The peak SNR at resonance is therefore

$$\text{SNR}_{\text{peak,Max}} = \frac{2\pi L}{\lambda p} \sqrt{\frac{P_L}{2h_P\nu}}\, h(\nu_g)$$

for a wide range of reference GW frequencies. For $f^{(0)}$ too small, however, the SNR falls to zero. Remark that this peak value scales as $1/p$, whereas the zero frequency limit of the (wideband) power recycling scales as $1/\sqrt{p}$. The spectral density of h equivalent to shot noise is :

$$h(f_0) = \sqrt{\frac{2h_P\nu}{P_L}} \frac{1}{\text{SNR}_{\text{peak,Max}}}$$

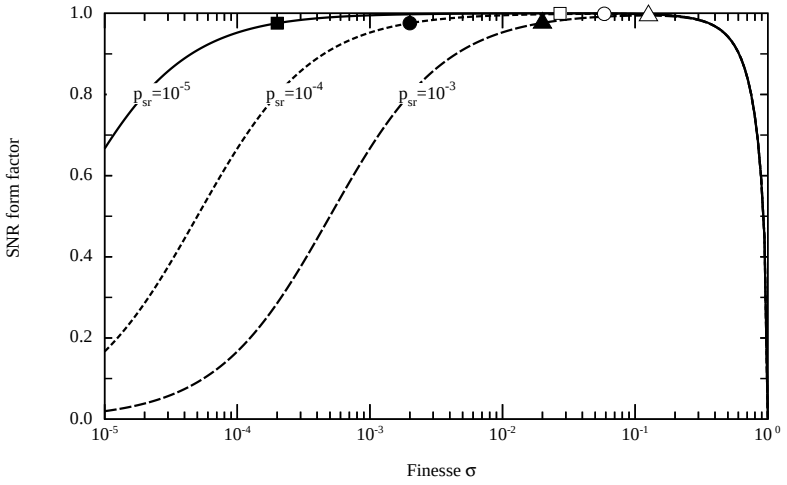

Figure 1.29: Form factor K for the SNR vs finesse $\sigma = p\mathcal{F}/\pi$. The white dots are the strict optima, the black dots mark the pseudo-optima

For cavity losses $p = 3\,10^{-5}$, l=3 km, $\lambda = 1.064\,10^{-6}$ m, P_L=20W, we have

$$h(f_0) \;\simeq\; 2.3\;10^{-25}\mathrm{Hz}^{-1/2}$$

It is now necessary to study the width of the resonance. For this purpose, we assume the laser being locked on the antisymmetric resonance, and the gravitational frequency in the neighbourhood of the gap $f_g^{(0)}$, i.e. $f_g = f_g^{(0)} + \delta f$, so that $\Delta f_A + f_g \;=\; \Delta f_S + \delta f$. Consider the SNR :

$$\mathrm{SNR}(\delta f) \propto \frac{16\mathcal{F}L}{\lambda}\,\frac{(1-\sigma/2)^2 t_r^2 f_g}{(1+4\Delta f_A^2)(1+4(\Delta f_A+f_g)^2)(1-r_r r_t \rho_A^2)\,(1-r_r r_t \rho_+^2 \mathrm{e}^{2i\Phi})}$$

In this expression, the varying terms are :

- The fast varying phase

  $$\Phi \;=\; \tan^{-1}\left[\frac{2(\Delta f_S+\delta f)}{1-\sigma}\right] + \tan^{-1}\left[2(\Delta f_S+\delta f)\right] - \tan^{-1}\left[\frac{2\Delta f_S}{1-\sigma}\right] - \tan^{-1}\left[2\Delta f_S\right]$$

  expanded at first order in δf this gives

  $$\Phi \;=\; A\delta f \quad \text{with} \quad A \;=\; \frac{4(2-\sigma)(1-\sigma+4\Delta f_S^2)}{\left[(1-\sigma)^2+4\Delta f_S^2\right]\left[1+4\Delta f_S^2\right]}$$

- The reflectivity of the cavities for the upper sideband :

$$\rho_+^2 \;=\; 1 - \frac{\sigma(2-\sigma)}{1+4(\Delta f_S + \delta f)^2}$$

This differs from unity by a small amount, whose variation is like second order. More specifically, the second order expansion gives

$$\rho_+^2 \;=\; \rho_S^2 + \frac{8\sigma(2-\sigma)\Delta f_S}{(1+4\Delta f_S^2)}\,\delta f + \frac{4\sigma(2-\sigma)(1-12\Delta f_S^2)}{(1+4\Delta f_S^2)^3}$$

We have already seen that the best value of σ is very small, in order to have a good reflectivity of the cavities. It can be thus understood, and numerically checked that the variations of ρ_+^2 around the S resonance can be neglected.

- The term,

$$\frac{f_g^{(0)} + \delta f}{1+4(\Delta f_S + \delta f)^2}$$

which varies very little.

The study of the shape of the resonance line can thus be carried out on the only term :

$$|1 - r_r r_t \rho_+^2 \mathrm{e}^{2i\Phi}| \;\simeq\; \left[(1 - r_r r_t \rho_S^2)^2 + 4 r_r r_t \sin^2(A\delta f)\right]^{1/2}$$

$$= \;(1 - r_r r_t \rho_S^2)\left[1 + \left(\frac{2\sqrt{r_r r_t \rho_S^2}\sin(A\delta f)}{1 - r_r r_t \rho_S^2}\right)^2\right]^{1/2}$$

expression very similar to a cavity resonance, with the *superfinesse*

$$\mathcal{SF} \;=\; \frac{\pi\sqrt{r_r r_t \rho_S^2}}{1 - r_r r_t \rho_S^2}$$

The linewidth (FWHM) od the SNR is thus :

$$\Delta f_g = \frac{\sqrt{3}(1 - r_r r_t \rho_s^2)}{A\sqrt{r_r r_t \rho_S^2}}$$

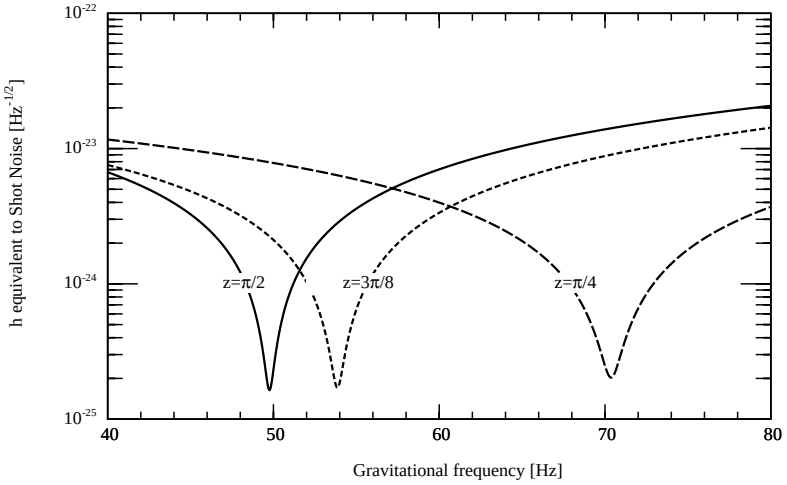

Figure 1.30: Effect of the detuning of the central cavity on the response of synchronous recycling interferometer

A simplified model will help to get simple estimates of the peak value and the linewidth of the SNR. We have seen that small values of σ are pseudo-optimal. We can then try a first order approximation in σ and a fortiori in the various losses. The SNR (with optimized recycling rate) becomes :

$$\mathrm{SNR}(f_g) \;=\; \frac{16\mathcal{F}L}{\lambda}$$

$$\frac{(1-\sigma)f_g(p_{RC}+2\sigma)}{(1+4\Delta f_A^2)(1+4\Delta f_S^2)(1-(1-p_{RC})(1-\sigma)\rho_A^2)|1-(1-p_{RC})(1-\sigma)\rho_S^2\,\mathrm{e}^{2i\Phi}|}\;\times$$

$$\times\;\sqrt{\frac{P_L}{2h_P\nu}}\;h(\nu_g)$$

It is easy to see that the 1st order expressions for the S and A detunings are respectively :

$$\Delta f_S \;=\; \frac{1-\sigma/2}{2\tan(z/4)}$$

$$\Delta f_A \;=\; -\,\frac{(1-\sigma/2)\tan(z/4)}{2}$$

where $z = 2kl$ is the tuning of the central cavity. we find then

$$1 + 4\Delta f_S^2 = \frac{1 - \sigma\cos^2(z/4)}{\sin^2(z/4)}$$

$$1 + 4\Delta f_A^2 = \frac{1 - \sigma\sin^2(z/4)}{\cos^2(z/4)}$$

whence

$$(1 + 4\Delta f_S^2)(1 + 4\Delta f_A^2) = \frac{4(1-\sigma)}{\sin^2(z/2)}$$

and also

$$\rho_S^2 = 1 - 2\sigma\sin^2(z/4)$$
$$\rho_A^2 = 1 - 2\sigma\cos^2(z/4)$$

The gravitational resonance frequency is

$$f_g^{(0)} = \Delta f_S - \Delta f_A = \frac{1 - \sigma/2}{\sin(z/2)}$$

If we can neglect the ring cavity losses p_{RC} (a few 10^{-5}) with respect to σ (up to 1%), we have simply

$$1 - (1 - p_{RC})(1 - \sigma)\rho_S^2 \simeq \sigma[1 + 2\sin^2(z/4)]$$

$$1 - (1 - p_{RC})(1 - \sigma)\rho_A^2 \simeq \sigma[1 + 2\cos^2(z/4)]$$

For the varying phase factor, we have

$$\Phi = 4(1 - \sigma/2)\sin^2(z/4)\,\delta f$$

The SNR is :

$$\mathrm{SNR} = \frac{8\pi L}{\lambda p}\,\frac{(1-\sigma/2) f_g^{(0)}\sin(z/2)}{(1-\sigma)[1+2\cos^2(z/4)][1+2\sin^2(z/4)]}$$

$$\times \left[1 + \left(\frac{8\sin^2(z/4)}{\sigma[1+2\sin^2(z/4)]}\,\delta f\right)^2\right]^{-1/2} \sqrt{\frac{P_L}{2h_P\nu}}\; h(\nu_g)$$

and finally :

$$\mathrm{SNR} = \frac{2\pi L}{\lambda}\,\frac{1}{p}\,(1-\sigma/2)\,\frac{4\sin(z/2)}{3+\sin^2(z/2)}$$

$$\times \left[1 + \left(\frac{8\sin^2(z/4)}{\sigma[1+2\sin^2(z/4)]}\,\delta f\right)^2\right]^{-1/2} \sqrt{\frac{P_L}{2h_P\nu}}\; h(\nu_g)$$

from where we conclude that the overall peak value, corresponding to $z = \pi/2$ is

$$\mathrm{SNR}_{peak,max} \;=\; \frac{2\pi L}{\lambda}\,\frac{1}{p} \tag{1.42}$$

This peak corresponds to the resonance frequency

$$f_g^{(0)} \;=\; 1 - \sigma/2$$

in other words, the minimum resonance frequency is given by the linewidth of the cavity, and the minimum gravitational linewidth (FWHM) :

$$\delta f_{FWHM,min} \;=\; \sigma\sqrt{3}$$

In terms of gravitational frequencies, we find the relation with the cavity linewidth :

$$\Delta\nu_{g,FWHM,min} \;=\; \sqrt{3} \;\times\; \delta\nu_{FWHM}$$

Let us summarize the results for small σ and z not far $\pi/2$:

- By varying the tuning of the central cavity, it is possible to adjust the resonance for a GW frequency equal to or larger than the linewidth of the cavities. The general formula is :

$$\nu_g^{(0)} \;=\; \frac{1-\sigma/2}{\sin(z/2)} \;\times\; \delta\nu_{FWHM} \tag{1.43}$$

- The best response of the interferometer is obtained for the lowest GW frequency, when the central cavity is exactly antiresonant ($z = \pi/2$), the value of the SNR resonance peak is:

$$\mathrm{SNR}_{peak} = \mathrm{SNR}_{peak,max} \times P(z) \tag{1.44}$$

  where the maximum peak value has been expressed above (Eq. 1.42), and $P(z)$ is a form factor, taking the value 1 for $z = \pi/2$:

$$P(z) \;=\; \frac{4\sin(z/2)}{3+\sin^2(z/2)} \tag{1.45}$$

- When the central cavity is progressively detuned from antiresonance, the GW resonance frequency increases, the sensitivity decreases, and the GW linewidth increases. The general formula for the GW linewidth is :

$$\delta\nu_{g,FWHM} \;=\; \sigma\sqrt{3} \;\times\; \frac{1+2\sin^2(z/4)}{4\sin^2(z/4)} \;\times\; \delta\nu_{FWHM} \qquad (1.46)$$

These approximations remain true as long as σ does'nt exceed a few %. For very low gravitational frequencies, the linewidth has to be very thin, and the finesse very high, σ cannot more be kept small and the approximation fails. In fact we already know from the preceding study that the SNR tends to zero when the resonance peak tends to zero. The ratio $\nu_g/\delta\nu_{g,FWHM}$ gives an idea of the equivalent Q of the resonator. For the optimal operation point ($z = \pi/2$), we have

$$Q \;\simeq\; \frac{1}{\sigma\sqrt{3}} \;=\; \frac{\pi}{\sqrt{3}p\mathcal{F}}$$

1.7.4 Signal recycling

Signal recycling was proposed some years ago by B. Meers [3]. The idea is to add one more mirror after the output port of the interferometer in order to store the sidebands generated by the GW. The dark fringe port plus the signal recycling mirror form a resonant cavity whose reflectivity can be tuned. The gravitational frequencies creating a sideband for which the signal cavity is *antiresonant* are enhanced. This allows to modify the sensitivity curve and have a gain factor at a given frequency range of special interest. We have seen other methods giving a comparable result. Here, one more benefit is to enhance the constrast of the interferometer by the spatial filtering effect of the extra Fabry-Perot installed at the output (But this is out of the scope of the present chapter). The sketch of the setup and the notation are shown on Fig.1.31. The lengths of the short arms are a and b, the length of the power recycling cavity is l, and the length of the dual recycling cavity is z. The parameters of the mirrors are labeled by r,s,d. The $\mathcal{S}$ operator corresponding to the whole setup may be constructed by successive shells. We first consider the Michelson (mic) as a black box having two inputs, West (as in the preceding sections) and South (because the dual recycling reinjects from the South). It has therefore an $\mathcal{S}$ reflectance R^W_{mic} and a transmittance $T^W_m ic$ (see Fig.1.32). It has also a reflectance R^S_{mic} and a transmittance T^S_{mic}

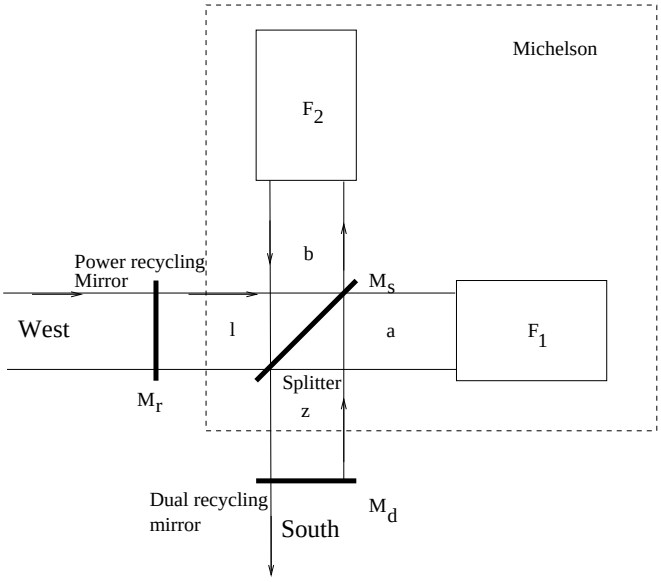

Figure 1.31: sketch of the Dual recycling configuration

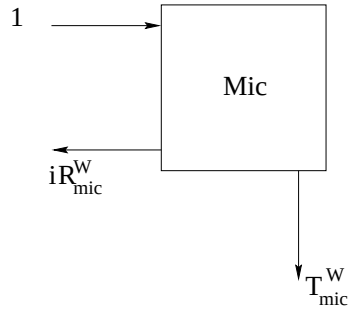

Figure 1.32: West input

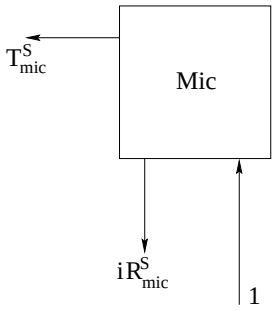

Figure 1.33: South input

for the South input port : The corresponding operators are easy to compute :

$$\begin{aligned} R^W_{mic} &= t_s^2 \mathrm{e}^{2ika} F_1 - r_s^2 \mathrm{e}^{2ikb} F_2 \\ T^W_{mic} &= -r_s t_s \left(\mathrm{e}^{2ika} F_1 + \mathrm{e}^{2ikb} F_2 \right) \\ R^S_{mic} &= -r_s^2 \mathrm{e}^{2ika} F_1 + t_s^2 \mathrm{e}^{2ikb} F_2 \\ T^S_{mic} &= -r_s t_s \left(\mathrm{e}^{2ika} F_1 + \mathrm{e}^{2ikb} F_2 \right) \end{aligned}$$

If we assume the splitter to be strictly symmetrical, and the Michelson tuned at a black fringe, we have simply, after setting $m = (a+b)/2$,

$$R^W_{mic} = -R^S_{mic} = \frac{i}{2}(1-p_s)\mathrm{e}^{2ikm}(F_1+F_2) = R_{mic}$$

$$T^W_{mic} = T^S_{mic} = -\frac{i}{2}(1-p_s)\mathrm{e}^{2ikm}(F_1-F_2) = T_{mic}$$

with

$$F_1 = \begin{pmatrix} F & 0 & 0 \\ G_+ & F_+ & 0 \\ G_- & 0 & F_- \end{pmatrix} \quad , \quad F_2 = \begin{pmatrix} F & 0 & 0 \\ -G_+ & F_+ & 0 \\ -G_- & 0 & F_- \end{pmatrix}$$

F, $F_\pm$ and $G_\pm$ having the definitions set in section 8. Now the power recycled interferometer (pritf) (see Fig.1.34 and Fig.1.35) has a transmittance T_{pritf} for a west input, and a reflectance R_{pritf} for a south input. The corresponding operators are :

$$T_{pritf} = t_r \mathrm{e}^{ikl} T_{mic} \left[1 + r_r \mathrm{e}^{2ikl} R_{mic} \right]^{-1}$$

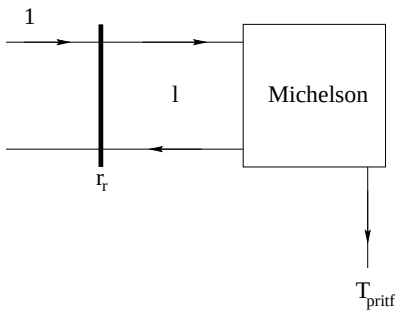

Figure 1.34: West input on a power recycled Michelson

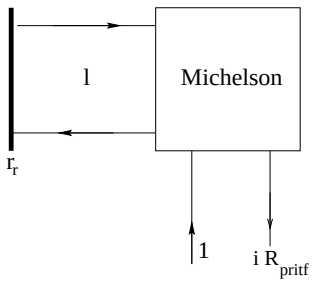

Figure 1.35: South input on a power recycled Michelson

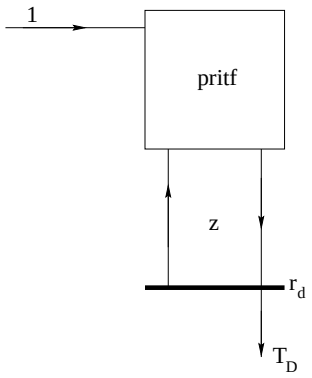

Figure 1.36: West input on a power and dual recycled Michelson

$$R_{pritf} = -R_{mic} + r_r e^{2ikl} T_{mic} \left[1 + r_r e^{2ikl} R_{mic}\right]^{-1} T_{mic}$$

Finally, the dual recycling setup (see Fig.1.36) has a transmittance for a west input T_D.

$$T_D = t_d e^{ikz} \left[1 + r_d e^{2ikz} R_{pritf}\right]^{-1} T_{pritf}$$

After some elementary algebra, we find :

$$T_{D,10} = -i \frac{t_r t_d (1-p_s) e^{ik(l+2m+z)} G_+}{[1 - i(1-p_s) r_d e^{2ik(m+z)} F_+][1 + i(1-p_s) r_r e^{2ik(l+m)} F]} \quad (1.47)$$

$$T_{D,20} = -i \frac{t_r t_d (1-p_s) e^{ik(l+2m+z)} G_-}{[1 - i(1-p_s) r_d e^{2ik(m+z)} F_-][1 + i(1-p_s) r_r e^{2ik(l+m)} F]} \quad (1.48)$$

It is easy ro recognize in these formulas the SNR for a power recycled Michelson, as already derived in a previous section, multiplied by an extra surtension factor :

$$S_D = \frac{t_d}{1 - i(1-p_s) r_d e^{2ik(m+z)} F_+}$$

Remark the opposite signs in the two factors of the denominators : The best efficiency is obtained for resonance in the recycling cavity, and antiresonance in the signal cavity. Obviously, the two sidebands cannot be both antiresonant (except at zero gravitational frequency). if we choose for instance, to make the (10)-component resonant. It is possible

- to tune the long Fabry-Perot's at resonance, so that $Arg(F) = \pi$,

- to tune the power recycling cavity so as to obtain resonance, by taking

$$2k(l+m)+\frac{\pi}{2} \equiv \pi$$

the signal surtension factor may be written as

$$S_D = \frac{t_d}{1-r_d(1-p_s)\,\rho_+\,e^{i[\pi/2+2k(m+z)+Arg(F_+)]}}$$

where, f being the gravitational reduced frequency,

$$\rho_+ = 1-\frac{\sigma(2-\sigma)}{1+4f^2}$$

$$Arg(F_+) = \pi + \tan^{-1}\left[\frac{2f}{1-\sigma}\right] + \tan^{-1}[2f]$$

clearly, it is always possible to tune the dual recycling cavity to meet resonance, with the condition :

$$2k(m+z)+\tan^{-1}\left[\frac{2f}{1-\sigma}\right]+\tan^{-1}[2f] \equiv \frac{\pi}{2}$$

The sharpness of the dual resonance is a function of r_d (see Fig.1.37) If σ is small, we conclude that the detuning giving the sensitivity peak at given f_0 is

$$\delta \sim \frac{\pi}{2} - 2\tan^{-1}(2f_0)$$

where we have set $\delta \equiv 4\pi(m+z)/\lambda$. (see Fig.1.38)

1.7.5 The signal extraction regime

We remark that for $\delta = -\pi/2$, which corresponds to $f_0 = \infty$, the sensitivity is almost flat (there is a knee at a higher frequency). This regime, exhibiting a broadband response (broader than the standard recycling, and thus losing in maximum sensitivity, for the same finesse) was called 'Signal extraction' by J. Mizuno [5], [6]. The explanation is that the flat curve is the result of a conflict between the low-pass response of the Michelson $(1/(1+4f^2)$ and the signal-recycling gain factor which starting from a low value at $f = 0$ (the SNR is out of resonance though the FP's are resonant), increases sharply to a high and

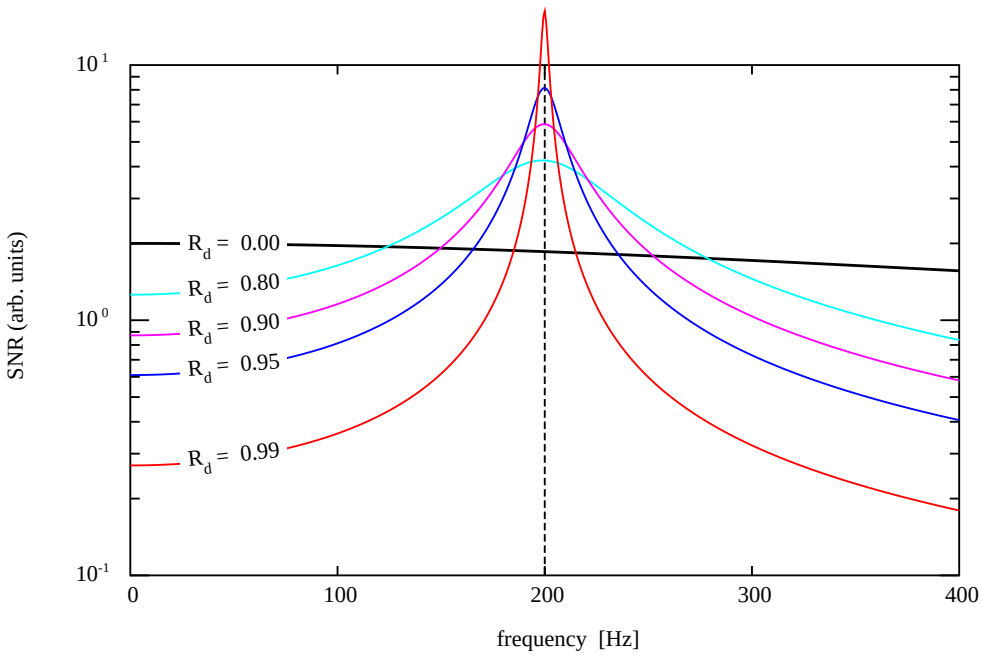

Figure 1.37: SNR of dual recycling configuration for various recycling rates (values of r_d)

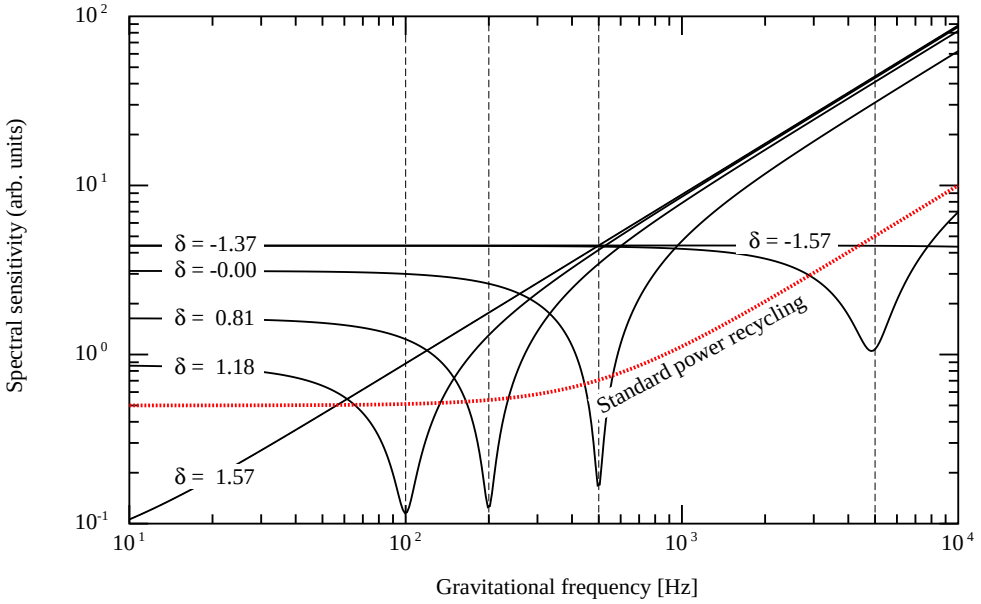

Figure 1.38: Spectral sensitivity of dual recycling configuration for various detunings of the signal recycling cavity $\delta \equiv 4\pi(m+z)/\lambda \pmod{2\pi}$

constant value when the FP's arrive to anti-resonance. (recall that there is a phase flip when a FP transits from resonance to anti, that the antiresonance frequency range is much larger than the resonance, especially at high finesses, and that the reflectance modulus is much higher at antiresonance than at resonance). This result can be understood by looking at the expression of the SNR (1.47). Recall that, when the cavities are at resonance, the upper sideband generated by the GW in one cavity is

$$G_+ \;=\; i\frac{2\mathcal{F}L(2-\sigma)}{\lambda}\;\frac{1}{1-2if_g}$$

and the reflectance of the cavity for that upper sideband is

$$\rho_+ \;=\; -\;\frac{1-\sigma+2if_g}{1-2if_g}$$

where f_g is the normalized gravitational frequency, i.e. the ratio of the gravitational frequency to the linewidth of the cavity ($f_g = \nu_g/\delta\nu$), and σ the coupling coefficient. The SNR takes thus the form (up to a phase factor and neglecting the length of the SR cavity), when power recycling is resonant and signal recycling antiresonant :

$$T_{D,10} \;=\; \frac{2\mathcal{F}L(2-\sigma)}{\lambda}\;\frac{1}{1-2if_g}\;G_r\;\frac{t_d}{1+(1-p_s)r_d\,\frac{1-\sigma+2if_g}{1-2if_g}}$$

where G_r is the resonant power recycling gain (unsensitive to GW frequency) :

$$G_r \;=\; \frac{t_r}{1-(1-p_s)r_r(1-\sigma)}$$

This yields

$$|T_{D,10}| \;=\; \frac{2\mathcal{F}L(2-\sigma)}{\lambda}\;G_r\left|\frac{t_d}{1-2if_g+(1-p_s)r_d\,[1-\sigma+2if_g]}\right| \;=$$

$$\frac{2\mathcal{F}L(2-\sigma)}{\lambda}\;G_r\left|\frac{t_d}{1+(1-p_s)(1-\sigma)r_d\;-2if_g\,[1-(1-p_s)r_d]}\right|$$

Which makes clear that the bandwidth is now

$$\delta\nu_g \;=\; \frac{\delta\nu}{1-(1-p_s)r_d}$$

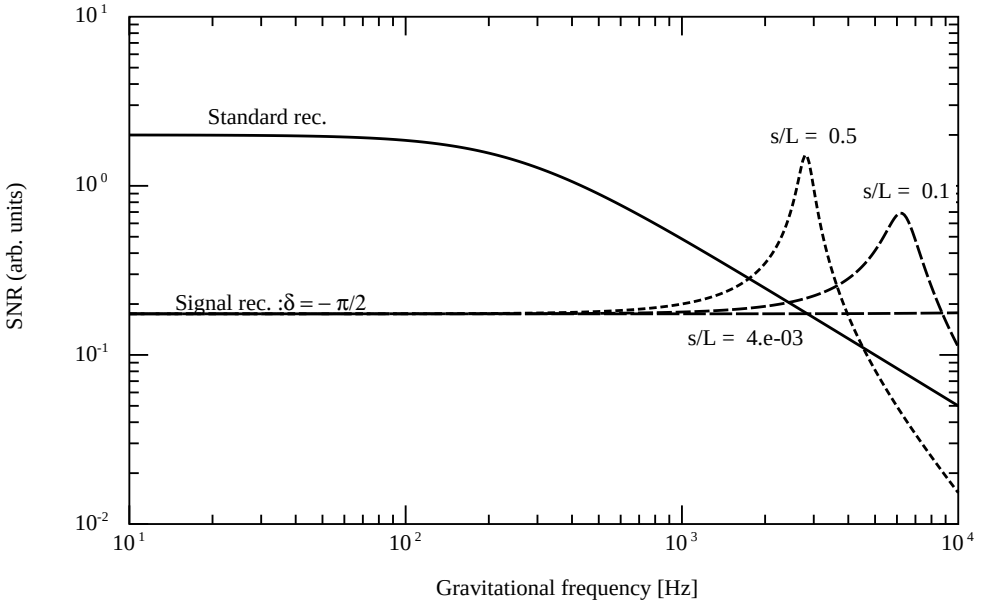

Figure 1.39: SNR in the regime of "signal extraction", i.e. $\delta \equiv -\pi/2 \pmod{2\pi}$, for several ratios s/L of the signal cavity. L is the length of the arms

so that, even if the finesse is very high, by increasing the recycling rate r_d, it is possible to keep constant the product $\mathcal{F}[1-(1-p_s)r_d]$ and thus the bandwidth of the detector.

It is even possible to play with the length of the signal cavity, assuming lengths much longer than the recycling cavity (see Fig.1.39). This creates local resonance effects.

It is interesting to note that it is possible, due to the effect mentionned above, to have almost exactly the same SNR spectral profile with standard power recycling, and with power recycling + signal extraction. The following extreme example will help to understand it.

- Assume a power recycling interferometer having finesse 100 long FP cavities. The optimum power recycling rate corresponds to a surtension ~ 800. Starting from a 20 W laser, this gives ~ 18 kW on the splitter, and finally about 500 kW in the FP cavities.

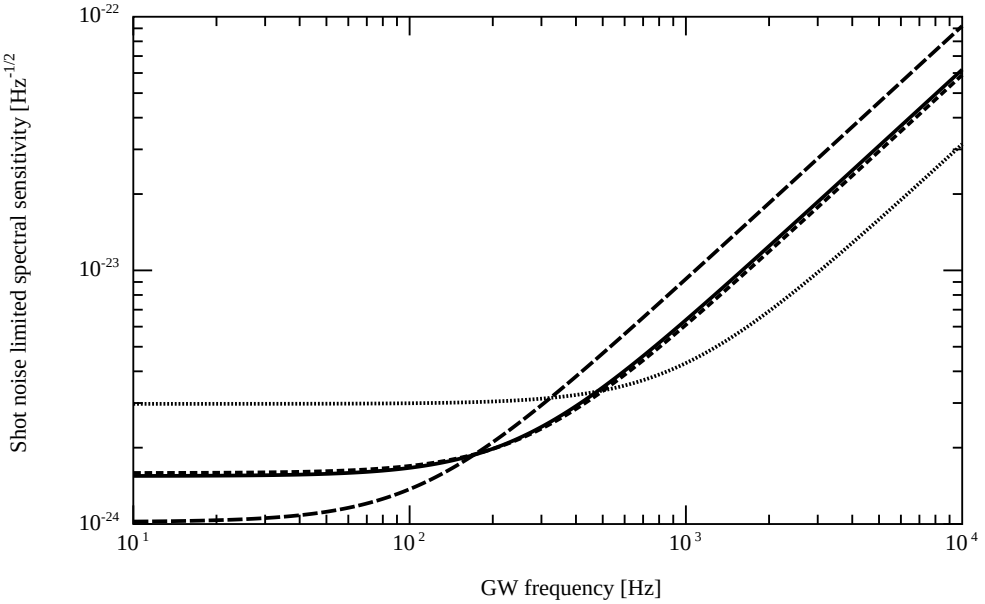

Figure 1.40: Solid curve : Standard power recyling, with $\mathcal{F} = 100$ and optimal recycling. Short dashed curve : Dual recycling-Signal extraction, $\mathcal{F} = 1000$, optimal recycling, $r_d^2 = 0.69$. Long dashed curve : $r_d^2 = 0.4$. Dotted line : $r_d^2 = 0.9$.

- Assume now a dual recycling interferometer in the signal extraction regime. The finesses of the long FP cavities are 1000, and under optimal power recycling, the power surtension is only ~ 80, which is ~ 1.6 kW on the splitter. The reflection coefficient of the signal recycling mirror is $r_d^2 = 0.69$. The power stored in the FP's is still about 500 kW.

- we can compare the SNR in the two situations (see Fig.1.40).

- the coincidence is caused by the particular choice of r_d. A smaller value would give a standard power recyling type response peaked at $f = 0$, a higher value would give a flat response but with a loss of sensitivity.

We see that the drawbacks caused by high powers (thermal lensing, thermal distortions, radiation pressure, ...) are identical in the FP cavities in both

cases, but very different in the power recycling cavity. This is of some importance when power dissipation is taken into account (see further chapters). The ultimate logics of the signal extraction regime is reached when the cavities are optimally coupled (all the light power is absorbed in the FP's), the power recycling rate being zero, and nevertheless, the bandwidth large.

Chapter 2

Beam optics and Interferometers

2.1 introduction

In interferometric GW detectors, we need to store light in long cavities in which light propagates back and forth. We have seen that a good reflectivity of these cavities is a key condition for efficiency in recycling. This reflectivity, combined with the ability to achieve a dark fringe have been an actual worry at the beginning of interferometer projects, and have triggered a lot of optical simulations of FP cavities and interferometers. It was essential to have theoretical models for light propagation. The theory used up to now for this purpose is the Scalar Diffraction Theory (SDT) (this seemed sufficient, owing to the very weak departure of the optical elements from an ideal shape). The basis of the SDT is the Kirchhoff equation, that is the basis of the paraxial approximation which is in fact more widely used.

2.2 A short theory of diffraction

2.2.1 The Kirchhoff integral

The diffraction theory can be found in classical courses as the famous Born & Wolff [7]. It can be shown starting from the wave equation that the electromagnetic field at the right of surface $z = 0$ is related to the field on the plane $z = 0$ by:

$$E(\vec{r}) \;=\; \iint_{z'=0} E(\vec{r'})\; K(\vec{r},\vec{r'})\; dx'\; dy' \tag{2.1}$$

where $K(\vec{r},\vec{r'})$ is the Kirchhoff diffraction kernel:

$$K(\vec{r},\vec{r'}) \;=\; -\;\frac{i}{\lambda}\;\frac{\mathrm{e}^{ik\rho}}{\rho}\;\left(1\;+\;\frac{i}{k\rho}\right)\;\frac{z}{\rho}$$

where $\rho \equiv \sqrt{(x-x')^2+(y-y')^2+z^2}$.

2.2.2 Application of the Kirchhoff equation

The preceding equation, establishing a relation between the field inside a volume and the field at the boundary is exact, but taken in the strict sense, of almost no practical interest: It could seem that in order to compute E, we first need to know E, because the correct way to impose boundary values is out of this theory. It can however be widely exploited, by slightly changing its meaning, in the following situation. Assume that the surface $z = 0$ contains a hole, and that a primary electromagnetic wave is coming from the left (see Fig.2.1). We can assume that at the immediate right of the surface $z = 0$, the field is simply the field at the left, transmitted through the hole. This means that on the right side of the plane, the field is zero outside the hole, and identical to the field coming from the left, within the hole. We can change the sense of the Kirchhoff equation (2.1) by introducing two fields, one is the coming one $E_1(\vec{r})$, which is assumed to be given throughout the aperture D, and the second one $E_2(\vec{r})$, which is to be computed from the preceding one by using a Kirchhoff-like formula:

$$E_2(\vec{r}) \;=\; -\;\frac{i}{\lambda}\;\iint_D E_1(\vec{r'})\;\frac{\mathrm{e}^{ik\rho}}{\rho}\;\left(1\;+\;\frac{i}{k\rho}\right)\;\frac{z}{\rho}\;\;dx'\;dy' \tag{2.2}$$

ρ having the same definition as above.

2.2.3 The Fresnel approximation and the paraxial diffraction equation (PDE)

The Fresnel approximation

As soon as the distance z separating the input aperture from the observation plane is much larger than the wavelength, the $1/k\rho$ term in Eq.(2.2) becomes

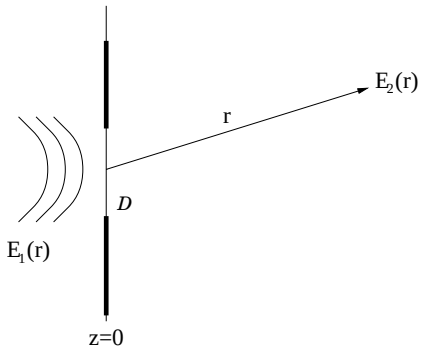

Figure 2.1:

negligible, and we can write:

$$E_2(\vec{r}) \;= -\frac{i}{\lambda}\oint_D E_1(\vec{r'})\,\frac{\mathrm{e}^{ik\rho}}{\rho}\,\cos(\theta)\,ds' \tag{2.3}$$

where θ is the angle under which the element of aperture centered at (x', y') is seen from the observation point (x, y). Eq.2.3 is often referred to as the "Huyghens-Fresnel" equation. It can be (and was) derived heuristically by considering all points of the aperture as elementary sources of spherical waves: At any point of the right hand side half space, the amplitude is the sum of all these wavelets, and we can for instance say that the elementary amplitude created at $\vec{r}$ by the small elementary source

$$ds(x', y') \;=\; E_1(x', y')dx'\,dy'$$

is:

$$dE_2(x, y) \;=\; \kappa \iint_D \frac{\mathrm{e}^{ik\rho}}{\rho} E_1(x', y')\,dx'\,dy'$$

where κ is some coefficient to be determined. For this purpose, we can require that the propagation of an indefinite plane wave is the same plane wave, up to a phase factor. This means that

$$\mathrm{e}^{ikz} \;=\; \kappa \iint_{\mathrm{R}^2} \frac{\mathrm{e}^{ik\rho}}{\rho}\,dx'\,dy'$$

The integral is easy to compute, being the value at $p = q = 0$ of the Fourier

transform of $e^{ik\rho}/\rho$ that is known, as said above, we have thus

$$e^{ikz} = \kappa \left[2i\pi \frac{e^{iz\sqrt{k^2-p^2-q^2}}}{\sqrt{k^2-p^2-q^2}} \right]_{p=q=0} = \frac{2i\pi e^{ikz}}{k} \kappa$$

It is therefore necessary that $\kappa = -i/\lambda$. This was known long before Kirchhoff's theory, which is the mathematical justification to the Huyghens principle and to the Fresnel formula. If θ in Eq.2.3 is small, we are in the paraxial regime. If the observation point is near the optical axis, and the distance Z long enough, we can neglect the quantity

$$\sqrt{(x-x')^2+(y-y')^2}$$

with respect to z, except in the phase factor. This leads to the paraxial diffraction integral:

$$E_2(x,y,z) = -\frac{i}{\lambda z} \exp(ikz) \times \tag{2.4}$$

$$\times \iint_D E_1(x',y',0) \exp\left[ik \frac{(x-x')^2+(y-y')^2}{2z} \right] dx'\, dy'$$

All consequences of this formula are said having been obtained within the Fresnel approximation. Remark that this equation is the convolution product of the field $E(z=0)$ with the simplified (paraxial) diffraction kernel

$$K_{\mathrm{P}}(x,y,z) = -\frac{i}{\lambda z} \exp\left[ik \frac{x^2+y^2}{2z} \right]$$

Use of the Fourier transform is especially convenient here, because the Fourier transform of K_{P} is easy to compute. For a function of the form

$$G(x,y) = e^{-Z(x^2+y^2)}$$

where Z is any complex number of positive real part, it can be shown that

$$\widetilde{G}(p,q) = \frac{\pi}{Z} e^{-\frac{p^2+q^2}{4Z}} \tag{2.5}$$

in particular the propagator is

$$\widetilde{K_{\rm P}}(p,q,z) \;=\; \exp\left[-i\frac{z(p^2+q^2)}{2k}\right] \tag{2.6}$$

Obviously, we could have deduced it from the "exact" propagator

$$\tilde{G}_{\rm exact}(p,q,z) \;=\; {\rm e}^{iz\sqrt{k^2-p^2-q^2}}$$

by assuming that the values of p,q are restricted to small values due to the behavior of the function to be propagated ("small" means $p,q \;\ll\; k$). This is one more version of the paraxial approximation, the diffraction is "adiabatic" along z (if z is regarded as an evolution parameter), so that the angles of the rays with respect to the axis are small. $p,q,\sqrt{k^2-p^2-q^2}$ may be thought of as the coordinates of the wave vector of an elementary plane wave. Then , θ being the direction of that elementary wave, we have $\theta \simeq \sin\theta \;=\; \sqrt{p^2+q^2}/\sqrt{k^2-p^2-q^2}$. If θ is small, we can thus write:

$$\tilde{G}(p,q,z) \;=\; {\rm e}^{ikz} \;\times\; {\rm e}^{-i\frac{z(p^2+q^2)}{2k}}$$

An alternative way of computing E_2 is therefore:

$$E_2(x,y,z) \;=\; \widetilde{K_{\rm P}}(p,q,z) \;\widetilde{\times}\; \widetilde{E_1}(p,q,0) \tag{2.7}$$

This is a very convenient way, as will be shown later.

The Paraxial Diffraction Equation

One can derive from the Helmholtz equation an approximate equation called **The paraxial diffraction equation** (PDE) which is equivalent to the paraxial diffraction integral. Consider the Helmholtz equation:

$$\left[\Delta + k^2\right]\mathcal{E} \;=\; 0 \tag{2.8}$$

If the field is expected to propagate mainly in the z direction, with a slow expansion in the transverse plane, we can use the slowly varying envelope approximation scheme, i.e.

$$\mathcal{E}(x,y,z) \;=\; {\rm e}^{ikz} \;\times\; E(x,y,z)$$

in which the envelope $E(x,y,z)$ is assumed to depend slowly on z, the rapidly oscillating factor having been extracted. More specifically, we intend to use the approximation

$$\frac{\partial E}{\partial z} \ll k\ E$$

for neglecting second order derivatives of E, so that the Helmholtz equation becomes:

$$[2ik\ \partial_z\ +\ \Delta_{\rm T}]\ E\ =\ 0 \tag{2.9}$$

where

$$\Delta_{\rm T}\ \equiv\ \partial_x^2 + \partial_y^2$$

is the transverse Laplace operator.This is the PDE. It is clearly equivalent to the Fresnel integral, for by taking the Fourier transform of Eq.(2.9) with respect to x, y, we obtain:

$$\left[2ik\ \partial_z\ -\ (p^2+q^2)\right]\ \tilde{E}(p,q,z)\ =\ 0$$

the solution of which is of the form

$$\tilde{E}(p,q,z+\Delta z)\ =\ \tilde{E}(p,q,z) \times \exp\left[-\ i\frac{(p^2+q^2)\Delta z}{2k}\right]$$

in which we recover the propagator (2.6).

2.2.4 The Fraunhofer approximation

The ultimate approximation for a diffracted wave holds when the very far field is considered. The Fresnel-Huyghens integral can be written as:

$$E(x,y,z)\ =\ -\ \frac{i}{\lambda z}\ \exp\left[i\pi\frac{x^2+y^2}{\lambda z}\right]\ \times$$

$$\int_{\mathbf{R^2}}\ \exp\left[i\pi\frac{x'^2+y'^2}{\lambda z}\right]\exp\left[-2i\pi\frac{xx'}{\lambda z}\right]\exp\left[-2i\pi\frac{yy'}{\lambda z}\right]\ E(x',y',0)\ dx'\,dy'$$

If we assume the transverse extension of the initial amplitude bounded by a radius a, the order of magnitude of the argument of the quadratic term in the complex exponential is

$$\delta\ <\ \pi\frac{a^2}{\lambda z}\ =\ \pi \times\ N_F$$

N_F is called *Fresnel number*. If the observation distance is so large that N_F may be neglected, we can write simply

$$E(x,y,z) \;=\; -\,\frac{i}{\lambda z}\,\exp\left[i\pi\frac{x^2+y^2}{\lambda z}\right]\;\times$$

$$\int_{\mathbf{R}^2}\exp\left[-2i\pi\frac{xx'}{\lambda z}\right]\exp\left[-2i\pi\frac{yy'}{\lambda z}\right]\;E(x',y',0)\;dx'\,dy'$$

which is nothing but the Fourier transform of the incoming amplitude:

$$E(x,y,z) \;=\; -\,\frac{i}{\lambda z}\,\exp\left[i\pi\frac{x^2+y^2}{\lambda z}\right]\;\tilde{E}\left(\frac{2\pi x}{\lambda z}\;,\;\frac{2\pi y}{\lambda z}\;,\;0\right)$$

This is the Fraunhoffer approximation, and allows to compute quickly the properties of the diffracted field for z very large. For instance, for a rectangular and uniform aperture $[-a,a]\times[-b,b]$, one finds immediately

$$|E(x,y,z)|^2 \;=\; \frac{16a^2b^2}{\lambda^2z^2}\;\left[\mathrm{sinc}\left(\frac{2\pi x}{\lambda z}\right)\mathrm{sinc}\left(\frac{2\pi y}{\lambda z}\right)\right]^2$$

explaining the pattern of Fig.**??**. For a uniform circular aperture, $r<a$, we find

$$|E(r,z)|^2 \;=\; \left[\frac{a}{r}\,J_1\left(\frac{2\pi ar}{\lambda z}\right)\right]^2$$

explaining the pattern of Fig.**??**. Anyway, in the very far field, when r/z is sufficiently small, we have

$$I(0) \;\sim\; I_0\times\left(\frac{S}{\lambda z}\right)^2$$

S being the area enclosed within the aperture, I(0) the intensity on axis in the far field, and I_0 the initial intensity. If we consider the total power P_0 passing through the aperture , we get

$$I(0) \;\sim\; \left(\frac{S}{\lambda^2z^2}\right)\,P_0$$

The total power received by an equal area in the far field is $P_1 = S\,I(0)$, so that we have the ratio

$$\frac{P_1}{P_0} \;=\; \left(\frac{S}{\lambda z}\right)^2$$

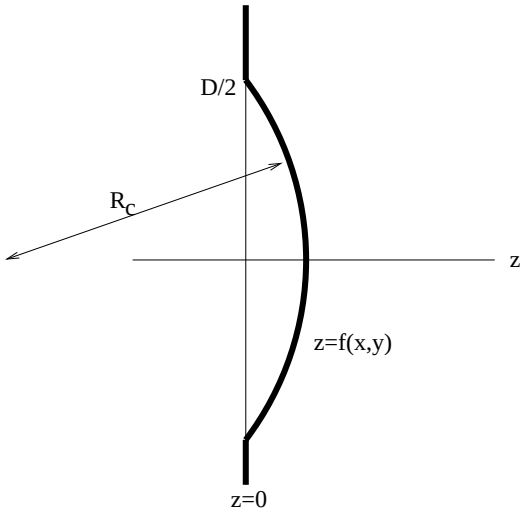

Figure 2.2: reflection off a curved mirror

2.2.5 Representation of optical elements

The action of thin optical elements, like thin lenses or nearly flat mirrors on the optical amplitudes can be modelled without using a diffraction integral. Consider for instance the reflection off a curved mirror of curvature radius R_c and diameter D. Assume the mirror to close the aperture in the plane $z = 0$ (see Fig.2.2). Strictly speaking, the field arriving on the mirror's surface should be computed fromn the field in the plane by Kirchhoff's equation. It is more convenient to discuss in the Fourier space. Calling $E_1(x, y, 0)$ the field in the plane $z = 0$, and $E_2(x, y, z)$ the field on the mirror's surface, we have as seen in (**??**):

$$\widetilde{E_2}(p, q, z) \;=\; \mathrm{e}^{iz\sqrt{k^2-p^2-q^2}} \;\times\; \widetilde{E_1}(p, q, 0)$$

The argument of the imaginary exponential can be written as:

$$z\sqrt{k^2 - p^2 - q^2} \;=\; kz \;+\; z\left(\sqrt{k^2 - p^2 - q^2} - k\right)$$

or

$$z\sqrt{k^2 - p^2 - q^2} \;=\; kz \;-\; \frac{z(p^2 + q^2)}{2k}\;\frac{2}{1 + \sqrt{1 - \frac{p^2+q^2}{k^2}}}$$

It is necessary to estimate the different orders of magnitude of these terms.

- The quantity p^2+q^2 is determined by the spatial behavior of the input wave. If the spatial frequencies are of the order of magnitude of w_0, for instance for a TEM mode of Fourier transform

$$\tilde{\phi}(p,q) \;=\; \exp\left(-\frac{w_0^2(p^2+q^2)}{4}\right)$$

we have

$$\frac{p^2+q^2}{k^2} \;\sim\; \frac{4}{k^2 w_0^2} \;\sim\; \left(\frac{\lambda}{\pi w_0}\right)^2 \;\sim\; \theta_g^2$$

θ_g being nothing but the divergence angle of the beam. For long baseline interferometers, this aperture is of the order of tens of microradians, for Virgo, $\theta_g \;=\; 1.7 \;\times\; 10^{-5}$Rd. It is clear that we can neglect this term.

- The argument of the imaginary exponential therefore reduces to

$$z\sqrt{k^2-p^2-q^2} \;=\; kz \;-\; \frac{z(p^2+q^2)}{2k}$$

but

$$\frac{z(p^2+q^2)}{2k} \;\sim\; \frac{z\lambda}{\pi w_0^2} \;\sim\; \frac{z}{z_R}$$

where z_R is the Rayleigh parameter of the beam (see below), about 1km for GW interferometers, whereas z is of the order of tens of micrometers. More precisely, we have for a parabolic mirror $z_{\max} \;=\; D^2/8R_c$, on the other hand, the Rayleigh parameter is related to the curvature radius (in a flat/parabolic cavity of length L) by

$$z_R \;=\; \sqrt{L(R_c-L)} \;=\; \frac{1}{\alpha} \;\times\; R_c$$

where

$$\alpha \;=\; \frac{R/L}{\sqrt{R/L-1}}$$

the factor α is of the order of the unity (For Virgo, $\alpha \;\simeq\; 2.97$). We have thus:

$$\frac{z(p^2+q^2)}{2k} \sim \frac{\alpha}{8}\left(\frac{D}{R_c}\right)^2$$

Taking again Virgo figures (D=35 cm, R_c=3.45 km) this is:

$$\frac{z(p^2+q^2)}{2k} \sim 3.8\times 10^{-9}$$

The conclusion is that we can write with a good accuracy

$$\widetilde{E_2}(p,q,z) = \mathrm{e}^{ikz} \times \widetilde{E_1}(p,q,0)$$

which by inverse Fourier transform gives simply

$$E_2(x,y,z) = \mathrm{e}^{ikz} \times E_1(x,y,0)$$

In other words, in the Fresnel equation

$$E_2(x,y,z) = \mathrm{e}^{ikz}\int K_p(x-x',y-y',z)\,E_1(x',y',0)\,dx'\,dy'$$

we have shown that the kernel K_p is a 2-D delta function for small z, so that if we consider the amplitude on a surface of equation $z=f(x,y)$, we can write simply

$$E_2(x,y) = \mathrm{e}^{ikf(x,y)} \times E_1(x,y)$$

For the reflected wave $E_3(x,y,z)$, we reverse the point of view. If we would compute E_2 knowing E_3 we would find (the propagation direction being reverse)

$$E_2(x,y) = \mathrm{e}^{-ikf(x,y)} \times E_3(x,y)$$

Therefore

$$E_3(x,y) = \mathrm{e}^{2ikf(x,y)} \times E_1(x,y)$$

and the reflection operator is simply the phase factor ;

$$R = \mathrm{e}^{2ikf(x,y)} \tag{2.10}$$

Let us recall that this only holds for "thin" optical elements, in the above discussed sense. In particular, for a parabolic mirror, well adapted to gaussian beams in the paraxial approximation, we have

$$R \;=\; \exp\left[i\;\frac{2\pi(x^2+y^2)}{\lambda R_c}\right] \tag{2.11}$$

2.3 Fundamental TEM mode

It is possible to find a special solution of 2.9 under the axially symmetrical form depending on two unknown functions of z:

$$\Psi(r,z) \;=\; \mathrm{e}^{\mathrm{A(z)}}\,\mathrm{e}^{ikr^2/2q(z)}$$

substituting this expression in 2.9 provides two coupled differential equations:

$$\frac{dq}{dz} \;=\; 1 \;\text{ and }\; \frac{dA}{dz} \;=\; -\,\frac{1}{q}$$

from where we get firstly

$$q(z) \;=\; q_0 + z$$

It is convenient to choose the constant q_0 in such a way that at $z=0$, the wave is a real gaussian function of parameter w_0. (i.e. of the form $\exp(-r^2/w_0^2)$). This clearly happens if

$$q_0 \;=\; -i\frac{kw_0^2}{2} \;=\; -i\,b$$

The parameter $b = kw_0^2/2$ is called **Rayleigh range**. We have then $q(z) = z - i\,b$, so that

$$A(z) \;=\; \ln\left[\frac{1}{z-i\,b}\right] + C$$

The arbitrary integration constant C may be chosen in order to have $A(0) = 0$, i.e. $C = -\ln(-1/ib)$, and then

$$A(z) \;=\; \ln\left[\frac{1}{1+iz/b}\right]$$

or as well

$$A(z) \;=\; \ln\left[\frac{1}{\sqrt{1+z^2/b^2}}\right] - \;i\,\arctan(z/b)$$

on the other hand we have, separating the real from the imaginary part of $1/q$:

$$\frac{ik}{2q(z)} = \frac{1}{z + b^2/z} + \frac{i}{b + z^2/b}$$

defining two new real functions , $w(z)$ and $R(z)$:

$$\frac{ik}{2q(z)} = -\frac{1}{w^2(z)} + \frac{ik}{2R(z)}$$

The definitions of $w(z)$ and $R(z)$ are consequently:

$$w(z) = w_0 \sqrt{1 + z^2/b^2}$$

$$R(z) = z(1 + b^2/z^2)$$

$w(z)$ is the beam half-width at abscissa z, and $R(z)$ is the curvature radius at the same point. These two real functions have concrete optical meanings, but contain the same information as the complex function $q(z)$ often called **complex curvature radius** We have finally the complete solution for the envelope:

$$\Psi(r, z) = \frac{1}{\sqrt{1 + z^2/b^2}} \, \mathrm{e}^{-r^2/w(z)^2} \, \mathrm{e}^{ikr^2/2R(z)} \, \mathrm{e}^{-i \arctan(z/b)}$$

The factor $\exp(ikz)$ may be added for representing the rapidly varying part. The extra phase $\arctan(z/b)$ appearing during propagation with respect to a plane wave is called **Gouy phase**. The solution $\Psi(r, z)$ is a very special one. One can find other solutions by considering the product of $\Psi(r, z)$ by polynomials in the variables $(x/w \ , y/w)$. The solution $\Psi(r, z)$ is called $\mathrm{TEM}_{(0,0)}$ propagation mode. It is the fundamental mode of two families of modes discussed below.

2.4 Discrete bases for free space propagation

The set $\mathcal{L}^2$ of all complex functions $f(x, y)$ of integrable square modulus may be given the structure of a Hilbert vector space, by introducing the scalar product:

$$\langle f \ , \ g \rangle = \int_{\mathbf{R^2}} dx \ dy \ \overline{f(x, y)} g(x, y) \tag{2.12}$$

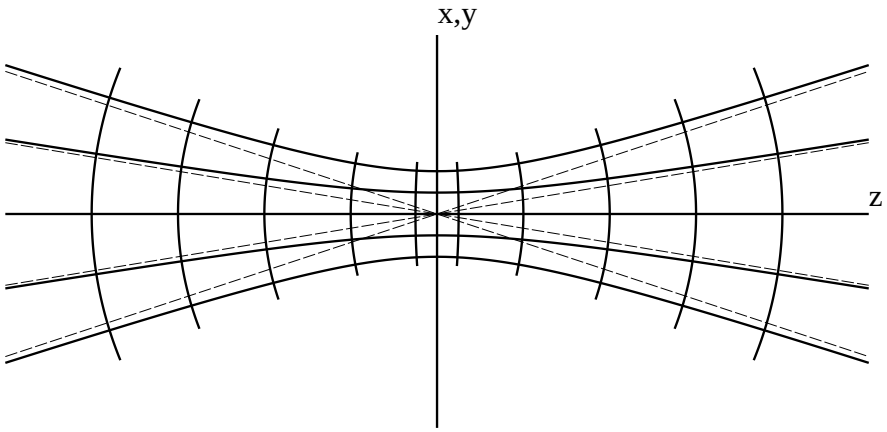

Figure 2.3: Diffraction of a gaussian wave: equal intensity and equal phase surfaces

If we think to these functions in terms of optical amplitudes at a given point of the path of a light beam having the preferred propagation direction z, we see that

$$\|f\|^2 \;=\; \langle\, f\;,\; f\,\rangle \;=\; \int_{\mathbf{R^2}} dx\; dy\; |f(x,y)|^2 \tag{2.13}$$

is nothing but the light power of the beam crossing the transverse plane at z: restriction to $\mathcal{L}^2$ is therefore not too demanding. Obviously, a number of bases can be constructed for this Hilbert space. It is possible to find discrete bases, whose corresponding vectors are called Transverse Electromagnetic Modes, and are labelled by two indices: $\mathrm{TEM}_{(\mathrm{m,n})}$. The more often employed bases for studying cavities and laser beams, are the Hermite-Gauss modes $\mathrm{HG}_{(\mathrm{m,n})}$ when rectangular coordinates are convenient, and the Laguerre-Gauss modes $\mathrm{LG}_{(\mathrm{m,n})}$ when polar coordinates are convenient. The fundamental mode has been defined above as: $\mathrm{TEM}_{(0,0)}(x,y;z) \;=\; \mathrm{HG}_{(0,0)}(x,y;z) \;=\; \mathrm{LG}_{(0,0)}(x,y;z)$ is, with $r^2 \;\equiv\; x^2+y^2$,

$$\mathrm{TEM}_{(0,0)}(x,y;z) \;=\; \sqrt{\frac{2}{\pi\, w(z)^2}}\; \mathrm{e}^{ikz}\;\; \mathrm{e}^{-i\arctan(z/b)} \mathrm{e}^{-r^2/w(z)^2}\; \mathrm{e}^{ikr^2/2R(z)} \tag{2.14}$$

where $w(z)$ gives the radius of the beam, $R(z)$ the curvature radius of the phase surface, b the Rayleigh range. The form of $w(z)$ suggests a widening of the beam (see Fig.2.3) during propagation, an angle aperture can be evaluated by

$$\lim_{z\to\infty} \frac{w(z)}{z}$$

This gives the gaussian aperture angle

$$\theta_g \;=\; \frac{\lambda}{\pi w_0}$$

2.4.1 Hermite-Gauss modes

Extended solution

The fundamental solution found above can be extended in the following scheme. Let us look for solutions of the form:

$$\Psi(x,y,z) \;=\; \mathrm{e}^{A(z)}\mathrm{e}^{ikr^2/2q(z)}P[u(z)x]\,Q[u(z)y]$$

where A and q are complex functions of z alone, whereas u is a real function of z, and P, Q real functions. The reason for these choices are firstly a separation of the variables x and y, and secondly the clear necessity to include a variable scaling factor in the transverse plane accounting for the extension of the wavefront, as seen in the fundamental mode. In this spirit, we expect the unknown function $u(z)$ to be inversely proportional to $w(z)$. After straightforward calculations, the paraxial diffraction equation becomes:

$$\begin{aligned} 2ik\left(\frac{\partial A}{\partial z}+\frac{1}{q}\right)\,P(X)\,Q(Y) + \frac{k^2r^2}{q^2}\left(\frac{\partial q}{\partial z}-1\right)\,P(X)\,Q(Y) + \\ +\,2ik\left(\frac{\partial u}{\partial z}+\frac{u}{q}\right)\left(x\frac{\partial P}{\partial X}Q(Y)+y\frac{\partial Q}{\partial Y}P(X)\right) \\ +u^2\left(\frac{\partial^2 P}{\partial X^2}Q(Y)+\frac{\partial^2 Q}{\partial Y^2}P(X)\right) \;=\; 0 \end{aligned} \tag{2.15}$$

where we used the notations $X \equiv u(z)x$ and $Y \equiv u(z)y$. Now we require the function $q(z)$ to be the same as in the fundamental solution, i.e.

$$\frac{\partial q}{\partial z} - 1 \;=\; 0$$

in order to keep the same dependence for the width of the beam, and for the curvature radius of the wavefront. Now we furthermore require that separately:

$$u^2 \frac{\partial^2 P}{\partial X^2} + 2ikx \left(\frac{\partial u}{\partial z} + \frac{u}{q} \right) \frac{\partial P}{\partial X} + \Lambda' P = 0 \tag{2.16}$$

and

$$u^2 \frac{\partial^2 Q}{\partial Y^2} + 2iky \left(\frac{\partial u}{\partial z} + \frac{u}{q} \right) \frac{\partial Q}{\partial Y} + \Lambda'' Q = 0 \tag{2.17}$$

where Λ', Λ'' are real arbitrary constants. Owing to the fact that u must be real, as also P and Q, it is necessary that

$$\frac{\partial u}{\partial z} + \frac{u}{q}$$

be purely imaginary. This is

$$\Re \left\{ \frac{\partial u}{\partial z} + \frac{u}{z - ib} \right\} = 0$$

or

$$\frac{1}{u} \frac{\partial u}{\partial z} = - \frac{z}{z^2 + b^2}$$

which gives the obvious solution

$$u(z) = \frac{\mu}{\sqrt{b^2 + z^2}}$$

where μ, an arbitrary constant, may be chosen in such a way that $u(0) = \sqrt{2}/w_0$. This is finally

$$u(z) = \frac{\sqrt{2}}{w(z)}$$

$w(z)$ being the function defined above in the fundamental solution. But now, we have:

$$\frac{\partial u}{\partial z} + \frac{u}{q} = \frac{ibu}{z^2 + b^2}$$
$$= i \frac{2\sqrt{2}}{kw^3}$$

so that eq.2.16 becomes:

$$\frac{2}{w^2} \frac{\partial^2 P}{\partial X^2} - \frac{4}{w^2} X \frac{\partial P}{\partial X} + \Lambda' P = 0$$

or

$$\frac{\partial^2 P}{\partial X^2} - 2X\frac{\partial P}{\partial X} + \frac{\Lambda' w^2}{2}P \;=\; 0 \tag{2.18}$$

We know that polynomial solutions of eq.2.18 exist, if

$$\frac{\Lambda' w^2}{2} \;=\; 2n$$

where n is any integer; in this case, eq.2.18 defines the Hermite polynomial of order n.

$$P(X) \;\equiv\; H_n(X)$$

Obviously, the same discussion holds for eq.2.17, and with

$$\frac{\Lambda'' w^2}{2} \;=\; 2m$$

we find

$$Q(Y) \;\equiv\; H_m(Y)$$

Now, eq.2.15 reduces to:

$$2ik\left(\frac{\partial A}{\partial z} + \frac{1}{q}\right) - (m+n)\frac{4}{w^2} \;=\; 0$$

or

$$\frac{\partial A}{\partial z} + \frac{1}{z - ib} + \frac{i(m+n)}{b(1 + z^2/b^2)} \;=\; 0$$

so that:

$$A(z) \;=\; \ln\left(\frac{1}{z - ib}\right) - i(m+n)\arctan\left(\frac{z}{b}\right)$$

and

$$\mathrm{e}^{A(z)} \;=\; (1 + z^2/b^2)^{-1/2}\,\mathrm{e}^{-i(m+n+1)\arctan(z/b)}$$

The HG basis

It has been shown that the PDE has Hermite-Gauss solutions of the form

$$\mathrm{HG}_{(m,n)}(x,y;z) \;=\; c_{m,n}\,\mathrm{e}^{ikz}\,H_m\left(\sqrt{2}\frac{x}{w(z)}\right)\,H_n\left(\sqrt{2}\frac{y}{w(z)}\right)\;\times$$

$$\mathrm{e}^{-i(m+n+1)\arctan(z/b)}\;\mathrm{e}^{-r^2/w(z)^2}\;\mathrm{e}^{ikr^2/2R(z)} \tag{2.19}$$

where the functions $H_n(X)$ are the Hermite polynomials and $c_{m,n}$ a normalization constant to be defined later.

Several properties of these functions are very convenient, and we recall them herafter without any proof.

- The Hermite polynomials are defined by:

$$H_n(x) \;=\; \mathrm{e}^{x^2}\left(-\frac{d}{dx}\right)^n \mathrm{e}^{-x^2} \tag{2.20}$$

- The explicit expression is:

$$H_n(x) \;=\; \sum_{s=0}^{[n/2]} (-1)^s \,\frac{n!}{(n-2s)!s!}\,(2x)^{n-2s} \tag{2.21}$$

  (the bracket means the integer part)

- They obey the following differential equation:

$$H''_n(x) - 2xH'n(x) + 2nH_n(x) \;=\; 0$$

- Their derivatives are given by:

$$H'_n(x) \;=\; 2n\, H_{n-1}(x)$$

- They obey a recurrence relation:

$$H_{n+1}(x) \;=\; 2x\; H_n(x) \;-\; 2n\; H_{n-1}(x) \tag{2.22}$$

- They obey an orthogonality relation

$$\int_{-\infty}^{\infty} H_m(x)\, H_n(x)\, \mathrm{e}^{-x^2}\, dx \;=\; \sqrt{\pi}\; 2^m m!\, \delta_{mn} \tag{2.23}$$

  The normalization constants for the HG modes are therefore:

$$c_{m,n} \;=\; \left[\frac{2}{\pi w^2}\;\;\frac{1}{2^{m+n} m!\; n!}\right]^{1/2} \tag{2.24}$$

- They obey as well a closure relation:

$$\frac{1}{\sqrt{\pi}} \sum_p \frac{1}{2^p p!}\; H_p(x) H_p(x')\; \mathrm{e}^{-(x^2+x'^2)/2} \;=\; \delta(x-x') \tag{2.25}$$

- There is a translation formula:

$$H_n(x+\Delta/2) \;=\; \sum_{k=0}^{n} C_n^k \; H_{n-k}(x)\; \Delta^k \tag{2.26}$$

(it can be shown using the recursion formula)

- There is a scaling formula:

$$H_n(\beta x) \;=\; \sum_{k=0}^{[n/2]} \frac{n!}{k!(n-2k)!}\, \beta^{n-2k} \; \left(\beta^2-1\right)^k \; H_{n-2k}(x) \tag{2.27}$$

- There is a reduction formula:

$$H_m(x)\, H_n(x) \;=\; \sum_{s=0}^{\min(m,n)} \frac{m!\, n!\, 2^s}{(m-s)!(n-s)!s!} \; H_{m+n-2s}(x) \tag{2.28}$$

- It is possible to give the general expression of the Fourier Transform of any mode ; We even give a more general formula under the following form. Let

$$\Psi_{(m,n)}(Z,x,y) \;=\; H_m\left(\sqrt{2}\frac{x}{w}\right)\; H_n\left(\sqrt{2}\frac{y}{w}\right)\; \exp\left(-Z\;\frac{x^2+y^2}{w^2}\right)$$

where Z is any complex number of positive real part. The Hermite-Gauss functions correspond to $Z=1$. The Fourier Transform is:

$$\widetilde{\Psi}_{(m,n)}(Z,p,q) \;=\; \frac{\pi w^2}{Z}\;\left(\frac{i}{Z}\right)^{m+n}\left(2Z-Z^2\right)^{(m+n)/2}\;\times$$

$$H_m\left(\frac{pw}{\sqrt{2}\sqrt{2Z-Z^2}}\right)\; H_n\left(\frac{qw}{\sqrt{2}\sqrt{2Z-Z^2}}\right)\; \exp\left[-\frac{w^2(p^2+q^2)}{4Z}\right] \tag{2.29}$$

For $Z=1$ (HG functions) this is simply:

$$\widetilde{\Psi}_{(m,n)}(1,p,q) \;=\; \pi w^2\, i^{m+n}\, H_m\left(\frac{pw}{\sqrt{2}}\right)\; H_n\left(\frac{qw}{\sqrt{2}}\right)\; \exp\left[-\frac{w^2(p^2+q^2)}{4}\right]$$

In a certain sense, we see that the HG modes are eigenvectors of the Fourier transform. The special case $Z=2$ gives

$$\widetilde{\Psi}_{(m,n)}(2,p,q) \;=\; \frac{\pi w^2}{2}\;\left(\frac{ipw}{2\sqrt{2}}\right)^m\;\left(\frac{iqw}{2\sqrt{2}}\right)^n\; \exp\left[-\frac{w^2(p^2+q^2)}{8}\right]$$

- There is a useful Fourier transform:

$$\frac{1}{\sqrt{\pi}} \int \mathrm{e}^{-x^2} H_n(x)\, \mathrm{e}^{ipx}\, dx \;=\; (ip)^n \mathrm{e}^{-p^2/4} \tag{2.30}$$

  note that this formula has nothing to do with the Fourier transform of a TEM mode, rather with the FT of the product of two modes.

- A consequence of the preceding integral (or an application of the generating function as well) is the expansion of a plane wave in terms of Hermite polynomials:

$$\mathrm{e}^{ipx} \;=\; \mathrm{e}^{-p^2/4} \sum_{n\geq 0} \frac{(ip)^n}{2^n n!} H_n(x)$$

- The first Hermite polynomials are explicitly:

$$H_0(x) \;=\; 1$$

$$H_1(x) \;=\; 2x$$

$$H_2(x) \;=\; 4x^2 - 2$$

$$H_3(x) \;=\; 8x^3 - 12x$$

$$H_4(x) \;=\; 16x^4 - 48x^2 + 12$$

$$H_5(x) \;=\; 32x^5 - 160x^3 + 120x$$

$$H_6(x) \;=\; 64x^6 - 480x^4 + 720x^2 - 120$$

  etc...

The intensity pattern of some HG functions is shown on the figures 2.4, 2.5, 2.6.

2.4.2 The Laguerre-Gauss modes

Using polar coordinates (r, ϕ) instead of (x, y) in the transverse plane, a new class of solutions to the PDE can be found, of the form

$$\mathrm{LG}_{\mathrm{m,n}}(r, \phi; z) \;=\; c_{m,n}\, \mathrm{e}^{ikz} \left(\sqrt{2}\frac{r}{w(z)}\right)^n L_m^{(n)}(2r^2/w(z)^2)\times$$

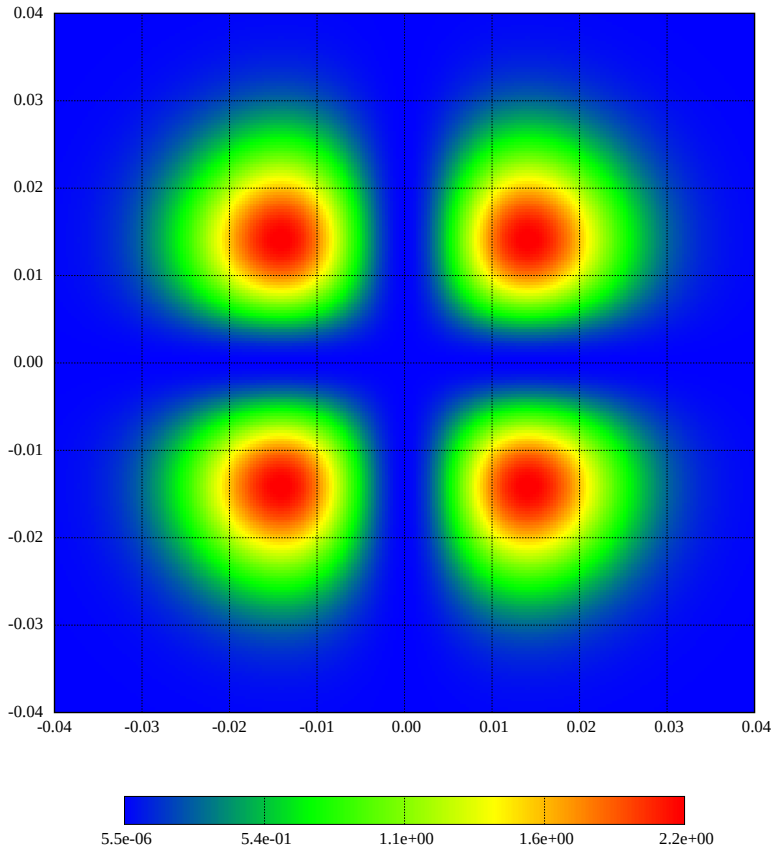

Figure 2.4: Intensity pattern of a HG_{11} mode for $w_0 = 0.02$ m

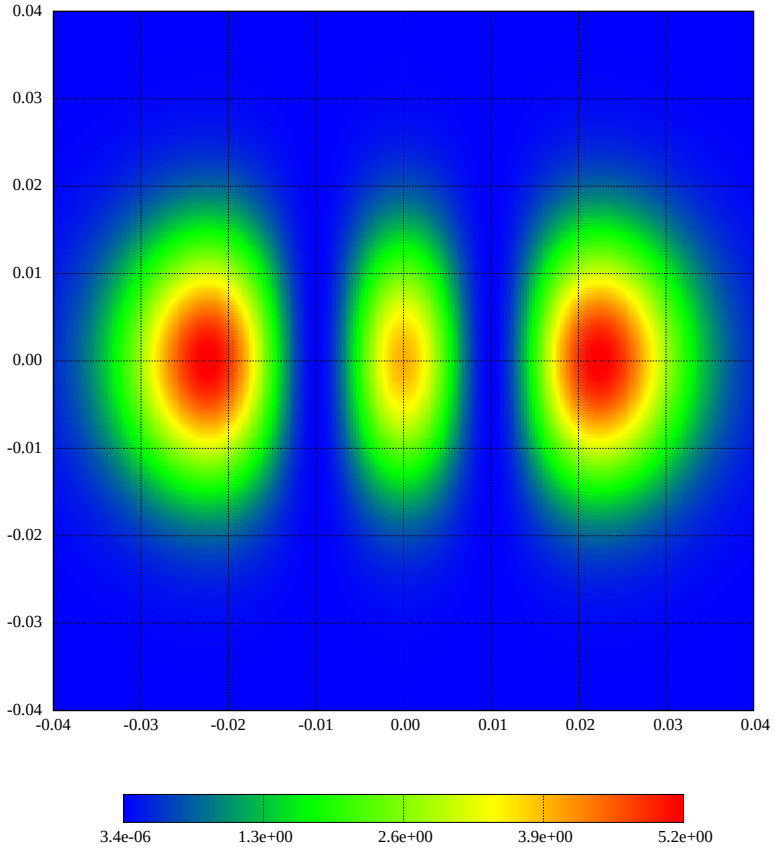

Figure 2.5: Intensity pattern of a HG_{20} mode for $w_0 = 0.02$ m

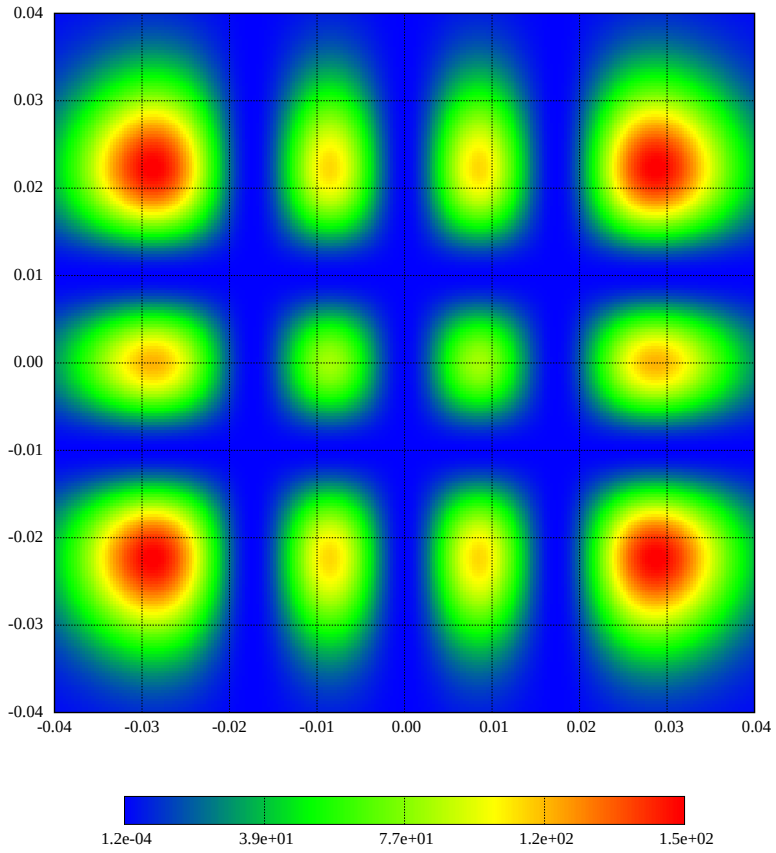

Figure 2.6: Intensity pattern of a HG_{32} mode for $w_0 = 0.02$ m

$$\mathrm{e}^{-i(2m+n+1)\arctan(z/b)}\ \mathrm{e}^{-r^2/w(z)^2}\ \mathrm{e}^{ikr^2/2R(z)}\ \cos(n\phi) \tag{2.31}$$

The functions $L_m^{(n)}(X)$ are the generalized Laguerre polynomials. They are defined by

$$L_m^{(n)}(x) \ = \ \frac{\mathrm{e}^x}{m!\ x^n}\ \left(\frac{d}{dx}\right)^m\ \left(x^{n+m}\mathrm{e}^{-x}\right)$$

They obey the recursion relation:

$$(m+1)L_{m+1}^{(n)}(x) \ = \ (2m+n+1-x)L_m^{(n)}(x) \ - \ (m+n)L_{m-1}^{(n)}(x)$$

The first ones are as follows:

$$L_0^{(n)}(x) \ = \ 1$$

$$L_1^{(n)}(x) \ = \ n+1-x$$

$$L_2^{(n)}(x) \ = \ \frac{(n+1)(n+2)}{2} - (n+2)\,x + \frac{x^2}{2}$$

$$L_3^{(n)}(x) \ = \ \frac{(n+1)(n+2)(n+3)}{6} \ - \frac{(n+2)(n+3)}{2}\,x \ + \ \frac{n+3}{2}\,x^2 \ - \ \frac{x^3}{6}$$

$$L_4^{(n)}(x) \ = \ \frac{(n+1)(n+2)(n+3)(n+4)}{24} \ - \frac{(n+2)(n+3)(n+4)}{6}\,x \ + \\ + \ \frac{(n+3)(n+4)}{4}\,x^2 \ - \ \frac{n+4}{6}\,x^4 \ + \ \frac{x^4}{24}$$

The normalization relation for the Laguerre polynomials comes from [11]:

$$\int_0^\infty L_m^{(n)}(x)^2\,x^n\,\mathrm{e}^{-x}\,dx \ = \ \frac{(m+n)!}{m!}$$

so that the normalization constants c_{mn} are:

$$c_{mn} \ = \ \frac{2}{w}\sqrt{\frac{m!}{\pi\,(1+\delta_{n0})\,(m+n)!}}$$

As a special case, we see that the $\mathrm{LG}_{m,0}$ modes have all the same normalization:

$$c_{m,0} \ = \ \sqrt{\frac{2}{\pi w^2}}$$

The intensity pattern of some LG modes is given in the maps 2.7,2.8,2.9,.

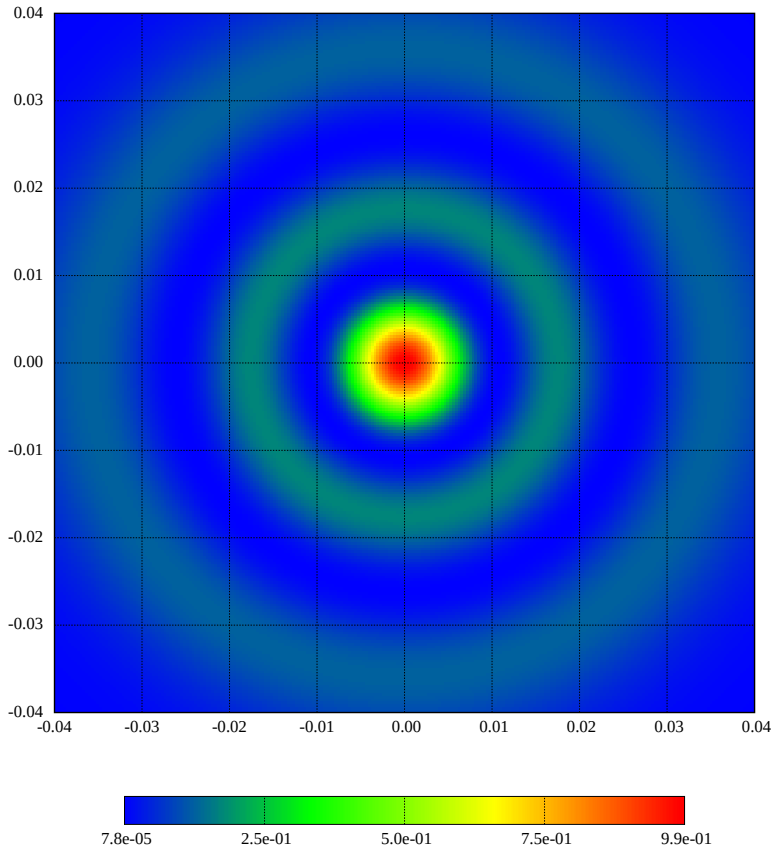

Figure 2.7: Intensity pattern of a LG_{20} mode for $w_0 = 0.02$ m

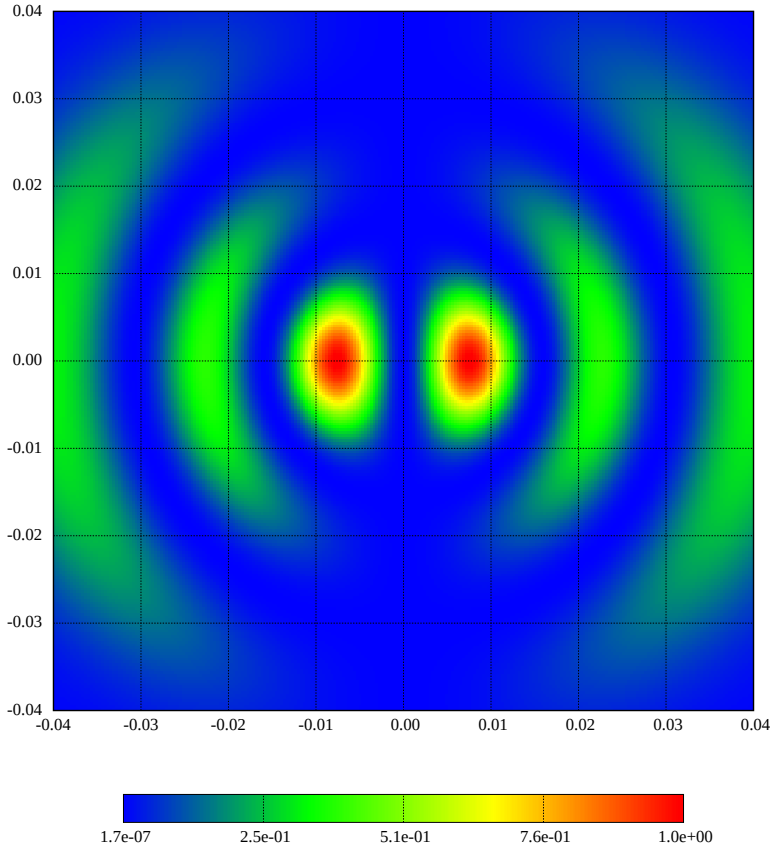

Figure 2.8: Intensity pattern of a LG_{21} mode for $w_0 = 0.02$ m

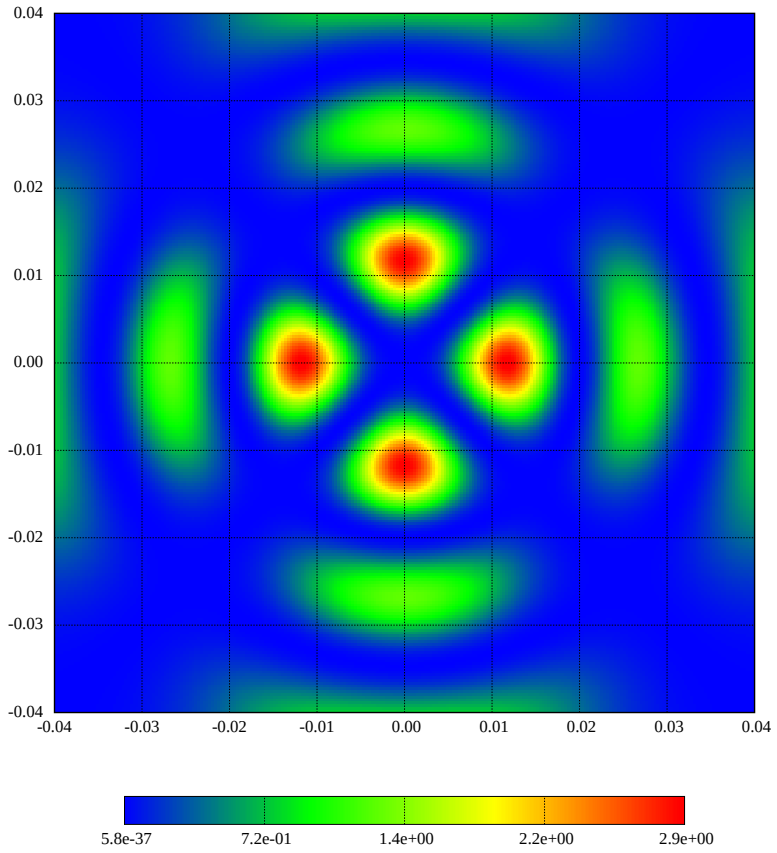

Figure 2.9: Intensity pattern of a LG_{22} mode for $w_0 = 0.02$ m

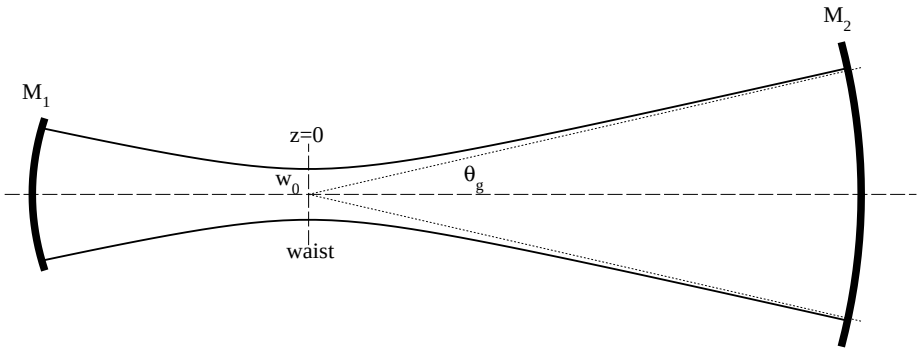

Figure 2.10: Any Fabry-Perot cavity with curved mirrors

2.5 Fabry-Perot: paraxial approximation

It has been seen that the free space propagation operator has, in a certain sense eigenmodes called $TEM_{m,n}$ modes. They have the significant two following properties:

- They are of finite transverse extension, there is already a storage in the transverse plane
- They have a parabolic equiphase surface

The second property allows to make "matched" mirrors, of shape adapted to the equiphase surface, reflecting the mode on itself (see Fig.2.10) A mode matching two parabolic mirrors not always exists, depending on the curvature radii of the mirrors and on the cavity length. Consider for instance a plane-spherical cavity with a plane input mirror M_1, and a spherical mirror M_2 of curvature radius R_c, at a distance L. in order to be matched to M_1, the stored wave must be at its waist at $z = 0$ on the input plane. Then, the

stored wave must have a phase curvature radius of R_c at $z = L$, so that we can write

$$R_c \;=\; L\left(1 \;+\; \frac{b^2}{L^2}\right)$$

b (Rayleigh parameter) having the definition previously encountered. This gives

$$b \;=\; \sqrt{L(R_c - L)}$$

Clearly, this is possible only if $R_c > L$. This is a stability condition for that type of cavity. If this condition is fulfilled, the cavity is able to store any $\mathrm{TEM_{m,n}}$ mode, provided it is near resonance. The size of the waist is

$$w_0 \;=\; \sqrt{\lambda b/\pi}$$

The resonance condition, assuming a $\pi/2$ dephasing at each reflection, is :

$$\pi \;-\; 2(m+n+1)\tan^{-1}\left(\frac{L}{b}\right) \;\equiv\; 2p\pi$$

the eigenmodes of the cavity are thus labeled by 3 integers, exactly as the modes of a closed box. The frequency spacing between modes is a very important feature in a cavity. If two modes have by chance close eigenfrequencies, a class of perturbations of the mirrors having the right symmetry will pump power from one mode to the other due to the finite linewidths (see below). In particular, if the cavity is operated on its fundamental mode, it is better to choose the geometrical parameters in such a way that the nearest transverse modes $(m,n) \neq (0,0)$ are well separated from the reference mode. The $\mathrm{TEM_{0,1}}$ and $\mathrm{TEM_{1,0}}$ modes are especially well coupled with the $\mathrm{TEM_{0,0}}$ in case of misalignment of mirrors. Let us discuss this issue now. We call $\Phi_{m,n,p}$ the total dephasing of the m,n,p mode over a round trip in the cavity. We have:

$$\Phi_{m,n,p} \;=\; \frac{4\pi\nu_{m,n,p}L}{c} \;-\; 2(m+n+1)\tan^{-1}\left(\frac{L}{b}\right) \;+\; \pi \;=\; 2p\pi$$

We see that the frequency gap between two successive longitudinal resonances, or Free Spectral Range (FSR), $(\Delta p = \pm 1)$, is $\Delta\nu_{FSR} \;=\; c/2L$. we see that the frequencies of the modes are given by

$$\nu_{m,n,p} \;=\; \Delta\nu_{FSR}\left(p - \frac{1}{2} + (m+n+1)\alpha\right)$$

with $\alpha = \tan^{-1}(L/b)/\pi$. Assume the operation mode has frequency $\nu_{0,0,p_0}$, the distances of the other modes are:

$$\delta\nu_{m,n,p} = \nu_{m,n,p} - \nu_{0,0,p_0} = (p - p_0 + (m+n)\alpha)\ \Delta\nu_{FSR} \qquad (2.32)$$

The distribution of resonances being periodic, it is sufficient to study it over a FSR. Given the length L of the cavity, the curvature radius R_c can be chosen under the following constraints:

- it must be larger than L
- it must not cause a too large magnification factor between the input mirror and the end mirror
- it must give a value of α such that equation 2.32 has no zero solutions for (m, n) small.

In the case of Virgo, the length of the arms is $L = 3$km and the curvature radius of the end mirror $R_c = 3.45$ km, so that $\alpha \simeq 0.38238$. The frequency offsets of the 15 nearest tranverse modes are given in the following table.

Mode order (m+n)	*Frequency offset* (Hz)
8	2950.62
3	7352.16
11	10302.78
6	14704.32
14	17654.94
1	19105.86
9	22056.48
4	26458.02
12	29408.64
7	33810.18
15	36760.79
2	38211.72
10	41162.34
5	45563.88
13	48514.49

Remark that the (0,1) and (1,0) modes are well separated from the (0,0), and that there is no coincidence for orders lower than 15. The nearest are the family (m+n=8) which are not easy to couple to (0,0) by a simple perturbation.

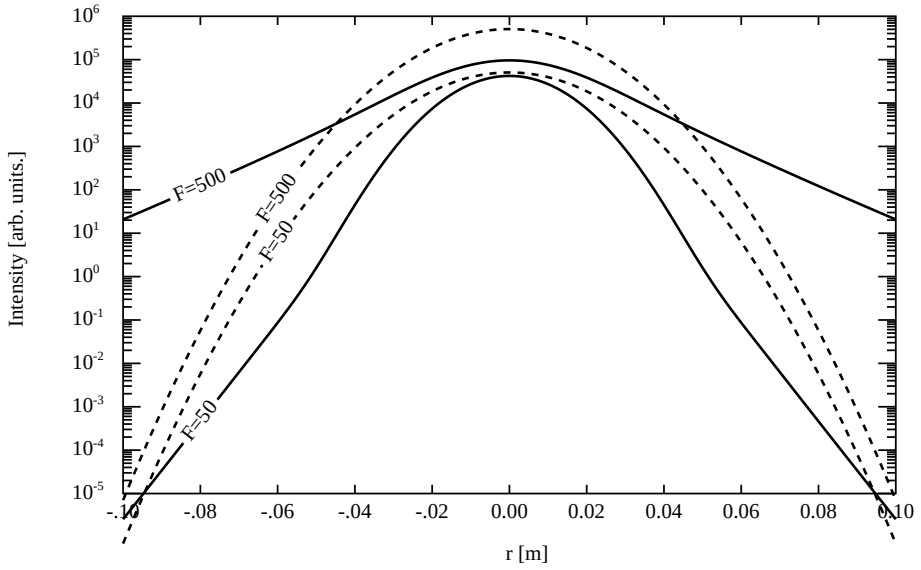

Figure 2.11: Intracavity mode intensity (solid lines) in a 12 m long flat/flat cavity for gaussian input wave w_0=2 cm for two finesses. Dashed lines : gaussian input wave times the surtension

2.6 flat cavities

It is intersting to check what happens when a gaussian mode is launched in a cavity involving flat mirrors. This would happen in the Virgo central zone, in the absence of cavity end mirrors. This is also what happens to the sidebands when antiresonant. Assume the input wave at its waist, of half width w_0. The reflection on flat and perfect mirrors does not affect the diffraction of the beam, so that the mode inside the cavity, of amplitude $E(r)$ can be expressed as the sum of gaussian waves with increasing width, curvature radius and Gouy phase. Let L be the length of the cavity and $b \equiv \pi w_0^2/\lambda$ the Rayleigh parameter of the beam. We have:

$$E(r) \;=\; t \sum_{n=0}^{\infty} R^n \, \mathrm{e}^{2inkL} \frac{w_0}{w_n} \exp\left[-\frac{r^2}{w_n^2} + i\,\frac{kr^2}{2R_n} - i \arctan 2inL/b \right]$$

where $R \equiv r_1\, r_2$ (the product of the reflectivities of the mirrors, t the transmission of the input mirror, and:

$$w_n \;=\; \sqrt{1 + \left(\frac{2nL}{b}\right)^2}$$

$$R_n \;=\; 2nL + \frac{b^2}{2nL}$$

It is easy to check that this is as well:

$$E(r) \;=\; t \sum_{n=0}^{\infty} R^n \, \mathrm{e}^{2inkL} \frac{1}{Z_n} \exp\left[-\frac{r^2}{w_0^2 Z_n}\right]$$

with $Z_n \equiv 1 + 2inL/b$. A numerical investigation shows that the maximum surtension is obtained for $2kL \equiv \pi$, and confirms the intuitive idea that the intracavity mode is close to the incoming one multiplied by the surtension of the cavity (see Fig.2.11), for a moderate finesse, and is widely spread for a high finesse. The reflected wave may have a distorted wavefront for high cavity finesses (see Fig.2.12).

2.7 Hypergaussian modes

2.7.1 construction

It will be shown in a foregoing section that the thermal noise (random motion of the mirror's surface) depends on the area of the light spot on the mirror. Large spots are better than sharp. With this respect, it appears than gaussian modes are not the best choice. The idea of constructing more homogeneous modes has been proposed long time ago by laser scientists in order to better exploit amplifier media: such modes are called hypergaussian. A way of constructing almost flat modes has been explored by D'Ambrosio ([?]). In this work, D'A. was dealing with a symmetrical cavity. In the case of plane-spherical cavities, we try a similar method. On the assumed flat input mirror, we consider the field as a superposition of gaussian modes according to :

$$\Psi(x, y, 0) \;=\; \frac{1}{\pi b^2} \int_{\Delta} dx_0\, dy_0\; \phi(x - x_0, y - y_0)$$

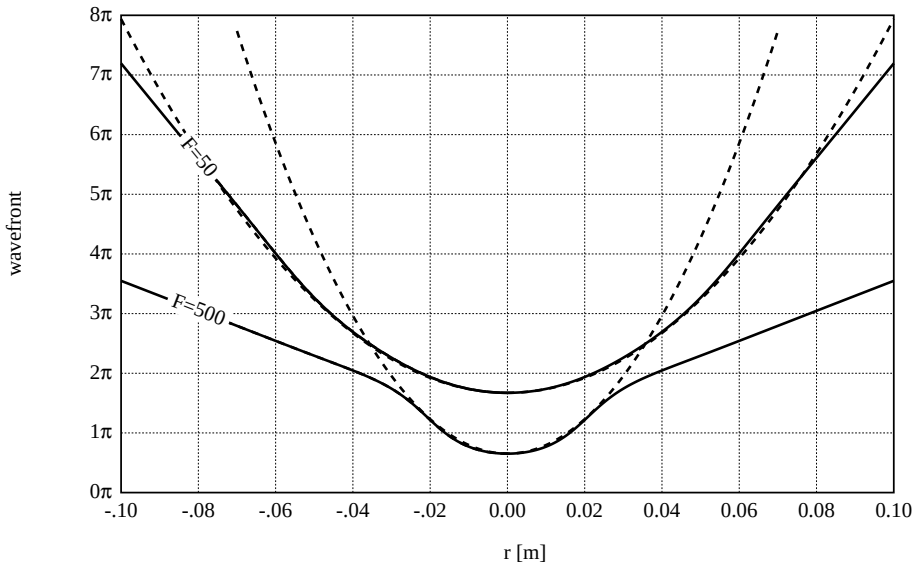

Figure 2.12: Wavefront of reflected wave (solid lines) in a 12 m long flat/flat cavity for gaussian input wave w_0=2 cm for two finesses. Dashed lines : fit of parabolic wavefronts: R=3000 m for F=50, R=1300 m for F=500

where Δ is the disk of radius b, centered at $(x = 0, y = 0)$, and where

$$\phi(x,y) \;=\; \sqrt{\frac{2}{\pi w_0^2}} \exp\left[-\frac{x^2+y^2}{w_0^2}\right]$$

is a classical TEM_{00} mode. In other words, Ψ is the superposition of such modes with various offsets, uniformly distributed on the disk of radius b. Remark (though it is fairly clear) that $\Psi(x,y,z)$ is actually a solution of the paraxial diffraction equation, for it is a linear combination of solutions. It is straightforward to express the field propagated at a distance z, propagation of each elementary gaussian mode being known:

$$\Psi(x,y,z) \;=\; 2\sqrt{\frac{2}{\pi w^2}}\,\frac{w^2}{b^2}\;\psi_{00}(r,z)\mathrm{e}^{-iArctan(z/z_R)} \qquad (r \;\equiv\; \sqrt{x^2+y^2})$$

with

$$\psi_{00}(r,z) \;\equiv\; \int_0^{b/w} \mathrm{e}^{-Z(r/w-u)^2}\;\mathrm{e}^{-2Zru/w}\;I_0(2Zru/w)\;u\,du$$

where $Z \equiv 1 - iz/z_R$ ($z_R \equiv \pi w_0^2/\lambda$ being the Rayleigh parameter), and where $I_0(z)$ denotes the 1st kind modified Bessel function. w is the beam width at the distance z, i.e.

$$w = w_0\sqrt{1 + z^2/z_R^2}$$

Following E.d'A, we have taken the following values (L being the length of the cavity):

$$w_0 \;=\; \sqrt{\frac{\lambda L}{\pi}} \;\simeq\; 3.2 \text{ cm}$$

$$b \;=\; 4w_0 \;\simeq\; 12.8 \text{ cm}$$

The integral $\psi_{00}(r,z)$ can be evaluated numerically by a simple Simpson numerical integration technique, the function $\exp(-z)I_0(z)$ having a quite simple behavior. The initial intensity profile is as shown on Fig.2.13 The intensity profile after 3 km propagation is plotted on Fig.2.14. The wavefront is shown on Fig.2.15

2.7.2 Angular aperture and Fourier transform

It is remarkable that the mode is practically unchanged along the propagation. The difficult point is to make a mirror having the profile shown on

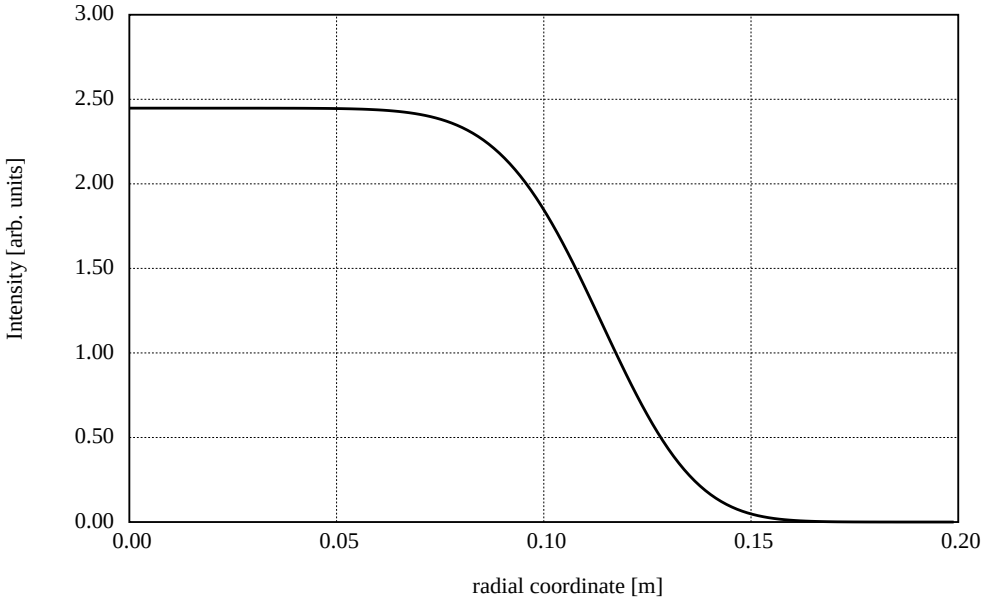

Figure 2.13: Intensity profile on the flat input mirror

Fig.2.15. The aperture angle of the beam is obviously much smaller than the gaussian's. On the flat mirror, The beam may be viewed as the convolution product of a gaussian of waist w_0 with a uniform distribution on the disk $r < b$. The Fourier transform of the beam amplitude is therefore the simple product of the Fourier transform of the elementary gaussian beam with that of the disk. A detailed calculation gives thus,

$$\tilde{\Psi}(p,q,0) \;=\; 2\sqrt{2\pi w_0^2}\,\exp\left(-w_0^2\rho^2/4\right)\,\frac{J_1(\rho b)}{\rho b}$$

where $\rho^2 \equiv p^2 + q^2$. By identifying $\rho = k\,\theta$, we get

$$|\tilde{\Psi}(p,q,0)|^2 \;=\propto\; \exp\left(-2\theta^2/\theta_g^2\right)\,\left[\frac{2J_1(\theta/\theta_b)}{\theta/\theta_b}\right]^2$$

where $\theta_g = \lambda/\pi w_0$ is the gaussian aperture angle, and $\theta_b = \lambda/2\pi b$ is the Bessel aperture angle. For $w_0 = 2$ cm and $b = 10$ cm, θ_b happens to be 10 times smaller than θ_g, and the aperture angle is practically determined by θ_b (see Fig. 2.16). This is consistent with the fact that the width of the beam is practically constant along the diffraction length.

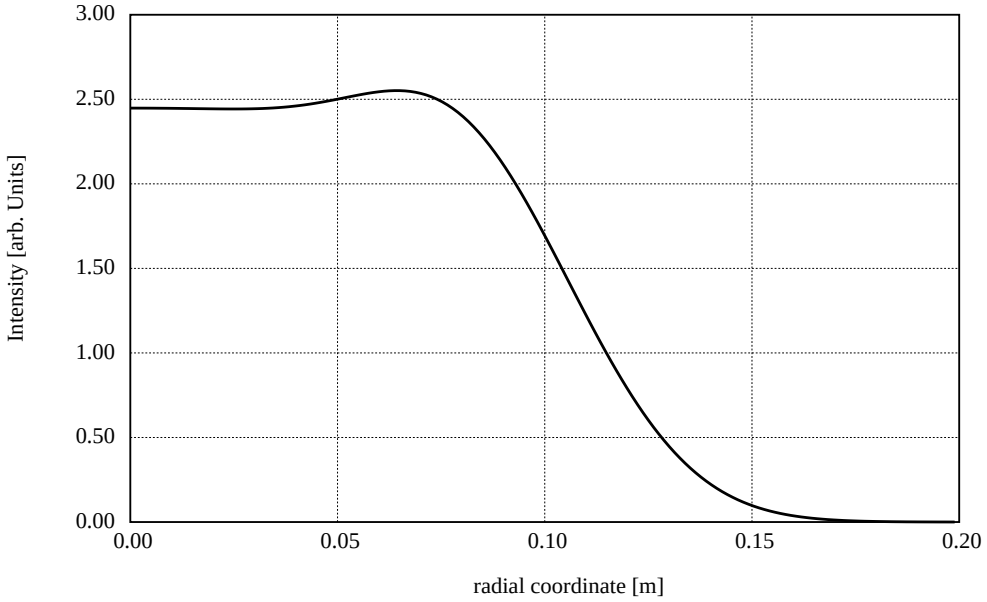

Figure 2.14: Intensity profile at 3 km

2.7.3 Normalization

It is difficult to compute directly the power carried by such a mode by simply integrating the intensity in the plane (x, y). Instead, we do it in the Fourier space. Owing to the Parseval-Plancherel theorem, we can write for the norm P:

$$P \;=\; \int |\Psi(x,y)|^2\, dx\, dy \;=\; \frac{1}{4\pi^2} \int |\tilde{\Psi}(p,q,0)|^2\, dp\, dq \qquad (2.33)$$

so that, using a precedent result:

$$P \;=\; 2\,\frac{w_0^2}{b^2} \;\times\; 2\int_0^\infty \exp(-w_0^2 x^2/2b^2)\,\frac{J_1(x)^2}{x}\, dx \qquad (2.34)$$

The integral can be carried out, yielding:

$$P(w_0, b) \;=\; 2\,\frac{w_0^2}{b^2}\, F_{00} \qquad (2.35)$$

with

$$F_{00} \;\equiv\; 1 \;-\; \exp(-b^2/w_0^2)\,\left[I_0(b^2/w_0^2) + I_1(b^2/w_0^2)\right]$$

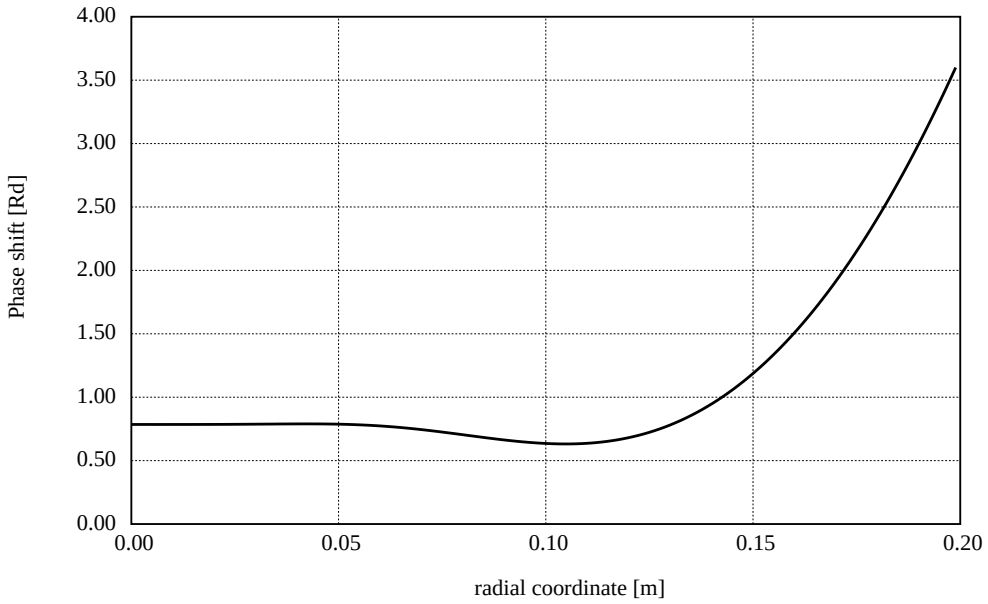

Figure 2.15: Wavefront at 3 km

where $I_0(z)$ and $I_1(z)$ are the modified Bessel functions of the 1st kind. When w_0 is small, so that b/w_0 is large, using the asymptotic values of the Bessel functions we get:

$$F_{00} \equiv 1 - \frac{2w_0}{\sqrt{\pi}b}\left[1 - \frac{w_0^2}{8b^2} - \frac{3w_0^4}{128b^4} - \frac{45w_0^6}{3072b^6} - ...\right] \tag{2.36}$$

The normalized flat mode at its waist is:

$$\Psi(x,y,0) = \frac{1}{\pi\, b\, w_0\, \sqrt{2F_{00}}} \int_\Delta dx_0\, dy_0\ \phi(x-x_0, y-y_0) \tag{2.37}$$

and finally, at any distance z:

$$\Psi(x,y,z) = \mathrm{e}^{-i\arctan(z/z_R)} \times$$
$$\times \frac{2w}{w_0 b\sqrt{\pi F_{00}}} \int_0^{b/w} \exp\left[-Z(r/w-\rho)^2\right] \exp(-2Zr\rho/w)\, I_0(2Zr\rho/w)\, \rho\, d\rho \tag{2.38}$$

with the same notation as above:

$$Z \equiv 1 - iz/z_R,\ z_R \equiv \pi w_0^2/\lambda,\quad w \equiv w_0\sqrt{Z.\overline{Z}}$$

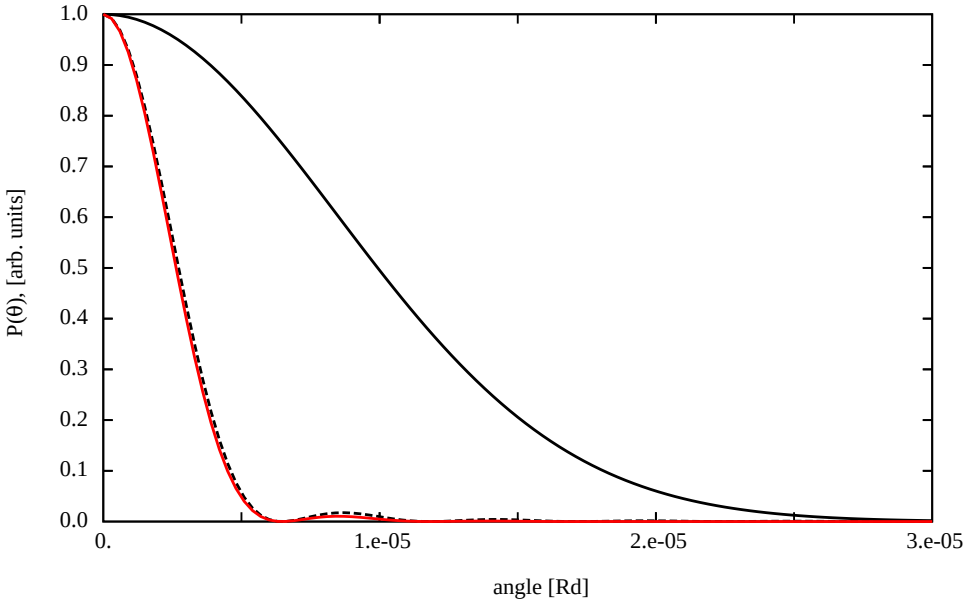

Figure 2.16: Angular distribution of the flat beam. Solid line: gaussian distribution, dashed line: circular aperture. Red dashed line: resulting angular distribution

2.7.4 Coupling with gaussian beams

It is of some importance to know the coupling rate of such flat beams with ordinary gaussian modes. We can for this compute the scalar product of the flat mode $\Psi(x,y)$ with for instance the fundamental gaussian mode of waist w : $\phi_{00}(x,y)$, at their common waist:

$$\Gamma_{00} \equiv \langle \Psi, \phi_{00} \rangle = \sqrt{\frac{2}{\pi w^2}} \sqrt{\frac{2}{\pi w_0^2}} \frac{1}{\pi b^2} \int_\Delta dx_0\, dy_0 \int_{\mathrm{R}^2} dx\, dy$$
$$\exp\left[-\frac{x^2+y^2}{w^2}\right] \exp\left[-\frac{(x-x_0)^2+(y-y_0)^2}{w_0^2}\right] \tag{2.39}$$

after some elementary algebra, we find:

$$\Gamma_{00} = \frac{2w_0 w}{b^2} \left\{1 - \exp\left[-\frac{b^2}{w_0^2+w^2}\right]\right\} \tag{2.40}$$

The power directly coupled from a gaussian beam into a flat beam (i.e. Γ_{00}^2) is thus extremely weak. We give on Fig.2.17 a plot of this power transfer versus the waist of the incoming gaussian beam, showing that only a few percent of the power can be this way injected in a flat beam. The coupling becomes worse and worse as the parameter b increases, and as the parameter w_0 decreases (the most the flat beam is interesting for thermal noise, the worst is its direct coupling to a gaussian beam). It is thus necessary to devise other ways of coupling power into flat-beam cavities.

2.7.5 Diffraction losses of flat beams

Flat beams have been seen to have a wide extension on the mirrors (this is exactly the reason why they have been designed). It may be useful to have an idea of the diffraction losses for such modes. How the clipping of the beam by a finite mirror reduces the reflected power. The following figure (2.18) shows the decrease of diffraction losses for two cases :b = 10 cm, 12 cm and w_0 = 3.2 cm. We see that for Virgo-like mirrors (a = 17.5 cm), the diffraction losses are negligible.

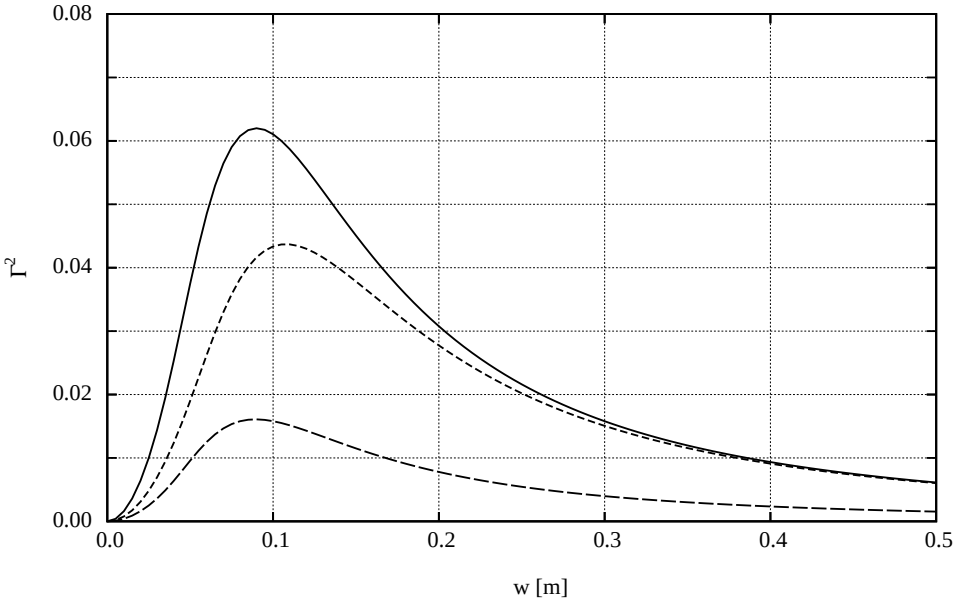

Figure 2.17: Coupling rate of a gaussian beam of waist w into a flat mode of parameters w_0, b. Solid line: $b = 10$ cm, $w_0 = 2$ cm. Short dashed line : $b = 12$ cm,$w_0 = 2$ cm. Long dashed line : $b = 10$ cm, $w_0 = 1$ cm.

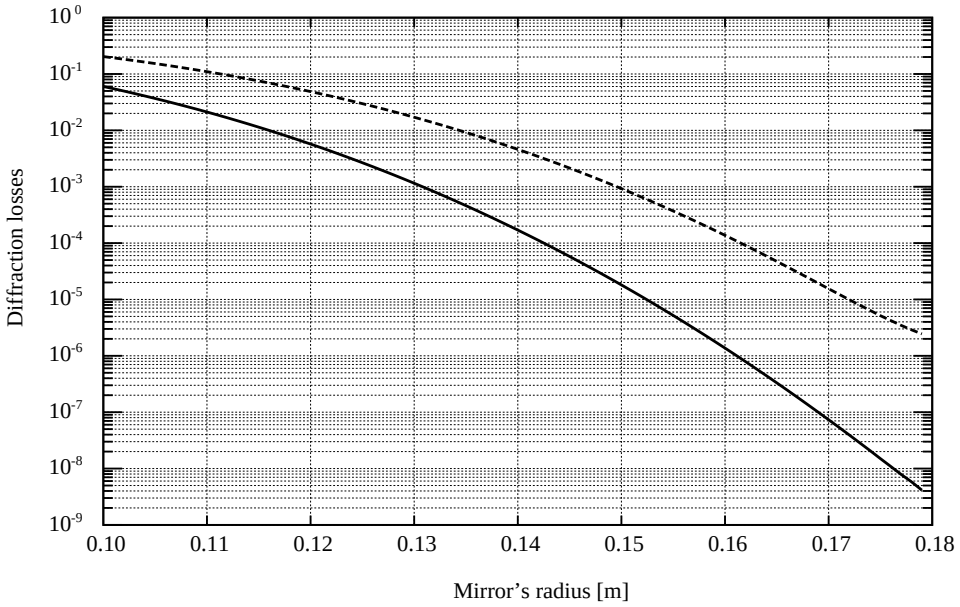

Figure 2.18: Diffraction losses of a flat beam of parameters $b = 10$ cm (solid line), $b = 12$ cm (dashed line) and $w_0 = 3.2$ cm

Chapter 3

Mirrors standard thermal noise

standard thermal noise is the phase noise caused by random motions of the reflecting faces of mirrors in a GW interferometer. A reflecting face can move either because it is displaced by its suspension system, or because it undergoes internal stresses. At finite temperature, the two effects are possible. We address here the internal stresses. Consider a massive body at temperature T. If $T > 0$, the atoms constituting the body are excited and have random motions around their equibrium position. The fact that they are strongly coupled to neighboring atoms makes possible propagation of elastic waves of various types, reflecting on the faces and the onset of stationary waves. One can show that, for a finite body (like for instance a cylinder of silica), there is a discrete infinity of such stationary waves, each corresponding to a particular elastic *normal mode*. At thermal equilibrium, the state of the body can be represented by a linear superposition of all the modes, with random relative phases, and, due to the energy equipartition theorem, the same energy $k_B T$ (k_B is the Boltzmann constant). The motion of atoms near a limiting surface of the body will slightly modify its shape, and if we consider the reflecting face of a mirror, a surface distortion is a possible cause of phase change in the reflected beam, in other words, of a noise. Estimation of the resulting spectral density of phase noise is the *internal thermal noise* problem in massive mirrors.

3.1 Damped harmonic oscillator

Each internal mode is characterized by its eigenfrequency, its geometry and its amplitude. Determination of the eigenfrequencies and of the eigenmodes of an arbitrary body is in general difficult, but the amplitude is a scalar x obeying a dynamical equation analogous to the harmonic oscillator's. If we consider the decoupled and undamped oscillator, this is :

$$\frac{d^2x}{dt^2} + \omega_0^2 x \;=\; 0$$

where $\omega_0/2\pi$ is the eigenfrequency of the mode. At thermal equilibrium with the environment (the heat bath), the amplitude follows a random walk so that the potential and kinetic energies have equal means, each being equal to $k_BT/2$ ($k_B \sim 1.38 \times 10^{-23}$J.K^{-1} is the Boltzmann constant). For the potential energy, we have

$$E_P \;=\; \frac{1}{2} m\omega_0^2 x^2$$

by taking the expectation value, and assuming a zero mean of x, this gives

$$V(x) \;=\; \frac{k_BT}{m\omega_0^2}$$

It is important to understand that though very small, the displacement-like variable x is, at room temperature much larger than GW induced ($x_{gw} \sim 10^{-18}$ m) displacements. Assume for instance a frequency of $2\pi \times 1000$ Hz and an equivalent mass of 10 kg (in fact the masses equivalent to modes are even smaller), we get a standard deviation

$$\sigma(x) \;=\; 3 \times 10^{-15} \text{ m}$$

At first sight, this seems to definitely forbid any GW detection. Even by cooling at very low temperature (say 1 mK), the result is still much too high.

In fact and fortunately, this is not true if we take into account the frequency distribution of the noise. If we introduce simultaneously a random driving force (Langevin force) $F(t)$ and a damping factor γ accounting for dissipation, we couple the oscillator to the heat bath : the driving force expresses action of the external world on the oscillator, whereas the damping factor releases the received energy, so that the energy of the oscillator is statistically stationary. The motion equation is (case of viscous damping) :

$$\frac{d^2x}{dt^2} + \gamma\,\frac{dx}{dt} + \omega_0^2\, x \;=\; F(t)/m$$

By taking the Fourier transform, this is

$$\tilde{x}(\omega) \;=\; \frac{1}{m}\,\frac{\tilde{F}(\omega)}{\omega_0^2-\omega^2+i\gamma\,\omega}$$

The relation between the spectral densities of x and F must therefore be :

$$S_x(f) \;=\; S_F(f)\,\frac{1}{m^2}\,\frac{1}{(\omega^2-\omega_0^2)^2+\gamma^2\omega^2}$$

S_F is a constant (white noise) , its value can be determined by requiring that

$$\int_0^\infty S_x(f)\,df \;=\; V(x) \;=\; \frac{k_BT}{m\omega_0^2}$$

We have obviously

$$\int_0^\infty S_x(f)\,df \;=\; \frac{1}{2}\int_{-\infty}^\infty S_x(\omega)\,\frac{d\omega}{2\pi}$$

so that

$$S_F\int_{-\infty}^\infty \frac{d\omega}{(\omega^2-\omega_0^2)^2+\gamma^2\omega^2} \;=\; \frac{4\pi k_BTm}{\omega_0^2}$$

For carrying out the integration, it is convenient to set

$$(\omega^2-\omega_0^2)^2+\gamma^2\omega^2=(\omega^2-\Omega^2)(\omega^2-\overline{\Omega}^2)$$

where

$$\Omega^2=\omega_0^2-\gamma^2/2+i\,\gamma\,\sqrt{\omega_0^2-\gamma^2/4}$$

so that

$$\Omega \;=\; \sqrt{\omega_0^2-\gamma^2/4}+i\,\gamma/2$$

then the integral can be split into two terms, giving

$$S_F\int_{-\infty}^\infty\left[\frac{1}{\omega^2-\Omega^2}-\frac{1}{\omega^2-\overline{\Omega^2}}\right]\frac{d\omega}{\Omega^2-\overline{\Omega^2}} \;=\; \frac{4\pi k_BTm}{\omega_0^2}$$

The Cauchy theorem gives (provided that $\gamma>0$) :

$$\int_{-\infty}^\infty \frac{d\omega}{\omega^2-\Omega^2} \;=\; \frac{i\pi}{\Omega}$$

so that the integral reduces to $\pi/\gamma\omega_0^2$, and the result for the spectral density of Langevin force is:

$$S_F = 4k_BTm\gamma$$

The spectral density of displacement is finally:

$$S_x(f) = \frac{4k_BT\gamma/m}{(\omega^2-\omega_0^2)^2+\gamma^2\omega^2} \tag{3.1}$$

The mechanical *quality factor* Q is defined as

$$Q = \omega_0/\gamma \tag{3.2}$$

The main features are:

$$\omega \to 0 \Rightarrow S_x(f) \to \frac{4k_BT}{mQ\omega_0^3}$$

$$\omega \to \omega_0 \Rightarrow S_x(f) \to \frac{4k_BQ}{m\omega_0^3}$$

$$\omega \to \infty \Rightarrow S_x(f) \to \frac{4k_BT\omega_0}{mQ\omega^4}$$

so that the spectral density is a constant for low frequencies, and the root spectral density is $1/Q$ the value at resonance. On Fig.3.1, one sees the general philosophy of thermal noise. The integral of the spectral density S_x is independent on Q, but by increasing Q, we can concentrate the SD in the neighborhood of the resonance, which becomes more and more narrow, and reduce the thermal noise outside the resonance. This is why high-Q material and fixations are searched for, in GW experiments. Heavy test masses and low temperatures have been also obviously proposed a number of times.

3.2 The FD theorem

There is a more general derivation of the spectral density, based on the *Fluctuation-Dissipation Theorem* (FD), due to Callen and Welton [21] : For an elementary dynamical system described by a degree of freedom x and any driving force F, one can consider the resulting velocity $\tilde{v} = i\omega\tilde{x}$, and compute a mechanical impedance as $Z = \tilde{v}/\tilde{F}$. Then, (this is the FD theorem):

$$S_x(f) = \frac{4k_BT}{\omega^2}\Re e[Z] \tag{3.3}$$

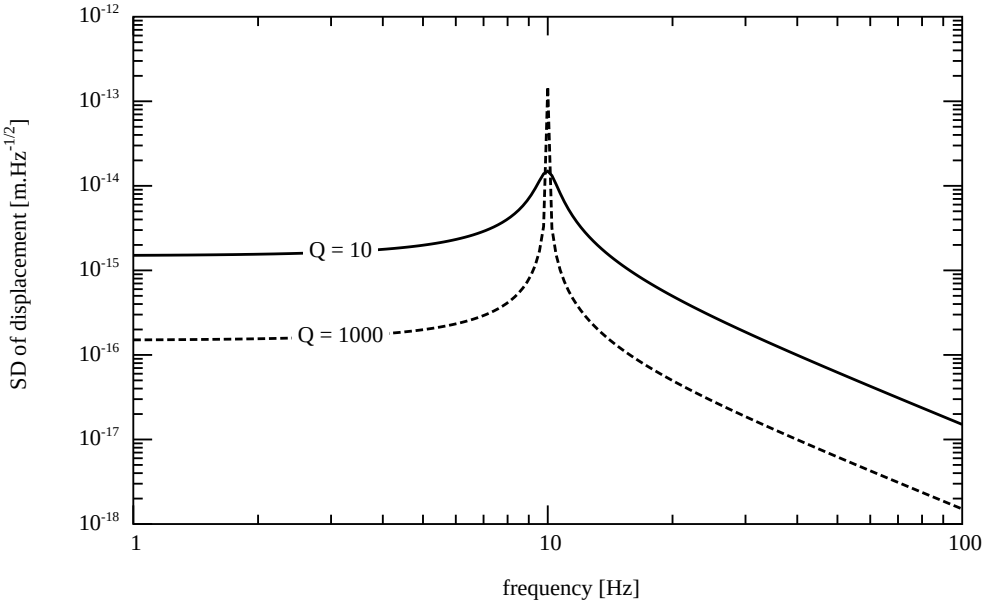

Figure 3.1: sqrt of spectral density of thermal displacement : viscous damping

In the preceding case, for instance, we had

$$Z(\omega) \;=\; \frac{i\,\omega/m}{\omega_0^2 - \omega^2 + i\,\gamma\omega}$$

from where 3.1 follows directly. But this approach allows to obtain results more difficult to derive by other means. For instance, if we consider a solid resonator, as for instance a mirror substrate, dissipation of the elastic energy is not caused by viscosity, but rather by thermoelastic processes: stressed regions are heated, and there is a heat flow from hot to cold regions due to finite thermal consuctivity leading to irreversibility. A very simple model of thermoelastic dissipation is given by a complex elastic stiffness, the motion equation being in some frequency domain:

$$\left[-\omega^2 + \omega_0^2\,(1 + i\Phi)\right]\,\tilde{x}(\omega) \;=\; \tilde{F}/m$$

where Φ is the so-called loss angle, often considered as independent on the frequency. It may be seen as the inverse of the quality factor. We have thus:

$$\tilde{x}(\omega) \;=\; \frac{\tilde{F}/m}{\omega_0^2 - \omega^2 + i\Phi\omega_0^2} \tag{3.4}$$

In order to determine the function F, we can no more use the direct approach of integrating over frequencies to recover the variance, because we know that the eq. 3.4 is only valid in some frequency domain. However, by using the FD theorem (eq.3.3), we get

$$S_x(f) \;=\; \frac{4k_BT\omega_0^2\Phi}{m\omega}\;\frac{1}{(\omega^2-\omega_0^2)^2+\omega_0^4\,\Phi^2}$$

This formula clearly holds above some cut-off frequency. It is essential to note the very different behavior of this thermoelastic spectral density with respect to the viscoelastic.

$$\omega \to 0 \;\Rightarrow\; S_x(f) \to \frac{4k_BT}{mQ\omega\omega_0^2}$$

$$\omega \to \omega_0 \;\Rightarrow\; S_x(f) \to \frac{4k_BQ}{m\omega_0^3}$$

$$\omega \to \infty \;\Rightarrow\; S_x(f) \to \frac{4k_BT\omega_0^2}{mQ\omega^5}$$

(see Fig.3.2) This is a common behavior for all internal modes of solid resonators, each being viewed as a thermoelastically damped harmonic oscillator. It is possible to numerically compute resonance frequencies of a cylindrical solid (as the mirror substrates), associate such a model to each corresponding mode (the question of the effective mass of the mode is raised), and sum up to find the global noise. Anyway, the increase of the thermal noise at low frequency is presently the main limitation to GW detectors.

3.3 The Levin generalized coordinate method

We can now address the problem of internal degrees of freedom in the mirrors. Internal elastic waves eventually distort the reflecting surface, causing a phase noise. We have already discussed the way of obtaining the information on

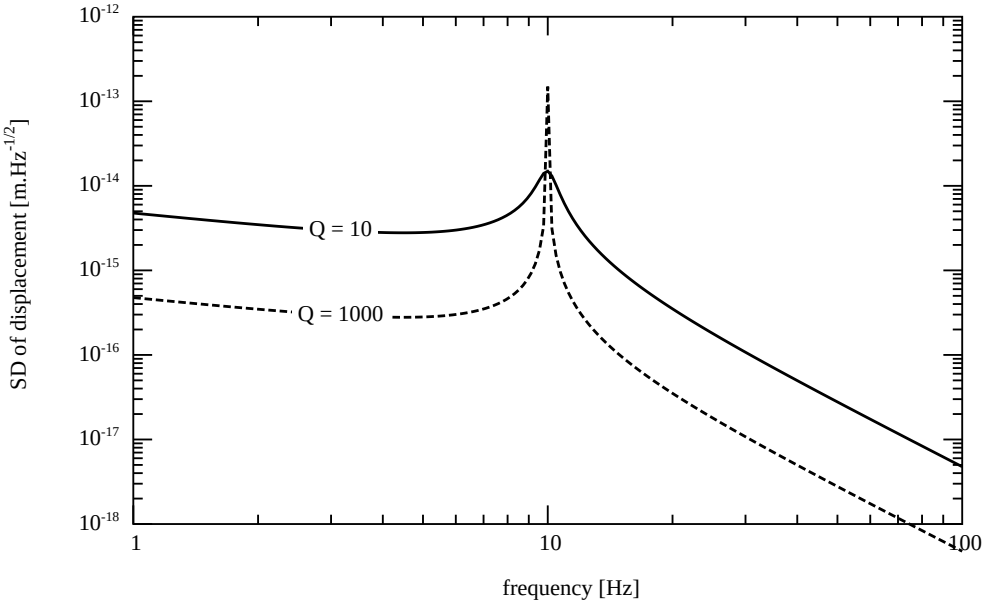

Figure 3.2: sqrt of spectral density of thermal displacement : thermoelastic damping

the surface relevant for the beam. Let $u_z(t,x,y)$ be the z component of the displacement vector of matter at the surface of the mirror. The equivalent displacement (generalized coordinate x) is

$$x(t) \;=\; \iint u_z(t,x,y)\, I(x,y)\, dx\, dy$$

where $I(x,y)$ is the normalized light intensity distribution in the TEM_{00} mode assumed to be the readout beam. We now follow the method proposed by Levin ([20]). Let $F(t)$ be the corresponding driving force. The interaction energy is

$$\mathcal{E} \;=\; -F(t)\, x(t)$$

or

$$\mathcal{E} \;=\; \iint u_z(t,x,y)\, F(t)\, I(x,y)\, dx\, dy$$

where the displacement u may be thought of as beeing caused by the pressure distribution $F \times I$. We address now the case of low frequencies. This case is

very relevant, because resonances of mirrors are at relatively high frequencies (several kHz) and the region where internal thermal noise is disturbing lies long before the first resonance, in the low frequency regime. Thus, although a general knowledge on internal thermal noise is useful, it is nevertheless extremely interesting to have the low frequency tail. This can be obtained as follows. If we consider a force $F(t) = F\mathrm{e}^{i\omega t}$ oscillating at very low frequency, the frequency will be lower than the cut-off for any standing waves. the pressure $F \times I$ will produce an oscillating stationary displacement u, of the form

$$u_z(t,x,y) = \mathrm{e}^{i(\omega t - \phi)} u(x,y)$$

this is equivalent to neglecting inertial forces in the motion of matter. The phase ϕ represents a retardation effect that dissipation may cause. In the Fourier domain, this is

$$u_z(\omega,x,y) \;=\; (1 - i\phi) u_z(x,y)$$

the impedance is

$$Z(f) \;=\; i\omega \, \frac{(1-i\phi) \int\int u_z(x,y)\, I(x,y)\, dx\, dy}{F}$$

so that

$$\Re e[Z] \;=\; \omega\, \phi \, \frac{\int\int u_z(x,y)\, F.I(x,y)\, dx\, dy}{F^2}$$

where the numerator of the fraction appears as the elastic energy stored in the solid stressed by the pressure distribution $F.I$. The strain energy is defined in classical elasticity theory by

$$W \;=\; \frac{1}{2} \int\int u_z(x,y) p(x,y)\, dx\, dy$$

where $p(x,y)$ is the pressure distribution causing the displacement $u_z(x,y)$ at the surface where it is applied. We can thus write for the spectral density of displacement :

$$S_x(f) \;=\; \frac{4k_B T}{\pi f}\, \phi\, \frac{W}{F^2}$$

in fact, W is proportional to F^2, so that $U \equiv W/F^2$ is the strain energy for a static pressure normalized to 1 N. The SD of displacement takes the general (low frequency) form :

$$S_x(f) \;=\; \frac{4k_B T}{\pi f}\, \phi\, U \tag{3.5}$$

The problem is reduced to the computation of U. This can be difficult in the general case of an arbitrary solid, but numerical finite element codes are able to give more or less accurate estimates. It is however possible to obtain analytic solutions in the case of axial symmetry.

3.4 Basic linear elasticity

We recall here the principles and master formulas of the linear elasticity theory.

3.4.1 displacement, strain, stress

Let a solid be decribed in the (x,y,z) coordinate system by its reference state, and its deformed state

$$x_i \to x_i + u_i(x_k)$$

The vector **u** is called *displacement* vector. The strain tensor E_{ij} is defined as

$$E_{ij} = \frac{1}{2}(\partial_i u_j + \partial_j u_i)$$

Its trace is

$$E = \sum_{i=1}^{3} E_{ii}$$

The stress tensor Θ_{ij} is linearly related to the strain tensor in a way generalizing Hooke's law. For isotropic solids (like silica), the relation is very simple :

$$\Theta_{ij} = \lambda\, \delta_{ij} E + 2\mu\, E_{ij}$$

the two parameters (λ, μ) are called Lamé coefficients. They are related to the Young modulus Y and the Poisson ratio σ by

$$\lambda = \frac{Y\sigma}{(1+\sigma)(1-2\sigma)}$$

$$\mu = \frac{Y}{2(1+\sigma)}$$

3.4.2 Elastodynamics equation

The elastodynamics equation is :

$$\partial_j \Theta_{ij} \;=\; \rho\, \partial_t^2 u_i$$

which in the static case reduces to the equilibrium equation

$$\partial_j \Theta_{ij} \;=\; 0$$

In polar coordinates (r, ϕ, z), the strain tensor has coordinates

$$E_{rr},\ E_{r\phi},\ E_{rz},\ E_{\phi\phi},\ E_{z\phi},\ E_{zz}$$

defined by :

$$\begin{aligned}
E_{rr} &= \partial_r u_r \\
E_{r\phi} &= \frac{1}{2}\left(\partial_r u_\phi - \frac{u_\phi}{r} + \frac{1}{r}\,\partial_\phi u_r\right) \\
E_{rz} &= \frac{1}{2}\left(\partial_r u_z + \partial_z u_r\right) \\
E_{\phi\phi} &= \frac{1}{r}\partial_\phi u_\phi + \frac{u_r}{r} \\
E_{z\phi} &= \frac{1}{2}\left(\frac{1}{r}\partial_\phi u_z + \partial_z u_\phi\right) \\
E_{zz} &= \partial_z u_z
\end{aligned}$$

The elastodynamics equation reads in detail

$$\left\{\begin{array}{l}
\partial_r \Theta_{rr} + \frac{1}{r}\left(\Theta_{rr} - \Theta_{\phi\phi}\right) + \frac{1}{r}\partial_\phi \Theta_{r\phi} + \partial_z \Theta_{rz} \;=\; \rho\, \partial_t^2 u_r \\
(\partial_r + \frac{2}{r})\Theta_{r\phi} + \frac{1}{r}\partial_\phi \Theta_{\phi\phi} + \partial_z \Theta_{\phi z} \;=\; \rho\, \partial_t^2 u_\phi \\
(\partial_r + \frac{1}{r})\Theta_{rz} + \frac{1}{r}\partial_\phi \Theta_{\phi z} + \partial_z \Theta_{zz} \;=\; \rho\, \partial_t^2 u_z
\end{array}\right. \tag{3.6}$$

In the special case of static axial symmetry, the system reduces to the *equilibrium* equation :

$$\left\{\begin{array}{l}
\partial_r \Theta_{rr} + \frac{1}{r}\left(\Theta_{rr} - \Theta_{\phi\phi}\right) + \partial_z \Theta_{rz} \;=\; 0 \\
(\partial_r + \frac{1}{r})\Theta_{rz} + \partial_z \Theta_{zz} \;=\; 0
\end{array}\right. \tag{3.7}$$

3.4.3 Boundary conditions

The boundary conditions express the balance between internal stresses and external pressures at the limiting surfaces :

$$[\sum_j \Theta_{ij} n_j]_\Sigma \;=\; p_i$$

where n_i is the normal to surface Σ

3.5 Mirror as a half-space

If the spot of the readout beam on a mirror is centered and small compared to the mirror's dimensions (radius, thickness), we can consider the substrate as an infinite half-space limited by a plane (the optical curvature is negligible here). The problem obeys the axial symmetry and it is easy to verify that there is a solution of 3.7 of the form :

$$u_r(r,z) \;=\; \left(\alpha - \frac{\lambda+2\mu}{\lambda+\mu}\,\beta + \beta\, kz\right)\,\mathrm{e}^{-kz} J_1(kr)$$

$$u_z(r,z) \;=\; \left(\alpha + \frac{\mu}{\lambda+\mu}\,\beta + \beta\, kz\right)\,\mathrm{e}^{-kz} J_0(kr)$$

where (α, β, k) are arbitrary constants. The J_n are the Bessel functions. The region occupied by the substrate is supposed to extend from $z = 0$ till infinity. The boundary conditions are

$$[\Theta_{rz}]_{z=0} \;=\; 0$$

and

$$[\Theta_{zz}]_{z=0} \;=\; p(r)$$

where $p(r)$ is the gaussian pressure having the beam's profile and normalized to 1 N (the integral over the whole plane of a pressure is a force):

$$p(r) \;=\; \frac{2}{\pi w^2}\mathrm{e}^{-2r^2/w^2}$$

It is easy to compute the stresses :

$$\Theta_{rz} \;=\; 2\mu\, k\,(\beta - \alpha - \beta\, kz) J_1(kr)$$

$$\Theta_{zz} \;=\; -2\mu\, k\,(\alpha + \beta\, kz) J_0(kr)$$

The first boundary condition gives $\alpha = \beta$. The solution depends now on two arbitrary constants (α, k). In fact the most general solution will be an integral over k :

$$u_r(r,z) \;=\; \int_0^\infty \alpha(k)\, \left(-\frac{\mu}{\lambda+\mu} + kz\right) \mathrm{e}^{-kz} J_1(kr) k\, dk$$

$$u_z(r,z) \;=\; \int_0^\infty \alpha(k)\, \left(\frac{\lambda+2\mu}{\lambda+\mu} + kz\right) \mathrm{e}^{-kz} J_0(kr) k\, dk$$

and now, $\alpha(k)$ refers to an arbitrary function of k. The Θ_{zz} stress component becomes :

$$\Theta_{zz}(r, z=0) \;=\; -2\mu \int_0^\infty \alpha(k) J_0(kr)\, k^2\, dk$$

so that the last boundary condition becomes

$$\int_0^\infty \alpha(k) J_0(kr)\, k^2\, dk \;=\; -\frac{1}{2\mu}\, p(r) \tag{3.8}$$

This expresses a Bessel transform. Recall that for functions admitting a Fourier transform, the two reciprocal Fourier transforms become, for axially symmetrical functions, reciprocal Bessel transforms :

$$\tilde{f}(\rho) \;=\; \int_0^\infty J_0(\rho r) f(r)\, r\, dr$$

and

$$f(r) \;=\; \int_0^\infty J_0(\rho r) \tilde{f}(\rho)\, \rho\, d\rho$$

we have thus, inverting the Bessel transform in 3.8 :

$$k\alpha(k) \;=\; -\frac{1}{2\mu} \int_0^\infty p(r)\, J_0(kr)\, r\, dr$$

It is possible to carry out the integration (see [17], Eq. **11.4.29**), obtaining

$$\alpha(k) \;=\; -\frac{1}{4\pi\mu k}\, \mathrm{e}^{-k^2 w^2/8}$$

and consequently a displacement

$$u_z(r, z=0) \;=\; -\frac{\lambda+2\mu}{\mu(\lambda+\mu)} \frac{1}{4\pi} \int_0^\infty \mathrm{e}^{-k^2 w^2/8}\, J_0(kr)\, dk \tag{3.9}$$

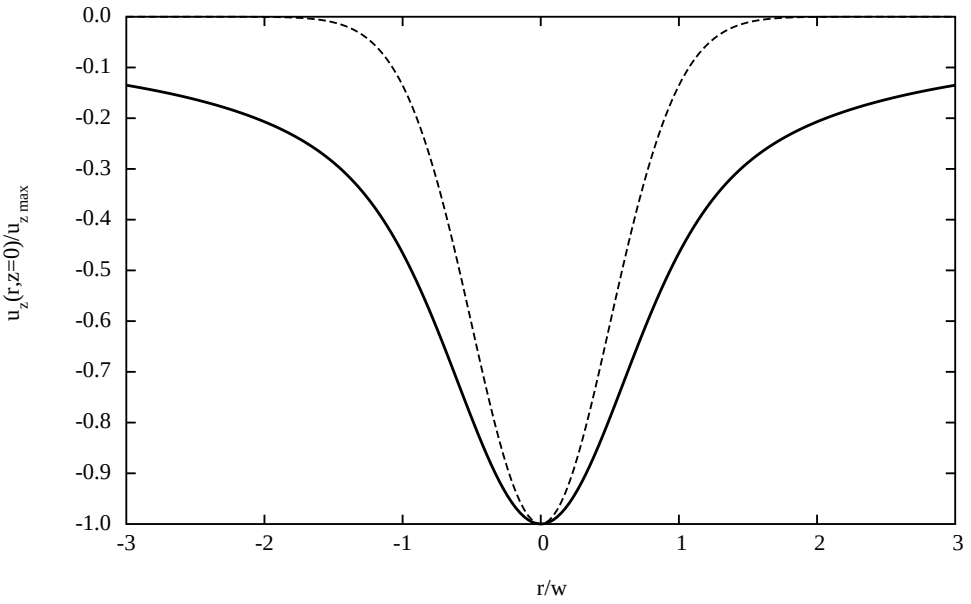

Figure 3.3: Displacement of the surface of an infinite substrate under gaussian pressure. The dashed line recalls the beam profile. The surface is assumed infinite (radius much larger than the beam width)

the integral can be found in tables of Bessel transforms [22], then converting (λ, μ) into (Y, σ) leads to :

$$u_z(r, z=0) \;=\; -\frac{1-\sigma^2}{Y}\sqrt{\frac{2}{\pi w^2}}\, I_0(r^2/w^2)\, \mathrm{e}^{-r^2/w^2}$$

where I_0 refers to the modified Bessel function. The profile of the displacement is shown in Fig.3.3. But we are interested in the strain energy, which can be calculated using

$$U \;=\; -\frac{1}{2}\int\!\!\int u_z(r, z=0)\, p(r)\, r\, dr\, d\phi$$

that is

$$U \;=\; \frac{1-\sigma^2}{Y}\,\frac{2}{\pi w^2}\int_0^\infty r\, dr\, \mathrm{e}^{-2r^2/w^2} \int_0^\infty dk\, \mathrm{e}^{-k^2 w^2/8} J_0(kr)$$

$$= \frac{1-\sigma^2}{Y}\frac{2}{\pi w^2}\int_0^\infty dk\,\mathrm{e}^{-k^2w^2/8}\int_0^\infty r\,dr\,\mathrm{e}^{-2r^2/w^2}\,J_0(kr)$$
$$= \frac{1-\sigma^2}{Y}\frac{2}{\pi w^2}\int_0^\infty dk\,\mathrm{e}^{-k^2w^2/8}\,\frac{w^2}{4}\,\mathrm{e}^{-k^2w^2/8}$$
$$= \frac{1-\sigma^2}{2\sqrt{\pi}Yw}$$

And finally, the spectral density of internal thermal noise takes the very simple expression

$$S_z(f) = \frac{4k_BT}{\pi f}\,\Phi\,\frac{1-\sigma^2}{2\sqrt{\pi}Yw} \tag{3.10}$$

with values such that $Y \sim 7.3\times10^{10}\mathrm{Nm}^{-2}$, $\sigma \sim 0.17$, $w = 0.02$ m, and a loss angle of $\Phi \sim 10^{-6}$, we get a root spectral density

$$S_z^{1/2}(f) \sim 10^{-18}\left[\frac{1\mathrm{Hz}}{f}\right]^{1/2}\ \mathrm{m\,Hz}^{-1/2}$$

3.6 Finite mirrors

The preceding calculation does not allow to study the effect of the aspect ratio of the actual mirror on the spectral density of thermal noise. We propose here an approximate model for a cylindrical mirror having a radius a and a thickness h. This model has been published in the BHV paper [28] with one wrong boundary condition. Then Yuk Tung Liu et al. (YT) have derived a correction to the BHV result.

3.6.1 A solution to the equilibrium equations

We consider a cylindrical mirror limited by:

$$0 \le r \le a, \quad 0 \le z \le h$$

The reflecting face is assumed at $z = 0$ In the case of a finite solid, we expect the displacement vector to be a discrete sum of Bessel modes, of the form:

$$\begin{cases} u_r(r,z) = \sum_m A_m(z)J_1(k_mr) \\ u_\phi(r,z) = 0 \\ u_z(r,z) = \sum_m B_m(z)J_0(k_mr) \end{cases} \tag{3.11}$$

Where A_m, B_m are arbitrary functions of z, and k_m arbitrary constants. The equilibrium equations however imply for each order:

$$\begin{cases} \mu(A''_m - k_m^2 A_m) - (\lambda+\mu)k_m(B'_m + k_m A_m) &= 0 \\ \mu(B''_m - k_m^2 B_m) + (\lambda+\mu)(B''_m + k_m A'_m) &= 0 \end{cases} \tag{3.12}$$

so that by combining the two, we get:

$$[\partial_z^2 - k_m^2](A'_m + k_m B_m) = 0$$

the solution of which is:

$$A'_m + k_m B_m = k_m \left(\alpha_m \mathrm{e}^{-k_m z} + \beta_m \mathrm{e}^{k_m z}\right)$$

where α_m, β_m are arbitrary constants. This allows to substitute B_m in the first of eq.3.12, and yields:

$$A''_m - k_m^2 A_m = -\frac{\lambda+\mu}{\lambda+2\mu} k_m^2 \left(\alpha_m \mathrm{e}^{-k_m z} - \beta_m \mathrm{e}^{k_m z}\right)$$

the solution of which is:

$$A_m(z) = \gamma_m \mathrm{e}^{-k_m z} + \delta_m \mathrm{e}^{k_m z} + \frac{\lambda+\mu}{2(\lambda+2\mu)} k_m z \left(\alpha_m \mathrm{e}^{-k_m z} + \beta_m \mathrm{e}^{k_m z}\right) \tag{3.13}$$

introducing two new series (γ_m, δ_m) of arbitrary constants. Now B_m is determined:

$$\begin{aligned} B_m(z) = &\left(\frac{\lambda+3\mu}{2(\lambda+2\mu)}\alpha_m + \gamma_m\right) \mathrm{e}^{-k_m z} + \left(\frac{\lambda+3\mu}{2(\lambda+2\mu)}\beta_m - \delta_m\right) \mathrm{e}^{k_m z} + \\ &+ \frac{\lambda+\mu}{2(\lambda+2\mu)} k_m z \left(\alpha_m \mathrm{e}^{-k_m z} - \beta_m \mathrm{e}^{k_m z}\right) \end{aligned} \tag{3.14}$$

The stress tensor has the following non zero components of order m:

$$\begin{cases} \Theta_{m,rr} &= \lambda(B'_m + k_m A_m) J_0(k_m r) + 2\mu k_m A_m J'_1(k_m r) \\ \Theta_{m,\phi\phi} &= \lambda(B'_m + k_m A_m) J_0(k_m r) + +2\mu \frac{A_m}{r} J_1(k_m r) \\ \Theta_{m,zz} &= [(\lambda+2\mu)B'_m + \lambda k_m A_m]\, J_0(k_m r) \\ \Theta_{m,rz} &= \mu(A'_m - k_m B_m) J_1(k_m r) \end{cases} \tag{3.15}$$

3.6.2 Boundary conditions

The boundary conditions we assume are:

- No shear on the cylindrical edge, i.e.

$$\Theta_{rz}(r = a, z) \;=\; 0$$

  this can be satisfied by requiring that $k_m a$ is a zero of J_1

$$k_m \equiv \zeta_m / a$$

  where the ζ_m are the strictly positive zeros of J_1.

- No shear on the two circular faces, i.e.

$$\Theta_{rz}(r, z = 0) \;=\; 0, \quad \Theta_{rz}(r, z = h) \;=\; 0 \tag{3.16}$$

- Pressure of the beam on the first face:

$$\Theta_{zz}(r, z = 0) \;=\; -p(r) \tag{3.17}$$

- No pressure on the second face:

$$\Theta_{zz}(r, z = h) \;=\; 0 \tag{3.18}$$

- No radial stress on the cylindrical edge:

$$\Theta_{rr}(r = a, z) \;=\; 0 \tag{3.19}$$

To the preceding constraints, Yuk Tung Liu et al. have pointed out that the pressure acting on the face $z = h$ results in a global force accelerating the solid, so that an acceleration field must be added to the equilibrium equations. This will be treated later. Now the pressure distribution can be expanded on the orthogonal family of functions $J_0(\zeta_m r/a)$:

$$p(r) \;=\; p_0 \sum_m p_m J_0(\zeta_m r/a)$$

where $p_0 \;=\; 1/\pi a^2$ is a normalisation constant such that the p_m are dimensionless. The orthogonality relations are:

$$\int_0^a J_0(\zeta_m r/a) J_0(\zeta_n r/a)\, r\, dr \;=\; \frac{1}{2} a^2 J_0^2(\zeta_m)$$

so that the p_m are obtained as:

$$p_m = \frac{2\pi}{J_0^2(\zeta_m)} \int_0^a p(r) J_0(\zeta_m r/a)\, r\, dr \tag{3.20}$$

The Θ_{rz} and Θ_{zz} components of the stress tensor are easily found from A_m and B_m:

$$\Theta_{m,rz}/k_m\mu = \left(2\delta_m - \frac{\mu}{\lambda+2\mu}\beta_m\right) \mathrm{e}^{k_m z} - \left(2\gamma_m + \frac{\mu}{\lambda+2\mu}\alpha_m\right) \mathrm{e}^{-k_m z} +$$

$$-\frac{\lambda+\mu}{\lambda+2\mu} k_m z \left(\alpha_m \mathrm{e}^{-k_m z} - \beta_m \mathrm{e}^{k_m z}\right) \tag{3.21}$$

and

$$\Theta_{m,zz}/k_m\mu = (\beta_m - 2\delta_m)\mathrm{e}^{k_m z} - (\alpha_m + 2\gamma_m)\mathrm{e}^{-k_m z} -$$

$$-\frac{\lambda+\mu}{\lambda+2\mu} k_m z \left(\alpha_m \mathrm{e}^{-k_m z} + \beta_m \mathrm{e}^{k_m z}\right) \tag{3.22}$$

The boundary conditions provide 4 equations. The two first are:

$$\beta_m - 2\delta_m - \alpha_m - 2\gamma_m = -p_m/k_m\mu \tag{3.23}$$

and

$$2\delta_m - \frac{\mu}{\lambda+2\mu}\beta_m - 2\gamma_m - \frac{\mu}{\lambda+2\mu}\alpha_m = 0 \tag{3.24}$$

They allow to compute γ_m and δ_m in terms of α_m, β_m:

$$\gamma_m = \frac{1}{4}\left[\frac{\lambda+\mu}{\lambda+2\mu}\beta_m - \frac{\lambda+3\mu}{\lambda+2\mu}\alpha_m + \frac{p_m}{k_m\mu}\right]$$

$$\delta_m = \frac{1}{4}\left[\frac{\lambda+3\mu}{\lambda+2\mu}\beta_m - \frac{\lambda+\mu}{\lambda+2\mu}\alpha_m + \frac{p_m}{k_m\mu}\right]$$

The next two boundary conditions imply:

$$\left[2\delta_m - \frac{\mu}{\lambda+2\mu}\beta_m\right] \mathrm{e}^{k_m h} - \left[2\gamma_m + \frac{\mu}{\lambda+2\mu}\alpha_m\right] \mathrm{e}^{-k_m h} +$$

$$+k_m h \frac{\lambda+\mu}{\lambda+2\mu}\left[\beta_m \mathrm{e}^{k_m h} - \alpha_m \mathrm{e}^{-k_m h}\right] = 0$$

and

$$(\beta_m - 2\delta_m)\mathrm{e}^{k_m h} - (\alpha_m + 2\gamma_m)\mathrm{e}^{-k_m h} - \frac{\lambda+\mu}{\lambda+2\mu} k_m h \left[\beta_m \mathrm{e}^{k_m h} + \alpha_m \mathrm{e}^{-k_m h}\right] = 0$$

by substituting the values found for γ_m, δ_m, we find

$$\alpha_m = p_0 \frac{p_m(\lambda+2\mu)}{k_m \mu(\lambda+\mu)} \frac{1 - q_m + 2q_m x_m}{(1-q_m)^2 - 4q_m x_m^2} \tag{3.25}$$

$$\beta_m = p_0 \frac{p_m(\lambda+2\mu)}{k_m \mu(\lambda+\mu)} \frac{q_m(1 - q_m + 2x_m)}{(1-q_m)^2 - 4q_m x_m^2} \tag{3.26}$$

then

$$\gamma_m = -p_0 \frac{p_m}{2k_m \mu} \frac{2q_m x_m^2 + \frac{\mu}{\lambda+\mu}(1 - q_m + 2q_m x_m)}{(1-q_m)^2 - 4q_m x_m^2} \tag{3.27}$$

$$\delta_m = -p_0 \frac{p_m q_m}{2k_m \mu} \frac{2x_m^2 - \frac{\mu}{\lambda+\mu}(1 - q_m + 2x_m)}{(1-q_m)^2 - 4q_m x_m^2} \tag{3.28}$$

with the notation $x_m \equiv k_m h$ and $q_m \equiv \exp(-2x_m)$. At this point, YT pointed out that the component of spatial frequency zero of the pressure has not been taken into account. Because the series involves only strictly positive zeros of J_1, the preceding displacement has a zero average on the strained face. One must consider the resulting force acting on the body under the uniform pressure

$$p_0 = 1/\pi a^2$$

producing a force of 1 N after integration on the disk. But this force produces an acceleration, so that an acceleration field should be added in the equilibrium equations (recall that our mirrors are practically free falling in the z direction). This can be done by adding to the preceding displacement an extra displacement of the form:

$$\begin{cases} \delta u_r(r,z) = \frac{\lambda p_0 r}{2\mu(3\lambda+2\mu)}(1 - z/h) \\ \delta u_\phi(r,z) = 0 \\ \delta u_z(r,z) = \frac{\lambda p_0 r^2}{4\mu h(3\lambda+2\mu)} - \frac{(\lambda+\mu)p_0}{\mu(3\lambda+2\mu)}(z - z^2/2h) \end{cases} \tag{3.29}$$

This extra displacement contributes only the axial stress:

$$\delta\Theta_{zz} = -p_0(1 - z/h)$$

all other stress components are identically zero. The equilibrium equations remain satisfied:

$$\partial_z \delta\Theta_{zz} \;=\; p_0/h \;=\; \rho \times \frac{1N}{\rho\pi a^2 h} \;=\; \rho \times (1\,N)/M \;=\; \rho\ddot{z}$$

where M is the mirror mass and ρ the density. Now the sum of the displacement 3.11 and the extra displacement 3.28 satisfies all boundary conditions, except the vanishing of the radial stress on the cylindrical edge. We have indeed

$$\Theta_{m,rr}(r=a,z) \;=\; \lambda(k_m A_m(z) + B'_m(z))J_0(\zeta_m) + 2\mu k_m A_m(z) J'_1(\zeta_m)$$

but due to the fact that $J'_1(\zeta_m) = J_0(\zeta_m)$, and after substituting the explicit values of A_m and B_m, we get

$$\begin{aligned}\Theta_{m,rr}(r=a,z) \;=\; p_0 \frac{J_0(\zeta_m)p_m}{(1-q_m)^2 - 4q_m x_m^2} \Big[&(1 - q_m + 2q_m x_m(1+x_m))\,\mathrm{e}^{-k_m z} - \\ &-q_m\,(1 - q_m + 2x_m(1-x_m))\,\mathrm{e}^{k_m z} - \\ &-k_m z q_m(1 - q_m + 2x_m)\mathrm{e}^{k_m z} - k_m z(1 - q_m + 2q_m x_m)\mathrm{e}^{-k_m z}\Big] \end{aligned} \tag{3.30}$$

It is numerically easy to check that this function of z is not very different from linear. It has even a vanishing average. It is therefore possible to find an approximate solution of the problem by using the De Saint-Venant principle: If we add to our displacement vector one more extra displacement giving a linear stress with suitable parameters, we compensate for the mean stress and torque on the edge, and the resulting solution is very accurate everywhere in the body, except maybe in the neighborhood of the edge, where the strain energy is likely weak. The second extra displacement is of the form:

$$\begin{cases} \Delta u_r(r,z) \;=\; \frac{\lambda+2\mu}{2\mu(3\lambda+2\mu)}(c_0 r + c_1 r z) \\ \Delta u_\phi(r,z) \;=\; 0 \\ \Delta u_z(r,z) \;=\; -\frac{\lambda}{\mu(3\lambda+2\mu)}(c_0 z + c_1 z^2/2) - \frac{\lambda+2\mu}{4\mu(3\lambda+2\mu)} c_1 r^2 \end{cases} \tag{3.31}$$

This displacement induces zero stresses, and thus leaves unchanged the boundary conditions, except for a radial contribution:

$$\Delta\Theta_{rr}(z) \;=\; c_0 + c_1 z$$

This linear stress can be adjusted to compensate for the first moments of the residual stress $\Theta_{rr}(r=a,z)$. We require for instance a minimum value for the integral

$$\int_0^h \left[\Theta_{rr}(r=a,z) + \Delta\Theta_{rr}(z)\right]^2 dz$$

If we define

$$I_0 = \frac{1}{h}\int_0^h \Theta_{rr}(r=a,z)dz$$

$$I_1 = \frac{1}{h^2}\int_0^h \Theta_{rr}(r=a,z)z\,dz$$

we have the values of c_0, c_1:

$$c_0 = 6I_1 - 4I_0, \quad c_1 = 6(I_0 - 2I_1)/h$$

The explicit expression of $\Theta_{rr}(r=a,z)$ (eq.3.30) allows to compute I_0, I_1. Firstly, one finds $I_0 = 0.$ and secondly

$$I_{1,m} = p_0\, J_0(\zeta_m) p_m / k_m^2 h^2$$

so that

$$I_1 = p_0 \times s$$

where

$$s = \frac{a^2}{h^2}\sum_m \frac{p_m J_0(\zeta_m)}{\zeta_m^2}$$

then

$$c_0 = 6sp_0, \quad c_1 = -12sp_0/h$$

3.6.3 Strain Energy

The global displacement vector has the form

$$\begin{cases} u_r(r,z) &= \sum_m A_m(z) J_1(\zeta_m r/a) + Pr + Qrz \\ u_\phi(r,z) &= 0 \\ u_z(r,z) &= \sum_m B_m(z) J_0(\zeta_m r/a) + Wr^2 + Tz + Sz^2 \end{cases}$$

where P, Q, W, T, S are known coefficients related to the two extra displacement terms defined above. The strain components are:

$$E_{rr}(r,z) = \sum_m k_m A_m(z) J_1'(\zeta_m r/a) + P + Qz$$

$$
\begin{aligned}
E_{\phi\phi}(r,z) &= \sum_m A_m(z)\frac{J_1(\zeta_m r/a)}{r} + P + Qz \\
E_{zz}(r,z) &= \sum_m B'_m(z) J_0(\zeta_m r/a) + T + 2Sz \\
E_{rz}(r,z) &= \sum_m \left(A'_m(z) - k_m B_m(z)\right) J_1(\zeta_m r/a)
\end{aligned}
$$

the trace of the strain tensor is thus:

$$
E(r,z) = \sum_m (B'_m(z) + k_m A_m(z))\, J_0(\zeta_m r/a) + 2P + T + 2(Q+S)z
$$

The strain energy per N^2(our target) is given by

$$
U = \int_0^{2\pi} d\phi \int_0^h dz \int_0^a r\, dr\, w(r,z)
$$

where the energy density w is defined as:

$$
w = \frac{1}{2}\left[\lambda E^2 + 2\mu\left(E_{rr}^2 + E_{\phi\phi}^2 + E_{zz}^2 + 2E_{rz}^2\right)\right] \tag{3.32}
$$

The squares of the stress components involve the squares of the main stresses, the squares of the extra stresses, plus crossed terms. It is possible to show that crossed terms vanish in the r integration. There is thus a perfect decoupling,and the extra terms in the displacement vector result in corrections to the global energy.

Main contribution to the strain energy

Now we can compute the main contribution. We recall the following integrals:

$$
\begin{aligned}
\int_0^a J_0(\zeta_m r/a) J_0(\zeta_m r/a) r\, dr &= \frac{a^2}{2} J_0^2(\zeta_m) \\
\int_0^a J_1(\zeta_m r/a) J_1(\zeta_m r/a) r\, dr &= \frac{a^2}{2} J_0^2(\zeta_m)
\end{aligned}
$$

For the Bessel modes contribution we have thus:

$$
U = \frac{\pi a^2}{2} \sum_m J_0(\zeta_m)^2 \int_0^h U_m(z)\, dz
$$

where

$$U_m = \lambda(B'_m + k_m A_m)^2 + 2\mu\left(k_m^2 A_m^2 + B_m'^2 + \frac{1}{2}(A'_m - k_m B_m)^2\right)$$

All the terms being known, the integration is straightforward, and the result is:

$$U = \frac{\pi a^3}{4}\frac{\lambda+2\mu}{\mu(\lambda+\mu)}\sum_m \frac{J_0^2(\zeta_m)p_m^2}{\zeta_m}\frac{1-q_m^2+4q_m x_m}{(1-q_m)^2-4q_m x_m^2}$$

or as well, using the Young modulus Y and the Poisson ratio σ instead of the Lamé coefficients:

$$U = \frac{1-\sigma^2}{\pi a Y}\sum_m \frac{J_0^2(\zeta_m)p_m^2}{\zeta_m}\frac{1-q_m^2+4q_m x_m}{(1-q_m)^2-4q_m x_m^2} \tag{3.33}$$

The dimension of U is J.N^{-2}.

Correction to strain energy

The contribution of the extra stresses to the strain energy is:

$$\Delta U = \int_0^{2\pi} d\phi \int_0^a r\, dr \int_0^h \Delta w(z) dz$$

where $\Delta w(z)$ is the extra density:

$$\Delta w(z) = \frac{1}{2}\left[\lambda\left(((2P+T+2(Q+S)z)^2 + 2\mu\left(2(P+Qz)^2 + (T+2Sz)^2\right)\right]\right.$$

The coefficients are:

$$P = \frac{p_0}{2\mu(3\lambda+2\mu)}(\lambda + 6s(\lambda+2\mu))$$

$$Q = -\frac{p_0}{2\mu(3\lambda+2\mu)h}(\lambda + 12s(\lambda+2\mu))$$

$$T = -\frac{p_0}{\mu(3\lambda+2\mu)}(\lambda+\mu+6s\lambda)$$

$$S = \frac{p_0}{2\mu(3\lambda+2\mu)h}(\lambda+\mu+12s\lambda)$$

The result is:

$$\Delta U = \frac{\pi a^2 h p_0^2}{6\mu(3\lambda+2\mu)}\left[6\lambda s + \lambda + \mu + 36(\lambda+2\mu)s^2\right]$$

After replacing the Lamé coefficients by Y, σ, this is:

$$\Delta U \;=\; \frac{a^2}{6\pi h^3 Y}\left[\left(\frac{h}{a}\right)^4 + 12\sigma\xi\left(\frac{h}{a}\right)^2 + 72(1-\sigma)\xi^2\right] \qquad (3.34)$$

with

$$\xi \;\equiv\; \sum_{m>0} p_m J_0(\zeta_m)/\zeta_m^2$$

Explicit coating displacement and edge stress

It is interesting to have the explicit expression for the reflecting surface displacement:

$$u_z(r, z=0) \;=\; \frac{2(1-\sigma^2)}{\pi a Y}\sum_{m>0}\frac{1-q_m^2+4q_m x_m}{(1-q_m)^2-4q_m x_m^2}\frac{p_m J_0(\zeta_m r/a)}{\zeta_m} +$$

$$+\frac{r^2/a^2}{2\pi h Y}\left[\sigma + 12\xi\frac{a^2}{h^2}(1-\sigma)\right]$$

units are m/N. See the displacement profile on figure 3.4

For the stress on the cylindrical edge before correction, we have as seen above (3.30):

$$\Theta_{rr}(r=a,z) \;=\; \frac{1}{\pi a^2}\sum_{m>0}\frac{J_0(\zeta_m)p_m}{(1-q_m)^2-4q_m x_m^2}\Big[(1-q_m+2q_m x_m(1+x_m))\,\mathrm{e}^{-\zeta_m z/a} -$$

$$-q_m\,(1-q_m+2x_m(1-x_m))\,\mathrm{e}^{\zeta_m z/a} -$$

$$-\zeta_m\frac{z}{a}\left[q_m(1-q_m+2x_m)\mathrm{e}^{\zeta_m z/a} + (1-q_m+2q_m x_m)\mathrm{e}^{-\zeta_m z/a}\right]\Big]$$

A plot of $\Theta_{rr}(r=a,z)$ (fig.3.5) shows the its quasi-linear behavior, justifying a posteriori the De Saint-Venant approximation.

Case of gaussian beams

if the beam intensity comes from a TEM_{00} wave of width w, we have

$$p_m \;=\; \frac{2\pi}{J_0(\zeta_m)^2}\frac{2}{\pi w^2}\int_0^a \exp(-2r^2/w^2)J_0(\zeta_m r/a)\,r\,dr$$

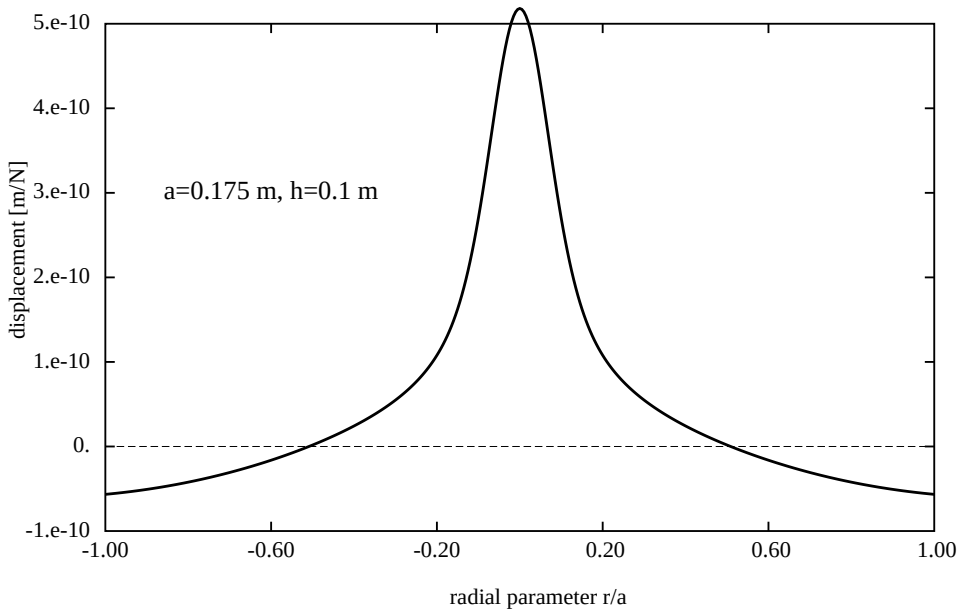

Figure 3.4: Displacement of the surface of a finite substrate under a gaussian pressure

The upper integration bound can be replaced by $+\infty$ if, as a mirror, the cylinder has negligible diffraction losses. Then the result can be found in [17] (eq. 11.4.29).

$$p_m = \frac{1}{J_0(\zeta_m)^2} \exp\left[-\frac{\zeta_m^2 w^2}{8a^2}\right]$$

The expansion of $p(r)$ on the orthogonal family $J_0(\zeta_m r/a)$ is rapidly convergent. A plot of $p(r)$ reconstructed from only 12 terms is shown on fig.3.6. A good accuracy is obtained for all the numerical calculations with only 50 terms. The expression 3.33 for U takes the special form

$$U_{\text{Gauss}} = \frac{1-\sigma^2}{\pi a Y} \sum_{m>0} \frac{\exp(-\zeta_m^2 w^2/4a^2)}{\zeta_m J_0(\zeta_m)^2} \frac{1-q_m^2+4q_m x_m}{(1-q_m)^2-4q_m x_m^2} \tag{3.35}$$

the ξ parameter involved in expression 3.34 for ΔU takes the special form:

$$\xi_{\text{Gauss}} = \sum_{m>0} \frac{\exp(-\zeta_m^2 w^2/8a^2)}{\zeta_m^2 J_0(\zeta_m)}$$

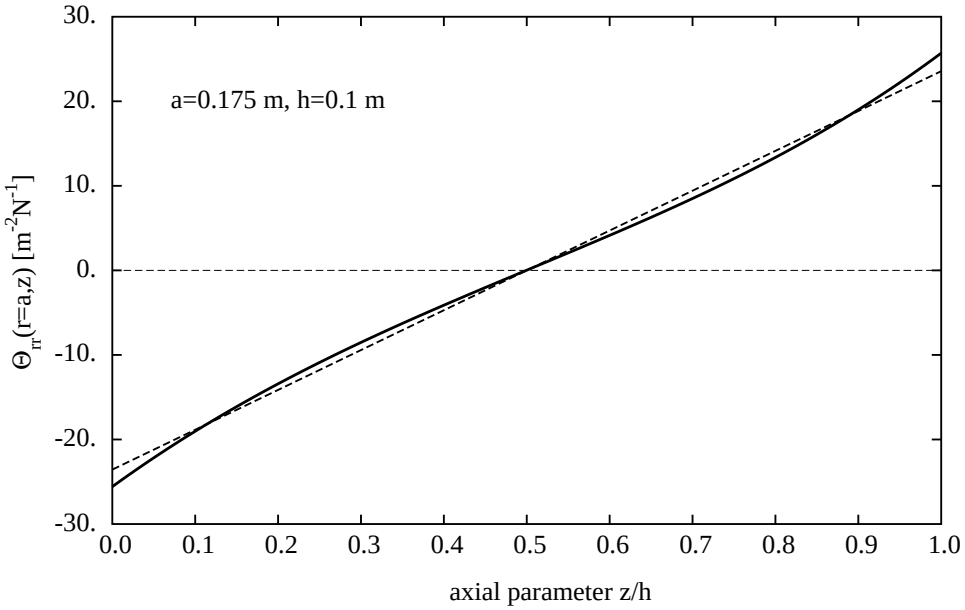

Figure 3.5: Radial stress along the edge of the cylindrical solid. Solid line : $\Theta_{rr}(r = a, z)$, Dashed line: linear fit $c_0 + c_1 z$

It is interesting to compare the results with the case discussed in the preceding section, of the half-space (infinite mirror) appproximation. If we note U_{HS} the corresponding strain energy and U_{FM} that of the finite mirror, we can plot the ratio for varying aspect ratios (see Fig.3.7). and it is clear that for a given thickness h, values of a as small as possible are desirable. Gong-like mirrors are worse than bar-like ones.

3.6.4 Some numerical results

For a Virgo input mirror, a =0.175m, h =0.1m, w =0.02m, we get

$$U \sim 1.81 \times 10^{-10} \text{ J.N}^{-2}$$

$$\Delta U \sim 2.08 \times 10^{-11} \text{ J.N}^{-2}$$

$$U_{\text{tot}} = U + \Delta U \sim 2.02 \times 10^{-10} \text{ J.N}^{-2}$$

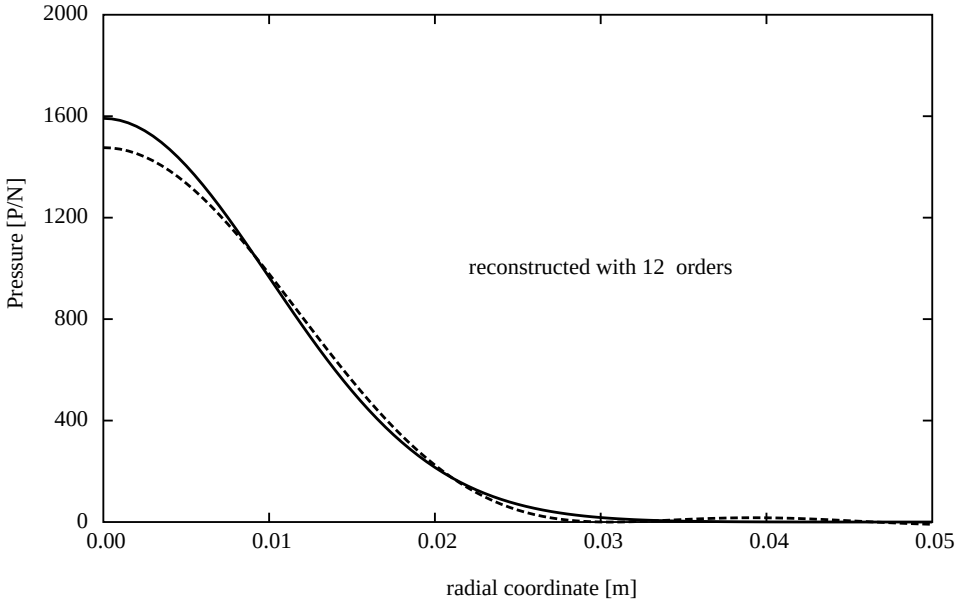

Figure 3.6: Solid line : gaussian pressure. Dashed line : reconstruction

The infinite mirror approximation was:

$$U_\infty \sim 1.88 \times 10^{-10} \text{ J.N}^{-2}$$

so that $U/U_\infty \sim 1.07$. The corresponding root spectral density of thermal noise is given by

$$S_x(f)^{1/2} = \sqrt{\frac{4k_BT}{\pi f}\Phi U_{\rm tot}}$$

so that we find (the loss angle being 10^{-6}:

$$S_x(f)^{1/2} \sim 1.03 \times 10^{-19} \text{ m.Hz}^{-1/2} \text{ at 100 Hz}$$

For a Virgo end mirror (a =0.175m, h =0.1m, w =0.0554m) we find:

$$U \sim 5.55 \times 10^{-11} \text{ J.N}^{-2}$$

$$\Delta U \sim 1.75 \times 10^{-11} \text{ J.N}^{-2}$$

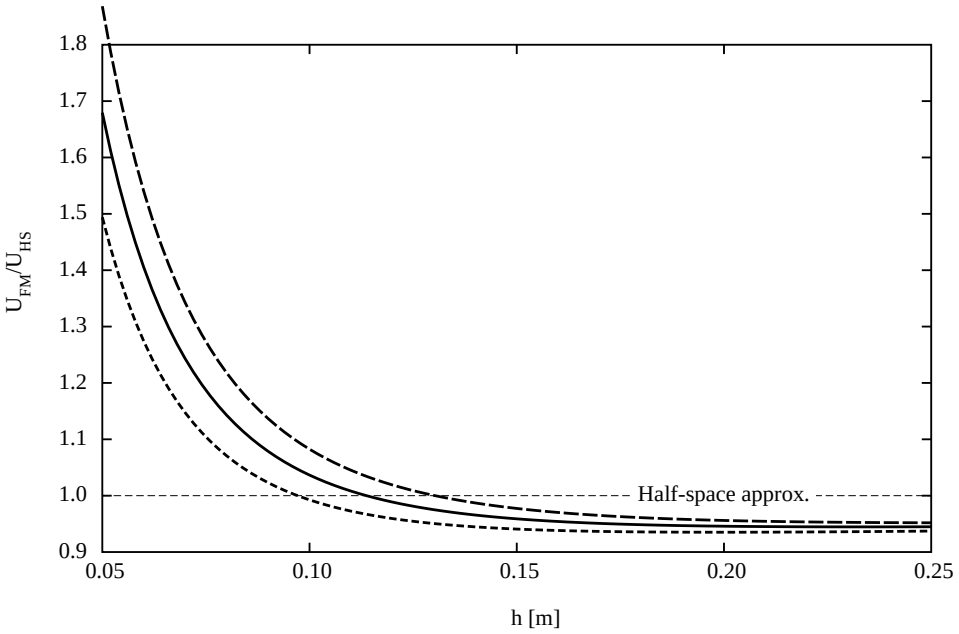

Figure 3.7: relative spectral density of Thermal noise for various aspect ratios. Solid line: a=0.175m, long dashed line: a=0.2m, short dashed line: a=0.15m

$$U_{\rm tot} \sim 7.30 \times 10^{-11} \text{ J.N}^{-2}$$

The beam width has changed (w=5.54cm), so that

$$U_\infty \sim 6.77 \times 10^{-11} \text{ J.N}^{-2}$$

so that $U/U_\infty \sim 1.08$. and

$$S_x(f)^{1/2} \sim 6.21 \times 10^{-20} \text{ m.Hz}^{-1/2} \text{ at 100 Hz}$$

Finally, it is interesting to check the convergence of $U_{\rm tot}$ to the infinite mirror approximation when the size of the mirror increases. This is shown on Fig.3.8.

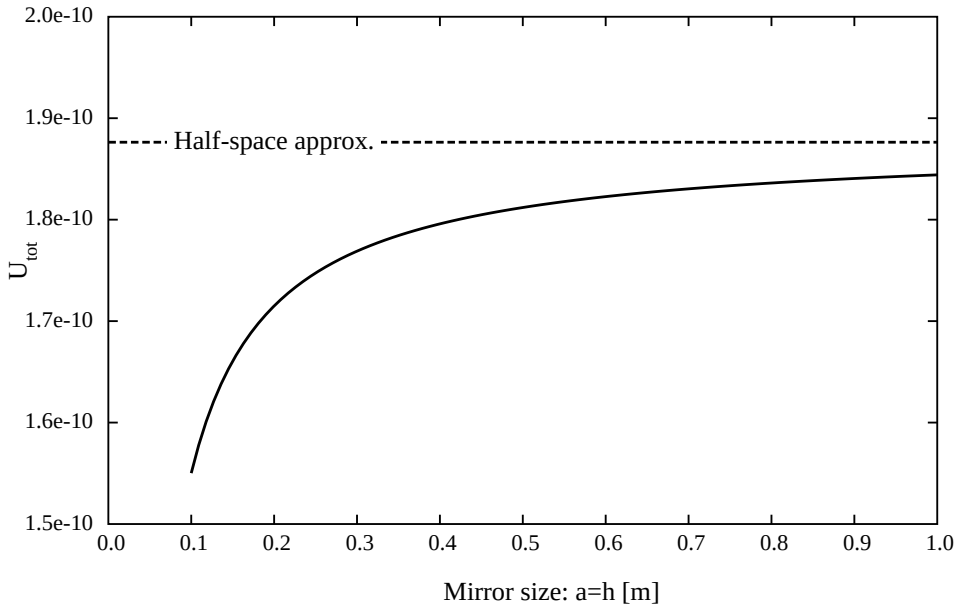

Figure 3.8: Convergence of the finite mirror model to the infinite, when the size of the mirror increases.

3.7 Non gaussian beams

3.7.1 Half-space approximation

It has been suggested ([32]) to use light beams with a flat profile in the long cavities instead of gaussian modes, in order to reduce the thermoelastic noise. It is expected that widen the beam will average the surface fluctuations and. The idea is convincing, but a quantitative model is obviously needed. We have addressed the question of how to generate these modes in a preceding section. For any pressure profile $p(r)$, the general expression of $\alpha(k)$ is, as already seen:

$$k\alpha(k) \;=\; -\,\frac{1}{2\mu}\int_0^\infty p(r)\,J_0(kr)\,r\,dr$$

so that the displacement of the surface of the half-space is:

$$u_z(r,z=0) \;=\; -\,\frac{\lambda+2\mu}{2\mu(\lambda+\mu)}\int_0^\infty dk\,J_0(kr)\int_0^\infty r'dr'\,J_0(kr')\,p(r')$$

or as well, using the Poisson ratio and the Young modulus:

$$u_z(r, z=0) \;=\; -\,\frac{2(1-\sigma^2)}{Y}\int_0^\infty dk\, J_0(kr)\int_0^\infty r'dr'\, J_0(kr')\, p(r') \qquad (3.36)$$

It is easy to see that the strain energy per N^2 is then given by

$$U \;=\; \frac{2\pi(1-\sigma^2)}{Y}\int_0^\infty dk\, \tilde{p}(k)^2$$

where

$$\tilde{p}(k) \;=\; \int_0^\infty r\, dr\, p(r)\, J_0(kr)$$

is nothing but the Fourier transform of the pressure distribution. In the special case of a distribution uniform on the disk $r < b$, representing a simplified version of a realistic mode (which would be only almost flat), we have

$$p(r) \;=\; \begin{cases} 1/\pi b^2 & (r < b) \\ 0 & (r \geq b) \end{cases}$$

so that

$$\tilde{p}(k) \;=\; \frac{J_1(kb)}{\pi kb}$$

and the energy integral reduces to

$$U \;=\; \frac{2(1-\sigma^2)}{\pi Y b}\int_0^\infty dx\, \left(\frac{J_1(x)}{x}\right)^2$$

the integral is of the Weber-Schafheitlin type (see [17] p.487), thus expressible in terms of a hypergeometric series:

$$\int_0^\infty dx\, \left(\frac{J_1(x)}{x}\right)^2 \;=\; \frac{1}{2}\, F\left(\frac{1}{2},\; -\frac{1}{2};\; 2\;;\; 1\right)$$

now (see [17] p.556),

$$F\left(\frac{1}{2},\; -\frac{1}{2};\; 2,\; 1\right) \;=\; \frac{8}{3\pi}$$

so that we have

$$\int_0^\infty dx\, \left(\frac{J_1(x)}{x}\right)^2 \;=\; \frac{4}{3\pi}$$

which yields the final result:

$$U \;=\; \frac{8(1-\sigma^2)}{3\pi^2 Y b}$$

It is worth to compare this value, denoted by $U_{\rm flat}$ with the gaussian value, denoted by $U_{\rm Gauss}$:

$$\frac{U_{\rm flat}}{U_{\rm Gauss}} \;=\; \frac{16}{3\pi^{3/2}}\,\frac{w}{b} \;\approx\; .96\,\frac{w}{b}$$

If it is possible to establish a flat mode of radius 10 cm where a gaussian mode of half-width 2 cm was used, the gain in thermal noise could be

$$\sqrt{\frac{U_{\rm flat}}{U_{\rm Gauss}}} \;\approx\; 0.44$$

which means a factor better than 2 in sensitivity, therefore 1 order of magnitude in the analyzed volume of space in the frequency band around 100 Hz. For curious readers, and though it is of no practical interest for our present purpose (but any result may always be re-used one day in a different context), we show the (virtual) distorted surface on Fig.3.9, and give the apex equation of the surface as:

$$u_z(r, z=0) \;=\; -\,\frac{2(1-\sigma^2)}{\pi Y b}\,\begin{cases} 1 & (r=0) \\ F\left(\frac{1}{2},\; -\frac{1}{2};\; 1\;;\; r^2/b^2\right) & (0<r<b) \\ 2/\pi & (r=b) \\ bF\left(\frac{1}{2},\; \frac{1}{2};\; 2\;;\; b^2/r^2\right)/2r & (r>b) \end{cases}$$

where $F(a,b;c;z)$ denotes the Gauss hypergeometric series.

In this case, the pressure distribution takes however significant values probably near the edge of the mirror, because the reduction of thermal noise operates only if a is much larger than w, and secondly because the size of actual mirrors has been defined as the minimum consistent with small diffraction losses, so that say 5 times w is near the physical edge for input mirrors, and outside the mirror for end mirrors of radius 35 cm. Approximate representation of the mirror as an infinite half-space is thus questionable in this case, and a theory with a finite mirror radius is needed.

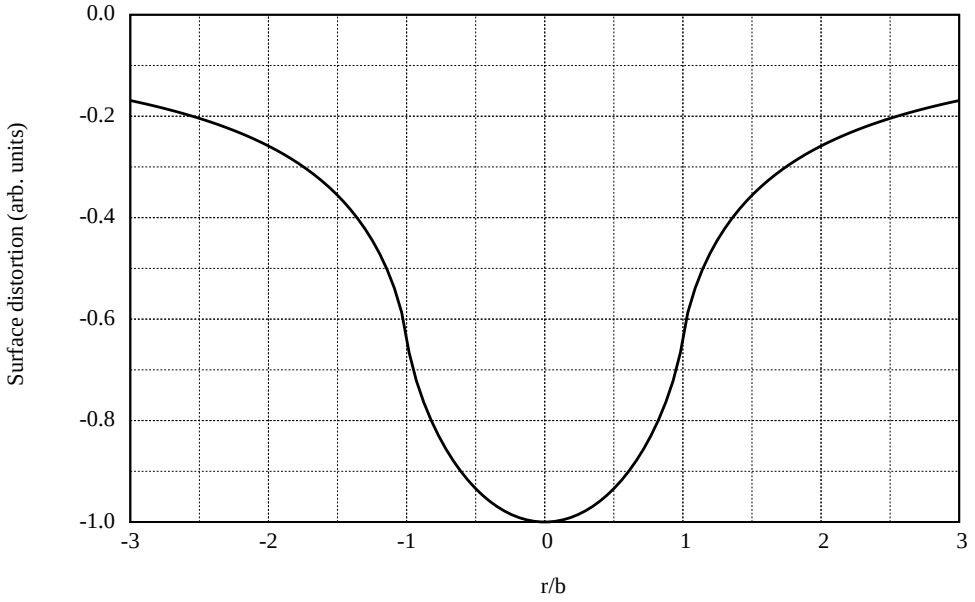

Figure 3.9: Displacement of the surface of an infinite substrate under a pressure uniform on the disk $r < b$. The surface is assumed infinite

3.7.2 Finite test mass approximation

The model developped for a finite mirror of radius a and thickness h can be extended to the case of a flat pressure

$$\begin{cases} p(r) &= 1/\pi b^2 \quad (r \leq b) \\ p(r) &= 0 \quad (r > b) \end{cases}$$

representing approximately a flat mode. The pressure coefficients are:

$$p_m = \frac{2a J_1(\zeta_m b/a)}{b\zeta_m J_0^2(\zeta_m)}$$

The p_m decrease much less rapidly for increasing m than in the case of a gaussian profile, so that reconstruction of $p(r)$ is numerically difficult. But The series giving U and ξ are still convergent, despite the new values for the p_m. In fact, these new p_m are decreasing like $1/\sqrt{m}$, so that the formal series giving $p(r)$ is valid in the sense of the distribution theory. But the terms in

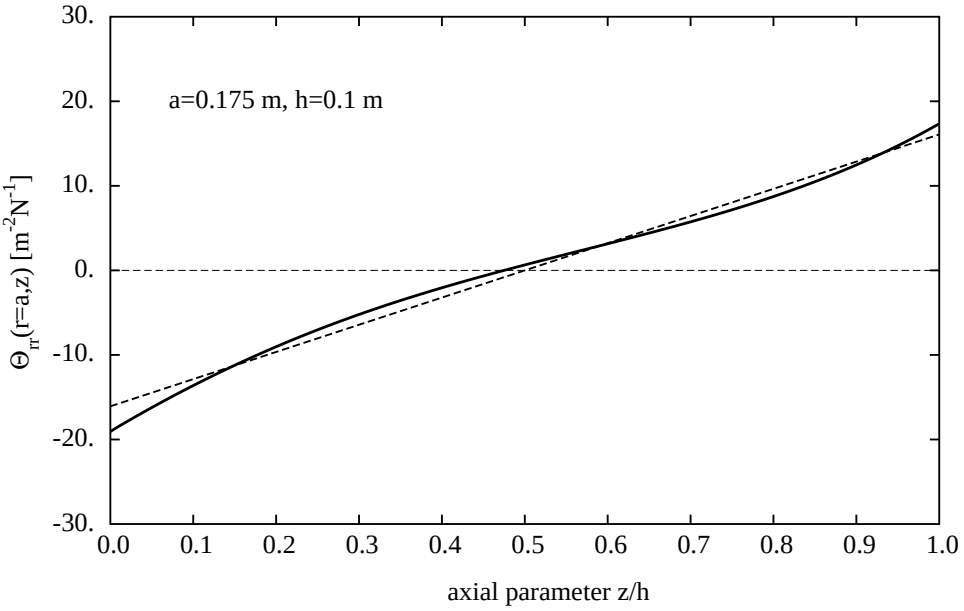

Figure 3.10: Radial stress and corresponding linear fit. b=0.1m

the series 3.33 fo r U, and in the series defining ξ are nevertheless decreasing like $1/m^3$, so that ordinary convergence is secured. All the formulas derived in the preceding section are unchanged, apart from the new values for p_m. It is nevertheless necessary to check that the correction for the radial stress on the edge is still reasonable. If we compute the stress $\Theta_{rr}(r = a, z)$ with the new coefficients, we get the following plot (fig.3.10), in the case of a mirror of radius 0.175m and a pressure flat in a disk of radius 0.1m. showing that the De Saint-Venant correction is still realistic. Even with a spot radius of 0.15m, the linear correction seems to make sense (see fig.3.11). The displacement of the reflecting surface is much less than in the gaussian case (fig.3.12), and distortion is very similar to the infinite case. It is especially intersting to compare the spectral densities of thermal noise in the gaussian mode regime to the flat mode regime. The following plot (3.13) shows again the large gain that could be achieved by increasing the spot radius. Comparison is made with a gaussian beam of width 2cm. It is interesting to remark that the case $b = a$ (the flat mode has the same radius as the mirror) leads to $U = 0$

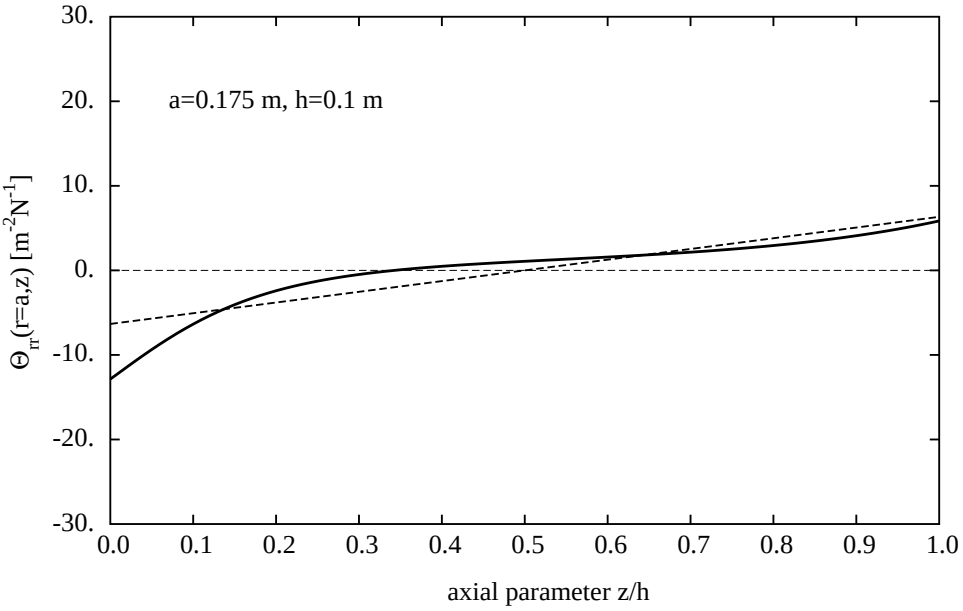

Figure 3.11: Radial stress and corresponding linear fit.b=0.15m

and $\xi = 0$. In this case the solution is exact, and the strain energy reduces, according to 3.34 to

$$\Delta U \;=\; h/6\pi a^2 Y$$

3.7.3 Numerical results

Let us assume such a flat mode in the Virgo cavities whose mirrors are assumed identical in size to the current situation. For the input mirrors, we find:

$$U \;\sim\; 1.60 \times 10^{-11}\ \mathrm{J.N}^{-2}$$

$$\Delta U \;\sim\; 1.06 \times 10^{-11}\ \mathrm{J.N}^{-2}$$

$$U_{\mathrm{tot}} \;\sim\; 2.65 \times 10^{-11}\ \mathrm{J.N}^{-2}$$

The infinite mirror approximation was:

$$U_{\infty} \;\sim\; 3.59 \times 10^{-11}\ \mathrm{J.N}^{-2}$$

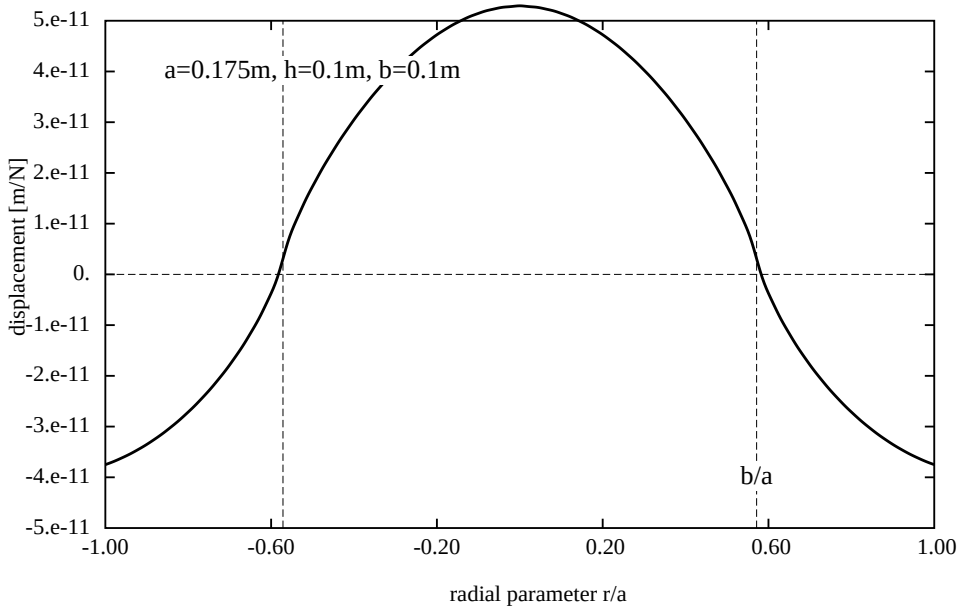

Figure 3.12: Displacement of the reflecting surface under a pressure uniform in a disk of radius 0.1m. (a=0.175m, h=0.1m)

so that $U/U_\infty \sim 0.74$. We find the spectral density (the loss angle being still 10^{-6}:

$$S_x(f)^{1/2} \sim 3.74 \times 10^{-20} \text{ m.Hz}^{-1/2} \text{ at 100 Hz}$$

For the end mirrors, the mode having almost exactly the same spot size after propagation, the numerical results are almost identical.

3.7.4 Realistic modes

The preceding approach is still questionable because the pressure distribution, as represented by an ideal flat top function is unrealistic from an optical point of view. It is thus necessary to check that taking a more realistic flat mode does not destroy the preceding conclusions. The more realistic model proposed by D'ambrosio et al.[32] consists in a superposition of elementary gaussian modes of waist w_0 on a disk of radius b. If we adapt the model to the Virgo parameters, for the sake of definiteness, we would have an amplitude

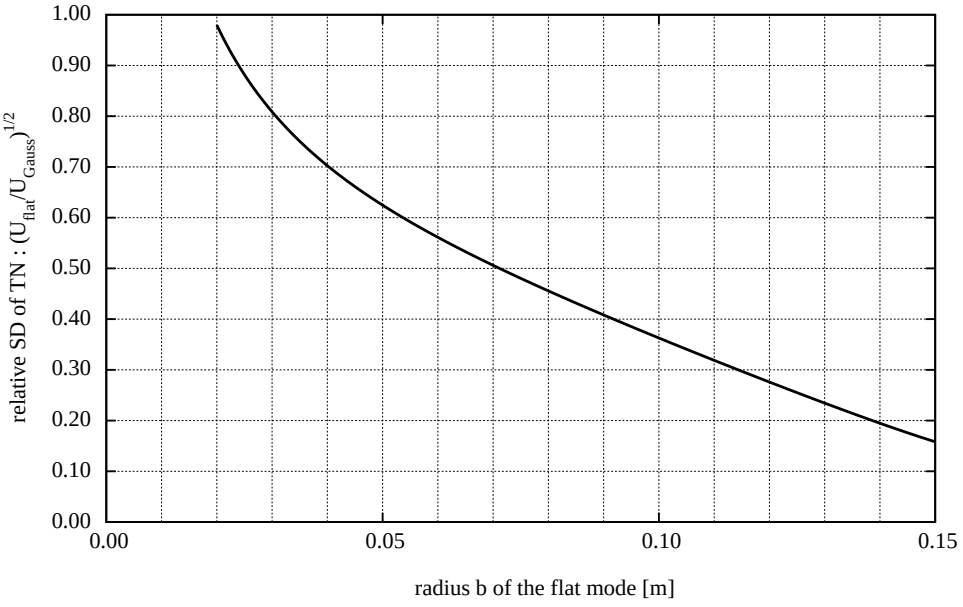

Figure 3.13: gain in SD of thermal noise vs spot radius.(a=0.175m, h=0.1m)

on the flat input mirror of the form:

$$A(x,y,0) \;=\; \int_{\Delta} \phi(x-x_0, y-y_0, 0)\, dx_0\, dy_0$$

where Δ is the disk of radius b, and $\phi(x,y,z)$ a gaussian TEM_{00} wave:

$$\phi(x,y,0) \;=\; \exp\left(-\frac{x^2+y^2}{w_0^2}\right)$$

The resulting amplitude has a quite flat maximum, with a gaussian-like edge Parameter w_0 determines the sharpness of this edge. It is easy to show that after propagation at a distance L, the amplitude is (up to a normalization factor):

$$A(x,y,L) \;\propto\; \int_0^{b/w} \exp\left[-Z(\rho-\rho_0)^2\right]\, \exp(-2Z\rho\rho_0)\, I_0(2Z\rho\rho_0)\, \rho_0\, d\rho_0$$

$z_R = \pi w_0^2/\lambda$ being the Rayleigh parameter, w is the beam half-width after propagation on the distance L:

$$w = w_0\sqrt{1+L^2/z_R^2}$$

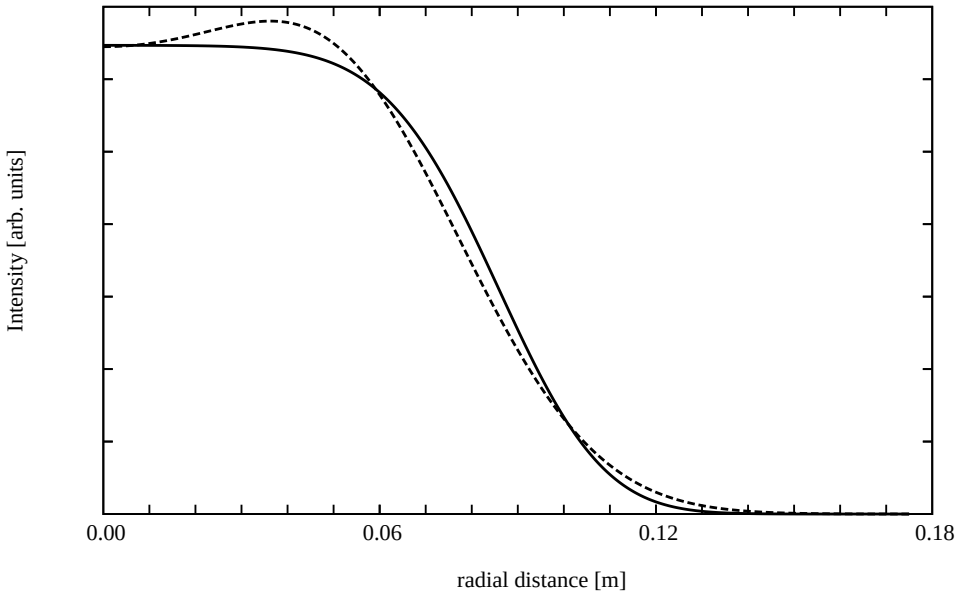

Figure 3.14: Intensity profile in the flat mode. Solid line : Profile on the input flat cavity mirror. Dashed line : Profile on the far mirror (3 km away).

$\rho \equiv \sqrt{x^2+y^2}/w$, and $Z \equiv 1 - iL/z_R$. $I_0(z)$ is the modified Bessel function of the first kind. There is no better analytical expression for the amplitude, but a numerical integration is straightforward, because the function $\exp(-z)I_0(z)$ has an easy behavior. On Fig.3.14, we have plotted the mode intensity profile for the following parameters: $w_0 \sim 3.2$ cm, $b = 0.1$ m, at the two ends of a cavity of length 3 km. Knowing A, we can compute numerically the p_m from $|A|^2$ after normalization. This can be done for the input mirrors (flat wavefront, $L = 0$) and for the end mirrors ('mexican hat' wavefront, L =3 km). The corresponding strain energies are almost the same, because the intensity distribution is weakly modified by diffraction for not too small w_0. Even for smaller w_0 resulting in more distorted intensity profiles on the end mirror, the strain energies are nearly identical at the two ends. In Fig.3.15, we plot the values found for several particular radii and several values of the parameter w_0. It is clear that by decreasing the parameter w_0 (sharping the edge), we get more and more close to the ideally flat model. However a too sharp edge is not desirable from an optical point of view, giving a too

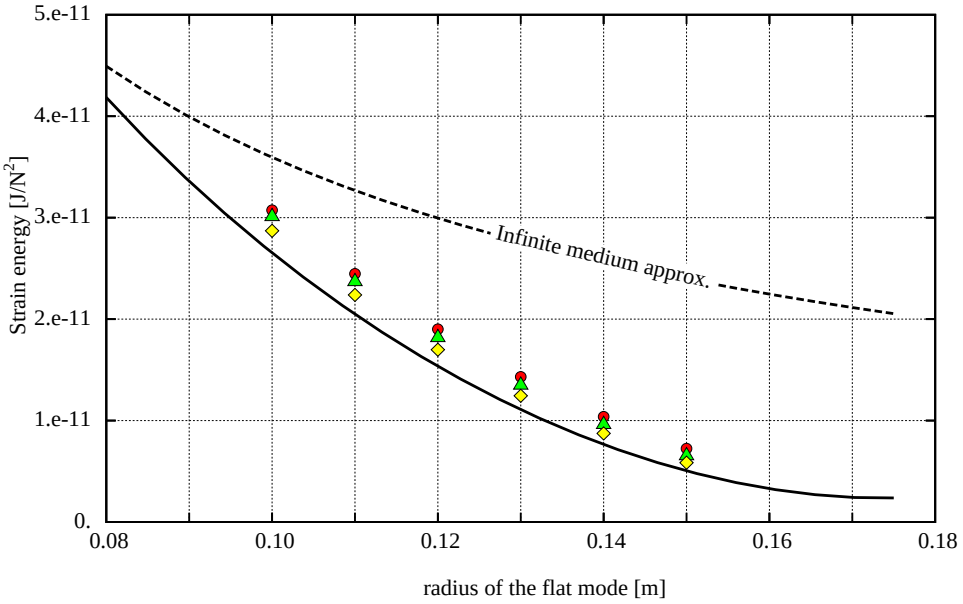

Figure 3.15: Strain energy U vs radius of the flat mode. Dashed line: Infinite mirror and ideally flat mode, Solid line : Mirror of radius 0.175 m, thickness 0.1 m and ideally flat mode. Circles: same finite mirror with realistic mode $w_0 \sim 3.2$ cm. Triangles: same finite mirror with realistic mode $w_0 \sim 2$ cm. Diamonds: same finite mirror with realistic mode $w_0 \sim 1$ cm

distorted wavefront (and consequently unfeasible mirrors). However, in the limit of reasonable parameters, we remark a good agreement between the ideal and realistic models.

3.8 Mirror distortions and energy maps

It is interesting to write explicitly the solution of the elastical problem. The expressions of the displacement vector components in the case of finite cylindrical mirrors are:

$$u_r(r,z) = u_{\mathrm{main},r}(r,z) + \Delta u_r(r,z)$$

$$u_z(r,z) = u_{\mathrm{main},z}(r,z) + \Delta u_z(r,z)$$

with the following expressions:

$$\Delta u_z(r,z) \;=\; \frac{1}{2\pi a^2 h Y}\left\{\left[\sigma+12s(1-\sigma)\right]r^2+(1+24s\sigma)z^2-2(1+12s\sigma)hz\right\}$$

(with $s\equiv\xi a^2/h^2$),

$$\Delta u_r(r,z) \;=\; \frac{r}{\pi a^2 Y}\left\{\sigma+6s(1-\sigma)-z\left[\sigma+12s(1-\sigma)\right]/h\right\}$$

$$u_{\mathrm{main},r}(r,z) \;=\; \frac{1+\sigma}{\pi a Y}\sum_{m>0}\frac{p_m J_1(\zeta_m r/a)}{\zeta_m D_m}P_m(z)$$

with $D_m\equiv(1-q_m)^2-4q_m x_m^2$, and

$$-P_m(z) \;=\; \left[2q_m x_m^2+(1-2\sigma)(1-q_m+2q_m x_m)\right]\exp(-\zeta_m z/a)+$$

$$+q_m\left[2x_m^2-(1-2\sigma)(1-q_m+2x_m)\right]\exp(\zeta_m z/a)-$$

$$-\zeta_m\frac{z}{a}\left[(1-q_m+2q_m x_m)\exp(-\zeta_m z/a)+q_m(1-q_m+2x_m)\exp(\zeta_m z/a)\right]$$

and

$$u_{\mathrm{main},z}(r,z) \;=\; \frac{(1+\sigma)}{\pi a Y}\sum_{m>0}\frac{p_m J_0(\zeta_m r/a)}{\zeta_m D_m}Q_m(z)$$

where

$$\frac{1}{2}Q_m(z) \;=\; \left[(1-\sigma)(1-q_m+2q_m x_m)-q_m x_m^2)\right]\exp(-\zeta_m z/a)+$$

$$+q_m\left[(1-\sigma)(1-q_m+2x_m)+x_m^2\right]\exp(\zeta_m z/a)+$$

$$+\zeta_m\frac{z}{2a}\left[(1-q_m+2q_m x_m)\exp(-\zeta_m z/a)-q_m(1-q_m+2x_m)\exp(\zeta_m z/a)\right]$$

Despite the apparent complexity, this is extremely fast to compute (see the "Heating issues" chapter for algorithmic details). These formulas allow to draw (see Fig.3.25) the distorted shape of the solid, and to check that the distortion is minimized by the flat mode. It is also possible to give the strain components. By derivating the preceding expressions, we get:

$$E_{i,j}(r,z) \;=\; E_{\mathrm{main},i,j}(r,z)+\Delta E_{i,j}(r,z)$$

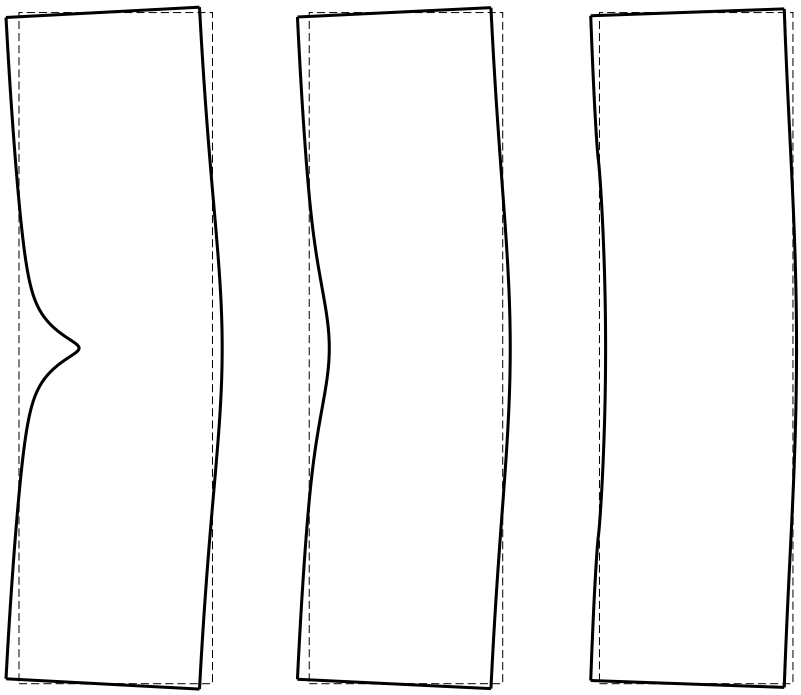

Figure 3.16: Distorted mirror for 1 N normalized pressure. From left to right: Gaussian mode, w=2cm, Gaussian mode w=5.54cm, flat mode of radius b =10cm. (exaggerated by a factor of 6×10^7)

with, in detail:

$$E_{\mathrm{main},rr}(r,z) = \frac{1+\sigma}{\pi a^2 Y}\sum_{m>0}\frac{p_m}{D_m}J_1'(\zeta_m r/a)\,P_m(z)$$

$$E_{\mathrm{main},\phi\phi}(r,z) = \frac{1+\sigma}{\pi a^2 Y}\sum_{m>0}\frac{p_m}{D_m}\,\frac{J_1(\zeta_m r/a)}{\zeta_m r/a}\,P_m(z)$$

$$E_{\mathrm{main},zz}(r,z) = \frac{1+\sigma}{\pi a^2 Y}\sum_{m>0}\frac{p_m}{D_m}J_0(\zeta_m r/a)\,\frac{a}{\zeta_m}Q_m'(z)$$

$$E_{\mathrm{main},rz}(r,z) = \frac{1+\sigma}{\pi a^2 Y}\sum_{m>0}\frac{p_m}{D_m}J_1(\zeta_m r/a)\,\frac{1}{2}\left[\frac{a}{\zeta_m}P_m'(z)-Q_m(z)\right]$$

$$E_{\mathrm{main}}(r,z) = \frac{1+\sigma}{\pi a^2 Y}\sum_{m>0}\frac{p_m}{D_m}J_0(\zeta_m r/a)\,\left[P_m(z)+\frac{a}{\zeta_m}Q_m'(z)\right]$$

The functions $P_m(z),\ Q_m(z)$ have been defined above. Moreover we have:

$$\frac{a}{\zeta_m}Q_m'(z)+P_m(z) = -2(1-2\sigma)\left[(1-q_m+2q_m x_m)\mathrm{e}^{-\zeta_m z/a}-q_m(1-q_m+2x_m)\mathrm{e}^{\zeta_m z/a}\right]$$

and

$$\frac{1}{2}\left[\frac{a}{\zeta_m}P_m'(z)-Q_m(z)\right] = \left(2q_m x_m^2-(1-q_m+2q_m x_m)\frac{\zeta_m}{a}z\right)\mathrm{e}^{-\zeta_m z/a}-$$

$$-\left(2q_m x_m^2-q_m(1-q_m+2x_m)\frac{\zeta_m}{a}z\right)\mathrm{e}^{\zeta_m z/a}$$

For the extra contributions, we have

$$\Delta E_{rr}(r,z) = \frac{1}{\pi a^2 Y}\left[\sigma+6s(1-\sigma)-z\left(\sigma+12s(1-\sigma)\right)/h\right]$$

$$\Delta E_{\phi\phi}(r,z) = \Delta E_{rr}(r,z)$$

$$\Delta E_{zz}(r,z) = \frac{1}{\pi a^2 Y}\left[(1+24s\sigma)z/h-1-12s\sigma)\right]$$

$$\Delta E_{rz}(r,z) = 0$$

$$\Delta E(r,z) = -\frac{1-2\sigma}{\pi a^2 Y}\left[1-12s-(1-24s)z/h\right]$$

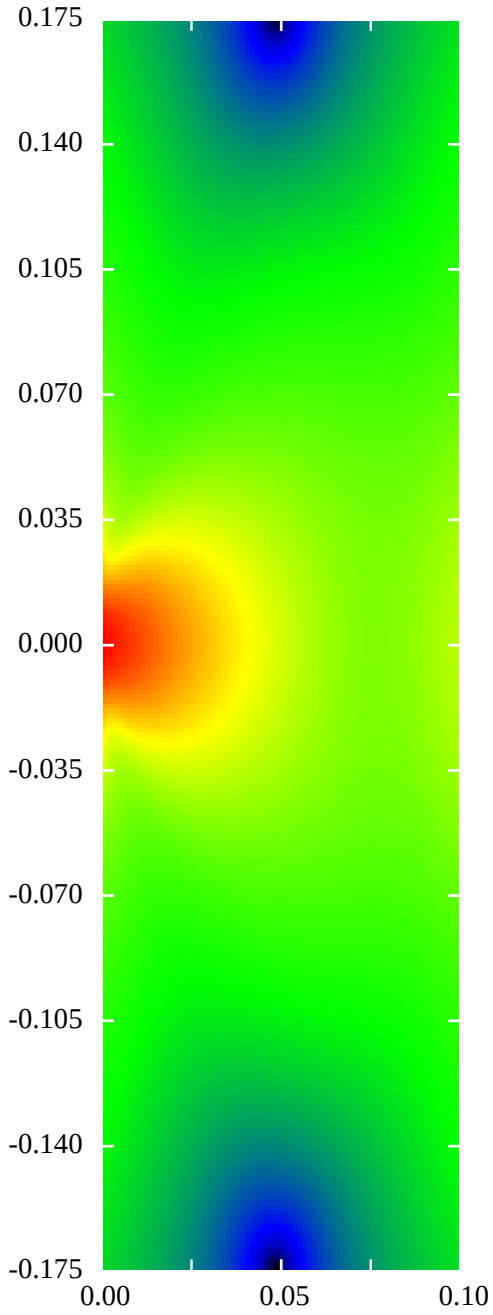

Figure 3.17: Distribution of strain energy in a cylindical mirror of radius a=17.5 cm, of thickness h=10 cm, under a gaussian pressure w=2 cm. Logarithmic scale

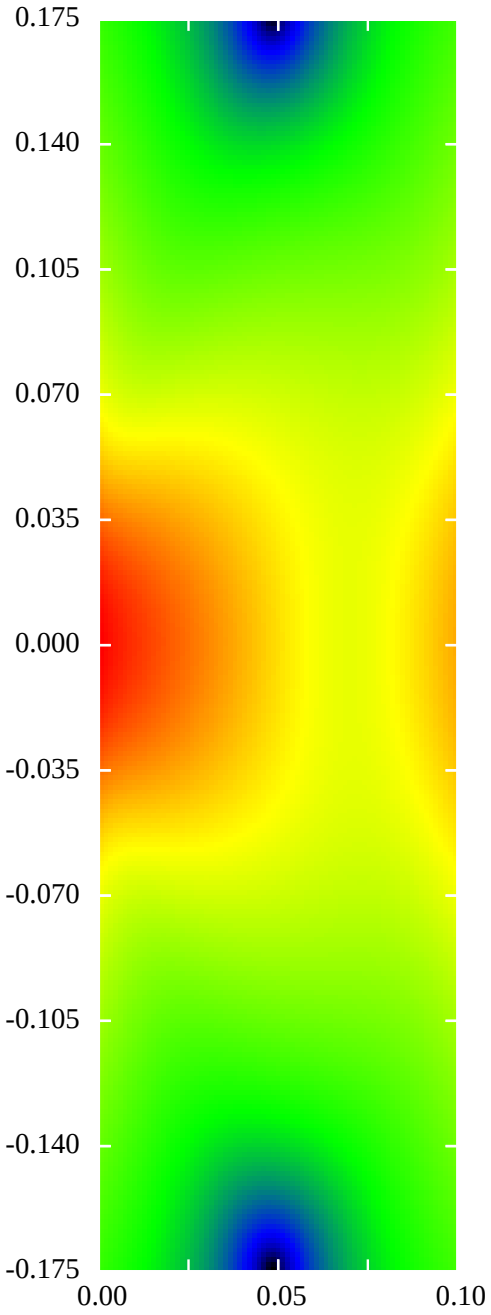

Figure 3.18: Distribution of strain energy in a cylindical mirror of radius a=17.5 cm, of thickness h=10 cm, under a gaussian pressure w=5.54 cm.Logarithmic scale

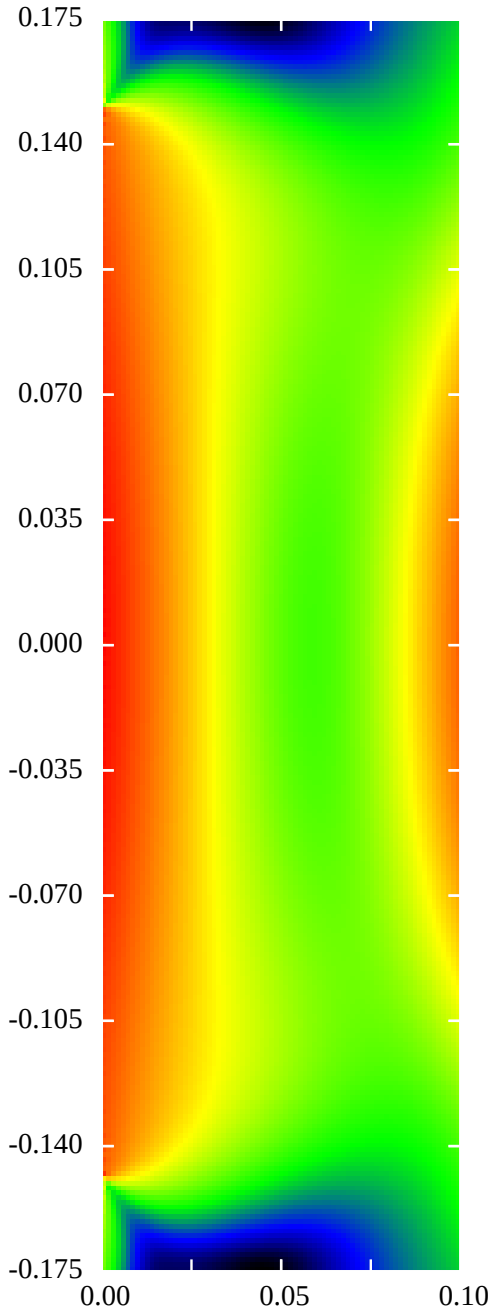

Figure 3.19: Distribution of strain energy in a cylindical mirror of radius a=17.5 cm, of thickness h=10 cm, under a flat top pressure b=15 cm.Logarithmic scale

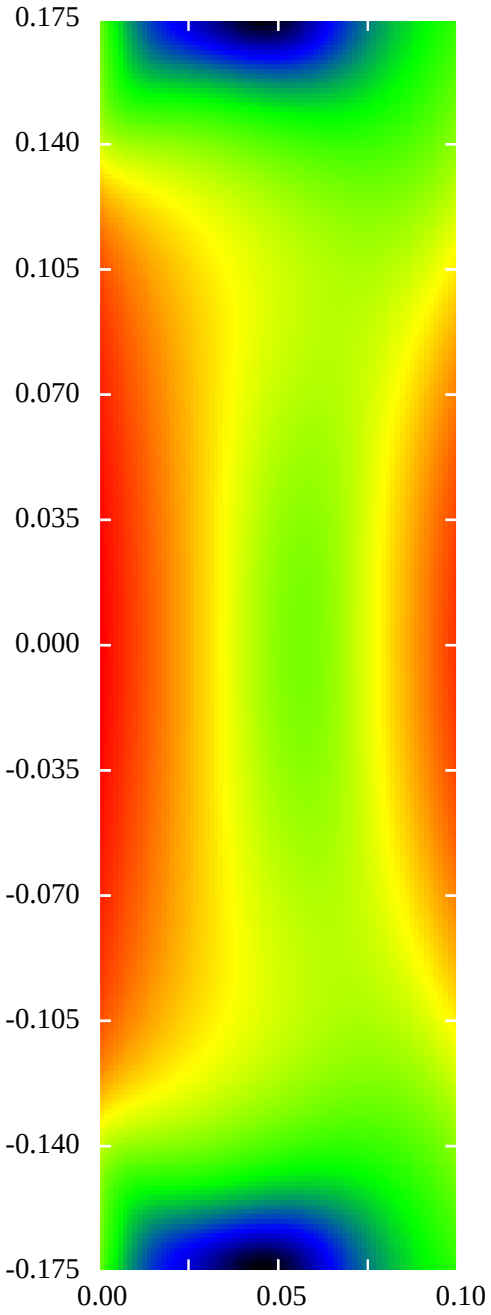

Figure 3.20: Distribution of strain energy in a cylindical mirror of radius a=17.5 cm, of thickness h=10 cm, under a realistically flat pressure b=15 cm.

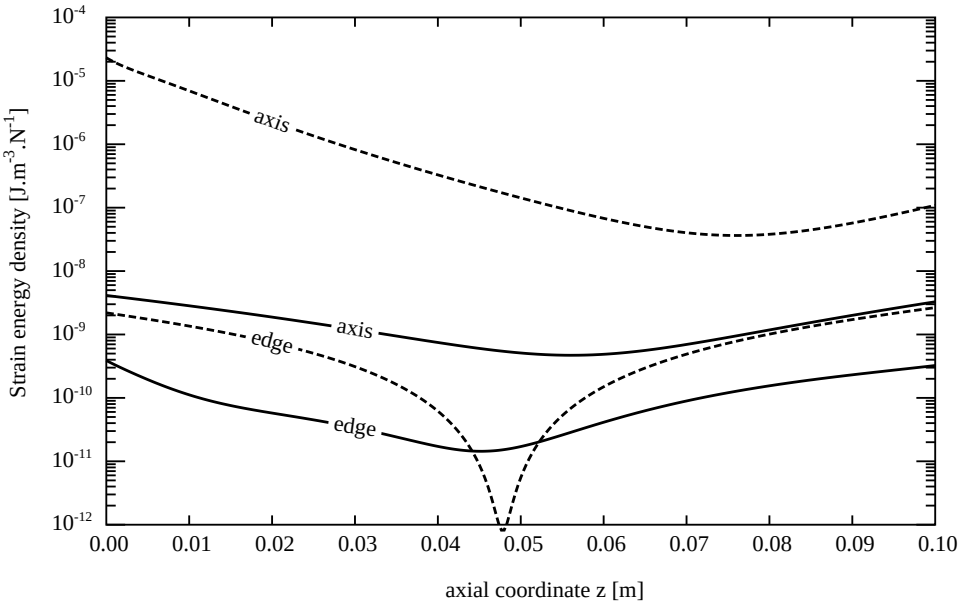

Figure 3.21: Distribution of strain energy on the axis and on the edge of a cylindrical mirror (a=17.5 cm, h=10 cm). Case of a gaussian (w=2 cm) beam (dashed lines), and of a realistic flat beam (b=0.15 m) (solid lines)

so that it is possible to compute explicitly the strain energy density:

$$w(r,z) \;=\; \frac{Y}{2(1+\sigma)}\left[\frac{E(r,z)^2}{1-2\sigma} + E_{rr}(r,z)^2 + E_{\phi\phi}(r,z)^2 + E_{zz}(r,z)^2 + 2E_{r,z}(r,z)^2\right]$$

The following pictures (Fig.3.17,3.18,3.19,3.20) show the distribution of w in some cases examined above. The energy density is weak on the edge, and this is even more clear for wider w and a fortiori, in average for flat beams and realistic flat beams. We show in Fig.3.21 the energy density on the axis and on the edge in the two extreme cases, namely a gaussian beam of width 2 cm, and a realistic flat mode of radius 15 cm. It can be seen that the energy density is much lower on the edge than on the hot point on the axis, in both cases, even if there is a sharp minimum for the gaussian beam, locally lower than the flat beam average.

3.9 Higher order LG modes

3.9.1 Introduction

Another interesting possibility is to spread power on the mirror's surface by using high order gaussian TEM modes. We restrict here our attention to axisymmetrical modes, for which the BHV model is relevant. The interest of using gaussian modes is to keep using spherical mirrors, instead of exotic surfaces. We hope the effect of misalignments to be significantly lower than with flat modes.

3.9.2 The BHV model

In the case where both the mirrors and the beam are assumed axisymmetrical, there exists a model allowing an accurate calculation of the low frequency tail of the spectral densities of internal noises. As a result of Levin's [?] theory The power spectral density (PSD) of displacement equivalent to thermal noise takes the general (low frequency) form :

$$S_x(f) \;=\; \frac{4k_BT}{\pi f}\,\phi\,U \tag{3.37}$$

where ϕ is a loss angle, and where U is the strain energy of the mirror under a pressure distribution having the same profile as the readout beam, and normalized to 1 N.

Let us summarize the results of the preceding chapter. the total internal energy is the sum of two contributions:

$$U \;=\; U_0 \;+\; \Delta U$$

that can be computed separately. Let a be the radius of the mirror and h its thickness. Let $J_\nu(x)$ be the Bessel functions, and $\{\zeta_k,\, k > 0\}$ the family of all non-zero solutions of $J_1(\zeta) = 0$. Let us note $x_k \equiv \zeta_k h/a$, and $q_k \equiv \exp(-2x_k)$. Let Y be the Young modulus of the mirror's material and σ its Poisson ratio.

Then we have:

$$U_0 \;=\; \frac{1-\sigma^2}{\pi a Y} \sum_{k>0} \frac{J_0^2(\zeta_k) p_k^2}{\zeta_k} \frac{1 - q_k^2 + 4 q_k x_k}{(1-q_k)^2 - 4 q_k x_k^2} \tag{3.38}$$

The dimension of U is J.N^{-2}.

In the preceding expression the Fourier-Bessel coefficients $\{p_k,\, k > 0\}$ are determined by the pressure profile. If we denote by $p(r)$ this pressure distribution, we have:

$$p_k \;=\; \frac{2\pi}{J_0^2(\zeta_k)} \int_0^a p(r) J_0(\zeta_k r/a)\, r\, dr \tag{3.39}$$

For the second contribution, we have:

$$\Delta U \;=\; \frac{a^2}{6\pi h^3 Y} \left[\left(\frac{h}{a}\right)^4 + 12\sigma\xi \left(\frac{h}{a}\right)^2 + 72(1-\sigma)\xi^2 \right] \tag{3.40}$$

with

$$\xi \;\equiv\; \sum_{k>0} p_k J_0(\zeta_k)/\zeta_k^2$$

At this level, the computation amounts to find the p_k.

3.9.3 Power profiles

In the case of an ideal flat-top mode of radius b, the pressure distribution is:

$$p_{\text{flat}}(r) \;=\; \begin{cases} 1/\pi b^2 & (r \le a) \\ 0 & (r > a) \end{cases} \tag{3.41}$$

As seen in the preceding section, the p_k coefficients are [?]

$$p_{k,\mathrm{flat}} \;=\; \frac{2aJ_1(\zeta_k b/a)}{b\zeta_k\, J_0^2(\zeta_k)}$$

In the case of a Gaussian TEM_{00} readout mode of normalized amplitude

$$\Psi_{0,0}(r) \;=\; \sqrt{\frac{2}{\pi w^2}}\,\exp(-r^2/w^2),$$

the pressure distribution is:

$$p(r) \;=\; |\Psi_{0,0}(r)|^2$$

and the p_k coefficients are:

$$p_{k,0}^{(0)} \;=\; \frac{1}{J_0(\zeta_k)^2}\,\exp\left[-\frac{\zeta_k^2 w^2}{8a^2}\right]$$

The preceding result can be extended to the case of any axisymmetrical Laguerre-Gauss mode $\mathrm{LG}_{n,m}$. It is well known that the paraxial diffraction equation (relevant for finding the eigenmodes of a resonant cavity with weakly spherical mirrors) admits solutions of the form (in polar coordinates)

$$\Psi_{n,m}(r,\phi,z) \;=\; \sqrt{\frac{2}{\pi w(z)^2}\,\frac{m!}{(m+n)!}}\,\exp(-r^2/w(z)^2)\,(2r^2/w(z)^2)^{n/2}\,L_m^{(n)}[2r^2/w(z)^2]\,\times$$

$$\times\;\exp(in\phi)\;\exp[-i(2m+n+1)\arctan(z/z_R)]\;\exp[i\pi r^2/\lambda R(z)]\;\exp(2i\pi z/\lambda) \tag{3.42}$$

where the $L_m^{(n)}(x)$ are the Generalized Laguerre polynomials. λ is the wavelength and z_R the Rayleigh parameter. The functions $w(z)$ and $R(z)$ determine respectively the width of the mode, and the curvature radius of its wavefront. In what follows, we only need $w(z)$. At the location z_M of a mirror, the normalized pressure distribution has therefore the general expression:

$$p_m^{(n)}(r) \;=\; \frac{2}{\pi w^2}\frac{m!}{(m+n)!}\,\exp(-2r^2/w^2)\,(2r^2/w^2)^n\,L_m^{(n)}(2r^2/w^2)^2$$

depending on the parameter $w \equiv w(z_M)$. If the ratio a/w is large enough that the diffraction losses are small, we can replace the finite upper bound of integral (3.39) by $+\infty$, and the Fourier-Bessel coefficients are simply:

$$p_{k,m}^{(n)} \;=\; \frac{1}{J_0(\zeta_k)^2}\,\exp\left[-\frac{\zeta_k^2 w^2}{8a^2}\right]\;L_m^{(0)}\left(\frac{\zeta_k^2 w^2}{8a^2}\right)\,L_{n+m}^{(0)}\left(\frac{\zeta_k^2 w^2}{8a^2}\right)$$

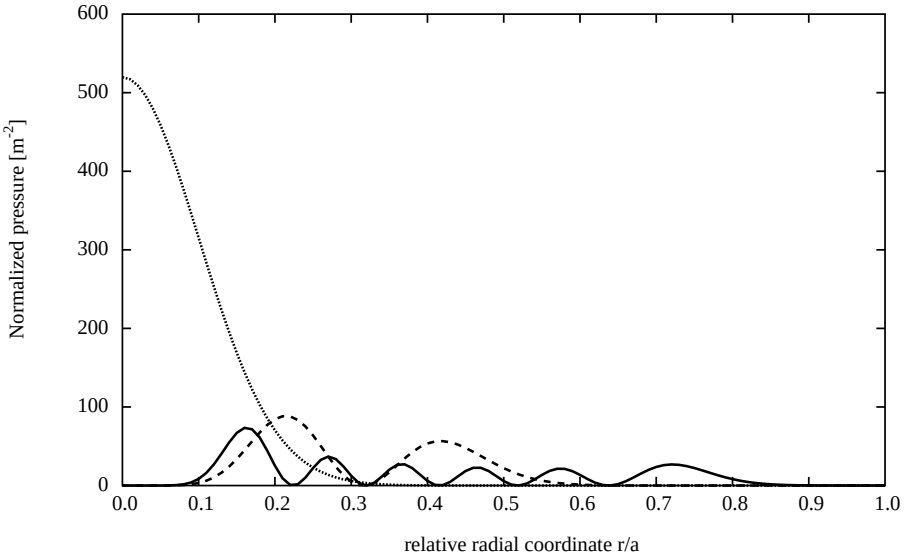

Figure 3.22: Pressure profiles. (0,0): dotted, (4,1): dashed, (5,5): solid

If the diffraction losses are not small, the preceding expression losses some accuracy, but simultaneously the corresponding mode losses its practical interest. The pressure profiles on the input mirror for some among the first Laguerre-Gauss modes of parameter $w = 3.5$ cm are represented on Fig.3.22. See on Fig.3.23 the intensity pattern of a $LG_{5,5}$ (for instance) mode. The integrated power (Fig.3.24) clearly shows a smoother distribution of power on the mirror's surface. Some examples of the virtual deformation of the mirror's surface under a pressure normalized to 1 N can be seen on Fig.3.25 with again w=3.5 cm. For the mirror's size, we assume a radius a= 17.5 cm and a thickness h= 10 cm. One clearly sees that the strain is a decreasing function of the orders (n, m) of the mode.

3.10 Relative gains on thermal noise

With the current parameters a= 17.5 cm, h = 10 cm, w= 2 cm of the Virgo input mirrors, if we insert the preceding $p_{k,m}^{(n)}$ in equations 3.38 and 3.40, we

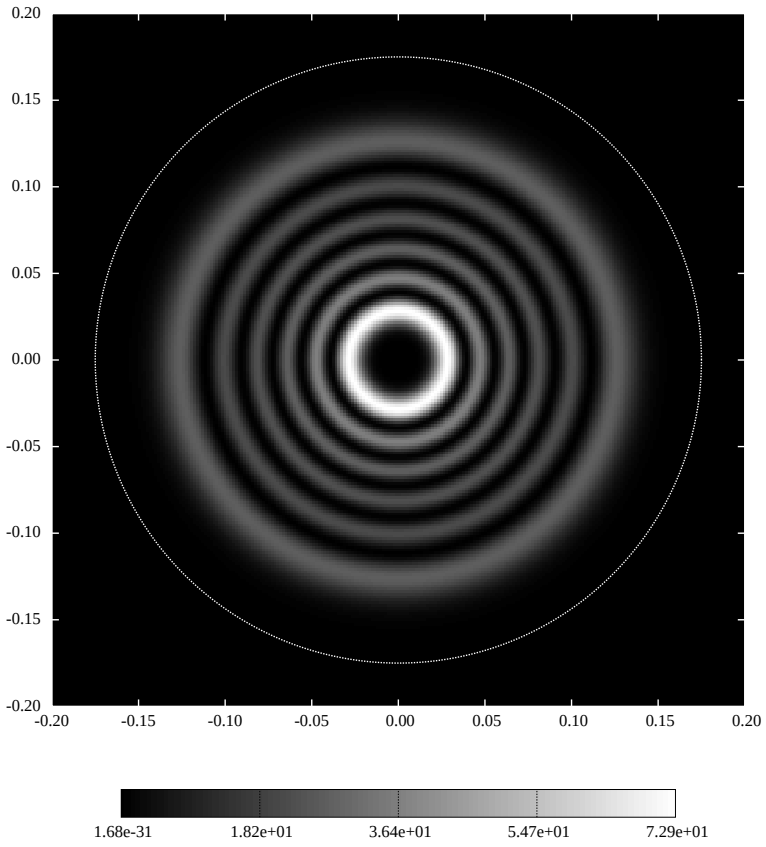

Figure 3.23: Intensity pattern of a $LG_{5,5}$ mode of Gaussian parameter $w = 3.5$ cm. The faint circle represents the edge of a 17.5 cm radius mirror (units: m).

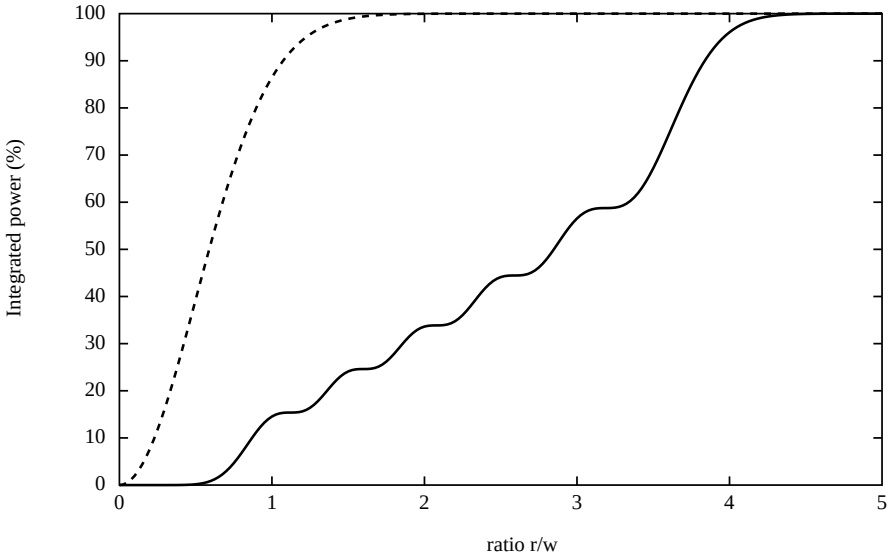

Figure 3.24: Integrated power for $LG_{5,5}$ (solid line) and $LG_{0,0}$ (dashed line) (w=3.5 cm)

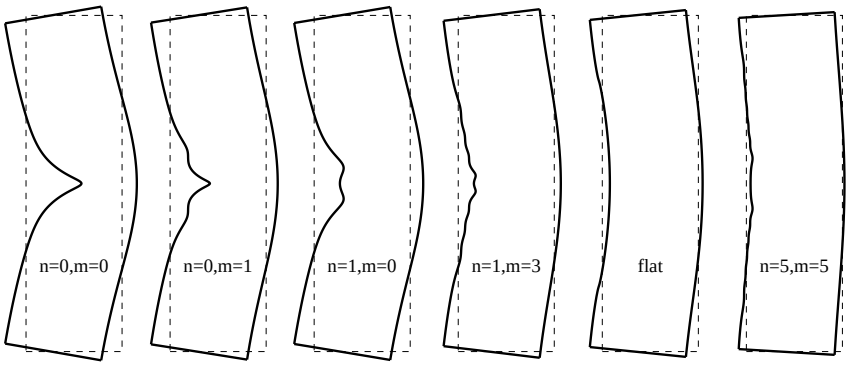

Figure 3.25: Deformation of a cylindrical mirror (a= 17.5 cm, h= 10 cm) under a $LG_{n,m}$ readout beam (w = 3.5 cm) normalized to 150 MW (1 N integrated radiation pressure), exaggerated by a factor of 2×10^8. The case of a flat beam b = 11.3 cm is also shown

find for the fundamental:

$$U^{(0)}_{\text{input},0} \;=\; 2.02\ 10^{-10}\text{J.N}^{-2} \tag{3.43}$$

then, for the Virgo end mirrors (w= 5.54 cm):

$$U^{(0)}_{\text{end},0} \;=\; 7.43\ 10^{-11}\text{J.N}^{-2} \tag{3.44}$$

For comparison, with a flat mode of radius 11.3 cm, we have

$$U_{\text{flat}} \;=\; 1.88\ 10^{-11}\text{J.N}^{-2} \tag{3.45}$$

The gain in thermal noise are:

$$g_{\text{end/input}} \;=\; \sqrt{\frac{U^{(0)}_{\text{end},0}}{U^{(0)}_{\text{input},0}}} \;\sim\; 0.6$$

$$g_{\text{flat/input}} \;=\; \sqrt{\frac{U_{\text{flat}}}{U^{(0)}_{\text{input},0}}} \;\sim\; 0.3$$

By increasing the order of the LG mode and the beam parameter w, it is possible to reach gains comparable to this flat mode. For instance, with a $\text{LG}_{0,3}$ mode of parameter w = 4.5 cm, or a $\text{LG}_{1,2}$ mode of parameter w = 4.78 cm, we get in both cases

$$U \;=\; 1.85\ 10^{-11}\text{J.N}^{-2}$$

meaning a gain of $\sim$ 0.3, and it is possible to do better. One must however consider the diffraction losses when the width w of the mode becomes too large compared to the mirror's radius a (see Fig.3.26). For each mode, there is a ratio a/w such that the losses fall to 1 ppm, and when comparing the gains for various orders, it is more relevant to take equal losses modes. On Fig.3.27 we show the ratio a/w insuring diffraction losses of 1 ppm, versus orders of the mode. We finally show (Fig.3.28) the gains relative to the worse situation of Virgo (input mirrors, $\text{LG}_{0,0}$, w=2 cm) for several higher order modes having each a w parameter adjusted to set diffraction losses at 1 ppm; the gain of the flat mode of size 11.3 cm (having the same losses) is also shown. Optimization of the beam parameter leads to symmetrical cavities having equally curved mirrors. Modes with $m \geq 2$ give already similar or better results than the flat mode.

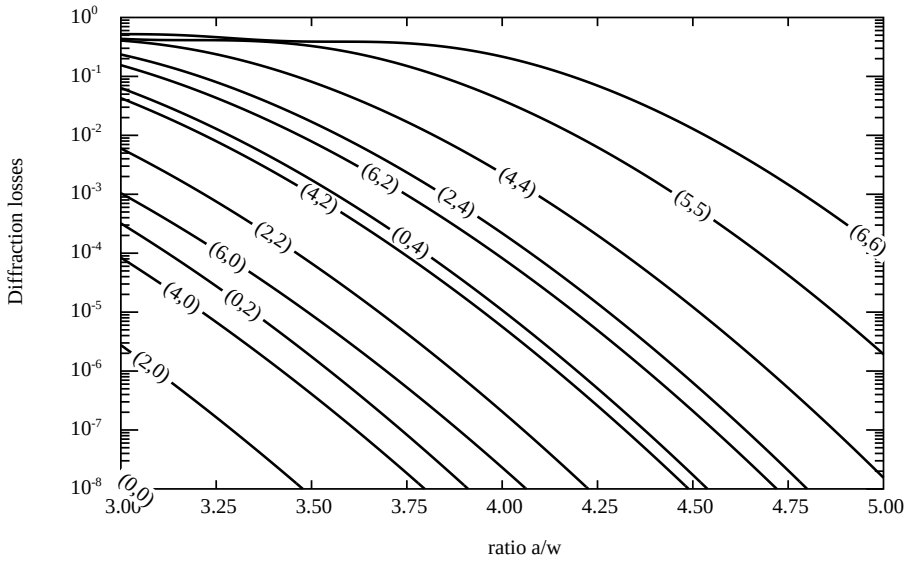

Figure 3.26: Diffraction losses vs ratio a/w for several LG modes

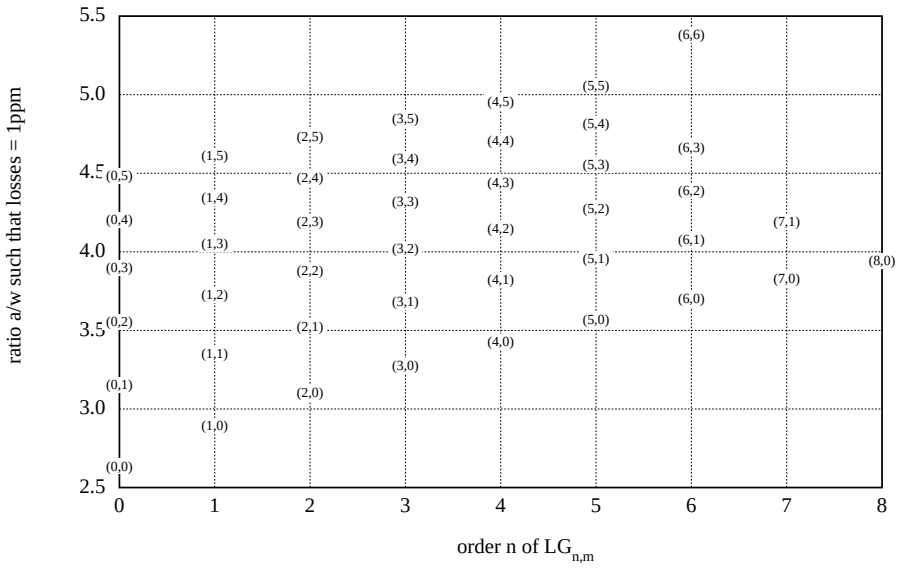

Figure 3.27: ratio a/w insuring 1 ppm diffraction losses vs order of the LG mode

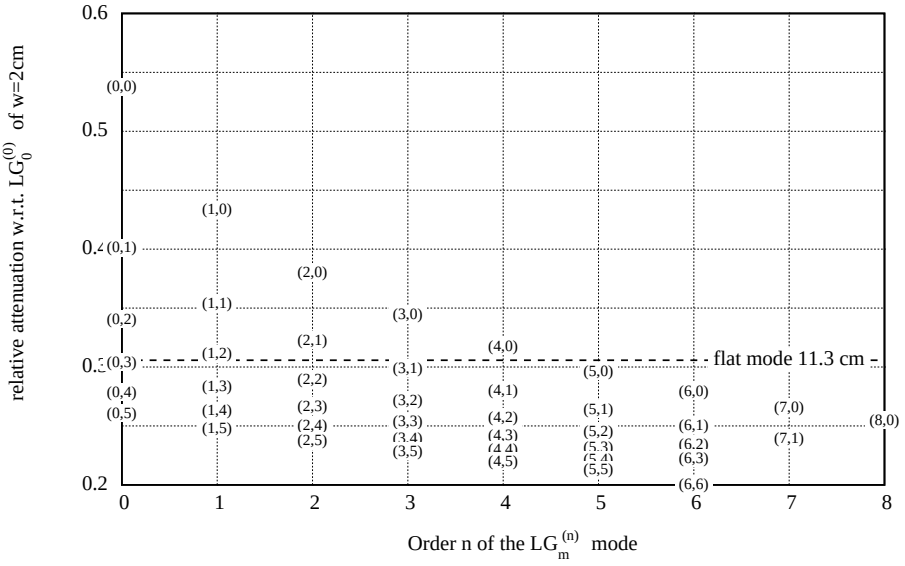

Figure 3.28: Relative reduction in root spectral density of thermal noise vs order (n, m) of the LG mode (each having a w tuned for 1 ppm diffraction losses).

To be specific, let us compute the spectral densities of displacement equivalent to thermal noise in some cases. We assume a loss angle of $\phi = 10^{-6}$. Firstly, in the case of a $\mathrm{TEM}_{0,0}$, $w = 2$ cm beam on a Virgo input mirror:

$$S_x^{1/2}(f) = 1.03\,10^{-19} \left[\frac{100\,\mathrm{Hz}}{f}\right]^{1/2} \mathrm{m.Hz}^{-1/2} \tag{3.46}$$

for $w = 3.5$ cm:

$$S_x^{1/2}(f) = 7.90\,10^{-20} \left[\frac{100\,\mathrm{Hz}}{f}\right]^{1/2} \mathrm{m.Hz}^{-1/2} \tag{3.47}$$

then for a flat mode of radius 11.3 cm:

$$S_x^{1/2}(f) = 3.15\,10^{-20} \left[\frac{100\,\mathrm{Hz}}{f}\right]^{1/2} \mathrm{m.Hz}^{-1/2} \tag{3.48}$$

and now for a $\mathrm{LG}_{5,5}$, $w = 3.5$ cm:

$$S_x^{1/2}(f) = 2.13\,10^{-20} \left[\frac{100\,\mathrm{Hz}}{f}\right]^{1/2} \mathrm{m.Hz}^{-1/2} \tag{3.49}$$

If we compare the 1st example (standard Virgo) to the third (in some "advanced Virgo"), we note a gain factor of ~ 5 in sensitivity in the 100 Hz region.

3.11 Conclusion and perspectives

It is possible to have a reduction of thermal noise comparable to or even better than that obtained with flat modes, by using moderately high order Laguerre-Gauss axisymmetrical modes. It seems beneficial that these modes are compatible with spherical cavity mirrors instead of "Mexican" surface shapes. The diffraction losses on the end mirror would however be too large in the present design (flat/spherical) of the Virgo cavities (2 cm waist on flat input mirror). If the flat/spherical cavities are replaced by symmetrical spherical/spherical cavities, that issue could be overcome. The question of generation of such modes having complex annular patterns could be solved by the recently developed fiber technology (Bragg fibers)[33], allowing to design fiber-lasers with analogous mode structures. A study of the optical stability of such a cavity operating with a $\mathrm{LG}_{n,m}$ mode is now necessary to confirm that it could be practically operated this way. In particular, the issue of the degeneracy of $\mathrm{LG}_{n,m}$ modes having the same $n + 2m$ is to be addressed.

Chapter 4

Thermoelastic noise

4.1 Introduction

The brownian motion of matter inside the substrates is not the only cause of noise in the optical readout. There is another cause due to temperature fluctuations in a finite volume of material. These fluctuations are called thermodynamical and can couple with strain via the thermal dilatation constant α, producing eventually random motions of the surface. A good way for modeling this kind of noise is to start from the general thermodynamical formulas as detailed by Landau and Lifshitz [31], and use the Levin approach already presented. As in the preceding chapter, we shall consider the low frequency tail of the spectral density of the effective motion of the surface (i.e. the readout noise) as depending on the energy dissipated when the body is under a virtual pressure having the same profile as the optical beam and excited at low frequency. In this case, the spectral density is still of the form (Levin's formula):

$$S_x(f) \;=\; \frac{4k_BT}{\omega^2}\,W \tag{4.1}$$

where W is the average dissipated energy. For the standard thermal noise, we had $W = 2U\omega\Phi$ as average dissipated energy, Φ being a global loss angle and U the static strain energy. But now W must be interpreted as the energy dissipated via coupling of the strain with the temperature field in the bulk. Obviously, the temperature field itself depends on the strain field. Using the same approach as used in [29], we first solve the static linear elastical problem (it is done in the preceding chapter), then we compute the resulting temperature field, and use it to compute the dissipated energy. For

computing the dissipated energy, we use the time dependence of the entropy S. The variations of the entropy density are related to the heat flux $\vec{q}$ by requiring conservation of the energy in the body:

$$T\,\frac{\partial S}{\partial t} \;=\; -\,\mathrm{div}(\vec{q}) \tag{4.2}$$

where $\vec{q} = -K\,\mathrm{grad}T$, K being the thermal conductivity of the material (cf.Landau and Lifshitz [31]). Or, as well:

$$\frac{\partial S}{\partial t} \;=\; -\,\frac{1}{T}\mathrm{div}(\vec{q})$$

The total entropy variation in the body is therefore:

$$\frac{dS_{\mathrm{tot}}}{dt} \;=\; -\int \frac{1}{T}\mathrm{div}(\vec{q})\,dV$$

where the integral is extended to the whole body. this is as well:

$$\frac{dS_{\mathrm{tot}}}{dt} \;=\; -\int \mathrm{div}\frac{\vec{q}}{T}\,dV + \int \vec{q}.\mathrm{grad}\left(\frac{1}{T}\right)\,dV$$

Owing to the fact that the heat flux is zero on the surface of the body, the first integral vanishes, and we have:

$$\frac{dS_{\mathrm{tot}}}{dt} \;=\; -\int \frac{1}{T^2}\,\vec{q}.\mathrm{grad}\,T\,dV$$

but using the definition of $\vec{q}$, this is:

$$\frac{dS_{\mathrm{tot}}}{dt} \;=\; \int \frac{K}{T^2}\,(\mathrm{grad}\,T)^2\,dV$$

so that the energy variation is :

$$W \;=\; T\,\frac{dS_{\mathrm{tot}}}{dt} \;=\; \int \frac{K}{T}\,(\mathrm{grad}\,T)^2\,dV \tag{4.3}$$

We shall say now that the temperature gradient field is caused by the small deformations of the body that we have computed precedingly, while T is the mean temperature. This becomes:

$$W \;=\; T\,\frac{dS_{\mathrm{tot}}}{dt} \;=\; \frac{K}{T}\int (\mathrm{grad}\,\delta T)^2\,dV \tag{4.4}$$

Where we have replaced T by a δT in the gradient for more clarity. On the other hand, it is well known (cf. Landau-Lifshitz) that the total entropy is the sum of two terms, one being the entropy in the reference state, and a second one proportional to the trace E of the strain tensor:

$$S = S_0 + \nu E$$

ν being the thermoelastic coefficient. so that there is in the bulk material a power source given by

$$P \;=\; T.\frac{dS}{dt} \;=\; \nu\, T\, \frac{dE}{dt}$$

where E is the trace of E_{ik}. The resulting temperature field obeys the Heat (Fourier) equation:

$$(\rho C \partial_t - K\,\Delta)\,\delta T \;=\; \nu\, T\, \frac{dE}{dt} \tag{4.5}$$

The trace of the strain tensor E_{ik} found in the preceding chapter is in any case a harmonic function, so that there is a trivial solution:

$$\delta T \;=\; \frac{\nu T}{\rho C}\, E$$

The boundary conditions (null heat flux on the surfaces) are considered satisfied in time average (δT is assumed oscillating at a few tens of Hz).In fact, they are exactly satisfied on the circular edge of the mirror. Now we reach the relevant equation for the dissipated energy:

$$W \;= \frac{K\nu^2 T}{\rho^2 C^2} \int (\text{grad}\; E)^2\, dV \tag{4.6}$$

ν is related to the linear dilatation coefficient α by

$$\nu \;=\; \frac{\alpha\, Y}{1-2\sigma}$$

where Y is the Young modulus, and σ the Poisson ratio. Finally:

$$W \;=\; KT \left[\frac{\alpha Y}{(1-2\sigma)\rho C}\right]^2 \int (\text{grad}\; E)^2\, dV \tag{4.7}$$

(see [29]). We have after the preceding chapter on standard thermal noise all the material for computing W.

4.2 Case of infinite mirrors

Let us recall the results obtained in the preceding chapter on standard thermal noise. Under beam pressure, the displacement vector is:

$$u_r(r,z) \;=\; \int_0^\infty u(k)\,[kz-1+2\sigma]\exp(-kz)\,J_1(kz)\,k\,dk \tag{4.8}$$

$$u_z(r,z) \;=\; \int_0^\infty u(k)\,[kz+2-2\sigma]\exp(-kz)\,J_0(kz)\,k\,dk \tag{4.9}$$

so that:

$$E(r,z) \;=\; \mathrm{div}\,\vec{u}(r,z) \;=\; -2(1-2\sigma)\int_0^\infty u(k)\,\exp(-kz)\,J_0(kz)\,k^2\,dk \tag{4.10}$$

The function $u(k)$ is determined by the virtual pressure distribution $p(r)$. Namely:

$$u(k) \;=\; -\frac{1+\sigma}{Y}\,\frac{\tilde{p}(k)}{k} \tag{4.11}$$

where $\tilde{p}(k)$ is the Fourier-Bessel transform of $p(r)$. As a result,

$$E(r,z) \;=\; -\,\frac{2(1-2\sigma)(1+\sigma)}{Y}\int_0^\infty \tilde{p}(k)\,\exp(-kz)\,J_0(kr)\,k\,dk$$

Which shows, in passing, that

$$E(r,0) \;=\; -\,\frac{2(1-2\sigma)(1+\sigma)}{Y}\,p(r)$$

We can thus already foresee that in the case of an ideally flat top beam, the gradient will involve Dirac distributions, and therefore the volume integration of its square will be problematic. Let us compute the gradient of E:

$$\frac{\partial E}{\partial r} \;=\; \frac{2(1-2\sigma)(1+\sigma)}{Y}\int_0^\infty \tilde{p}(k)\,\exp(-kz)\,J_1(kz)\,k^2\,dk$$

$$\frac{\partial E}{\partial z} \;=\; \frac{2(1-2\sigma)(1+\sigma)}{Y}\int_0^\infty \tilde{p}(k)\,\exp(-kz)\,J_0(kz)\,k^2\,dk$$

Now, using the closure relation

$$\int_0^\infty J_\nu(kr)\,J_\nu(k'r)\,r\,dr \;=\; \frac{\delta(k-k')}{k} \tag{4.12}$$

for $\nu = 0, 1$. It is now possible to carry out the volume integration:

$$2\pi \int_0^\infty r\,dr \int_0^\infty dz\,(\vec{\mathrm{grad}}E)^2 \;=\; 8\pi\,\frac{(1-2\sigma)^2(1+\sigma)^2}{Y^2}\int_0^\infty \tilde{p}(k)^2\,k^2\,dk \quad (4.13)$$

so that

$$W \;=\; \frac{KT\alpha^2(1+\sigma)^2}{\rho^2 C^2}\int_0^\infty \tilde{p}(k)^2\,k^2\,dk \quad (4.14)$$

This expression shows that the function $\tilde{p}(k)$ must have an asymptotic behavior better than $k^{-3/2}$ for the integral to converge. This is a strong requirement on the Fourier transform of the pressure distribution.

4.2.1 Gaussian beams

For a gaussian profile of half width w, we have seen that:

$$\tilde{p}(k) \;=\; \frac{1}{2\pi}\,\exp\left[-k^2w^2/8\right]$$

giving

$$\int (\vec{\mathrm{grad}}E)^2\,dV \;=\; \frac{4(1-2\sigma)^2(1+\sigma)^2}{\sqrt{\pi}Y^2w^3} \quad (4.15)$$

so that the spectral density of thermoelastic noise is, using (4.1) and (4.7):

$$S_x(f) \;=\; \frac{4k_BKT^2\alpha^2(1+\sigma)^2}{\sqrt{\pi}\,\rho^2\,C^2\,f^2w^3} \quad (4.16)$$

This result has been found firstly by Braginsky et al.[30], then by Liu et al.[29], using the preceding approach. For silica parameters:

$$K \;\sim\; 1.4\ \mathrm{W.m^{-1}.K^{-1}}$$
$$\alpha \;\sim\; 5.4\,10^{-7}\ \mathrm{K^{-1}}$$
$$\rho \;\sim\; 2,202\mathrm{kg.m^{-3}}$$
$$C \;\sim\; 7,500\ \mathrm{J.kg^{-1}.K^{-1}}$$

on finds:

$$S_x(f)^{1/2} \;=\; 2.68\,10^{-20}\,\left[\frac{1\ \mathrm{Hz}}{f}\right]\ \mathrm{m.Hz^{-1/2}}$$

which is lower than the standard thermal noise, but almost significant. For the end mirrors ($w = 5.54$ cm) , this is:

$$S_x(f)^{1/2} \;=\; 5.81\,10^{-21}\,\left[\frac{1\ \mathrm{Hz}}{f}\right]\ \mathrm{m.Hz^{-1/2}}$$

4.2.2 Flat beams

If we now consider a flat beam modeled by its ideal representation:

$$p(r) \;=\; \begin{cases} 1/\pi b^2 & (r < b) \\ 0 & (r \geq b) \end{cases}$$

we have the Fourier-Bessel transform:

$$\tilde{p}(k) \;=\; \frac{J_1(kb)}{\pi\, kb}$$

which shows that the requirement on the decreasing rate for large k is not fulfilled, $J_\nu(k)$ having an asymptotic behavior in $k^{-1/2}$. If we try to compute the integral, we get:

$$\int (\vec{\mathrm{grad}}\, E)^2\, dV \;=\; \frac{8(1-2\sigma)^2(1+\sigma)^2}{\pi b^3} \int_0^\infty J_1(x)^2\, dx$$

wich is a divergent integral.This is the consequence of our preceding remark on the discontinuity of the pressure. For fun, we note that "Mathematica" nevertheless gives a finite (and rather strange) result:

$$\int_0^\infty J_1(x)^2\, dx \;=\; \frac{\mathrm{Ln}(64) - 4 + 2\gamma}{2\pi}$$

(γ = Euler's constant). We meet two conclusions: the first is that we must carry out a numerical integration with the "realistic" flat modes detailed in the preceding chapter, the second is that we must be cautious with results of symbolic computation softwares.

4.3 Case of finite mirrors

In the case of finite mirrors, the model developped for standard thermal noise provides the explicit expressions for the trace E of the strain tensor:

$$E(r,z) \;=\; E_0(r,z) + \Delta E(r,z)$$

with

$$E_0(r,z) \;=\; -\,\frac{2(1-2\sigma)(1+\sigma)}{\pi a^2 Y} \sum_{m>0} \frac{p_m}{D_m} J_0(\zeta_m r/a) \left[u_m\, \mathrm{e}^{-\zeta_m z/a} - v_m\, \mathrm{e}^{\zeta_m z/a} \right]$$

where the p_m are the Fourier-Bessel coefficients of the pressure distribution, and where the D_m have been defined in the preceding chapter. The u_m, v_m are:

$$u_m = 1 - q_m + 2q_m x_m, \quad v_m = q_m(1 - q_m + 2x_m)$$

q_m and x_m have also the same definitions. Moreover,

$$\Delta E(r,z) = -\frac{1-2\sigma}{\pi a^2 Y}\left[1 - 12s - (1-24s)z/h\right]$$

so that the gradient of E is:

$$\frac{\partial E_0}{\partial r} = \frac{2(1-2\sigma)(1+\sigma)}{\pi a^3 Y}\sum_{m>0}\frac{p_m\zeta_m}{D_m}J_1(\zeta_m r/a)\left[u_m\,\mathrm{e}^{-\zeta_m z/a} - v_m\,\mathrm{e}^{\zeta_m z/a}\right] \tag{4.17}$$

$$\frac{\partial E_0}{\partial z} = \frac{2(1-2\sigma)(1+\sigma)}{\pi a^3 Y}\sum_{m>0}\frac{p_m\zeta_m}{D_m}J_0(\zeta_m r/a)\left[u_m\,\mathrm{e}^{-\zeta_m z/a} + v_m\,\mathrm{e}^{\zeta_m z/a}\right] \tag{4.18}$$

$$\frac{\partial \Delta E}{\partial z} = \frac{1-2\sigma}{\pi a^2 h Y}(1-24s) \tag{4.19}$$

Owing to the orthogonality relations for the $J_\nu(\zeta_m r/a)$, we get

$$\int(\vec{\mathrm{grad}}\,E_0)^2\,dV = \frac{4(1-2\sigma)^2(1+\sigma)^2}{\pi a^3 Y^2}\sum_{m>0} w_m \tag{4.20}$$

where

$$w_m = \frac{p_m^2\zeta_m}{D_m^2}J_0(\zeta_m)^2(1-q_m)\times$$
$$\times\left[(1-q_m)(1-q_m^2) + 8q_m(1-q_m)x_m + 4q_m(1+q_m)x_m^2\right]$$

and obviously,

$$\int(\vec{\mathrm{grad}}\,\Delta E)^2\,dV = \frac{(1-2\sigma)^2}{\pi a^2 h Y^2}(1-24s)^2$$

(NB: $\vec{\mathrm{grad}}\,\Delta E$ and $\vec{\mathrm{grad}}\,E_0$ are orthogonal in the r integration). We have successively:

$$W = \frac{4KT\alpha^2}{\pi a^3\rho^2 C^2}\left[(1+\sigma)^2\sum_{m>0} w_m + (1-24s)^2\frac{a}{4h}\right]$$

And for the spectral density:

$$S_x(f) = \frac{4k_B KT^2\alpha^2}{\pi a^3\rho^2 C^2 f^2}\left[(1+\sigma)^2\sum_{m>0} w_m + (1-24s)^2\frac{a}{4h}\right] \tag{4.21}$$

4.3.1 Gaussian beams

For gaussian beams, we substitute the p_m's in the preceding formulae. For the parameters corresponding to Virgo input mirrors (w =2 cm, a = 17.5 cm, h = 10 cm, we find:

$$S_x^{1/2}(f) \;=\; 2.76\,10^{-20}\ \mathrm{m.Hz}^{-1/2}\left[\frac{1\ \mathrm{Hz}}{f}\right]$$

slightly worse than the infinite case. For w = 5.54 cm (end mirrors):

$$S_x^{1/2}(f) \;=\; 8.20\,10^{-21}\ \mathrm{m.Hz}^{-1/2}\left[\frac{1\ \mathrm{Hz}}{f}\right]$$

in Fig.4.1, one sees the distribution of $(\mathrm{grad}E)^2$ in the case of an input Virgo mirror. which is worse than the infinite case.

4.3.2 Flat modes

The same drawback happens in the case of ideally flat modes. The sharp edge generates high spatial frequencies that forbid the Fourier-Bessel coefficients p_m to have a decreasing rate able to secure the convergence of the series. One more time we have to numerically compute the p_m for realistic flat modes. The result for a Virgo-like mirror (a = 17.5 cm, h = 10 cm) and for a realistic mode (b = 10 cm, w_0 = 3.2 cm), is:

$$S_x^{1/2}(f) \;=\; 4.89\,10^{-21}\ \mathrm{m.Hz}^{-1/2}\left[\frac{1\ \mathrm{Hz}}{f}\right] \tag{4.22}$$

It is weakly dependent on the parameter w_0 (sharpness of the beam's edge). To be specific, for w_0 = 1 cm, this is

$$S_x^{1/2}(f) \;=\; 4.92\,10^{-21}\ \mathrm{m.Hz}^{-1/2}\left[\frac{1\ \mathrm{Hz}}{f}\right]^2$$

On Fig.4.2, we have represented the distribution of $(\mathrm{grad}E)^2$ for a realistic flat mode (b = 10 cm, w_0 = 1 cm). Note the two "hot" points corresponding to the regions where the gradient is the largest. When sharping the edge, these points become hoter and hoter, yielding a singularity in the limit of an ideal flat top beam.

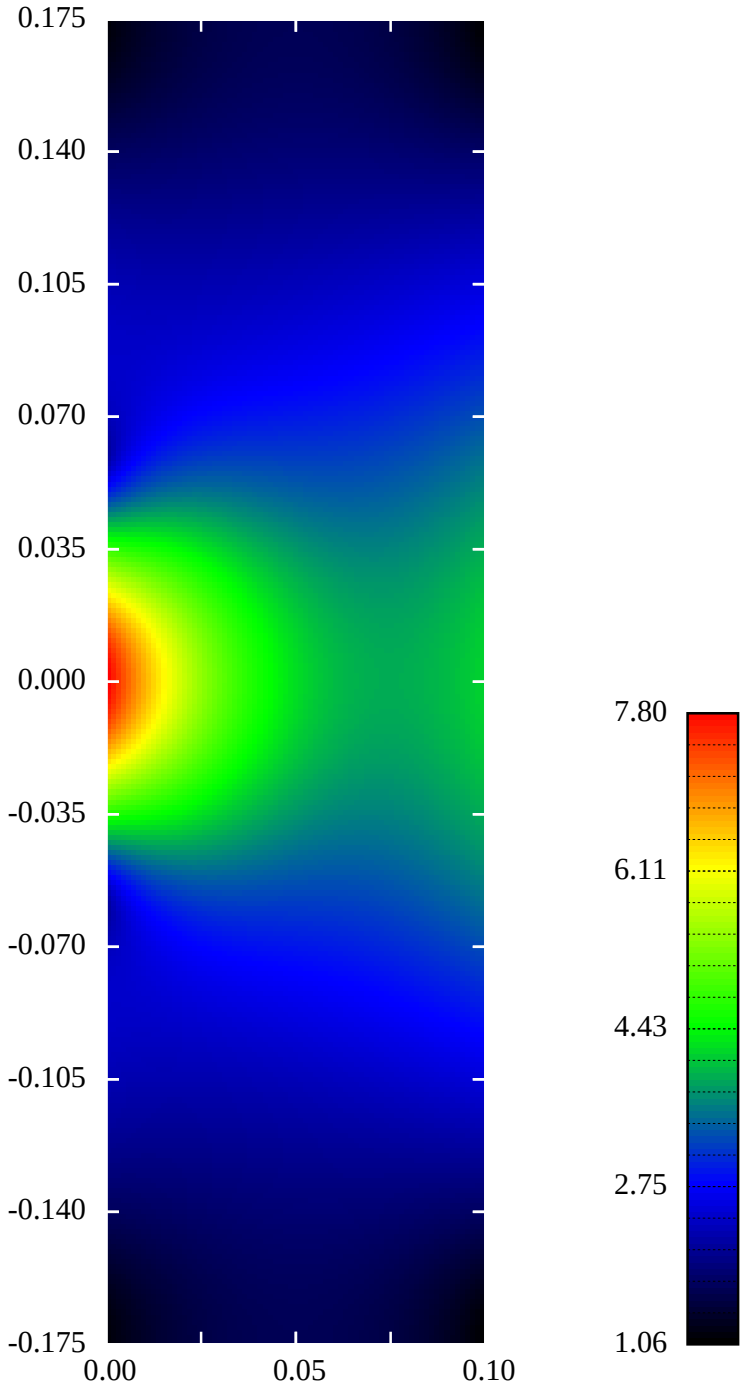

Figure 4.1: Distribution of the square gradient of the temperature in the case of a gaussian beam. (Logarithmic scale, arbitrary units)

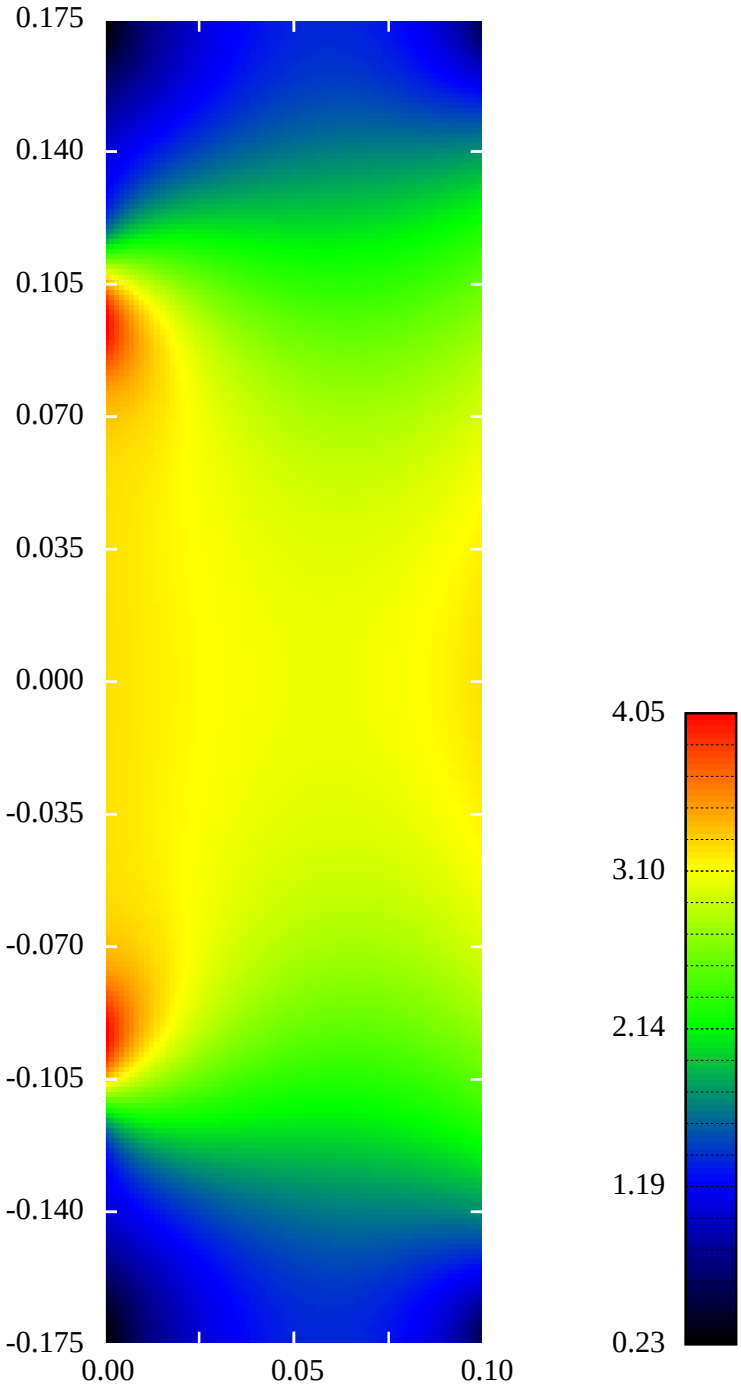

Figure 4.2: Distribution of the square gradient of the temperature in the case of a realistic flat beam. (Logarithmic scale, arbitrary units)

Chapter 5

Fundamentals of the LISA Formation flight

In order to escape the seismic perturbation caused at low frequency by the Newtonian gravity gradients, it has been proposed since a long time to install low frequency (below 1 Hz) antennas in space, where most of terrestrial perturbations vanish and where long range optical beams can be sent in a good vacuum. Long range means several millions of km, and it is not clear at first sight at what accuracy level a formation flight of several spacecraft having that mutual distances can stay in a stable configuration. We discuss here the ideas brought mainly by Peter Bender (JILA, Colorado, USA) for solving that issue.

5.1 Elementary LISA orbitography

By "elementary", we mean a classical (Newtonian) theory involving a central potential and three test particles (the LISA spacecraft)

5.1.1 Keplerian LISA orbits

As a first approximation, neglecting n-body effects and other perturbations, the three LISA spacecraft follow Keplerian orbits of the form **??**. It is desirable to have a triangular configuration of the constellation as stable as possible, distance fluctuations having spurious effects to be discussed later. The center of mass of the system is required to follow a circular orbit of radius

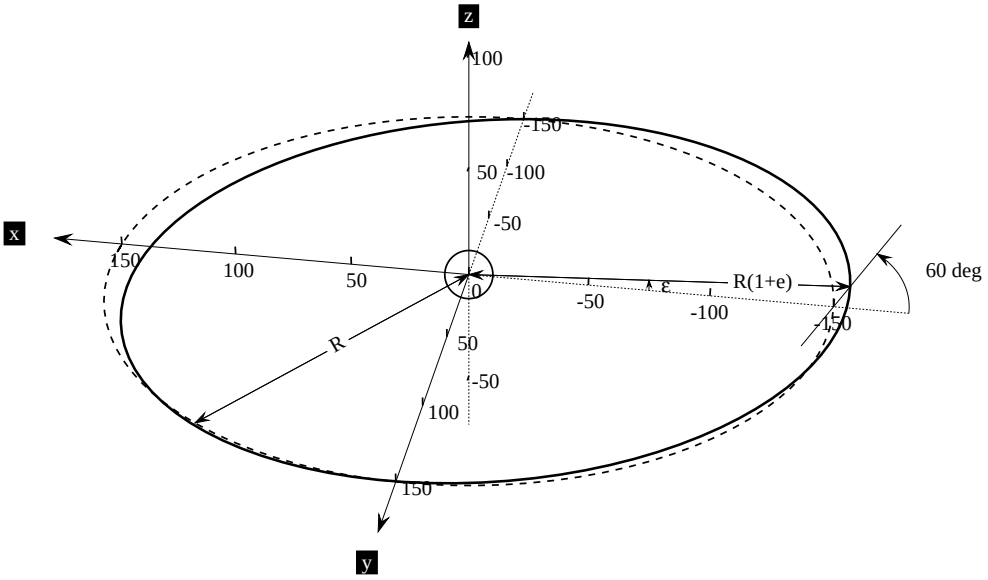

Figure 5.1: Dashed : reference circular orbit. Solid : orbit of one spacecraft .

1 AU, so that the constellation is approximately at a constant distance from the Earth. This result is obtained by placing each spacecraft on a weakly elliptical orbit weakly inclined on the ecliptic. Namely, if we denote by L the nominal inter spacecraft distance ($\sim$ 5 Mkm) and R the radius of the circular orbit ($\sim$ 150 Mkm) then the ratio $\alpha = L/2R$ is small ($\sim 1/60$), and the inclination angle on ecliptic is chosen as:

$$\epsilon = \arctan\left[\frac{\alpha}{1+\alpha/\sqrt{3}}\right] \tag{5.1}$$

(voir Fig.5.1) The eccenctricity is given by:

$$e = \sqrt{1+\frac{2\alpha}{\sqrt{3}}+\frac{4\alpha^2}{3}}-1 \tag{5.2}$$

This correlated choice of inclination and eccentricity is necessary for obtaining a 60 degrees angle between the ecliptic and the plane defined by the

constellation. This will be explained hereafter. The three orbits are then defined by the following criterions:

- The three orbits are identical up to a rotation
- The semi major axis of the second orbit is 120 degrees shifted with respect to the first one, and also the third with respect to the second.
- The eccentric anomalies are shifted in the same order

For spacecraft #i, one solves for the eccentric anomaly:

$$E_i - e \sin E_i \;=\; \Omega t - (i-1)\frac{2\pi}{3}$$

Then the coordinates are found after a first rotation of angle ϵ of **??** in the (x, z) plane:

$$\begin{cases} x &= R(\cos E_i - e)\cos\epsilon \\ y &= R\sqrt{1-e^2}\,\sin E_i \\ z &= -R(\cos E_i - e)\sin\epsilon \end{cases} \tag{5.3}$$

It is worth to note in passing that the average of z is not zero. Due to the ellipticity, a spacecraft stays longer far from the Sun than close. When the orbit undergoes a rotation in the (x, z), the result is that the spacecraft is longer above or below the ecliptic (above in our case), so is it also for the center of mass. The center of mass is consequently not on the ecliptic, as one could believe at first sight. Indeed:

$$\frac{1}{T}\int_0^T \cos E(\Omega t)\,dt \;=\; \frac{1}{2\pi}\int_0^{2\pi} \cos E(\phi)\,d\phi \;=\; \frac{1}{2\pi}\int_0^{2\pi} \cos E(\phi)\,\frac{d\phi}{dE}\,dE$$

$$= \;\frac{1}{2\pi}\int_0^{2\pi} \cos E(\phi)\,(1 - e\cos E)\,dE \;=\; -\frac{e}{2}$$

whence

$$< z > \;=\; \frac{3}{2}\,e\,\sin\epsilon$$

It is obviously the same for any spacecraft , so that the center of mass of the constellation is located on a circle offset by $< z >$ with respect to ecliptic. Then we carry out a rotation of angle $\theta_i = (i-1)\frac{2\pi}{3}$ in the (x, y) plane:

$$\begin{cases} X &= x\,\cos\theta_i \;-\; y\,\sin\theta_i \\ Y &= x\,\sin\theta_i \;+\; y\,\cos\theta_i \\ Z &= z \end{cases} \tag{5.4}$$

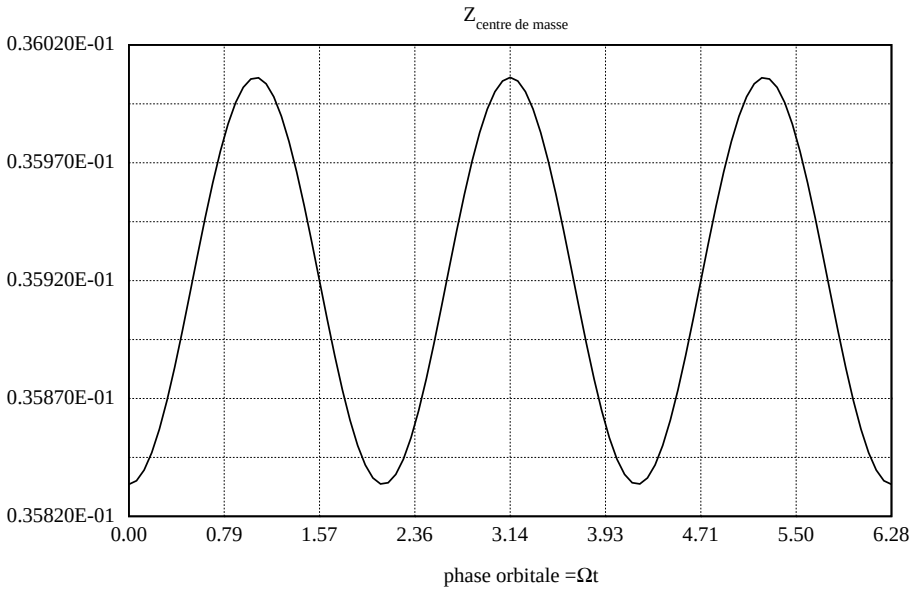

Figure 5.2: Weak oscillations of the LISA mass center around a mean altitude above the ecliptic

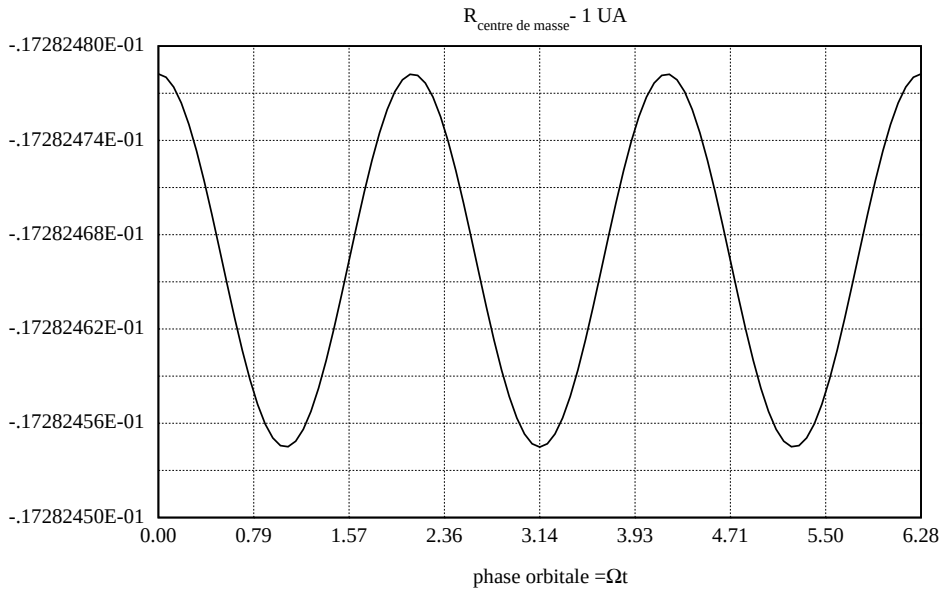

Figure 5.3: Small oscillations of the mass center around a mean radius (deviations from 1 UA).

The average of Z not only does not vanish, but is oscillating along the year (see Fig.5.2). The radius of the trajectory of the mass center is almost constant, slightly smaller than 1 AU, having a small residual oscillation around a mean value (see Fig.5.3). Seen by a co-moving observer bringing her own frame with gyroscopic axes (fixed orientation with respect to fixed stars), the three spacecraft apparently draw Lissajous curves (see 5.4). If she carries aout a continuous rotation in the (x, y) plane so as to absorb the rotation due to orbital motion, the three spacecraft follow a circle inclined at about 60 degrees (see again Fig.5.4). In this frame, the barycenter of the constellation draw a circle above the ecliptic (see voir Fig.5.5). We can moreover flip the LISA plane by a 60 degrees rotation and freeze it by a new inverse synchronous rotation. One then obtain the trajectory shown on Fig.5.6. The reference point is the nominal position assuming a rigid regular triangle. On obtient alors la trajectoire We see (Figs.5.7 and 5.8) that the motion is not planar.

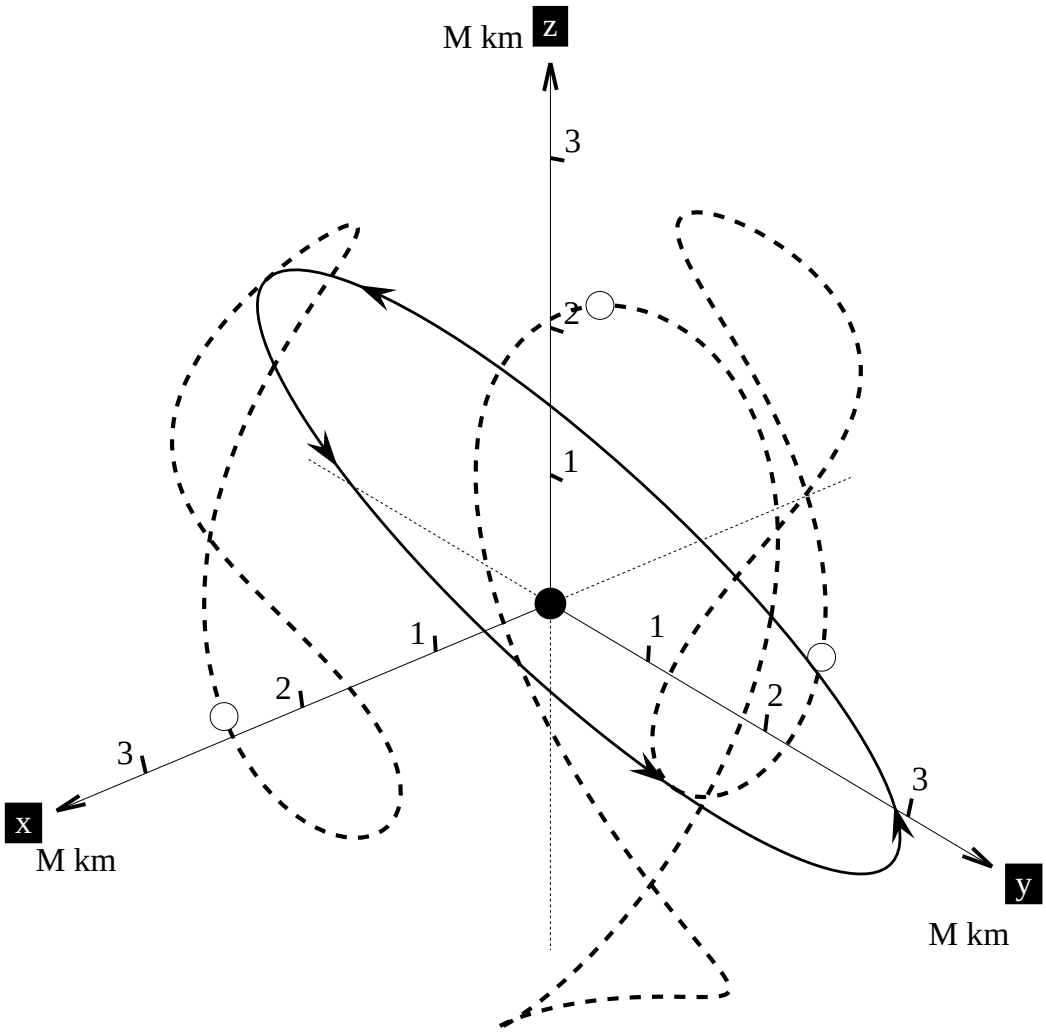

Figure 5.4: Apparent motion of the spacecraft for a comoving observer. Dashed: gyroscopic axes. Solid: synchronous rotation.

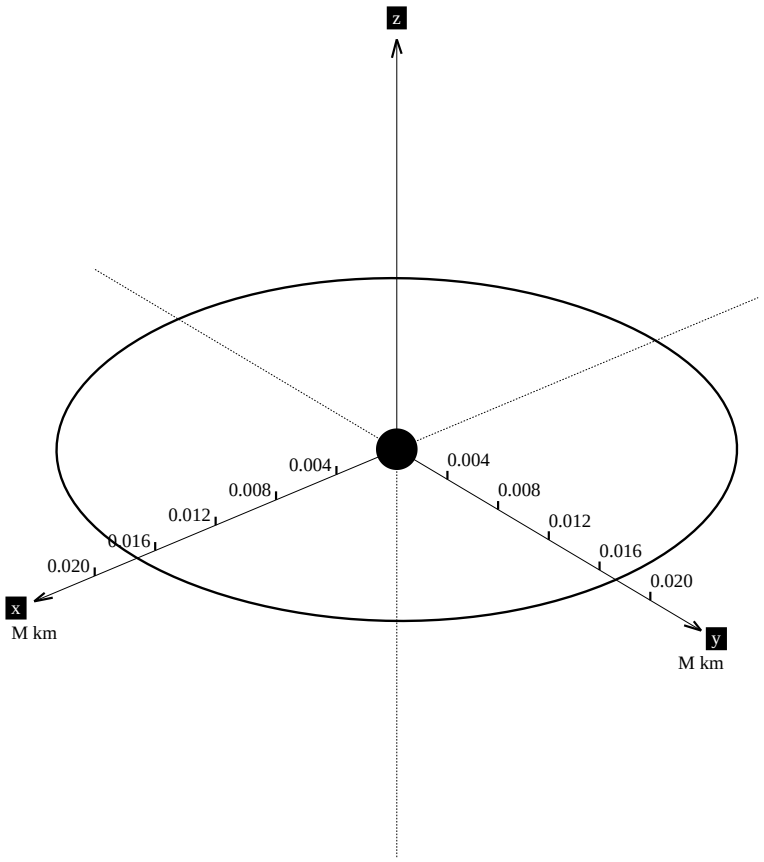

Figure 5.5: Motion of the mass center of the constellation with respect to the reference point staying on the ecliptic

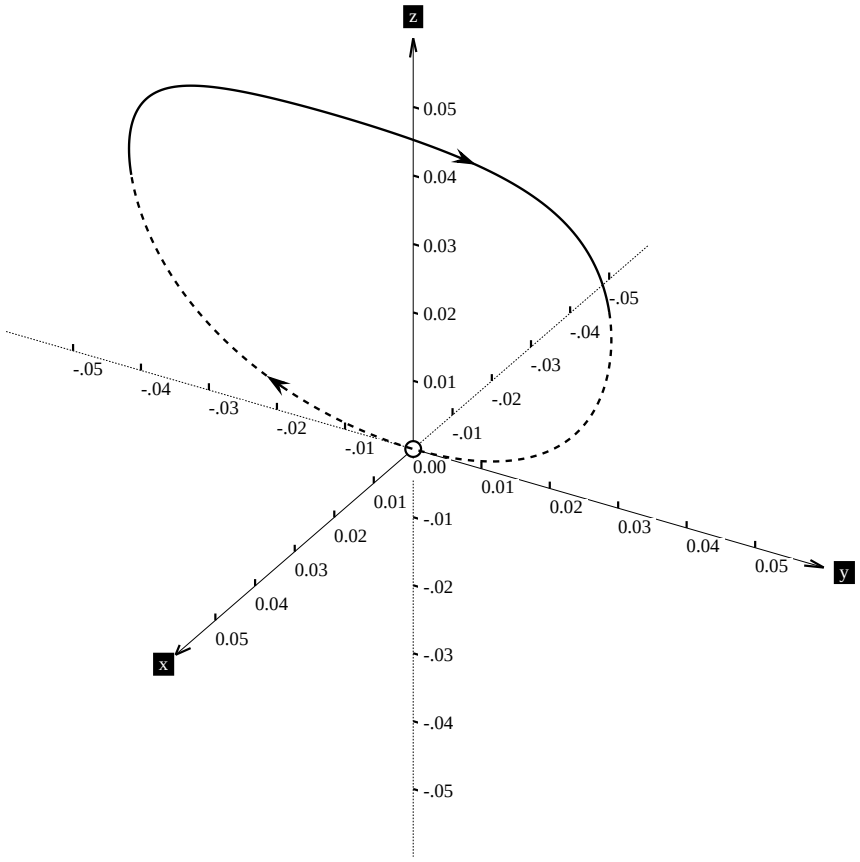

Figure 5.6: Motion of spacecraft #1 in a comoving and corotating frame. The small sphere shows the location of the reference point, where the spacecraft would stay if no second order effets were acting.

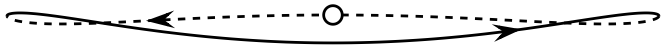

Figure 5.7: Motion of spacecraft #1 in a comoving and corotating frame seen under 73 degrees

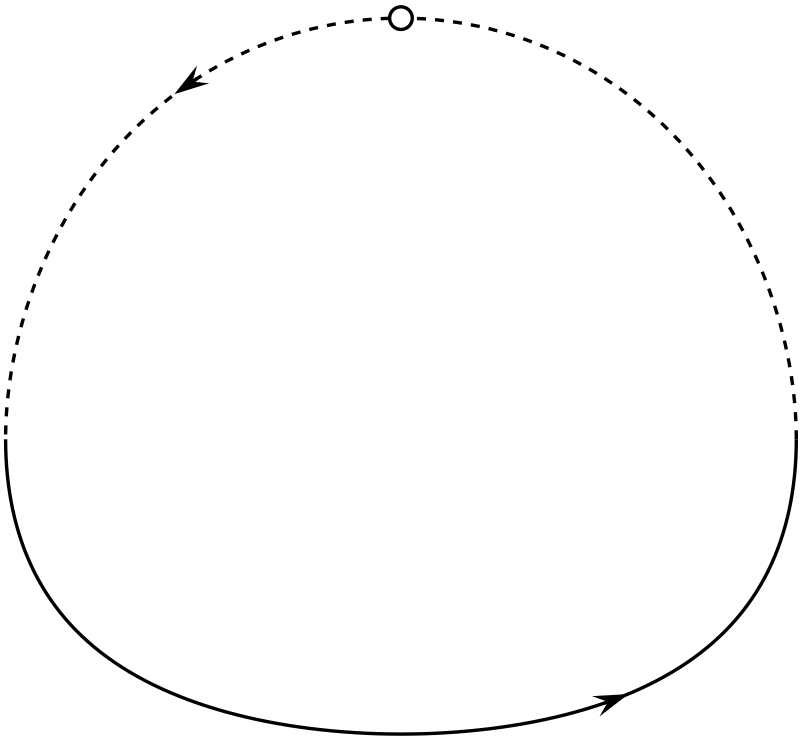

Figure 5.8: Motion of spacecraft #1 in a comoving and corotating frame: orientation orthogonal to the preceding

5.1.2 A model at first order in e

It can be checked that the inter spacecraft distances are stable at first order in e (or in α as well). Consider the spacecraft #1 and 2. With $\phi \equiv \Omega t$ one finds

$$\begin{cases} X_1 &= R[\cos\phi - e(1+\sin^2\phi)] + \mathcal{O}(e^2) \\ Y_1 &= R[\sin\phi + e\sin\phi\,\cos\phi] + \mathcal{O}(e^2) \\ Z_1 &= -R\sqrt{3}\,e\,\cos\phi + \mathcal{O}(e^2) \end{cases}$$

then

$$\begin{cases} X_2 &= R\left[\cos\phi + e\,\left(\frac{3}{4} - \frac{1}{4}\cos 2\phi + \frac{\sqrt{3}}{4}\sin 2\phi\right)\right] + \mathcal{O}(e^2) \\ Y_2 &= R\left[\sin\phi - e\,\left(\frac{3\sqrt{3}}{4} + \frac{\sqrt{3}}{4}\cos 2\phi + \frac{1}{4}\sin 2\phi\right)\right] + \mathcal{O}(e^2) \\ Z_2 &= -R\sqrt{3}\,e\,\left[-\frac{1}{2}\cos\phi + \frac{\sqrt{3}}{2}\sin\phi\right] + \mathcal{O}(e^2) \end{cases}$$

The distance is now:

$$D^2 \;=\; (X_2-X_1)^2 + (Y_2-Y_1)^2 + (Z_2-Z_1)^2 = 12e^2R^2 + \mathcal{O}(e^3)$$

But at 1st order, we have

$$e = \frac{\alpha}{\sqrt{3}}$$

so that

$$D \;=\; \sqrt{12}\,\frac{\alpha}{\sqrt{3}}\,R \;=\; L$$

This makes possible a stable formation flight for LISA. Higher order terms however produce annual variations that we shall discuss later, so that the triangle undergoes periodic deformations (see Fig.5.9).

5.1.3 The Clohessy & Wiltshire theory

Clohessy & Wiltshire [34] have proposed a classical geodesic deviation theory giving motion equations in the neighborhood of a reference point located on a reference orbit. If that orbit is circular, if we take the origin on the reference point, the x axis along the radial direction, the y axis tangent to the orbit in the direction of the motion and the z axis making a direct reference frame with the preceding (see Fig.5.10), on can expand the gravitational potential in a multipole series in the neighborhood of the reference point, and write the orbital differential in this neighborhood as fictitious forces. Assuming no

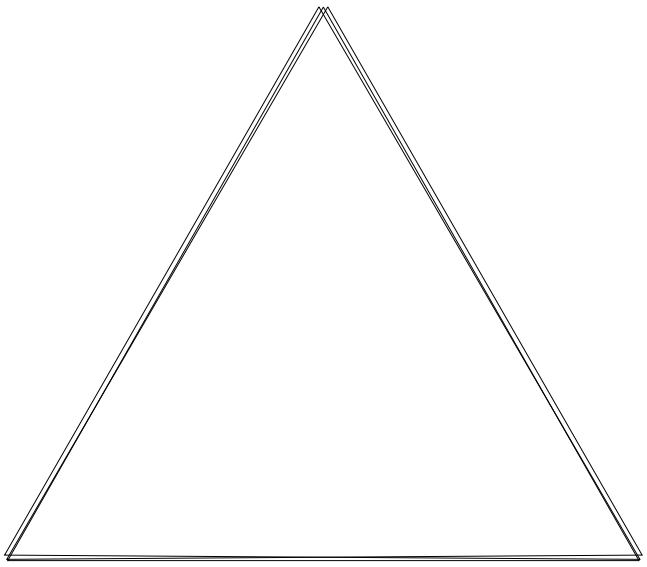

Figure 5.9: The LISA triangle seen from a comoving and corotating frame along the year

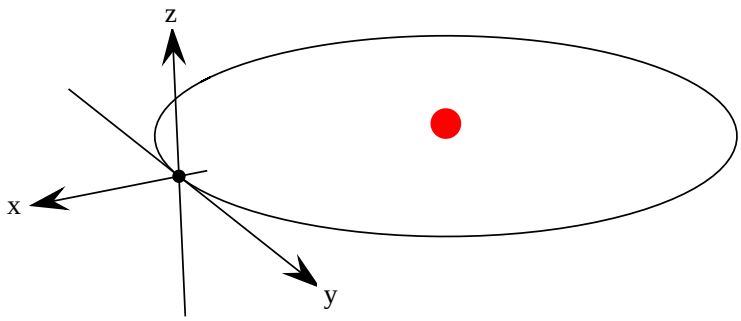

Figure 5.10: C-W Comoving frame

applied force (drag free operation), the motion equation read in this frame:

$$\begin{cases} \ddot{x} - 2\Omega\dot{y} - 3\Omega^2 x &= 0 \\ \ddot{y} + 2\Omega\dot{x} &= 0 \\ \ddot{z} + \Omega^2 z &= 0 \end{cases} \tag{5.5}$$

where Ω is the (constant) angular velocity of the reference point. The general solution, depending on 6 arbitrary constants is:

$$\begin{cases} x(t) &= \frac{\dot{x}_0}{\Omega}\sin\Omega t - \left(3x_0 + 2\frac{\dot{y}_0}{\Omega}\right)\cos\Omega t + 2\left(2x_0 + \frac{\dot{y}_0}{\Omega}\right) \\ y(t) &= \left(6x_0 + 4\frac{\dot{y}_0}{\Omega}\right)\sin\Omega t + 2\frac{\dot{x}_0}{\Omega}\cos\Omega t - 3(2\Omega x_0 + \dot{y}_0)t + \left(y_0 - 2\frac{\dot{x}_0}{\Omega}\right) \\ z(t) &= z_0\cos\Omega t + \frac{\dot{z}_0}{\Omega}\sin\Omega t \end{cases} \tag{5.6}$$

There is in $y(t)$ an obvious drift term correlated with an offset in $x(t)$ or, in other words, a "bad" radial choice of the reference point. We are allowed to require a no drift solution. We therefore set:

$$\dot{y}_0 + 2\Omega x_0 = 0$$

Now, the offset in $y(t)$ can be seen as a "bad" longitudinal choice of the reference point. We can therefore require without any loss of generality that:

$$\dot{x}_0 - \frac{1}{2}y_0 = 0$$

The centered solution reduces then to:

$$\begin{cases} x(t) &= \frac{1}{2}y_0\sin\Omega t + x_0\cos\Omega t \\ y(t) &= y_0\cos\Omega t - 2x_0\sin\Omega t \\ z(t) &= z_0\cos\Omega t + \frac{\dot{z}_0}{\Omega}\sin\Omega t \end{cases} \tag{5.7}$$

The distance from the current point to the reference is:

$$d^2 = x(t)^2 + y(t)^2 + z(t)^2 =$$

$$\left(\frac{y_0^2}{4} + 4x_0^2 + \frac{\dot{z}_0^2}{\Omega^2}\right)\sin^2\Omega t + (x_0^2 + y_0^2 + z_0^2)\cos^2\Omega t + \left(\frac{2z_0\dot{z}_0}{\Omega}\right)\sin\Omega t\cos\Omega t$$

On can obtain $d = cste$ by requiring that the terms of frequency Ω et 2Ω in phase and in quadrature identically vanish. This is equivalent to:

$$z_0^2 - \frac{\dot{z}_0^2}{\Omega^2} = 3\left(x_0^2 - \frac{y_0^2}{4}\right)$$

and

$$\frac{2z_0\dot{z}_0}{\Omega} = 3x_0y_0$$

The solution of the problem is found by adding the first equation to i times the second, giving one complex equation:

$$\left(z_0 + i\,\frac{\dot{z}_0}{\Omega}\right)^2 = 3\left(x_0 + i\frac{y_0}{2}\right)^2$$

which yields immediately:

$$z_0 = \mu\sqrt{3}x_0, \quad \frac{\dot{z}_0}{\Omega} = \frac{1}{2}\mu\sqrt{3}y_0$$

with $\mu \equiv \pm 1$, so that the motion equations reduce again:

$$\begin{cases} x(t) = \frac{1}{2}\rho_0\cos(\Omega t - \phi_0) \\ y(t) = -\rho_0\sin(\Omega t - \phi_0) \\ z(t) = \mu\rho_0\frac{\sqrt{3}}{2}\cos(\Omega t - \phi_0) \end{cases} \tag{5.8}$$

where:

$$\rho_0 = \sqrt{4x_0^2 + y_0^2}, \quad \tan\phi_0 = \frac{y_0}{2x_0}$$

After a rotation of angle $\mu\pi/3$ around the y axis then a rotation of angle $-\Omega t$ around the new z axis, we get in the new coordinates:

$$x'(t) = \rho_0\cos\phi_0, \quad y'(t) = \rho_0\sin\phi_0, \quad z'(t) = 0$$

We conclude that requiring the stability of the distance to the reference point leads to install the body in such a way that it is at rest with respect to a plane inclined at $\mu\pi/3$ on the ecliptic and contrarotating with a period of 1 yer. The final conclusion is that any constellation having such nodes is stable (at least at 1st order in α).

5.1.4 Higher order approximation and optimization

If we use the exact orbital equations given in 5.4, we can plot the time evolution of the inter spacecraft distances along a year. One sees that these distances are oscillating around the nominal value of 5 Mkm with a peak to peak amplitude around 150,000 km (see Fig.5.11). It is strongly desirable to look for a way of reducing the amplitude of these spurious variations

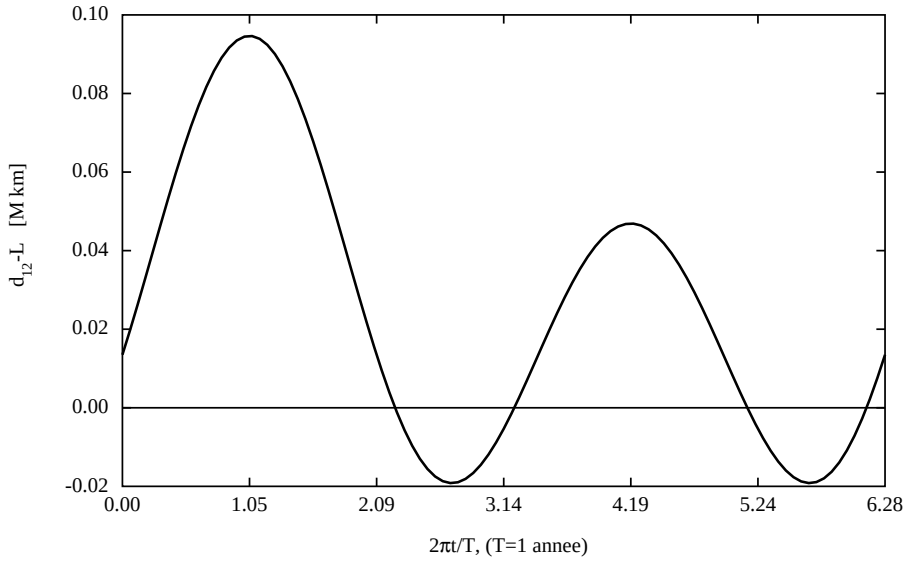

Figure 5.11: Annual variations of the inter spacecraft distances for a 60 degrees inclination on the ecliptic of the LISA plane

that have a number of negative effects. I has been shown [35] that there is a minimum in this flexing, and that this minimum can be attained by slightly increasing the "magical" angle of 60 degrees. This angle was found using a 1st order theory. One easily imagine that a 2d order theory would allow to find a correction to the initial conditions resulting in a reduced flexing. Following [35], we can take the same equations (5.4), but in which the definitions of the orbital inclination ϵ and of the eccentricity e take into account an inclination of the LISA plane corrected by a first order quantity, giving a 2d order correction to inter spacecraft distances. One firstly define the new inclination angle of the LISA plane:

$$\beta = \frac{\pi}{3} + \delta\alpha \tag{5.9}$$

where δ is a quantity of order unity, then

$$\tan\epsilon = \frac{2}{\sqrt{3}} \frac{\alpha \sin\beta}{1 + \frac{2}{\sqrt{3}}\alpha \cos\beta} \tag{5.10}$$

and

$$e = \left[1 + \frac{4}{3}\alpha^2 + \frac{4}{\sqrt{3}}\alpha cos\beta\right]^{1/2} - 1 \tag{5.11}$$

Starting from here, one can expand to 2d order the orbital equations and compute the distances d_{ij} up to second order. One the shows that the optimal value of δ, which minimizes the variances of the d_{ij}, their peak to peak amplitudes or the Doppler shifts as well is:

$$\delta = \frac{5}{8}$$

It is remarkable that this apparently special result (we have worked with the only parameter δ) is actually general. This results from two features [35]:

- The expansion to 2d order of the orbital equations is numerically very close to the exact calculation due to the very weak eccentricity. This allows to discuss on analytical expressions without loss of generality.
- On can then derive a 2d order version of the Clohessy & Wiltshire equations by expanding the gravity potential up to octupolar term, and the optimality can be shown analytically.

The only restriction to this result is that it holds for three orbits identical up to a 120 degrees rotation. Finally, the reduction of the inter spacecraft distances fluctuations is by a factor of 3 (see Fig.5.12).

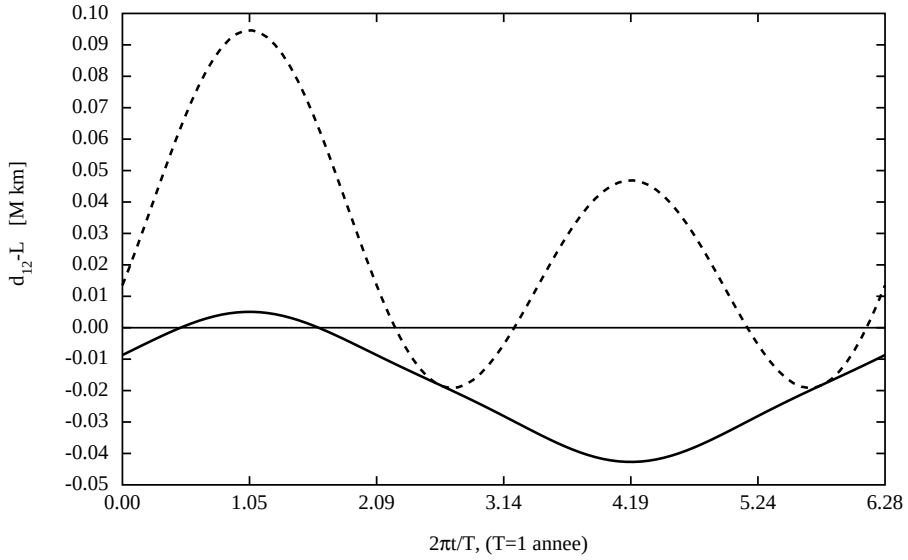

Figure 5.12: Annual variations of the inter spacecraft distances for an optimal inclination angle of the LISA plane (solid curve). The former solution (60 degrees) is recalled (dashed curve).

Chapter 6

Time Delay Interferometry

LISA is not a hard built interferometer as Virgo or LIGO. In a classical Michelson interferometer, the two arms are carefully symmetrized in order to be the less sensitive as possible to the light source frequency fluctuations. In LISA, we mix two beams, one coming from 5 Mkm, with one coming from a few cm. In this crude situation, the sensitivity in terms of $\delta L/L$ would be the same order of magnitude as the $\Delta\nu/\nu$ of the laser in the relevant frequency range, namely $\sim 10^{-15}$. This is clearly far from a significant sensitivity. Time Delay Interferometry (TDI) aims to restablish the symmetry of a Michelson by a numerical processing of the 6 data streams. The three LISA spacecraft are in a triangular flight formation approximately regular and rigid. It is more efficient,from a pedagogical point of view to discuss the rationale of the data flows starting from the simplest situation (static LISA) to a more realistic one (orbiting LISA). We shall see that at low GW frequency (the case for a number of galactic sources), the simplest model is sufficient for studying the response of the system. On the contrary for suppressing the instrumental noise, a realistic model is necessary.

6.1 Basic static LISA

6.1.1 The triangle

In the simplest scheme, the LISA constellation is a structure rigid in an inertial frame. The inter spacecraft distances are however not equal due to an imperfect positionning. Beside the positioning, it has been seen that

the triangle is continuously flexing in reality, so that at a given date, it has different arm lengths. The nodes of the formation are numbered from 1 to 3, and the lengths L_i connecting them wear the figure of the opposite node, so for the unit vectors $\mathbf{n}_i, (i = 1, 2, 3)$. (see Fig.6.1). The elementary data are the frequency shifts between the incoming beams and the local laser. We have thus for spacecraft #1 two data flows that we denote respectively U_1 and V_1, defined by:

$$\begin{cases} U_1(t) &= C_3(t - L_2) - C_1(t) \\ V_1(t) &= C_1(t) - C_2(t - L_3) \end{cases} \tag{6.1}$$

NB: From now on, we take $c = 1$. NB: à partir de maintenant, on prend $c = 1$. The $C_i(t)$ are the instantaneous frequencies of the lasers. One notes the delays ~ 17 s due to propagation of light along the arms. The other data flows on other spacecraft are obtained by circular permutation of the indices. The fact that a circular index permutation $(1 \to 2 \to 3 \to 1)$ gives y from x will be denoted by $x \succ y$

6.1.2 Noise cancelling combinations

In absence of GW signal, the 6 different lasers have anyway intrinsic frequency fluctuations. It will be shown that the effect of a GW on a long optical link is to produce a frequency shift of the order of $h \times \nu_L$ where h is the GW amplitude (less than 10^{-20}), and ν_L the laser nominal frequency. For being able to detect such a wave, a spectral stability better than 10^{-6} Hz/$\sqrt{\text{Hz}}$ in the dtection band of LISA (0.1 mHz à 0.1 Hz) should be achieved, which is out of question. The leading idea of TDI is to make numerically on the data, the equivalent of an interferometer, in which the frequency fluctuations are strongly rejected by symmetrical optical paths so that at any time the recombined waves have the same frequency even if it varies in time. The relevant combinations of data have been found some years ago by colleagues at JPL: Tinto, Estabrook and Armstrong [36]. By introducing, as in [37] delay operators D_i, defined by their action on a function of time:

$$(D_i f)(t) \;=\; f(t - L_i) \tag{6.2}$$

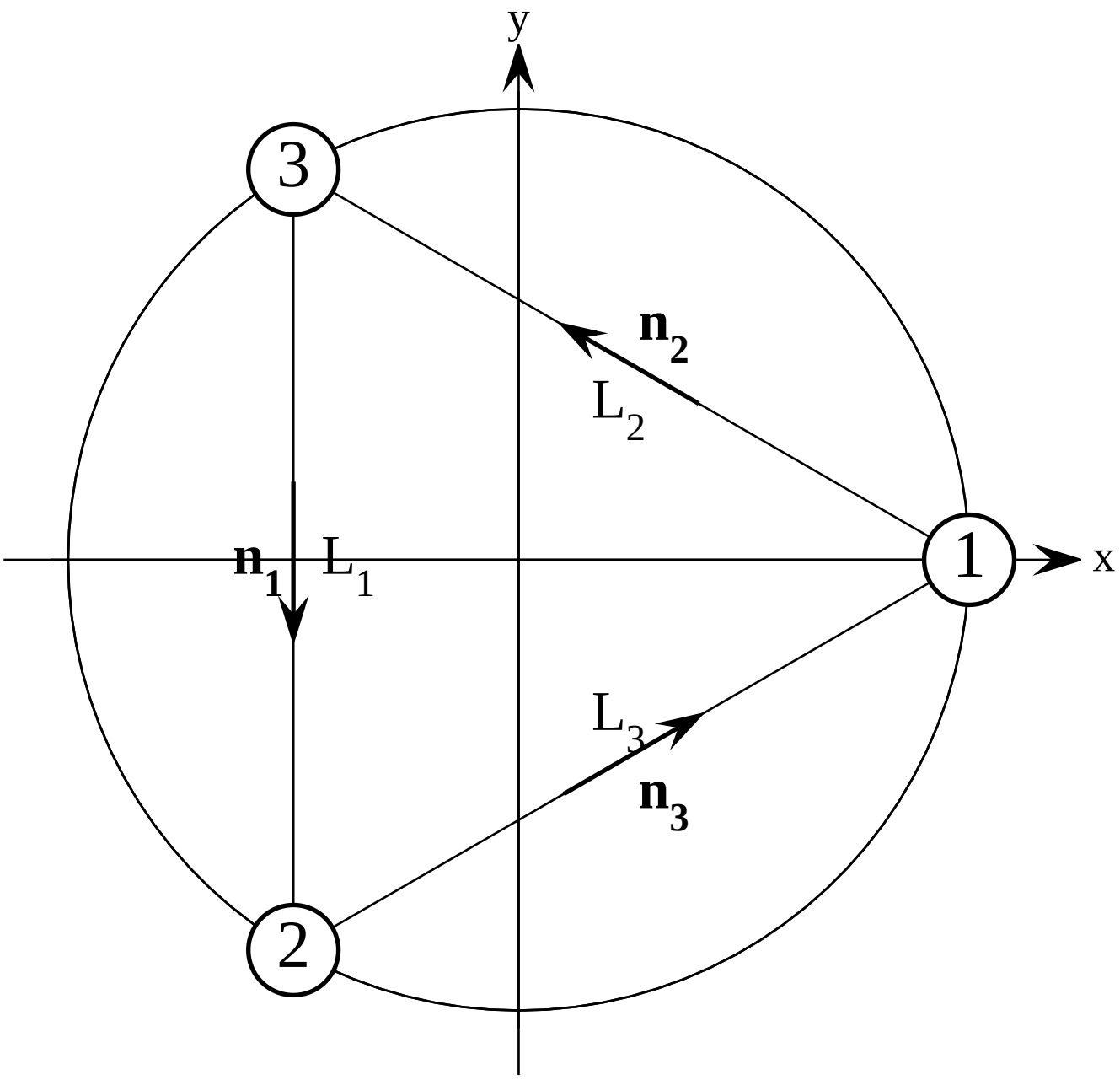

Figure 6.1: Notations

On can cast the data flows defined by 6.1 and containing only laser noise under the following form:

$$\begin{aligned} U_1 &= D_2C_3 - C_1 \\ U_2 &= D_3C_1 - C_2 \\ U_3 &= D_1C_2 - C_3 \\ V_1 &= C_1 - D_3C_2 \\ V_2 &= C_2 - D_1C_3 \\ V_3 &= C_3 - D_2C_1 \end{aligned} \tag{6.3}$$

We look for a combination of these elementary time series with possible delays, giving identically zero. There is an obvious solution. By forming the sums $U_i + V_i$, one gets a kind of vector having the same algebraic structure as a curl:

$$\mathbf{U} + \mathbf{V} = \mathbf{D} \times \mathbf{C} \tag{6.4}$$

applying the divergence operator yields an identically zero result:

$$\mathbf{D}.(\mathbf{U} + \mathbf{V}) = 0$$

In terms of data flows, this reads:

$$\sum_{i=1}^{3} D_iU_i + \sum_{i=1}^{3} D_iV_i = 0$$

This exhibits an example of a combination of delayed data unsensitive to individual frequency fluctuations. We clearly have to look for all combinations having the same property. These combiantions, as pointed out in [37] have the form of a scalar product of a vector of formal polynomials in D_i with the data 6-uple $U = (U_i, V_i)$. A generic X combination with delays is of the form:

$$\sum_{i=1}^{3} (p_iV_i + q_iU_i) = \langle X|U\rangle$$

where the 6-uple $X = (p_i, q_i)$ contains the polynomials. The simplest case, as just shown is:

$$\zeta = (\mathbf{p}, \mathbf{q}) = (D_1, D_2, D_3, D_1, D_2, D_3)$$

The other combinations found by Tinto and colleagues are, besides ζ:

$$\alpha = (1,\ D_3,\ D_1D_3,\ 1,\ D_1D_2,\ D_2)$$

with the two circular permutations (of the indices and of the places in the sub-3-uple of the 6-uple):

$$\beta \;=\; (D_1D_2,\ 1,\ D_1,\ D_3,\ 1,\ D_2D_3)$$

$$\gamma \;=\; (D_2,\ D_2D_3,\ 1,\ D_1D_3,\ D_1,\ 1)$$

or, after ournotation:

$$\alpha \succ \beta \succ \gamma \succ \alpha$$

The set $\mathcal{P}_3$ of all polynomials in three variables (D_1, D_2, D_3) has the algebraical structure of a ring. The following properties are satisfied:

- It is a commutative additive group. In other words, the addition of polynomials is associative:

  $$\forall p_1, p_2, p_3 \in \mathcal{P}_3 \;:\; p_1 + (p_2 + p_3) \;=\; (p_1 + p_2) + p_3 = \; p_1 + p_2 + p_3$$

  There exists a zero polynomial:

  $$\exists 0 \in \mathcal{P}_3 \ ,\ \forall p \in \mathcal{P}_3 \;:\; p + 0 \;=\; 0 + p \;=\; p$$

  Any polynomial has an opposite one:

  $$\forall p \in \mathcal{P}_3, \exists(-p) \in \mathcal{P}_3 \;:\; p + (-p) \;=\; 0$$

- The product is associative:

  $$\forall p_1, p_2, p_3 \in \mathcal{P}_3 \;:\; p_1(p_2p_3) \;=\; (p_1p_2)p_3 \;=\; p_1p_2p_3$$

- The product is distributive on the right and on the left on a sum:

  $$\forall p_1, p_2, p_3 \in \mathcal{P}_3 \;:\; (p_1+p_2)p_3 \;=\; p_1p_3+p_2p_3,\ \ p_1(p_2+p_3) \;=\; p_1p_2+p_1p_3$$

$\mathcal{P}_3$ is not a field because a key property is missing: in general a polynomial, even different from zero has no inverse. However, certain polynomials may happen to have other divisors than 1. This results nevertheless in the fact that the set of all 6-uples of polynomials has not the structure of a vector space, and the notion of basis makes no sense here. On the other hand, it is clear that any linear combination of $(\alpha, \beta, \gamma, \zeta)$ with arbitrary polynomials coefficients (of $\mathcal{P}_3$) will inherit of the property of cancelling the phase

noise. We call "silent" combinations cancelling the noise, and their set will be denoted by $\mathcal{S}$.

An essential point is to know wether the set of all combinations of $(\alpha, \beta, \gamma, \zeta)$ is equal to $\mathcal{S}$ or only to a part of it. The answer has been given in [37]. The set $(\alpha, \beta, \gamma, \zeta)$ actually generates $\mathcal{S}$. It is analogous to a basis. The difference with a basis is that other generative parts may exist, having a different number of elements thsi will be discussed in a specific section. Let us only say that $\mathcal{S}$ has the structure of a module on $\mathcal{P}_3$. The elements $(\alpha, \beta, \gamma, \zeta)$ are an example of a set of generators of the module.

The technique of processing the data only through silent combinations has been called "Time Delay Interferometry" (TDI) by Tinto and colleagues.

Generators α, β, γ are called "Sagnac" generators, since it is easily seen that they express the difference between the sum of the data in both clockwise and anticlockwise senses with time delays insuring a consistent addition. The locus where the difference is evaluated is spacecraft # 1 for α, 2 for β, 3 for γ.

The generator ζ is called "symmetric Sagnac" since it expresses the sum of all differences for round trips alogs the three sides. Generators α, β, γ are deduced successively (modulo 3) by circular permutations. ζ is invariant under a circular permutation ($\zeta \succ \zeta$).

6.1.3 Interferometric combinations

Tinto and colleagues have also proposed configurations analogous to a Michelson interferometer. For instance:

$$X_1 \;=\; \alpha - D_3\beta - D_2\gamma + D_2D_3\zeta$$

The result is:

$$X_1 \;=\; (1 - D_2^2,\; 0,\; -D_2(1 - D_3^2),\; 1 - D_3^2,\; -D_3(1 - D_2^2),\; 0) \qquad (6.5)$$

Two other similar combinations are obtained by circular permutations:

$$X_1 \succ X_2 \succ X_3$$

namely:

$$X_2 \;=\; (-D_3(1 - D_1^2),\; 1 - D_3^2,\; 0,\; 0,\; 1 - D_1^2,\; -D_1(1 - D_3^2)) \qquad (6.6)$$

$$X_3 \;=\; (0,\; -D_1(1-D_2^2),\; 1-D_1^2,\; -D_2(1-D_1^2),\; 0, 1-D_2^2) \qquad (6.7)$$

The link with a Michelson appears when checking the effect on data. We have for instance:

$$\langle X_1|U\rangle \;=\; (1-D_2^2)[V_1 - D_3U_2] \;-\; (1-D_3^2)[D_2V_3 - U_1]$$

combinations $V_1 - D_3U_2$ et $D_2V_3 - U_1$ represent coherent sums evaluated at node # 1 in which the link D_1 is absent: only the links 12 and 13 (D_3, D_2) are involved. On can regard X_1 as an interferometer having its splitter at 1, and two arms 12 and 13. Tinto et al. have also proposed 3 other series of combinations frequently invoked in the literature and useful for dealing with the case where one or two optical links are lost: The beacon series

$$B_1 \;=\; \zeta - D_1\,\alpha$$

or in detail:

$$B_1 \;=\; (0,\; D_2 - D_1D_3,\; D_3(1-D_1^2),\; 0,\; D_2(1-D_1^2),\; D_3 - D_1D_2) \qquad (6.8)$$

two others are found by circular permutation:

$$B_1 \succ B_2 \succ B_3$$

yielding:

$$B_1 \;=\; (D_1(1-D_2^2),\; 0,\; D_3 - D_1D_2,\; D_1 - D_2D_3,\; 0,\; D_3(1-D_2^2)) \qquad (6.9)$$

$$B_1 \;=\; (D_1 - D_2D_3,\; D_2(1-D_3^2),\; 0,\; D_1(1-D_3^2),\; D_2 - D_1D_3,\; 0) \qquad (6.10)$$

6.2 Inertial LISA with internal motions

6.2.1 Extended data flow

The precedent discussion must be extended for taking into account more realistic details. For instance, we have not one laser per spacecraft but two different, each pointing respectively towards the two other spacecraft . We mark with an * the ray propagating counterclockwise, and without an * the other one (see Fig.6.2). We must also consider the motions of the various

parts of the payload and use the results found in **??**. The detail of the data flow can be summarized by generalizing the 6-uples as follows:

$$U_1(t) \;=\; C_3(t-L_2) - C_1^*(t) - \mathbf{V}_3(t-L_2).\mathbf{n}_2 - \mathbf{V}_1^*(t).\mathbf{n}_2 + 2\,\mathbf{v}_1^*(t).\mathbf{n}_2 + y_1^* + g_2^* \tag{6.11}$$

This recalls **??**. One can note the changes of sign due to the fact that the unit vector $\mathbf{n_2}$ is now pointing from the receiver to the emitter, the opposite of **??**. y_1^* represents the quantum noise generated in 1*, and all analogous noises; g_2^* represents the GW signal caused during the propagation from 3 towards 1*. Motions of optical benches are represented by vectors $\mathbf{V}_i$, $\mathbf{V}_i^*$, and residual motions of the proof masses by vectors $\mathbf{v}_i$, $\mathbf{v}_i^*$. U_2 and U_3 are found as usual by circular permutations of the indices. The same way, V_1 is found as:

$$V_1(t) \;=\; C_1(t) - C_2^*(t-L_3) - \mathbf{V}_2^*(t-L_3).\mathbf{n}_3 - \mathbf{V}_1(t).\mathbf{n}_3 + 2\,\mathbf{v}_1(t).\mathbf{n}_3 + y_1 + g_3 \tag{6.12}$$

It is again a new version of **??** where the couple emitter/receiver has been inversed (one sign flip), but where the unit vector $\mathbf{n_3}$ is pointing from the emitter towards the receiver (second sign flip). Signs of scalar products are eventually unchanged with respect to 6.11. y_1 is the shot noise generated in 1, and g_3 the GW signal caused by propagation from 2* to 1. V_2 and V_3 are found by circular permutation of the indices. NB: the notation V_i for this data flow and $\mathbf{V}_i, \mathbf{V}_i^*$ for the bench velocities could be misleading and deserve criticism. We also must introduce two new data flows produced by comparing the frequencies of the two lasers in the same spacecraft . Following **??**, we have in the left/right comparison aboard 1:

$$z_1 \;=\; C_1(t) - C_1^*(t) + 2(\mathbf{v}_1^*(t) - \mathbf{V}_1^*(t)).\mathbf{n}_2 \;+\; \sigma_1 \tag{6.13}$$

and for the right/left comparison:

$$z_1^* \;=\; C_1^*(t) - C_1(t) - 2(\mathbf{v}_1(t) - \mathbf{V}_1(t)).\mathbf{n}_3 \;+\; \sigma_1 \tag{6.14}$$

One can note the extra noise σ_1 caused by propagation in the fiber.

6.2.2 New silent combinations

With respect to the simple situation analyzed in 6.1.2, we have 6 noise sources instead of 3, but also 6 new data flows. This allows to generalized the silent

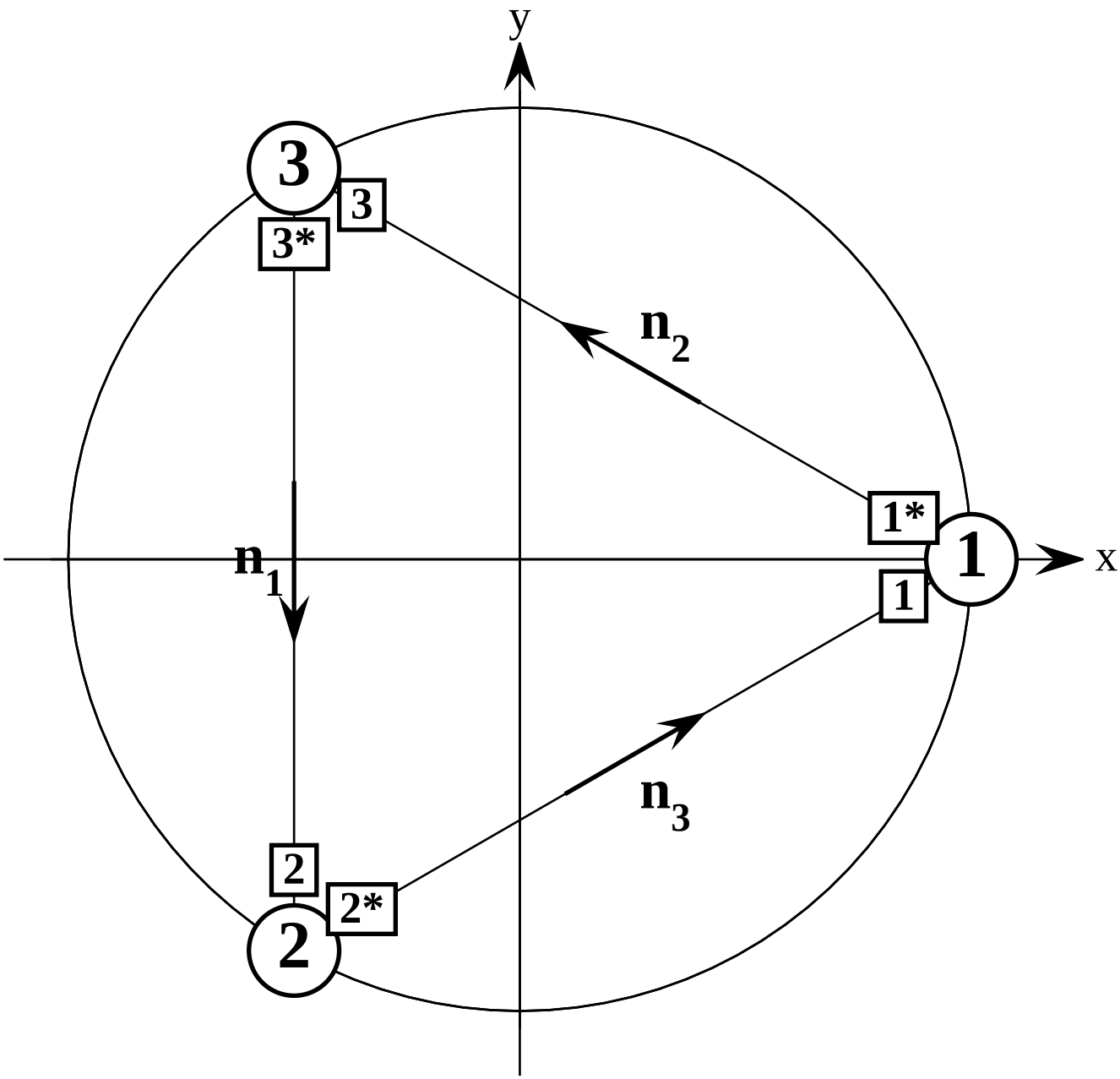

Figure 6.2: Notation for links

combinations. On physical basis one indeed expects that spurious motions of optical benches cause Doppler shifts cannot be separated from laser phase fluctuations. Combinations suppressing the latter must therefore also suppress the former. Remark that eq.6.11 and 6.12 may be rewritten if we forget the proof masses and the GW signal: under the following form:

$$U_1 = D_2 [C_3 - \mathbf{V}_3.\mathbf{n}_2] - [C_1^* + \mathbf{V}_1^*.\mathbf{n}_2] \tag{6.15}$$

$$V_1 = [C_1 - \mathbf{V}_1.\mathbf{n}_3] - D_3 [C_2^* + \mathbf{V}_2^*.\mathbf{n}_3] \tag{6.16}$$

One can also form a new data flow:

$$Z_1 = \frac{z_1 - z_1^*}{2} = -\mathbf{V}_1.\mathbf{n}_3 - \mathbf{V}_1^*.\mathbf{n}_2 \tag{6.17}$$

which eliminates the fiber noise. It is thus very convenient to introduce the new variables:

$$\tilde{C}_1 = C_1 - \mathbf{V}_1.\mathbf{n}_3 \tag{6.18}$$

et

$$\tilde{C}_1^* = C_1^* + \mathbf{V}_1^*.\mathbf{n}_2 \tag{6.19}$$

Then eq.6.15, 6.16 and 6.17 become simply:

$$U_1 = D_2\tilde{C}_3 - \tilde{C}_1^* \tag{6.20}$$

$$V_1 = \tilde{C}_1 - D_3\tilde{C}_2^* \tag{6.21}$$

$$Z_1 = \tilde{C}_1 - \tilde{C}_1^* \tag{6.22}$$

The algebraical structure of the U_i, V_i is now identical to that described in 6.1.2 and it will not be too surprising to find the same module $\mathcal{S}$. For being rigourous, we point that the overall data flow is now a set of 9-uples (U_i, V_i, Z_i). Silent combinations must now be generated by a family of 9-uples of polynomials of $\mathcal{P}_3$. Let us note

$$X = (p_i, q_i, r_i)$$

a generic silent combination. It can be shown that the 6 first coordinates of the searched silent 9-uples are nothing but the 6-uples (p_i, q_i) already found in the simple discussion; the remaining 3 coordinates are imposed by these first 6. Let us examine in detail the simplest case of generator ζ. recall that:

$$\zeta \equiv (D_1, D_2, D_3, D_1, D_2, D_3)$$

If we coonsider only the first 6 coordinates, we have thus:

$$\langle\zeta|U\rangle \;=\; D_1V_1 + D_2V_2 + D_3V_3 + D_1U_1 + D_2U_2 + D_3U_3$$

by substituting the new definitions of the U, V, we get:

$$\langle\zeta|U\rangle \;=\; (D_1{+}D_2D_3)(\tilde{C}_1{-}\tilde{C}_1^*){+}(D_2{+}D_3D_1)(\tilde{C}_2{-}\tilde{C}_2^*){+}(D_3{+}D_1D_2)(\tilde{C}_3{-}\tilde{C}_3^*)$$

When in 6.1.2 we were confusing the left and the right laser and were ignoring the motions of the optical benches, we had $\tilde{C}_i = \tilde{C}_i^*$ and consequently the preceding expression was identically zero. This is no more true, but extension to a 9-uple allows to restore the situation. On sees that

$$\langle\zeta|U\rangle \;=\; (D_1 + D_2D_3)Z_1 + (D_2 + D_3D_1)Z_2 + (D_3 + D_1D_2)Z_3$$

so that extension of ζ to the 9-uple

$$\zeta \;=\; (D_1,\, D_2,\, D_3,\, D_1,\, D_2,\, D_3,\, -(D_1{+}D_2D_3),\, -(D_2{+}D_3D_1),\, -(D_3{+}D_1D_2)) \tag{6.23}$$

applied to the 9-uple of data

$$U \;=\; (V_1, V_2, V_3, U_1, U_2, U_3, Z_1, Z_2, Z_3)$$

Allows to retreive a silent combination at the price of a wider data acquisition. One can show that the same happens for other generators. The extensions of $\alpha,\ \beta,\ \gamma$ are as follows:

$$\alpha \;=\; (1,\, D_3,\, D_1D_3,\, 1,\, D_1D_2,\, D_2,\, -1{-}D_1D_2D_3,\, -(D_1D_2{+}D_3),\, -(D_1D_3{+}D_2)) \tag{6.24}$$

$$\beta \;=\; (D_1D_2,\, 1,\, D_1,\, D_3,\, 1,\, D_2D_3,\, -(D_1D_2{+}D_3),\, -1{-}D_1D_2D_3,\, -(D_2D_3{+}D_1)) \tag{6.25}$$

$$\gamma \;=\; (D_2,\, D_2D_3, 1,\, D_1D_3,\, D_1,\, 1,\, -(D_1D_3{+}D_2),\, -(D_2D_3{+}D_1), -1{-}D_1D_2D_3) \tag{6.26}$$

This very simple extension of the module, ore more precisely the evidence of a module homomorphism is the algebraic counterpart of the physical impossibility of distinguishing between laser phase shifts Doppler shifts induced by the supporting bench motions. Let us note also that algebraical suppression is restricted to noises that appear several times in the data, with time delays. The purely local noises (residual proof mass motions, shot noise...) cannot be suppressed by any TDI combination (this is the same in an actual interferometer). It will also be interesting to check that the GW signal survives

to that kind of filtering. Let us mention the extensions of the Michelson combinations. For more convenience, we only give the complementary 3-uples with respect to the 6-uples already given in 6.5, 6.6, 6.7:

$$X_{1,Z} = (D_2^2 + D_3^2 - D_2^2 D_3^2 - 1,\ 0,\ 0) \tag{6.27}$$

$$X_{2,Z} = (0,\ D_3^2 + D_1^2 - D_3^2 D_1^2 - 1,\ 0) \tag{6.28}$$

$$X_{3,Z} = (0,\ 0,\ D_1^2 + D_2^2 - D_1^2 D_2^2 - 1) \tag{6.29}$$

6.3 Rotating LISA

6.3.1 The Sagnac effect

The fact that the LISA triangle is in permanent rotation makes it necessary to treat thoroughly light propagation between spacecraft . Up to what degree of accuracy can we consider the LISA frame as inertial? The first objection comes from the Sagnac effect that makes non reciprocal the light distances in a rotating frame. A rigorous treatment can be carried out using principles of General Relativity. Consider firstly a reference frame with coordinates $x^{\mu'} = (ct', x', y', z')$ such that the metric tensor is Minkowskian:

$$g_{\mu'\nu'}(x^{\lambda'}) = \begin{pmatrix} 1 & 0 & 0 & 0 \\ 0 & -1 & 0 & 0 \\ 0 & 0 & -1 & 0 \\ 0 & 0 & 0 & -1 \end{pmatrix}$$

(This is a simplified version of the barycentric frame) The change for a reference frame rotating around the z axis with angular velocity Ω induce a coordinate change:

$$\begin{cases} t = t' \\ x = x' \cos \Omega t' + y' \sin \Omega t' \\ y = -x' \sin \Omega t' + y' \cos \Omega t' \\ z = z' \end{cases}$$

The new components of the metric tensor are found through the Jacobian:

$$g_{\mu\nu} = \frac{\partial x^{\mu'}}{\partial x^{\mu}} \frac{\partial x^{\nu'}}{\partial x^{\nu}} g_{\mu'\nu'}$$

after some calculations, this is:

$$g_{\mu\nu}(x,y) \;=\; \begin{pmatrix} 1-\Omega^2 r^2/c^2 & \Omega y/c & -\Omega x/c & 0 \\ \Omega y/c & -1 & 0 & 0 \\ -\Omega x/c & 0 & -1 & 0 \\ 0 & 0 & 0 & -1 \end{pmatrix}$$

with $r \equiv \sqrt{x^2+y^2}$. A photon propagates along a null geodesic. Along the optical path, we have thus:

$$ds^2 \;\equiv\; g_{\mu\nu}\,dx^\mu\,dx^\nu \;=\; g_{00}\,c^2dt^2 \;+\; 2\,g_{0i}\,c\,dt\,dx^i \;+\; g_{ij}\,dx^i\,dx^j \;=\; 0$$

this allows to compute the time coordinate lag between two events separated by dx^i along the optical path:

$$dt \;=\; \frac{-g_{0i}\,dx^i \;\pm\sqrt{(g_{0i}\,g_{0j}-g_{00}\,g_{ij})\,dx^i\,dx^j}}{c\,g_{00}}$$

The sign indetermination is caused by the absence of causality in the preceding process. If we require a causal sequence, the time lag must be positive and we must take the absolute value of the preceding expression:

$$dt = |dt| \;=\; \frac{\sqrt{(g_{0i}\,g_{0j}-g_{00}\,g_{ij})\,dx^i\,dx^j}\pm\,g_{0i}\,dx^i}{c\,g_{00}}$$

It is now clear that the coordinate time lag between two events on the optical path depends of the direction of the path. The angular velocity and the inter spacecraft distances are such that $\Omega r/c \;\sim\; 2\,10^{-6} \;\ll 1$. We can therefore limit the expression to the 1st order in v/c:

$$dt \;=\; \frac{1}{c}\left(\sqrt{\delta_{ij}\,dx^i\,dx^j}\pm\,g_{0i}\,dx^i\right)$$

By integrating along the path from point A to point B, we get:

$$t_B \;-\; t_A \;=\; \frac{L}{c} \;\pm\; \int_A^B \frac{\Omega}{c^2}(y\,dx - x\,dy)$$

$$= \;\frac{L}{c} \;\mp\; \frac{\Omega}{c^2}\int_A^B r^2\,d\phi \;=\; \frac{L}{c} \;\mp\, 2\,\frac{\Omega}{c^2}\,S$$

where S is the area swept by the position vector during the trip AB and L the ordinary euclidean distance between A and B (r, ϕ are the polar coordinates corresponding to x, y). For the AB trip, we have:

$$t_B = t_A + \frac{L}{c} - 2\frac{\Omega}{c^2} S$$

and for the opposite trip BA:

$$t_A = t_B + \frac{L}{c} + 2\frac{\Omega}{c^2} S$$

The time difference between the two trips is thus:

$$\Delta t_{AB} = 4\frac{\Omega}{c^2} S$$

For LISA, the area swept between two nodes of the triangle of side length L is the third of the triangle area or:

$$S_{AB} = \frac{L^2}{4\sqrt{3}}$$

so that

$$\Delta t_{AB} = \frac{1}{\sqrt{3}} \Omega \left(\frac{L}{c}\right)^2$$

The equivalent optical path is:

$$c\,\Delta t_{AB} = \frac{\Omega L}{c\sqrt{3}} L \sim 10 \text{ km}$$

Remark that if we denote by ΔL the difference in light-distance between the two paths, we have

$$\Delta L / L = v/c$$

where v is the velocity of the spacecraft with respect to the center of the constellation. Anyway, the result is much larger than the accuracy in time delay required for an efficient noise cancellation by TDI. It is thus now necessary to distinguish the direction of the paths for chosing the time delays in TDI. A native relativistic study of the optical links allows to obtain systematically not only the 1st order sagnac effect described here in order to show the existence of non reciprocal time delays, but more generally all relativistic corrections to these time delays. This will be done in chapter **??**.

6.3.2 Aberration

The most important effect is however the aberration. This effect arises frome the Lorentz transformation of time between the coordinate time in the LISA frame and in the barycentric frame. For understanding this effect we consider the simplest experiment in which two spacecraft A and B are moving with constant velocity v along the x axis in the barycentric frame (S). Denote by (ct, x) the barycentric coordinates and (ct', x') the coordinates in the frame (S') attached to the two spacecraft (i.e. in which the two spacecraft are at rest). In (S'), the distance between the two spacecraft is constant and equal to L. Emission of a photon from A to B happens at time $t'_A = 0$ when the spacecraft A is at the location $x'_A = 0$. Its detection in B happens at time $t'_B = L/c$, when the spacecraft B is at location $x'_B = L$. In the barycentric frame, the same events have coordinates we can deduce from the preceding ones via a special Lorentz transform with $\gamma = \frac{1}{\sqrt{1-v^2/c^2}}$:

$$\begin{cases} ct_A = \gamma(ct'_A - v\,x'_A/c) &= 0 \\ x_A = \gamma(x'_A - v\,t_A) &= 0 \end{cases}$$

and

$$\begin{cases} ct_B = \gamma(ct'_B - v\,x'_B/c) &= \gamma\frac{L}{c}\left(1 - \frac{v}{c}\right) \\ x_B = \gamma(x'_B - v\,t_B) &= \gamma L\left(1 - \frac{v}{c}\right) \end{cases}$$

The light distance in (S) is thus:

$$c\Delta t_{AB} = c(t_B - t_A) = \gamma\, L\left(1 - \frac{v}{c}\right)$$

Consider now the opposite sequence. Emission happens from B at time $t'_B = 0$ and at abscissa $x'_B = L$ in (S'). Detection happens at time $t'_A = L/c$ and location $x'_A = 0$ The same transformation gives:

$$\begin{cases} ct_B = \gamma(ct'_B - v\,x'_B/c) &= -\gamma L\,v/c \\ x_B = \gamma(x'_B - v\,t_B) &= \gamma L \end{cases}$$

and

$$\begin{cases} ct_A = \gamma(ct'_A - v\,x'_A/c) &= \gamma L/c \\ x_A = \gamma(x'_A - v\,t_A) &= -\gamma v L/c \end{cases}$$

the light distance in (S) is now

$$c\Delta t_{BA} = c(t_A - t_B) = \gamma\, L\left(1 + \frac{v}{c}\right)$$

we have consequently a non reciprocal path:

$$c(\Delta t_{BA} - \Delta t_{AB}) \;=\; 2L\frac{v}{c}$$

(we have $\gamma \sim 1$). During short periods of time, it happens that two LISA spacecraft have a nearly inertial motion, like in the preceding discussion, due combination of orbital motions. But in general, the LISA spacecraft have motions more complex that this simple example. The effect is however still existing. In order to give an order of magnitude, the orbital velocities are about 30 km/s giving $v/c \sim 10^{-2}$. One could therefor have non reciprocal distances of the order of 1000 km. A numerical model shows that this upper bound is never reached. A maximum is 100 km.

6.3.3 Non reciprocal delay operators: A new module

We are now faced with 6 delay operators instead of 3. Refer to Fig.6.1, we keep the notation D_i for the counterclockwise delays , and D'_i for the clockwise delays. The elementary data are now:

$$U_1 \;=\; D'_2C_3 - C_1, \quad V_1 \;=\; C_1 - D_3C_2 \tag{6.30}$$

and the 4 other flows by circular permutation of the indices. The equation that determines the module is more complex and the module itself is on the ring of polynomials in 6 formal variables ($(D_1, D_2, D_3, D'_1, D'_2, D'_3)$). One can however find by using the algebraical methods reported at chapter **??** a generating system [**?**]:

$$\begin{cases} g^{(1)} &= [D_2(1 - D'_1D_1),\ D_2D_3 - D'_1,\ 1 - D'_1D_1,\ 0,\ 0,\ 1 - D_1D_2D_3] \\ g^{(2)} &= [D'_1(1 - D'_2D_2),\ 0,\ D_3 - D'_1D'_2,\ D'_1 - D_2D_3,\ 0,\ D_3(1 - D'_2D_2)] \\ g^{(3)} &= [0,\ 1 - D'_2D_2,\ D_1 - D'_2D'_3,\ D'_3 - D_1D_2,\ 1 - D'_2D_2,\ 0] \\ g^{(4)} &= [D'_3 - D_1D_2,\ D'_3D_3 - 1,\ D_1(D'_3D_3 - 1),\ 0,\ D_1D_2D_3 - 1,\ 0] \\ g^{(5)} &= [D'_1D_1 - 1,\ D'_1D'_2 - D_3,\ 0,\ D'_1D_1 - 1,\ 0,\ D_1D_3 - D'_2] \\ g^{(6)} &= [D_2 - D'_1D'_3,\ 0,\ 1 - D'_3D_3,\ 0,\ D'_1 - D_2D_3,\ 1 - D'_3D_3] \end{cases} \tag{6.31}$$

One can retrieve generators analogous to the "Sagnac" combinations found in the inertial picture:

$$\alpha \;=\; D_1\, g^{(2)} - D'_1D'2\, g^{(4)} - g^{(5)} \tag{6.32}$$

$$\beta \;=\; D_1D'_3\, g^{(2)} - g^{(4)} - D'_3\, g^{(5)} \tag{6.33}$$

$$\gamma \;=\; (1 - D'_3 D_3)\, g^{(1)} + D'_3\, g^{(2)} - D'_1\, g^{(4)} - D'_3 D_3 D_2\, g^{(5)} \tag{6.34}$$

There are now 3 symmetric Sagnac instead of 1:

$$\zeta_1 \;=\; D'_2\, g^{(1)} - D_1\, g^{(2)} - D'_2\, g^{(6)} \tag{6.35}$$

$$\zeta_2 \;=\; g^{(3)} + g^{(4)} + D'_3\, g^{(5)} \tag{6.36}$$

$$\zeta_3 \;=\; -g^{(1)} - D'_1\, g^{(3)} + g^{(6)} \tag{6.37}$$

or in detail:

$$\alpha \;=\; [1 - D'_1 D'_2 D'_3,\; D_3(1 - D'_1 D'_2 D'_3),\; D_1 D_3(1 - D'_1 D'_2 D'_3),$$

$$1 - D_1 D_2 D_3,\; D'_1 D'_2 (1 - D_1 D_2 D_3),\; D'_2 (1 - D_1 D_2 D_3)] \tag{6.38}$$

$$\beta \;=\; [D_1 D_2 (1 - D'_1 D'_2 D'_3),\; 1 - D'_1 D'_2 D'_3,\; D_1 (1 - D'_1 D'_2 D'_3),$$

$$D'_3 (1 - D_1 D_2 D_3),\; 1 - D_1 D_2 D_3,\; D'_2 D'_3 (1 - D_1 D_2 D_3)] \tag{6.39}$$

$$\gamma \;=\; [D_2 (1 - D'_1 D'_2 D'_3),\; D_2 D_3 (1 - D'_1 D'_2 D'_3),\; 1 - D'_1 D'_2 D'_3,$$

$$D'_1 D'_2 (1 - D_1 D_2 D_3),\; D'_1 (1 - D_1 D_2 D_3),\; 1 - D_1 D_2 D_3] \tag{6.40}$$

Consider a triplet of 9-uples (a, b, c). We call $\mathcal{C}$ the transformation in which simultaneously the 9-uples (a, b, c), the components of theirs sub-3-uples and the indices are circularly permuted. It is easily seen that the triplet (α, β, γ) is invariant under $\mathcal{C}$, which can be written $\alpha \succ \beta \succ \gamma$. The inertial case is retrieved up to a polynomial factor by suppressing the primes. We have also:

$$\zeta_1 \;=\; [D'_1 (D'_2 D'_3 - D_1),\; D'_2 (D_2 D_3 - D'_1)\, D_3 (D'_2 D'_3 - D_1),$$

$$D_1 (D_2 D_3 - D'_1),\; D'_2 (D_2 D_3 - D'_1)\, D_3 (D'_2 D'_3 - D_1)] \tag{6.41}$$

the $\zeta_{2,3}$ are found by $\mathcal{C}$ suppressing the primes leads to only one ζ, up to a polynomial factor. The following "Mathematica notebook" checks that the preceding expressions cancel the phase noise out.

6.3.4 Notebook Mathematica

Notations are obvious: Di $\equiv D_i$, DPi $\equiv D'_i$.

```
In[1]:=

Definition of elementary data

In[2]:=
U1:= DP2 C3 - C1
In[3]:=
U2:=DP3 C1 - C2
In[4]:=
U3:=DP1 C2 - C3
In[5]:=
V1:=C1- D3 C2
In[6]:=
V2:=C2 - D1 C3
In[7]:=
V3:=C3- D2 C1

 "Noise" 6-uple

In[8]:=
Noise:={V1,V2,V3,U1,U2,U3}



First generator of the module:

In[14]:=
gen1:={D2(1-DP1 D1), D2 D3 - DP1,1-DP1 D1, 0, 0, 1 -D1 D2 D3}

Checking cancellation of noise:

In[15]:=
gen1.Noise
```

```
Out[15]=
(C2-C3 D1) (D2 D3-DP1)+(1-D1 D2 D3) (-C3+C2 DP1)+(C3-C1 D2) (1-D1 DP1)+
  D2 (C1-C2 D3) (1-D1 DP1)

In[16]:=
FullSimplify[%]

Out[16]=
0


Second generator:

In[17]:=
gen2:={DP1(1 - DP2 D2),0,D3-DP1 DP2,DP1-D2 D3,0,D3(1-DP2 D2)}

checking:

In[18]:=
FullSimplify[gen2.Noise]
Out[18]=
0

third generator

In[19]:=
gen3:={0,1- DP2 D2, D1- DP2 DP3, DP3 - D1 D2, 1- DP2 D2, 0}
In[20]:=
FullSimplify[gen3.Noise]
Out[20]=
0

fourth generator:

In[21]:=
gen4:={DP3 - D1 D2, DP3 D3 -1, D1(DP3 D3 - 1),0, D1 D2 D3 -1,0}
In[22]:=
FullSimplify[gen4.Noise]
```

```
Out[22]=
0

fifth generator

In[23]:=
gen5:={DP1 D1- 1, DP1 DP2 - D3, 0, DP1 D1 -1, 0, D1 D3-DP2}
In[24]:=
FullSimplify[gen5.Noise]
Out[24]=
0

sixth generator:

In[25]:=
gen6:={D2-DP1 DP3,0, 1-DP3 D3, 0, DP1 - D2 D3, 1 - DP3 D3}
In[26]:=
FullSimplify[gen6.Noise]
Out[26]=
0

Combination  \[Alpha]

In[27]:=
\[Alpha]:= D1 gen2 - DP1 DP2 gen4 - gen5
In[28]:=
FullSimplify[\[Alpha]]
Out[28]=
{1-DP1 DP2 DP3,D3-D3 DP1 DP2 DP3,D1 D3 (1-DP1 DP2 DP3),
  1-D1 D2 D3,-(-1+D1 D2 D3) DP1 DP2,DP2-D1 D2 D3 DP2}
In[29]:=
FullSimplify[\[Alpha].Noise]
Out[29]=
0

Combination \[Beta]

In[30]:=
```

```
\[Beta]:= D1 DP3 gen2 - gen4 - DP3 gen5
In[31]:=
FullSimplify[\[Beta]]
Out[31]=
{D1 D2 (1-DP1 DP2 DP3),1-DP1 DP2 DP3,D1-D1 DP1 DP2 DP3,DP3-D1 D2 D3 DP3,
  1-D1 D2 D3,(1-D1 D2 D3) DP2 DP3}

Combination \[Gamma]

In[34]:=
\[Gamma]:=(1-DP3 D3)gen1 + DP3 gen2 - DP1 gen4 - DP3 D3 D2 gen5
In[35]:=
FullSimplify[\[Gamma]]

Out[35]=
{D2-D2 DP1 DP2 DP3,D2 D3 (1-DP1 DP2 DP3),1-DP1 DP2 DP3,(1-D1 D2 D3) DP1 DP3,
  DP1-D1 D2 D3 DP1,1-D1 D2 D3}


the \[Zeta]i:

In[36]:=
\[Zeta]1:=DP2 gen1 - D1 gen2 - DP2 gen6
In[37]:=
FullSimplify[\[Zeta]1]

Out[37]=
{-D1 DP1+DP1 DP2 DP3,(D2 D3-DP1) DP2,-D1 D3+D3 DP2 DP3,
  D1 (D2 D3-DP1),(D2 D3-DP1) DP2,-D1 D3+D3 DP2 DP3}

In[42]:=
\[Zeta]2:=gen3 + gen4 + DP3 gen5
In[43]:=
FullSimplify[\[Zeta]2]

Out[43]=
{D1 (-D2+DP1 DP3),-D2 DP2+DP1 DP2 DP3,(D1 D3-DP2) DP3,D1 (-D2+DP1 DP3),
  D2 (D1 D3-DP2),(D1 D3-DP2) DP3}
```

```
In[44]:=
\[Zeta]3:=-gen1 - DP1 gen3 + gen6
In[45]:=
FullSimplify[\[Zeta]3]

Out[45]=
{DP1 (D1 D2-DP3),D2 (-D3+DP1 DP2),-D3 DP3+DP1 DP2 DP3,DP1 (D1 D2-DP3),
  D2 (-D3+DP1 DP2),D3 (D1 D2-DP3)}
```

The "Michelson" combinations have the following new definitions:

$$X_1 \;=\; [1 - D'_1 D_1,\; 0,\; D'_2(D'_3 D_3 - 1),\; 1 - D'_3 D_3,\; D_3(D'_1 D_1 - 1),\; 0]$$

and as in the preceding:

$$X_1 \succ X_2 \succ X_3$$

As above, one must take into account the existence of 2 lasers and the random motions of the benches. The technique used for extending the module works a similar way. The Z_i variables are unchanged because non-reciprocal effects make no sense within one spacecraft . We only give the extensions of the generators (complementary 3-uples)

$$\begin{aligned}
g_1 &= (D'_1 D_1 - 1)\,[D_2,\; D_2 D_3,\; 1] \\
g_2 &= (D'_2 D_2 - 1)\,[D'_1,\; D_3 D'_1,\; D_3] \\
g_3 &= (D'_2 D_2 - 1)\,[D'_3,\; 1,\; D_1] \\
g_4 &= (1 - D'_3 D_3)\,[D_1 D_2,\; 1,\; D_1] \\
g_5 &= (1 - D'_1 D_1)\,[1,\; D_3,\; D'_2] \\
g_6 &= (D'_3 D_3 - 1)\,[D_2,\; D'_1,\; 1]
\end{aligned}$$

6.4 Flexing LISA: Second generation TDI module

It has been shown in the "orbitography" chapter that the distances between spacecraft is only approximately constant. Annual variations of about 50,000 km can be foreseen. As a result, the time deays required by TDI are not only non reciprocal, but also variable in time. A first consequence is the loss of commutativity of the delay operators. A new module must be found.

6.5 Response of LISA to GW

The LISA mission aims in fine to detect various kinds of gravitational signals. Let us see how the LISA system transduces a gravitational wave into the data stream. Consider one of the optical links, propagating from spacecraft A to spacecraft B. The unit vector of direction AB is $\mathbf{n}$. The distance between A and B is L=AB (the celebrated ~ 5 Mkm). The gravitational wave amplitude may in general be represented as a transverse traceless tensor. The only non zero components are the spatial ones h_{ij} given by ($c = 1$):

$$h_{ij}(t) \;=\; h'_+(t - \mathbf{w}.\mathbf{r})(a_i a_j - b_i b_j) + h'_\times(t - \mathbf{w}.\mathbf{r})(a_i b_j + a_j b_i) \qquad (6.42)$$

This is the so called "TT gauge". Vector $\mathbf{w}$ represents the direction of the source. If this direction is located by angles (θ, ϕ), we have

$$\mathbf{w} \;=\; \begin{bmatrix} \sin\theta\cos\phi \\ \sin\theta\sin\phi \\ \cos\theta \end{bmatrix} \qquad (6.43)$$

$\mathbf{r}$ is the current point ($\mathbf{r} = (x, y, z)$), the $\mathbf{a}, \mathbf{b}$ are unknown unit vectors related to the polarization of the source; they are orthogonal to $\mathbf{w}$ and mutually. Functions $h'_+(t)$ et $h'_\times(t)$ are unkown functions of time expressing the time variaitions of the source. In the frame where the unit vectors are $(\mathbf{a}, \mathbf{b}, \mathbf{w})$, the spatial part of tensor $\mathbf{h}$ is simply:

$$h_{ij} \;=\; \begin{pmatrix} h_+ & h_\times & 0 \\ h_\times & -h_+ & 0 \\ 0 & 0 & 0 \end{pmatrix}$$

We have therefore

$$w_i h_{ij} \;=\; 0$$

(transverse)

$$h_{ii} \;=\; 0$$

(traceless). It is convenient to consider an orthogonal basis directly linked to the source:

$$\mathbf{w}, \quad \theta \;\equiv\; \frac{\partial \mathbf{w}}{\partial \theta}, \quad \phi \;\equiv\; \frac{1}{\sin\theta}\frac{\partial \mathbf{w}}{\partial \phi} \qquad (6.44)$$

In the corresponding frame, the unkown vectors $\mathbf{a}, \mathbf{b}$ are obtained from θ, ϕ through a rotation the unknown angle ψ of which will be the scalar parameter defining the polarization state of the wave.

$$\begin{cases} \mathbf{a} &= \cos\psi\,\theta \;-\; \sin\psi\,\phi \\ \mathbf{b} &= \sin\psi\,\theta \;+\; \cos\psi\,\phi \end{cases}$$

Then

$$h_{ij}(t) \;=\; h_+(\theta_i\theta_j - \phi_i\phi_j) + h_\times(\theta_i\phi_j + \theta_j\phi_i) \tag{6.45}$$

where the functions h_+ and $h_\times$ are obtained from h'_+ and $h'_\times$ via a rotation (spin 2):

$$\begin{cases} h_+ &= \cos 2\psi\; h'_+ + \sin 2\psi\; h'_\times \\ h_\times &= -\;\sin 2\psi\; h'_+ + \cos 2\psi\; h'_\times \end{cases} \tag{6.46}$$

If now we consider a photon coming from A and propagating to B, on a time interval dt, its coordinates dx^i obey the null geodesic equation:

$$0 \;=\; ds^2 \;=\; dt^2 - dx^2 - dy^2 - dz^2 + h_{ij}dx^i dx^j$$

If λ is a scalar parameter parametrizing the path from A to B, we can write:

$$\mathbf{r} \;=\; \mathbf{r}_A + \lambda\,\mathbf{n} \quad (\lambda \in\; [O, L])$$

then:

$$0 \;=\; dt^2 - d\lambda^2 + h_{ij}n^i n^j d\lambda^2$$

yielding:

$$d\lambda \;=\; dt\,\left[1 + \frac{1}{2}\,H(t - \mathbf{w}.\mathbf{r})\right] \tag{6.47}$$

where:

$$H \;=\; h_{ij}n^i n^j \;=\; h_+\xi_+ + h_\times\xi_\times$$

with

$$\xi_+ \;=\; (\theta.\mathbf{n})^2 - (\phi.\mathbf{n})^2, \quad \xi_\times \;=\; 2\,(\theta.\mathbf{n})(\phi.\mathbf{n}) \tag{6.48}$$

If we denote by t_r the photon emission date (retarded time), and t the current date, the vector $\mathbf{r}$ apparent in the argument of H may be parametrized as follows:

$$\mathbf{r} \;=\; \mathbf{r}_A + (t - t_r)\,\mathbf{n}$$

so that by integrating 6.47 we get:

$$L \;=\; t - t_r + \frac{1}{2}\int_{t_r}^{t} H(t' - \mathbf{w}.(\mathbf{r}_A + (t'-t_r)\,\mathbf{n})\,dt'$$

or as well:

$$L \;=\; t - t_r + \frac{1}{2}\int_{t_r}^{t} H((1-\mathbf{w}.\mathbf{n})t' - \mathbf{w}.\mathbf{r}_A + \mathbf{w}.\mathbf{n}\,t_r)\,dt' \qquad (6.49)$$

The retarded time t_r is thus an implicit function of the current date t. However at first order in h we have:

$$t_r \;=\; t - L + \frac{1}{2}\int_{t-L}^{t} H[(1-\mathbf{w}.\mathbf{n})t' - \mathbf{w}.\mathbf{r}_A + \mathbf{w}.\mathbf{n}\,(t-L)]\,dt' \qquad (6.50)$$

6.5.1 Time domain

It is convenient to use a Fourier transform. Assume that

$$H(t) \;=\; \int_{\mathbf{R}} d\omega\; \tilde{H}(\omega)\; \mathrm{e}^{-i\omega t}$$

then

$$t_r \;=\; t - L + \frac{1}{2}\int_{\mathbf{R}} d\omega\; \tilde{H}(\omega)\int_{t-L}^{t} \exp\left[-i\omega(1-\mathbf{w}.\mathbf{n})t' + i\omega\mathbf{w}.\mathbf{r}_A - i\omega\mathbf{w}.\mathbf{n}\,(t-L)\right]$$

after some algebra one finds (with $\mathbf{r}_B = \mathbf{r}_A + L\mathbf{n}$):

$$t_r \;=\; t - L + \frac{1}{2}\int_{\mathbf{R}} d\omega\; \tilde{H}(\omega)\; \mathrm{e}^{-i\omega t}\; \frac{\mathrm{e}^{i\omega\mathbf{w}.\mathbf{r}_B} \;-\; \mathrm{e}^{i\omega(\mathbf{w}.\mathbf{r}_A + L)}}{-i\omega(1-\mathbf{w}.\mathbf{n})} \qquad (6.51)$$

The fluctuating phase detected at B is:

$$\Phi(t) \;= 2\pi\,\nu_0\,t_r$$

where ν_0 is the nominal frequency of the emitting laser. The fluctuating phase is then:s

$$\nu(t) \;=\; \frac{1}{2\pi}\,\frac{d\Phi(t)}{dt}$$

or:

$$\nu(t) \;=\; \nu_0 + \frac{\nu_0}{2(1-\mathbf{w}.\mathbf{n})}\int_{\mathbf{R}} d\omega\; \tilde{H}(\omega)\; \mathrm{e}^{-i\omega t}\; \left[\mathrm{e}^{i\omega\mathbf{w}.\mathbf{r}_B} \;-\; \mathrm{e}^{i\omega(\mathbf{w}.\mathbf{r}_A + L)}\right]$$

the relative expression (analogous to a Doppler shift) is:

$$\frac{\delta\nu}{\nu}(t) \;=\; \frac{1}{2(1-\mathbf{w}.\mathbf{n})}\left[H(t-\mathbf{w}.\mathbf{r}_B)-H(t-\mathbf{w}.\mathbf{r}_A-L)\right] \tag{6.52}$$

We have to translate this result in terms of the observables U, V. We have thus:

$$V_1(t) \;=\; \frac{1}{2(1-\mathbf{w}.\mathbf{n}_3)}\left[H_3(t-\mu_1)-H_3(t-\mu_2-L_3)\right] \tag{6.53}$$

$$U_1(t) \;=\; -\frac{1}{2(1+\mathbf{w}.\mathbf{n}_2)}\left[H_2(t-\mu_1)-H_2(t-\mu_3-L_2)\right] \tag{6.54}$$

where we have taken into account the directions of the unit vectors along the arms. We successively set:

$$\mu_i \;=\; \mathbf{w}.\mathbf{r}_i$$

et

$$\begin{cases} \xi_{+,i} \;=\; (\theta.\mathbf{n}_i)^2-(\phi.\mathbf{n}_i)^2, \\ \xi_{\times,i} \;=\; 2\,(\theta.\mathbf{n}_i)(\phi.\mathbf{n}_i) \end{cases} \tag{6.55}$$

then

$$H_i \;=\; h_+\,\xi_{+,i} \;+\; h_\times\,\xi_{\times,i}$$

Other observables (U_2, U_3, V_2, V_3) are found as usual by using the $\mathcal{C}$ transformation.

6.5.2 Frequency domain

In the frequency domain, the Fourier transforms of the observables are directly derived from 6.51. We have thus ($\omega \equiv 2\pi f$):

$$V_1(f) \;=\; H_3(\omega)\,\frac{1}{2(1-\mathbf{w}.\mathbf{n}_3)}\left[\mathrm{e}^{i\omega\mu_1} \;-\; \mathrm{e}^{i\omega(\mu_2+L_3)}\right] \tag{6.56}$$

$$U_1(f) \;=-\; H_2(\omega)\,\frac{1}{2(1+\mathbf{w}.\mathbf{n}_2)}\left[\mathrm{e}^{i\omega\mu_1} \;-\; \mathrm{e}^{i\omega(\mu_3+L_2)}\right] \tag{6.57}$$

which gives the transfer functions for the two polarization components:

$$F_{V_1,+,\times} \;=\; \frac{1}{2(1-\mathbf{w}.\mathbf{n}_3)}\left[\mathrm{e}^{i\omega\mu_1} \;-\; \mathrm{e}^{i\omega(\mu_2+L_3)}\right]\,\xi_{3,+,\times} \tag{6.58}$$

$$F_{U_1,+,\times} = -\frac{1}{2(1+\mathbf{w}.\mathbf{n}_2)}\left[\mathrm{e}^{i\omega\mu_1} - \mathrm{e}^{i\omega(\mu_3+L_2)}\right]\xi_{2,+,\times} \qquad (6.59)$$

For the GW part of the observables, one has simply at the end:

$$U_{i,\mathrm{gw}} = F_{U_i,+}h_+ + F_{U_i,\times}h_\times$$

$$V_{i,\mathrm{gw}} = F_{V_i,+}h_+ + F_{V_i,\times}h_\times$$

Bibliography

[1] Ronald Drever
in *Gravitational Radiation*
edited by N. Deruelle and T. Piran (North Holland 1983) p.321

[2] Jean-Yves Vinet, Brian Meers, Catherine Nary Man and Alain Brillet
Optimization of long-baseline interferometers for gravitational-wave detection
Phys. Rev. D , Vol **38**, N.2 (1988) p. 433

[3] Brian J. Meers
Recycling in laser-interferometric GW detectors
Phys. Rev. D , Vol **38**, N.2 (1988) p. 2317

[4] F. Pegoraro, L.A. Radicati, Ph. Bernard and E. Picasso
Phys. Lett. **A68** (1978) p.165

[5] J. Mizuno, K.A. Strain, P.G. Nelson, J.M. Chen, R. Schilling, A. Rüdiger, W. Winkler and K. Danzmann
Phys. Lett. **A175** (1993) p.273

[6] Jun Mizuno in
Comparison of optical configurations for laser-interferometric gravitational-wave detectors
PHD Thesis, Max-Planck-Institut für Quantenoptik (MPQ 203) 1995

[7] Max BORN & Emil WOLF
Principles of Optics
Pergamon Press 1980

[8] Fritz Oberhettinger
Tables of Bessel Transforms
Springer 1972

[9] Fritz Oberhettinger
Tabellen zur Fourier Transformation
Springer 1957

[10] J.W. Cooley and J.W. Tukey
An algorithm for the machine calculation of complex Fourier series
Math. Comput.**19**, pp.297-301 (1965)

[11] Anthony E. Siegman
Lasers
Univ. Sc. Book (Oxford University Press) 86

[12] H. Kogelnik, Tingye Li
Laser beams and resonators Appl. Opt. **5**, p.1550 (1966)

[13] E. Sziklas, A. E. Siegman
Mode calculation in unstable resonators with flowing saturable gain I : Hermite-Gaussian expansion
Appl. Opt.**13**, p.2775 (1974)
Mode calculation in unstable resonators with flowing saturable gain II : FFT methods
Appl. Opt.**14**, p.1874 (1975)

[14] Patrice Hello, Jean-Yves Vinet
Simulation of beam propagation in off-axis optical sytems J. Opt. Paris, 1996 vol 27, N6, pp.265-276

[15] Michael Hercher
The spherical mirror Fabry-Perot interferometer
Appl. Opt. **7**, p.951 (1968)

[16] Patrice Hello
Modèle physique et simulation de l'antenne interférométrique gravitationnelle Virgo
Thèse de Doctorat en Sciences, Université Paris-Sud (1990)

[17] M. Abramowitz and I. Stegun
Handbook of mathematical functions
Dover

[18] Patrice Hello and Jean-Yves Vinet
Analytical models of thermal aberrations in massive mirrors heated by high power laser beams
J. Phys. France 51 (1990) p.1267

[19] Patrice Hello and Jean-Yves Vinet
Analytical models of transient thermoelastic deformations of mirrors heated by high power cw laser beams
J. Phys. France 51 (1990) p. 2243

[20] Yu. Levin
Internal thermal noise in the LIGO test masses : a direct approach
Phys. Rev. D 57 (1998) p.659

[21] H.B. Callen and T.A. Welton
Phys. Rev. 83 (1951) p.34

[22] Fritz Oberhettinger
Tables of Bessel Transforms
Springer-Verlag (1972)

[23] Jean-Yves Vinet
Journal de Physique (Paris) 10 (1985) p.252

[24] Timoshenko S. and Goodier J.N.
Theory of elasticity
Mc Graw & Hill 1951

[25] F.Bondu and J-Y. Vinet
Phys. Lett. A 198 (1995) p. 74-78

[26] A.Gillespie and F. Raab
Phys. Lett. A 178 (1993) P. 357

[27] C. Cagnoli, L. Gammaitoni, F. Marchesoni, M. Punturo
Virgo note PJT94/032

[28] F. Bondu, P. Hello, J-Y. Vinet
Phys. Lett. A 246 (1998) p.227

[29] Yuk Tung Liu, Kip S. Thorne
in press for Phys. Rev D (gr-qc/0002055)

[30] V.B Braginsky, M.L. Gorodetsky and S.P. Vyatchanin
Phys. Lett. A 264 (1999)

[31] Landau & Lifshitz
Course of theoretical physics, Vol.7 Pergamon, 1959

[32] Erika D'ambrosio, Kip S. Thorne
Phys. Rev. D 67 102004

[33] S. Ramachandran et al.
Proceedings of the optical fibre communication conference, paper K2 (March 5-10 2006)

[34] Clohessy and Wiltshire, Jour. of Aerospace Siences, 653-658 (1960)

[35] Nayak, Koshti, Dhurandhar, Vinet
On the minimum flexing of LISA
Class. Quant. Grav. 23 (2006), 1763-1778

[36] Tinto, Armstrong, Estabrook
Time-Delay interferometry for space-based gravitational wave searches
The Astroph. Jour. 527:814-826 (1999)

[37] Dhurandhar, Nayak, Vinet
Algebraic approach to time-delay data analysis for LISA
Phys. Rev. D 65 (2002) 102002